Materials Science Forum Vols. 567-568 (2007) pp. 269-272
online at http://www.scientific.net

Online available since 2007/12/06

Cell adhesion and proliferation on modified polyethylene

Nikola Kasálková[1, a], Kateřina Kolářová[1], Lucie Bačáková[2], Martin Pařízek[2], Anna Macková[3], Václav Švorčík[1]

1Department of Solid State Engineering, Institute of Chemical Technology, 166 28 Prague, Czech Republic

2 Institute of Physiology, Academy of Sciences of the Czech Republic, 142 20 Prague, Czech Republic

3Nuclear Physics Institute, Academy of Sciences of the Czech Republic, 250 68 Řež, Czech Republic

[a]nikola.kasalkova@vscht.cz

Keywords: polyethylene, plasma modification, grafting, cell adhesion and proliferation

Abstract

The interaction of cells with polymers is important for their potential applications in medicine and various areas of biotechnology. Their physico-chemical surface properties strongly influence the cell morphology, adhesion and growth. Physical and chemical properties of pristine and modified polyethylene (PE) films were studied. PE was modified by Ar plasma (0–400 s, 2.0 W) and than grafted with amino acid (glycine). Structural and morphological changes of polymer were studied by goniometry and Rutherford back-scattering (RBS). The interaction of these samples with vascular smooth muscle cell (VSMC) from the rat aorta was studied. Number and morphology of the adhered and proliferated cell on the pristine and modified PE was studied in vitro method. It was found that wetting angle of the modified films decreased with exposure time. Experiments in vitro indicated that the adhesion and proliferation of VSMC is increasing function of degradation time and glycine grafting.

Introduction

Study of materials with potential applications in medicine, information technologies and other fields is topical in present polymer chemistry [1]. Polymers find applications in tissue engineering as materials suitable for tissue reconstruction or as substrates for cultivation of cells skin coverage. For these applications the polymer surface can be tailored and its surface morphology, wettability and affinity to living cells can be changed in required manner [2].

One of the techniques of modification of polymer surface is exposure to plasma discharge. The plasma treatment initiate complex changes of polymer physico-chemical properties, the character of which depends on working gas composition, exposure time and discharge power [3,4]. Plasma discharge initiates cleavage of macromolecular chains or cross-linking. The plasma modified polymer surface exhibits increased chemical activity, due to presence of free radicals and unsaturated bonds, and it can easily be grafted with suitable agents [5,6]. By the grafting new functional groups or molecules are permanently bonded on the polymer surface [7].

In this study the polyethylene (PE) is modified in Ar plasma and subsequently grafted with glycine. The formation of oxidized structures is examined by RBS technique and surface wettability by goniometry. The modified PE is used as a carrier for cultivation of smooth muscle cells (VSMC), the adhesion and proliferation of which is studied by standard techniques.

Experimental

Experiments were performed on oriented polyethylene (PE, supplied by Granitol Ltd., CR), in the form of 40 μm thick foils. High density polyethylene (HDPE, ρ=0.951 g cm^{-3}) and low density polyethylene (LDPE, ρ=0.922 g cm^{-3}) were studied. The samples were modified in Ar plasma, exposure times were from 0 to 400 s. Discharge power was 1.7 W and the treatment was accomplished at room temperature. Modified PE was grafted with water solution of glycine (12 h, RT, 2 wt.%). Since the PE modified in plasma exhibits partial solubility in water parallel, control experiment was accomplished in which PE samples were etched in deionized water at RT for 12 hours.

Surface wettability was measured by goniometry. Contact angle (with error ±5%) was measured with distilled water at RT at 5 positions. Total content of oxygen and its concentration depth profile in pristine and modified PE was determined by Rutherford Back Scattering (RBS) method. Analyses were performed with 2.0 MeV He^+ ions from NPI Van de Graaff accelerator at NPI. He^+ ions scattered the laboratory scattering angle of 170°. The oxygen concentration profiles were obtained before and after 24 hour water etching.

Number and morphology of the adhered and proliferated vascular smooth muscle cell (VSMC) on the pristine and modified PE was studied in vitro. Polymer samples were sterilized for 1 hour in ethanol before cell cultivation. VSMC were seeded on the samples with density 30000 cells per cm^{-2} into1.5 ml of Dulbecco´s modification of Eagle´s minimal essential medium (DMEM) containing 10 % of fetal bovine serum. Cells were cultivated at 37°C and 5% content of CO_2. Cells adhesion was determined after 24 hours and cell proliferation after 2nd, 5th a 7th days after seeding. Cells were rinsed in phosphate-buffered saline (PBS), fixed in 70% ethanol and colored with hematoxylin and eosin. The cell membranes were colored with Texas Red colour and colour Hoechst were used for decorating of cell nuclei. The number of cells in the samples grafted with glycine and cultivated for 5 and 7 days was too high and different techniques had to be used for the determination of cell number. The cells were rinsed by PBS, released with trypsin-EDTA solution and counted in Cell Viability Analyzer (VI-cell XR, Beckman Coulter).

Results and discussion

The Ar plasma discharge causes cleavage of C-C and C-H bonds at exposed PE surface [8], rearrangement of modified macromolecules and molecular fragments and oxidation the PE surface layer [9]. These changes lead to changes in the PE surface morphology and wettability. The plasma modified surface exhibit increased chemical activity and it can be grafted with various agents [7].

The dependence of the contact angle on the plasma exposure time is shown in Fig.1. It is evident that the contact angle decreases with exposure time. Contact angle from HDPE is lower that from LDPE. The decline is faster for HDPE possibly due to higher content of new, oxidized structures [9]. Decline in the contact angle observed on water etched samples is probably due to dissolution of oxidized structures from the surface of plasma modified PE. Contact angles on the samples grafted with glycine are lower that those of the samples modified only with plasma. Since the glycine contains a polar group, this result proves

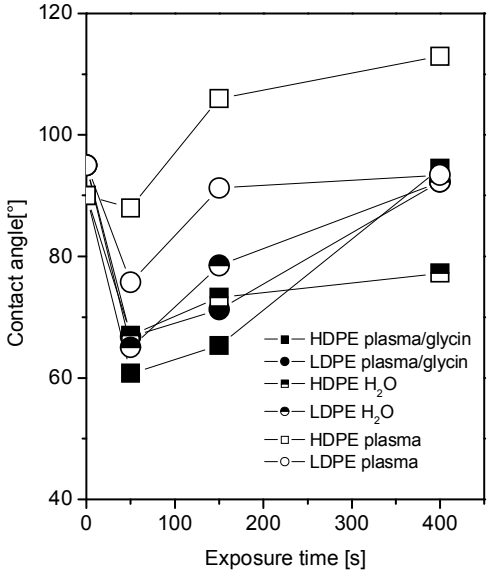

Fig. 1 Dependence of the contact angle on the plasma exposure time for pristine, plasma and plasma/glycin modified HDPE and LDPE.

glycine binding at the surface of plasma modified PE. The changes in contact angle may be affected also by changes in PE surface morphology. In previous experiments it was shown that, after the plasma treatment, the surface roughness of HDPE is higher that that of LDPE [9]. This may be due to the fact that during the plasma treatment PE amorphous regions are preferentially degraded followed by crystalline ones [10].

Plasma treatment leads to creation of free radicals [8] and an oxidation either from ambient atmosphere in reaction tank or later by air. Concentration depth profile of oxygen modified LDPE and HDPE was determined from RBS measurement. The oxygen content in plasma modified LDPE is higher (1,64 at.%) than in plasma modified and water etched LDPE (0,49 at.%). This may be explained by removal of a part of modified surface layer containing oxidized structures by etching. On the oxygen depth profile (Fig.2) from plasma modified LDPE an oxygen concentration maximum is seen at 20 nm depth. After etching the very surface layer of PE is removed and surface concentration increases. It could be due to binding of -COOH groups onto free radicals in the surface layer [8]. Concentration of oxygen in plasma modified and glycine grafted samples is comparable with that observed in plasma modified samples at the depth of 50 nm.

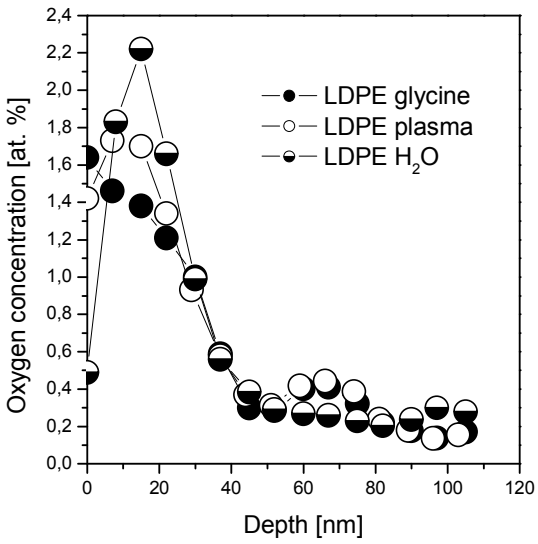

Fig. 2 Oxygen concentration depth profile of plasma, water and plasma/glycine modified LDPE.

Adhesion and proliferation of cells on both PE species was followed microscopically. For the sake of clarity, the proliferation of VSCM cells on pristine HDPE and LDPE is shown in Figs.3 A, B, the proliferation on plasma modified HDPE and LDPE in Figs 3C, D and on plasma modified and glycine grafted HDPE and LDPE in Figs. 3E, F. It is evident that the plasma modification enhances homogeneity of proliferating cells on both PE species. The subsequent grafting increases both homogeneity and proliferation, the effect being more pronounced on LDPE. In Fig. 4 the dependence of the cell number on the time of plasma treatment for plasma treated and plasma treated and grafted samples are shown. The plasma treatment leads to an increase of the number of adhering cells in comparison with pristine PE. The cell number is higher on LDPE probably due to higher oxygen content in the polymer surface layer. On both

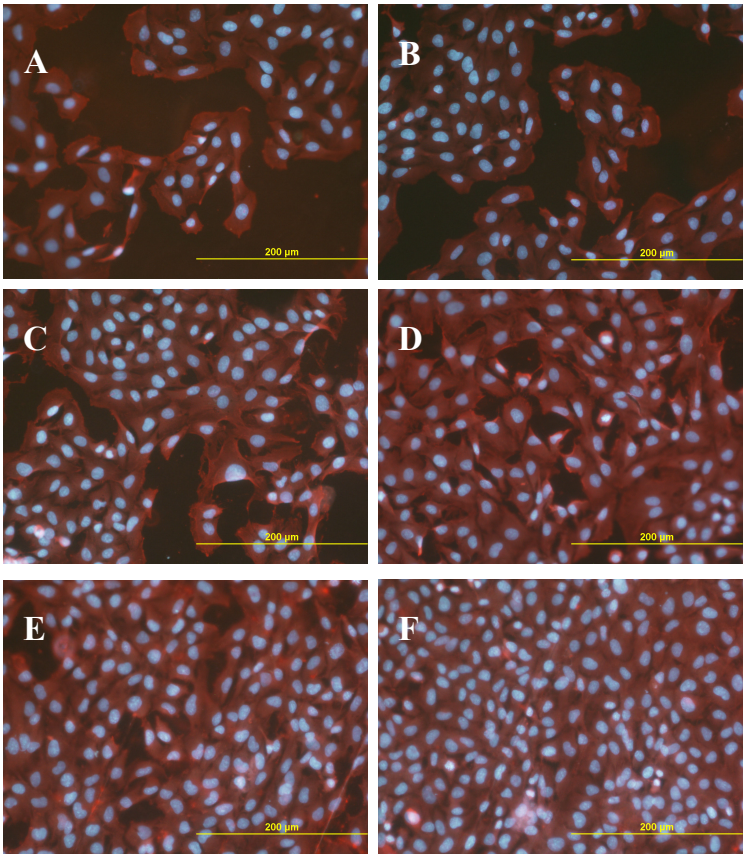

Fig. 3 The photographs show proliferation of VSMC (after 48 h) on pristine HDPE (A) and LDPE (B), plasma modified HDPE (C) and LDPE (D) and plasma/glycine modified HDPE (E) and LDPE (F).

polymer species the glycine grafting shows a positive effect on cell proliferation.

Conclusion

The plasma treatment leads to changes in the PE surface morphology (surface wettability), the changes being more pronounced on HDPE. Modification by plasma discharge itself and subsequent glycine grafting result in contact angle decline. Plasma modification of both, HDPE and LDPE and subsequent glycine grafting enhance adhesion and proliferation of VSCM cells.

Acknowledgements

The work was supported by GA CR under project No. 204/06/0225, by GAAS CR under the projects Nos. KAN400480701 and A 5011301 and by Ministry of Education of the CR under No. LC 06041 and by ICT in Prague No. 126080017.

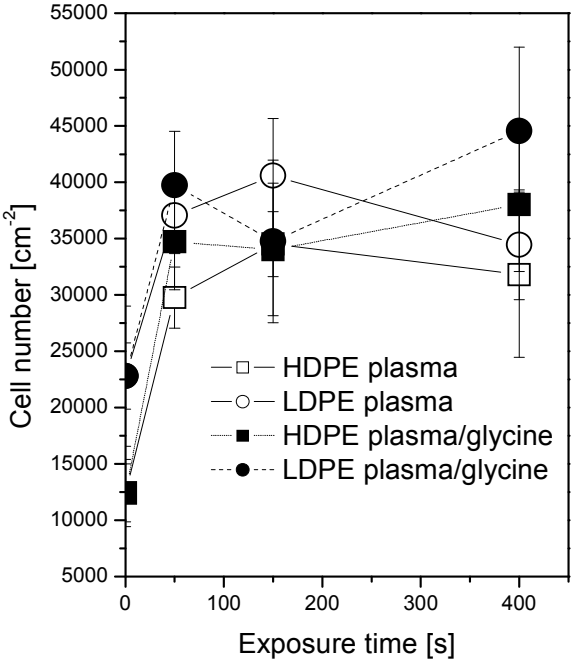

Fig. 4 Dependence the number of cells on the plasma exposure time for plasma/glycine modified HDPE and LDPE after adhesion (24 hours).

[1] information on http://www.imc.cas.cz/czisol2/imc/prospekt.html

[2] information on http://skripta.ft.tul.cz/data/2006-04-07/12-32-06.pdf

[3] D. Hegemann, H. Brunner and C. Oehr, Surf. Coat. Tech., Vol. 174-175 (2003), p. 253.

[4] C. Oehr, M. Müller, B. Elkin, D. Hegemann and U. Vohrer, Surf. Coat. Tech., Vol. 116-119 (1999), p. 25.

[5] information on http:/www.ft.vslib.cz/depart/ktm/files.20060106/VlastnostiVlaken-prednaska 14.pdf

[6] information on http://216.239.59.104/search?q=cache:stHN15xEXfw J:web.vscht. cz/sajdlp/la ng_cs.

[7] V. Švorčík, V. Hnatowicz, P. Stopka, L. Bačáková, J. Heitz, R. Öchsner and H. Ryssel, Rad. Phys. Chem., Vol. 60 (2001), p. 89.

[8] V. Švorčík, V. Rybka, V. Hnatowicz and K. Smetana. J. Appl. Mater. Sci. Mater. Med., Vol. 8 (1997), p. 435.

[9] V. Švorčík, K. Kolářová, P. Slepička, A. Macková, M. Novotná and V. Hnatowicz, Polym. Degr. Stab., Vol. 91 (2006), p. 1219.

[10] V.Kotál, V.Švorčík, P.Slepička, O.Bláhová, P.Šutta and V.Hnatowicz, Plasma Proc. Polym., Vol. 4 (2007), p. 69.

Int. J. Mol. Sci. **2009**, *10*, 4352-4374; doi:10.3390/ijms10104352

OPEN ACCESS

International Journal of
Molecular Sciences
ISSN 1422-0067
www.mdpi.com/journal/ijms

Article

Improved Adhesion, Growth and Maturation of Vascular Smooth Muscle Cells on Polyethylene Grafted with Bioactive Molecules and Carbon Particles

Martin Parizek [1], Nikola Kasalkova [2], Lucie Bacakova [1,*], Petr Slepicka [2], Vera Lisa [1], Martina Blazkova [3] and Vaclav Svorcik [2]

[1] Centre for Cardiovascular Research, Institute of Physiology, Academy of Sciences of the Czech Republic / Videnska 1083, CZ-14220 Prague 4, Czech Republic;
E-Mail: parizek@biomed.cas.cz (M.P.)

[2] Department of Solid State Engineering, Institute of Chemical Technology / Technicka 5, 16628 Prague 6, Czech Republic; E-Mails: Nikola.Kasalkova@vscht.cz (N.K.); Petr.Slepicka@vscht.cz (P.S.); Vaclav.Svorcik@vscht.cz (V.S.)

[3] Department of Biochemistry and Microbiology, Institute of Chemical Technology / Technicka 5, 16628 Prague 6, Czech Republic; E-Mail: Martina.Blazkova@vscht.cz (M.B.)

* Author to whom correspondence should be addressed; E-Mail: lucy@biomed.cas.cz (L.B.); Tel.: +420-2-9644-3743; Fax: +420-2-9644-2844.

Received: 9 July 2009; in revised form: 5 September 2009 / Accepted: 30 September 2009 / Published: 12 October 2009

Abstract: High-density polyethylene (PE) foils were modified by an Ar^+ plasma discharge and subsequent grafting with biomolecules, namely glycine (Gly), polyethylene glycol (PEG), bovine serum albumin (BSA), colloidal carbon particles (C) or BSA and C (BSA + C). As revealed by atomic force microscopy (AFM), goniometry and Rutherford Backscattering Spectroscopy (RBS), the surface chemical structure and surface morphology of PE changed dramatically after plasma treatment. The contact angle decreased for the samples treated by plasma, mainly in relation to the formation of oxygen structures during plasma irradiation. A further decrease in the contact angle was obvious after glycine and PEG grafting. The increase in oxygen concentration after glycine and PEG grafting proved that the two molecules were chemically linked to the plasma-activated surface. Plasma treatment led to ablation of the PE surface layer, thus the surface morphology was changed and the surface roughness was increased. The materials were then seeded with vascular smooth muscle cells (VSMC) derived from rat aorta and

incubated in a DMEM medium with fetal bovine serum. Generally, the cells adhered and grew better on modified rather than on unmodified PE samples. Immunofluorescence showed that focal adhesion plaques containing talin, vinculin and paxillin were most apparent in cells on PE grafted with PEG or BSA + C, and the fibres containing α-actin, β-actin or SM1 and SM2 myosins were thicker, more numerous and more brightly stained in the cells on all modified PE samples than on pristine PE. An enzyme-linked immunosorbent assay (ELISA) revealed increased concentrations of focal adhesion proteins talin and vinculin and also a cytoskeletal protein β-actin in cells on PE modified with BSA + C. A contractile protein α-actin was increased in cells on PE grafted with PEG or Gly. These results showed that PE activated with plasma and subsequently grafted with bioactive molecules and colloidal C particles, especially with PEG and BSA + C, promotes the adhesion, proliferation and phenotypic maturation of VSMC.

Keywords: plasma irradiation; bioactivity; biocompatibility; tissue engineering and reconstruction

1. Introduction

Synthetic polymers, such as polyethylene, polystyrene, polyurethane, polytetrafluoroethylene and polyethyleneterephthalate, are commonly used in various industrial applications, as well as in biotechnology and medicine. These materials not only serve as growth supports for cell cultures *in vitro*, but can also be used for constructing replacements for various tissues or organs, *e.g.*, non-resorbable or semi-resorbable vascular prostheses, artificial heart valves, bone and joint replacements, and implants for plastic surgery (for reviews, see [1–3]).

Materials designed for the construction of body implants must be biocompatible, *i.e.*, matching the mechanical properties of the replaced tissue and not acting as cytotoxic, mutagenic or immunogenic. Biocompatible materials can also behave as bioinert, *i.e.*, not promoting cell adhesion and proliferation. For example, such types of materials have been applied in the construction of artificial eye lenses and in articular surfaces of joint prostheses, *i.e.*, implants requiring transparency or smoothness, and thus completely cell-free surfaces. Bioinert materials have also been used for fabricating polymeric vascular prostheses in order to prevent adhesion and activation of thrombocytes and immunocompetent cells on the inner surface of these grafts (for reviews, see [2,4]).

An alternative and more advanced approach, widely accepted in recent tissue engineering, is to create surfaces that support colonization with cells and good integration of a replacement with the surrounding tissues of the patient's organism. This concept is used *e.g.*, for constructing bone prostheses that will persist in the patient's organism for many years, and is being developed for the creation of bioartificial replacements of blood vessels, liver, pancreas and even nervous system tissue. In these replacements, the artificial materials have a similar function as the natural extracellular matrix, and they serve as templates for regeneration of the damaged tissue. For example, in vascular tissue engineering, such a material should enable reconstruction of the *tunica intima*, formed by a

confluent layer of endothelial cells, and also reconstruction of the *tunica media* containing vascular smooth muscle cells. For such purposes, advanced artificial materials cannot merely be passively tolerated by cells, but should act as bioactive or biomimetic, *i.e.,* inducing the required cell responses in a controllable manner (for reviews, see [2–4]).

The cell-material interaction is strongly dependent on the physical and chemical properties of the material surface. The main properties decisive for colonization of a material with cells are polarity, wettability, electrical charge, roughness and topography. No less important is the presence of various chemical functional groups and biomolecules on the surface of these materials (for reviews, see [4,5]).

Unfortunately, many potential materials for the construction of tissue replacements have properties that are not so appropriate for integration with the surrounding tissues, and they need further modification in order to enhance their attractiveness for cell colonization and new tissue formation. The synthetic polymers mentioned above are a typical example. In their pristine state, these materials are characterized by relatively high hydrophobicity, *i.e.*, the water drop contact angle on their surface is higher than 90° (for reviews, see [4,5]).

There are various ways of modifying the surfaces of polymers to make them convenient for cell adhesion. For this purpose, the surfaces have been exposed to ultraviolet (UV) irradiation [6,7], to a beam of various ions (*e.g.*, oxygen, nitrogen, noble gases or halogens for biological applications [1–3,8]) or to a plasma discharge [9–12]. For more pronounced changes in the physicochemical properties of the modified surface, some of these processes can be realised in a gas atmosphere, *e.g.*, in acetylene or ammonia [6,7,13]. These modifications change the stability, roughness, morphology, mechanical properties and chemical composition of the polymer surface by creating chemical functional groups containing oxygen or nitrogen, *e.g.*, carbonyl, carboxyl or amine groups, on the surface of the material. These groups increase the surface wettability, support the adsorption of cell adhesion-mediating extracellular matrix proteins in an appropriate geometrical conformation and stimulate cell adhesion and growth [1–3,7].

An alternative and more exact approach for polymer surface modification can be to graft the polymer surfaces directly with various biomolecules, *e.g.*, with amino-acids, oligopeptides or protein molecules, which can influence the cell behavior in a more controllable manner. This grafting occurs spontaneously by exposing the material to biological environments, such as solutions of various biomolecules, blood, intercellular liquid or cell culture media, immediately after plasma activation. The biomolecules then bind to radicals created on the polymer surface by plasma activation [11,12].

Therefore, in this study, high-density polyethylene, a model material for potential biomedical use, was modified by an Ar^+ plasma discharge and subsequent grafting of glycine (Gly), bovine serum albumin (BSA), polyethyleneglycol (PEG), colloidal carbon particles (C) or BSA + C. The aim of these modifications was to create surfaces attractive for cell colonization. On the modified polymer, we evaluated the adhesion, proliferation and phenotypic maturation of vascular smooth muscle cells in cultures derived from rat aorta.

2. Results and Discussion

2.1. Physicochemical Properties of Polymer Samples

It is well known that chemical structure and surface morphology have a significant effect on surface wettability [12,14,15], which in turn may affect adhesion and proliferation of living cells [12,14]. The contact angle, as a measure of surface wettability, is shown in Figure 1 for pristine PE, plasma treated PE and plasma-treated and biomolecule-grafted samples. The contact angle decreases for samples treated by plasma, which is mainly related to the formation of oxygen structures during plasma-irradiation [16]. Obviously, the oxygen from the ambient residual atmosphere interacts with the plasma activated PE surface, and creates various oxidized structures. Creation of carbonyl, carboxyl and ester groups on plasma-treated PE was proven earlier in similar experiments [17,18]. A further decrease in the contact angle is obvious after glycine and PEG grafting, where the hydrophilicity of the sample increases in comparison to PE treated only with plasma. This finding supports the idea that the polar molecules (Gly, PEG) are linked to the activated PE chain [14]. By contrast, after BSA, C and BSA + C grafting, the values of the contact angle were higher than after plasma treatment, but lower than in the case of pristine PE. In our previous studies, covalent grafting of the mentioned molecules to the polymer surface was proved by the decrease in the concentration of radicals and double bonds on the modified polymer surface [19,20].

Figure 1. The contact angle of pristine PE (PE), plasma-treated PE (PE/pl), PE plasma-treated and then grafted with glycine (PE/pl/Gly), PEG (PE/pl/PEG), BSA (PE/pl/BSA), C (PE/pl/C) or BSA + C (PE/pl/BSA + C).

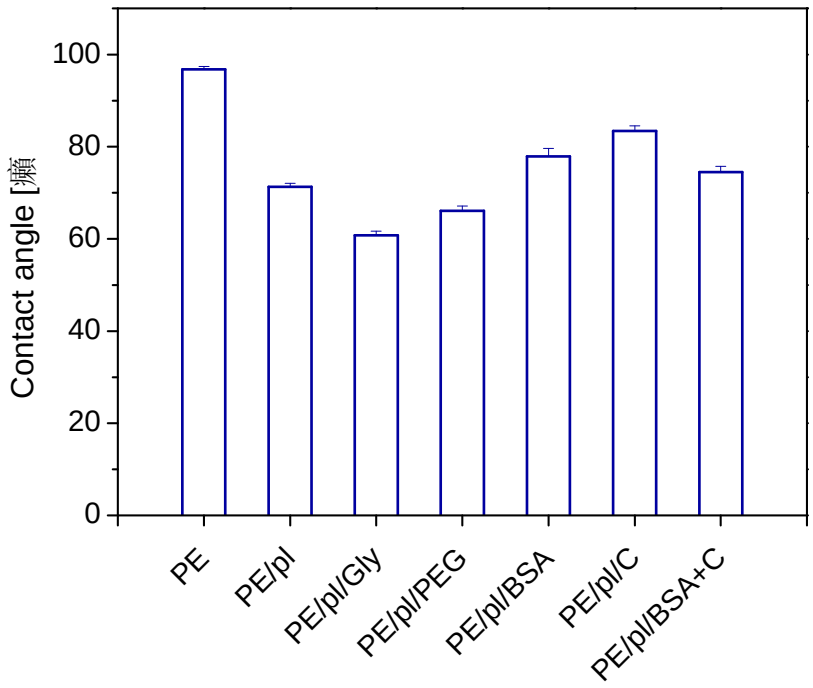

The presence of oxygen in the surface layer of the plasma-treated PE was examined using the RBS method. The oxygen depth concentration profile on the polymer surface is shown in Figure 2 for

plasma-treated PE, plasma-treated PE immersed in water, and plasma-treated PE grafted with glycine. Water-treating experiments were performed because all the biomolecules and C were grafted from a water solution, and then the samples were exposed to a water-based cell culture environment. Thus, it was necessary to know what influence the water has on the plasma-treated PE surface. It is apparent that oxygen is present not only on the very surface of the sample, but also in the near surface layer about 50 nm in thickness. The oxygen concentration reached its maximum at a depth of about 20 nm, and then decreased to the bulk. The presence of oxygen beneath the PE surface may indicate an inward diffusion of oxygen, which could be facilitated by the structure of the PE surface altered by the preceding plasma treatment. The results given in Figure 2 indicate that water-treating of plasma-treated PE leads to a dramatic decrease in oxygen concentration in the PE surface layer, caused by dissolution in water of the polymer macromolecules, degraded by plasma irradiation [21]. On the other hand, the increase in oxygen concentration after glycine grafting proves that this amino-acid was chemically linked to the plasma-activated surface [12]. The oxygen concentration in plasma-treated PE, the plasma-treated and water-immersed sample, and the plasma-treated and PEG-grafted sample is shown in Table 1. Similarly as in Figure 2, it is evident that the oxygen concentration decreases after water-treating. After PEG grafting, however, the oxygen concentration increases compared to the water-etched sample, which proves that there is chemical linking of the oxygen compound on the activated polymer chain. In pristine PE, no oxygen content was detected by RBS measurement. Also pristine PE exposed to water, PEG or Gly was oxygen-free. There are no radicals and double bonds on a pristine PE surface, and therefore it is not possible to graft PEG and Gly to this material.

Figure 2. Depth concentration profile of oxygen, determined from RBS measurement, on the sample exposed to plasma discharge (PE/plasma), plasma-treated sample immersed in water (PE/plasma/H_2O) and plasma-treated sample grafted with glycine (PE/plasma/Gly).

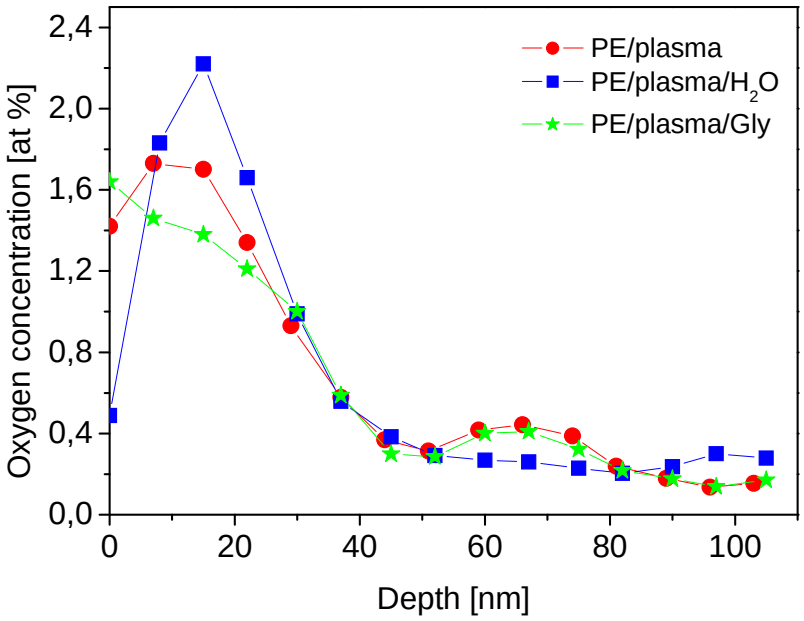

Table 1. Surface oxygen concentration determined from RBS measurement in plasma-treated PE (PE/plasma), plasma-treated and water-immersed PE (PE/plasma/H_2O), and plasma-treated PE then grafted with PEG (PE/plasma/PEG).

Sample	O concentration (10^{16} at cm^{-2})
PE/plasma	2.63
PE/plasma/H_2O	1.23
PE/plasma/PEG	2.19

Figure 3. AFM images of pristine PE (A), plasma-treated PE (B), PE treated with plasma and immersed in water (C), PE treated with plasma and grafted with glycine (D), PEG (E), BSA (F), colloidal carbon particles (G) or BSA + C (H). R_a is a parameter of measured surface roughness in nm.

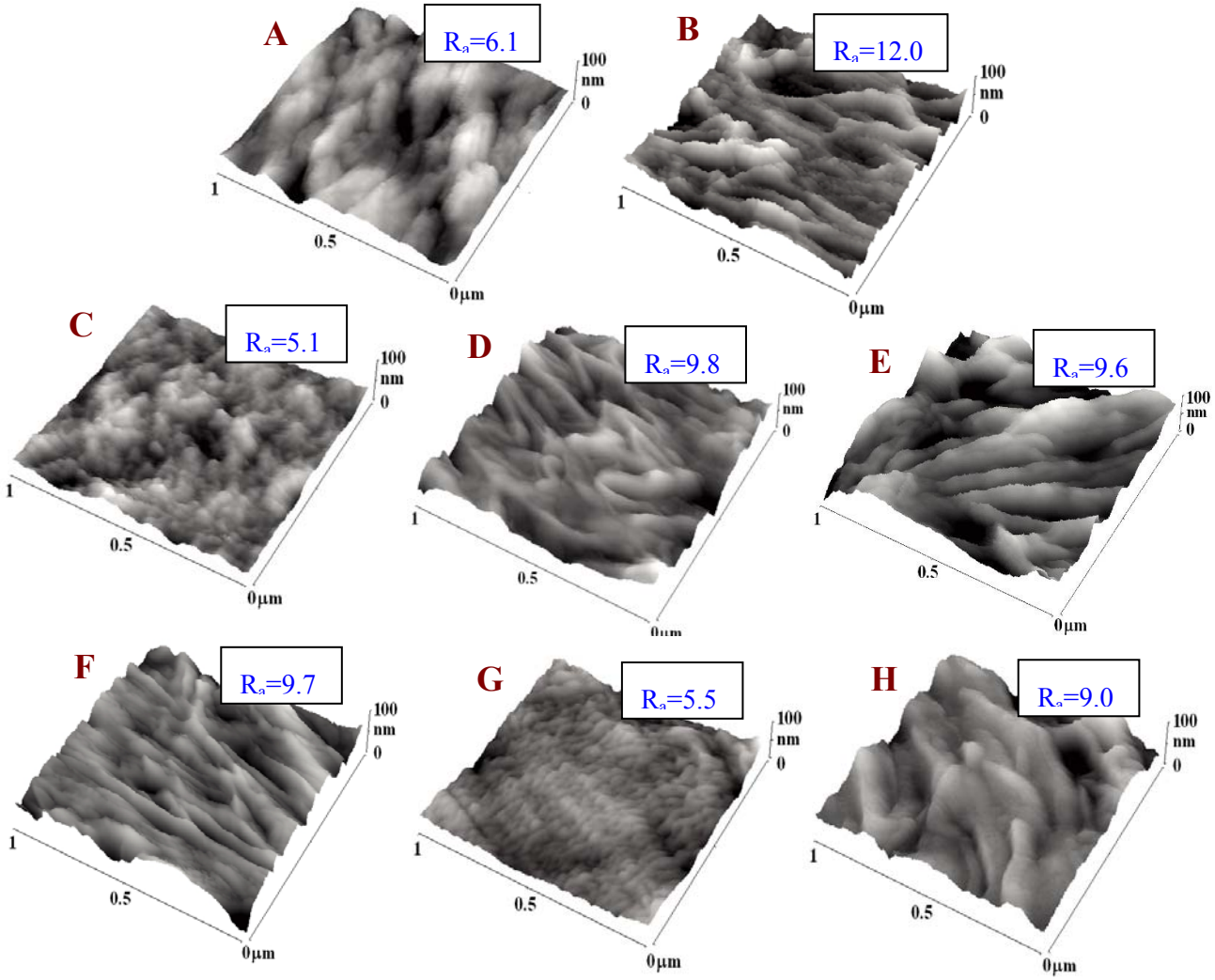

The surface morphology of pristine PE and PE exposed to a plasma discharge and then etched or grafted was examined using the AFM method (Figure 3). Plasma treatment led to ablation of the PE surface layer [17,18]. As a result, the surface morphology changed dramatically and the nanoscale surface roughness increased. Also a lamellar structure appeared on the PE surface, which could be due to the different ablation rates of the amorphous and crystalline phases [21]. Further changes in the

surface morphology and a decrease in the surface roughness occurred after exposure of the samples to a water environment. These changes were probably due to preferential etching of short molecular fragments formed by the plasma treatment [18]. Figure 3 also demonstrates changes in the surface morphology and a further increase in surface roughness after grafting the plasma-activated PE with glycine, PEG, BSA and BSA + C. Interestingly, when we compare the water-treated samples and the samples grafted by molecules of very different molecule weights (*i.e.*, glycine *vs*. PEG), the increase in material surface roughness does not depend on the molecular weight of the grafted molecule.

2.2. Initial Adhesion of VSMC on Polymer Samples

On day 1 after seeding, the numbers of initially adhered cells on all PE samples, including those unmodified, ranged between 9,340 ± 740 to 13,310 ± 1,430 cells/cm², while on the control PS, only 7,060 ± 770 cells/cm² were found. The highest cell numbers, significantly higher than those on PS, were found on PE grafted with PEG (13,310 ± 1,430 cells/cm²), C (12,280 ± 1,070 cells/cm²) and Gly (12,130 ± 1,130 cells/cm², Figure 4A). This was a favourable result, because tissue culture polystyrene (*i.e.*, PS usually modified by a glow discharge, *i.e.,* a similar technique as the plasma-irradiation used in our study) is considered as an ideal material for cell adhesion and proliferation. However, it is generally known that irradiation of polymers with a plasma discharge improves cell adhesion and growth. This beneficial effect has been attributed to the creation of oxygen-containing functional groups on the polymer surface. Fourier Transform Infrared Spectroscopy (FTIR) has indicated the presence of peroxide, ester, carbonyl, carboxyl, hydroxyl and amide groups, as well as excessive double bonds in polyethylene modified with a plasma discharge [21]. Also in this study, RBS proved an increase in oxygen concentration in PE after plasma treatment and plasma treatment followed by grafting Gly or PEG molecules, *i.e.*, donors of additional oxygen-containing groups (Table 1, Figure 2). These groups are known to increase surface wettability and improve the adsorption of cell adhesion-mediating extracellular matrix molecules (*e.g.*, vitronectin, fibronectin) from the serum of the culture medium. These molecules are adsorbed in an appropriate and flexible spatial conformation, enabling good accessibility of specific sites on these molecules (*e.g.*, RGD-containing oligopeptides) by cell adhesion receptors, such as integrins (for a review, see [2,4,5]). A similar effect has been described for nanostructured surfaces [22]. Therefore, from this point of view, the nanostructured surfaces act synergetically with oxygen-containing and wettable surfaces. As revealed by AFM, the nanoscale surface roughness of PE in our study became more apparent after plasma irradiation, and was also retained in a water environment and after grafting the polymer with biomolecules and C (Figure 3).

2.3. Spreading of VSMC on Polymer Samples

The cells on the modified PE samples were better spread, *i.e.*, adhering by a larger cell-material projected area, than on pristine PE (Figure 4B, C). On the 1st day after seeding, the largest spreading areas were found in cells adhering to the polystyrene dishes (546 ± 90 μm²), and PE grafted with BSA (453 ± 47 μm²), C (390 ± 53 μm²) or PEG (354 ± 32 μm²), whereas on non-modified PE the value was only 187 ± 29 μm². On day 2 after seeding, the largest cell spreading area was again achieved on the

polystyrene dishes (1440 ± 137 μm²) and on PE grafted with PEG (993 ± 52 μm²), compared to only 492 ± 42 μm² in VSMC on pristine PE. Also in our earlier studies, PE in its pristine non-modified form proved to be a substrate not very suitable for cell adhesion and spreading [8,11,14]. This behaviour of pristine PE can be attributed to its relatively high hydrophobicity, characterized by a water drop contact angle of almost 100° (Figure 1) compared with 102.5 ± 2.3° found in our earlier study [21], and also to the lack of oxygen-containing groups.

Figure 4. The number of initially adhered cells (A) and the size of the cell spreading area (B, C) of rat aortic smooth muscle cells in cultures on non-modified PE (Pristine), PE irradiated with plasma (Plasma), PE irradiated with plasma and grafted with glycine (Gly), polyethyleneglycol (PEG) bovine serum albumin (BSA), colloidal carbon particles (C) or bovine serum albumin and C (BSA + C). As a reference material, a tissue culture polystyrene dish (PS dish) was used.

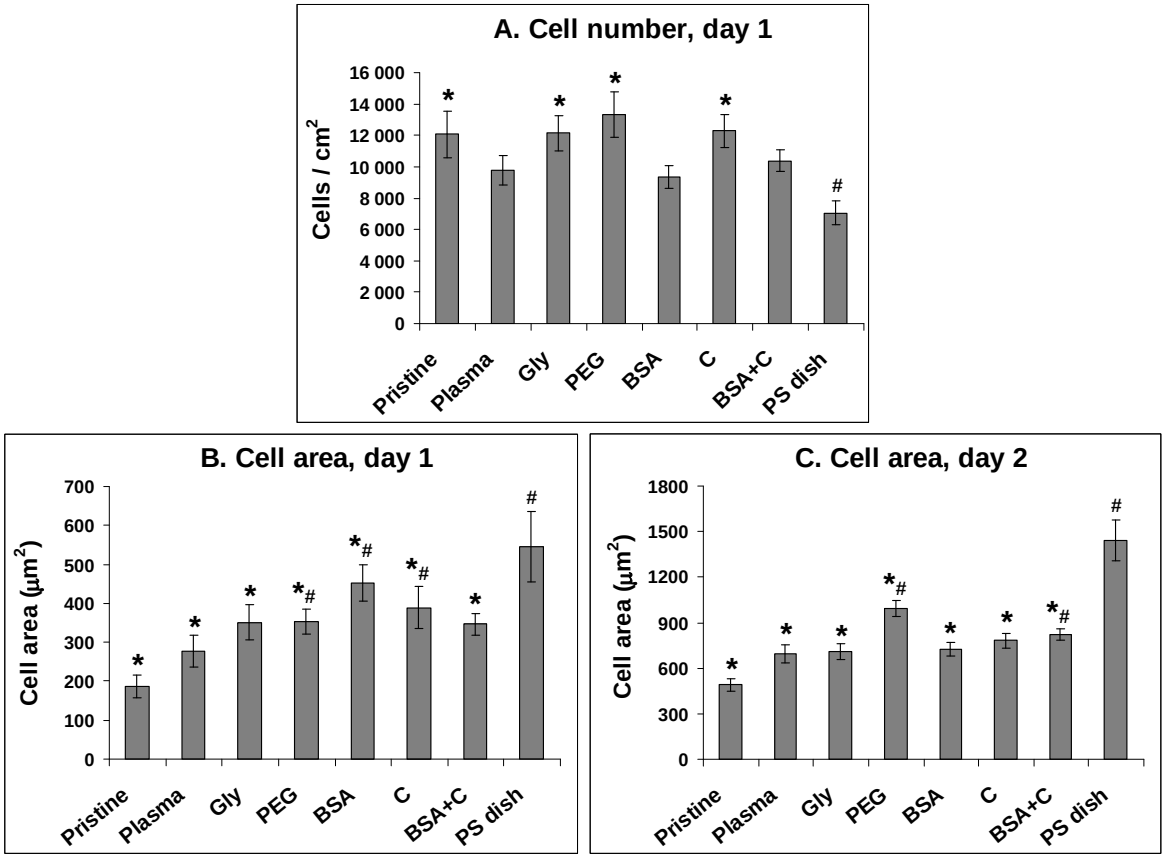

Means ± S.E.M. from 3 samples, each measured for 50 times (A) or from 72 to 142 cells for each experimental group (C, D). ANOVA, Student-Newman-Keuls method. Statistical significance: *, #: $p \leq 0.05$ compared to the value on pristine PE and polystyrene dish, respectively.

2.4. Proliferation of VSMC on Polymer Samples

Despite a lower number of initially adhered cells on PS, on day 2 after seeding, the cells on PS were in the exponential phase of growth, while the cells on most PE samples still remained in the lag phase (except plasma-irradiated PE and PE grafted with BSA + C, Figure 5). As a result, the cell number on PS (15,370 ± 2,240 cells/cm²) became significantly higher than that on non-modified PE

(8,240 ± 1,500 cells/cm²) and similar to the values found on all modified PE samples. Among these, the highest cell population densities were obtained on PE irradiated with plasma (17,650 ± 2,080 cells/cm²) and subsequently grafted with BSA and C (15,660 ± 1,690 cells/cm²), and these values were significantly higher than that on pristine PE (Figure 6A).

Figure 5. Growth dynamics of rat aortic smooth muscle cells in cultures on non-modified PE (Pristine), PE irradiated with plasma (Plasma), PE irradiated with plasma and grafted with glycine (Gly), polyethyleneglycol (PEG) bovine serum albumin (BSA), colloidal carbon particles (C) or bovine serum albumin and C (BSA + C). As a reference material, a tissue culture polystyrene dish (PS dish) was used.

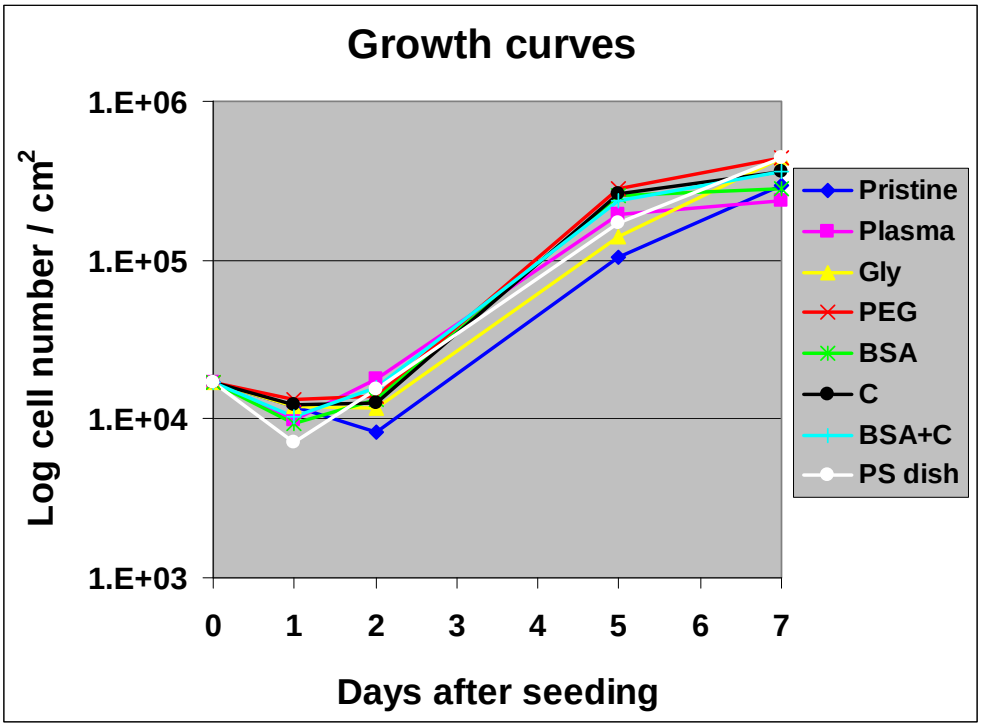

Means from three samples for each experimental group and time interval (each sample measured for 50 times).

On day 5 after seeding, the highest cell numbers were obtained on samples modified with PEG (285,000 ± 35,000 cells/cm^2), C (265,000 ± 14,000 cells/cm^2), BSA (256,000 ± 40,000 cells/cm^2) and BSA + C (236,000 ± 19,000 cells/cm^2). On PE grafted with PEG, the cell number was even significantly higher than that on PS (171,000 ± 23,000 cells/cm^2). The lowest number of cells persisted on pure PE (104,000 ± 19,000 cells/cm², Figure 6B).

On day 7, the cell numbers on PE grafted with PEG (442,000 ± 24,000 cells/cm^2) and Gly (436,000 ± 24,000 cells/cm^2) became significantly higher, not only in comparison with pristine PE (299,000 ± 23,000 cells/cm^2), but also in comparison with PE modified only with plasma irradiation (235,000 ± 20,000 cells/cm^2). Also on PE grafted with C and BSA + C, the cell numbers were significantly higher than on plasma-irradiated PE. On the latter sample, the cell number was significantly lower than that found on polystyrene culture dishes (440,000 ± 135,000 cells/cm²; Figure 6C). As documented by the growth curves, from day 5 to 7, the cells on the plasma-modified

samples entered the stationary phase, *i.e.,* did not significantly change their number (Figsures 5, 6B, C). A usual explanation for such cell behaviour is that confluence of the cells is attained and their growth ceases due to contact inhibition. However, as mentioned above, the cells in other materials were able to continue their growth, though more slowly. VSMC are able to form multilayered regions *in vitro*, referred to as "hills" [22], thus they become contact-inhibited at relatively high population densities. Another explanation for the cessation of VSMC growth on the plasma-modified PE could be that the plasma irradiation did not sufficiently increase the wettability of PE, which still remained lower than that of the cell culture polystyrene. The contact angle of traditional tissue culture polystyrene has been reported to range between 55.8° and 63.5° [24], while the plasma-irradiated PE in our study reached a higher value of about 70° (Figure 1). The concentration of oxygen, which is also supportive for cell adhesion and proliferation, was 17.2 % in tissue culture PS as measured by the Electron Spectroscopy for Chemical Analysis (ESCA) [24], whereas in plasma-treated PE, it was only about 0.5 at.% immediately on the polymer surface (which enters into contact with adsorbed proteins and attached cells), and about 1.7 at a depth of 10-20 nm (Figure 2). As mentioned above, the exposure of plasma-treated PE to a water environment used for grafting biomolecules (and also for cell cultivation), caused a further decrease in the oxygen content in the surface layer of the polymer. Last but not least, plasma modification is known to create radicals on the polymer surface [21]; for reviews, see [5,12], which can damage the cells and thus they can hamper the process of cell adhesion and proliferation.

Figure 6. Proliferation activity of rat aortic smooth muscle cells measured by cell numbers achieved on day 2 (A), 5 (B) and 7 (C) after seeding on non-modified PE (Pristine), PE irradiated with plasma (Plasma), PE irradiated with plasma and grafted with glycine (Gly), polyethyleneglycol (PEG) bovine serum albumin (BSA), colloidal carbon particles (C) or bovine serum albumin and C (BSA + C). As a reference material, a tissue culture polystyrene dish (PS dish) was used.

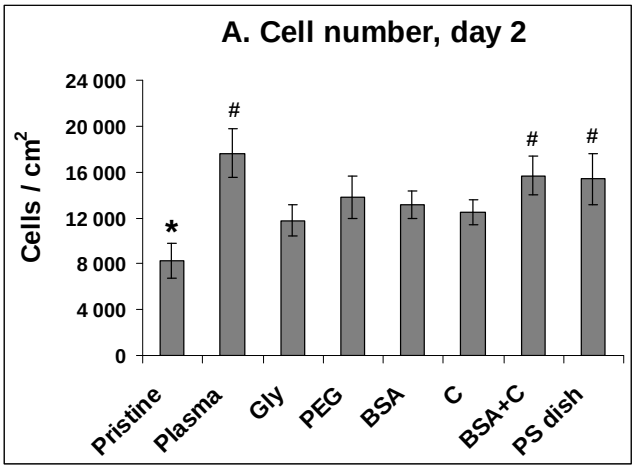

Figure 6. *Cont.*

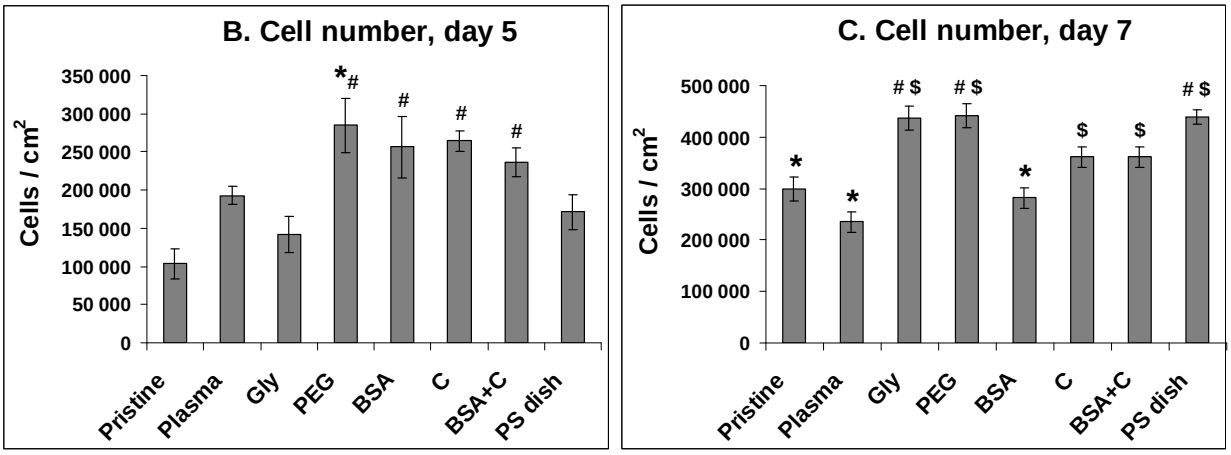

Means ± S.E.M. from three samples for each experimental group, each measured for 50 times. ANOVA, Student-Newman-Keuls method. Statistical significance: $^{*, \#, \$}$: $p \leq 0.05$ compared to the value on pristine PE, polystyrene dish and PE irradiated with plasma, respectively.

On the other hand, the radicals present on the surface of plasma-irradiated polymers can be efficiently used for grafting biomolecules. The results of this study proved that grafting PE with biomolecules, such as glycine, PEG, BSA and/or carbon particles, can create surfaces which are suitable for the adhesion and growth of VSMC. On all grafted samples, the cells were able to create confluent layers at the end of the experiment, *i.e.*, on day 7 after seeding (Figure 7). All modified PE samples seemed not to have any considerable cytotoxic effects, as suggested by the numbers of viable cells determined by the ViCell Analyser, which ranged between 73 and 97%. The number of viable cells increased from day 1 to day 7 of cultivation, which suggests that the cells were damaged by trypsinization and the counting procedure rather than by exposure to the modified PE samples.

Figure 7. Morphology of rat aortic smooth muscle cells on day 5 after seeding on pristine PE (A), tissue culture polystyrene dish (B), PE irradiated with Ar^+ plasma (C), PE irradiated with plasma and grafted with glycine (D), polyethyleneglycol (E) bovine serum albumin (F), colloidal carbon particles (G) or bovine serum albumin and C (H).

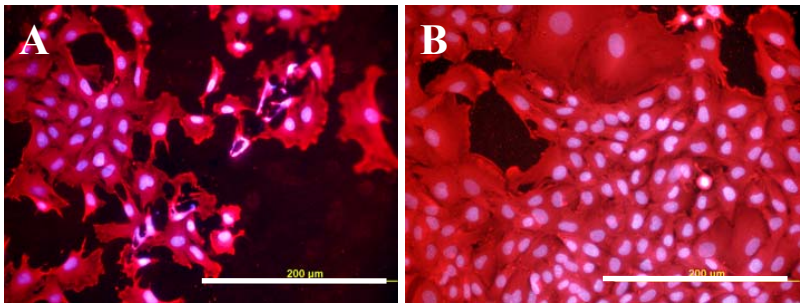

Figure 7. *Cont.*

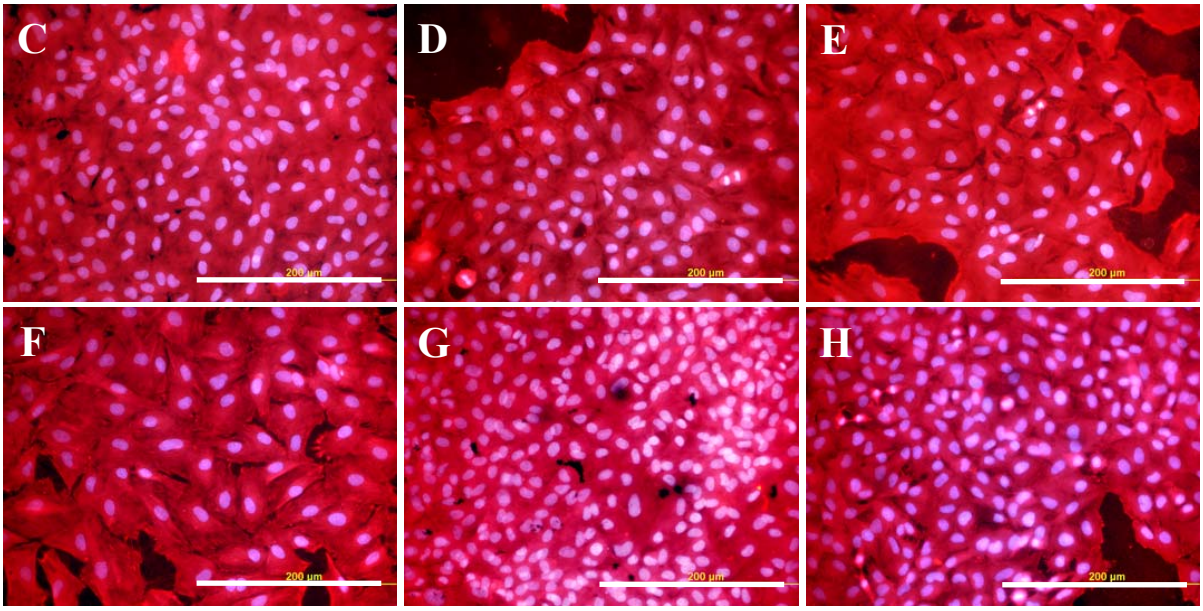

Cell membrane and cytoplasm stained with Texas Red C2-maleimide (red fluorescence), cell nuclei with Hoechst #33342 (blue fluorescence). Olympus IX 51 microscope, DP 70 digital camera, obj. 20×, bar = 200 µm.

The increase in the cell number and the size of the cell spreading area from day 1 to 7 was usually well-apparent on PE samples grafted with PEG or BSA. In other studies, however, both PEG and BSA have often been reported to be non-adhesive for cells and have even been used for constructing inert cell non-adhesive surfaces (for a review, see [25]). The anti-adhesive action of PEG is based on its very high hydrophilia and the mobility of its chain, which hamper stable adsorption of the proteins that mediate cell adhesion. However, at the same time, the anti-adhesive action of PEG is dependent on its concentration on the polymer surface and on the length of its chain. In our earlier studies performed on copolymers of poly(DL-lactide) (PDLLA) and PEG, the negative effect of PEG on the adhesion and proliferation of VSMC was most pronounced at intermediate concentrations of the PEG phase on the surface of the polymeric film (33-45 wt.%) and also at an intermediate length (m.w. 11,000) of the PEG chains. Both lower and higher concentrations (*i.e.*, 5 to 18 wt.% and 70 wt.%, respectively) and lengths (m.w. 5,000 and 23,800, respectively) permitted the attachment, spreading and formation of vinculin-containing focal adhesion plaques in VSMCs to an extent comparable to that observed on pure PDLLA and standard cell culture substrates, such as polystyrene dishes or microscopic glass coverslips [25,26]. Also the PEG chains used in the present study were rather long, having a molecular weight of 20,000.

As for BSA, this protein cannot be directly bound by cells. However, it has been reported to promote the adsorption of vitronectin and fibronectin in advantageous spatial conformations, supporting the accessibility of these molecules by cell adhesion receptors [27,28]. These molecules can be adsorbed over the albumin from the serum of the culture medium, and also synthesized and deposited by VSMCs themselves. When adsorbed on albumin, these molecules promote cell adhesion even if their concentrations are too low to support cell attachment alone [29].

The cell adhesion and proliferation on PE grafted with BSA was often improved after additional grafting of C. In our earlier studies, and also in studies by other authors, enrichment of cell adhesion substrate with carbon, *e.g.*, after ion irradiation [2,30], coating with amorphous carbon [31] or by deposition of carbon nanoparticles [32] (for a review, see [5]) often resulted in enhanced adhesion and growth of cells in cultures on these materials.

Grafting with glycine also improved the cell colonization of PE in the present study. This amino acid is a component of RGD-containing oligopeptides, which act as ligands for cell adhesion receptors. Although Gly alone cannot directly bind these receptors, it provides the grafted polymer surface with additional oxygen-containing groups and positively charged amine groups, which improve the adsorption of cell adhesion-mediating molecules from the serum of the culture medium [6,13,33].

2.5. Distribution and Concentration of Molecular Markers of Adhesion and Maturation in VSMCs

In accordance with the data obtained on the cell number and the cell spreading area, immunofluorescence staining revealed that focal adhesion plaques containing talin, vinculin and paxillin were generally better developed in cells on modified PE samples, particularly those grafted with PEG and BSA + C, than in cells on pristine PE samples (Figure 8). ELISA showed that the cells on PE modified with PEG or BSA + C contained higher concentrations of talin, a protein associated with integrin adhesion receptors (about twice compared to pristine PE and about 1.5 times compared to PE modified only by plasma irradiation, Table 2). The concentration of vinculin, another protein of focal adhesion plaques associated with cell adhesion receptors, in cells on PE with BSA + C was almost 1.9 and 1.7 times higher than in cells on pristine PE and PS dishes, respectively (Table 2). The concentration of focal adhesion protein paxillin was similar in cells on all studied samples. However, the concentration of β-actin, a protein of the cytoplasmic cytoskeleton associated with focal adhesions and thus an important marker of cell adhesion and spreading, was increased by 1.7 to 2 times in cells grown on PE modified with PEG, BSA, C and BSA + C compared to cells on PS dishes (Table 2).

Figure 8. Immunofluorescence staining of talin, an integrin-associated protein of focal adhesion plaques, in rat aortic smooth muscle cells on day 5 after seeding on pristine PE (A), a reference material represented by a microscopic glass coverslip (B), PE irradiated with plasma (C), PE irradiated with plasma and grafted with glycine (D), polyethyleneglycol (E) bovine serum albumin (F), colloidal carbon particles (G) or bovine serum albumin and C (H).

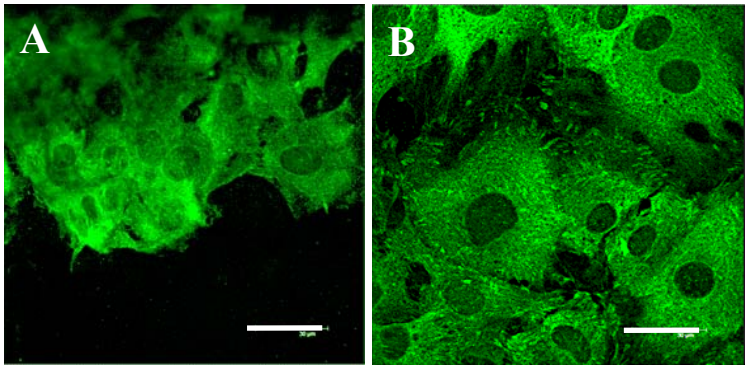

Figure 8. *Cont.*

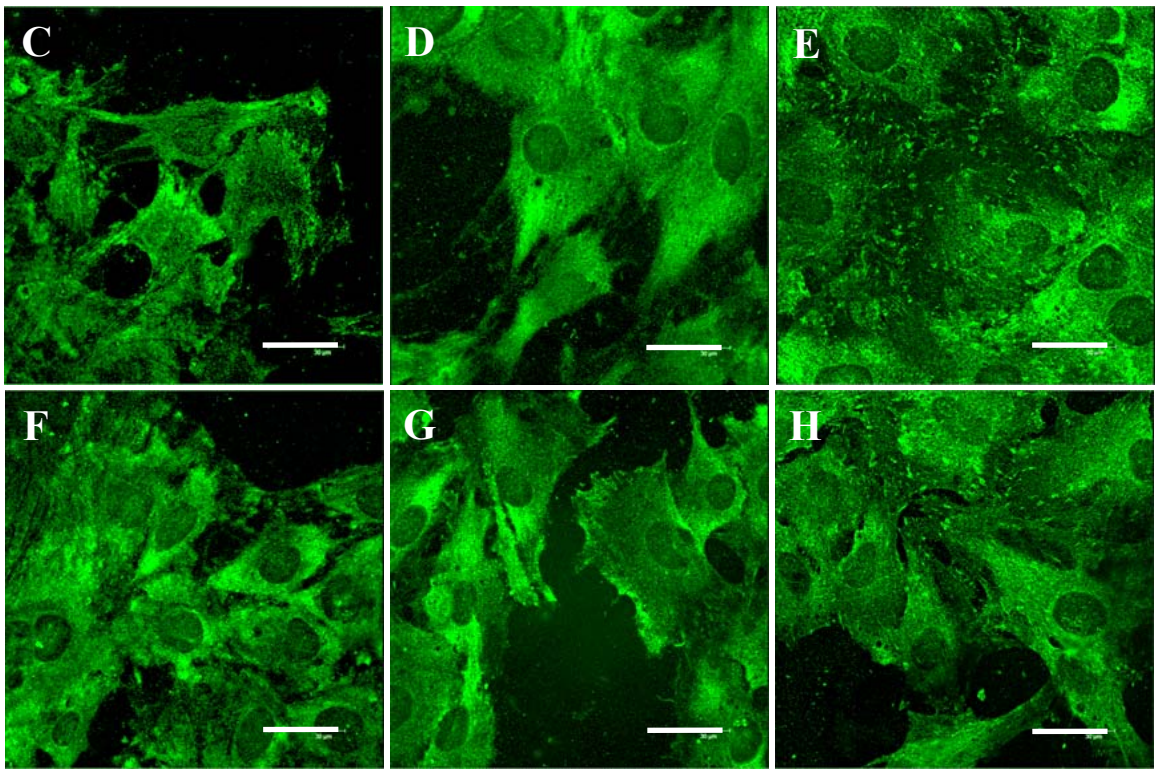

Leica confocal laser scanning microscope (TCS SP2, Germany), obj. 100x, bar = 30 μm.

Immunofluorescence also revealed that fibres containing cytoskeletal protein β-actin, and particularly α-actin or SM1 and SM2 myosins, *i.e.*, markers of phenotypic maturation of VSMCs toward a more differentiated contractile phenotype [22,34], were thicker, more numerous and more brightly stained in cells on all modified PE samples than on pristine PE (Figure 9). The concentration of α-actin, measured by ELISA per mg of protein, was significantly increased in cells on the polymer grafted with PEG (by about 1.4 times compared to polystyrene and plasma-modified PE) or with Gly (1.3 times compared to PS, Table 2). The highest average concentration of SM1 and SM2 myosins was found in cells growing on PE with PEG (128% of the value found on pristine PE), but this difference did not reach statistical significance (Table 2). The concentration of α-actinin, a protein associated with α-actin filaments, was the highest in cells cultured on plasma-modified PE. In these samples, it was even significantly higher than in cells on other modified samples, namely with Gly (1.6 times), PEG (1.5 times) and BSA (2.5 times, Table 2).

It should be pointed out that the conventional ELISA applied in this study measured the total numbers of the investigated molecules in the cells, *i.e.*, not only those bound in focal adhesion plaques or cytoskeletal and contractile fibres, but also those present in cytoplasm and organelles, such as the Golgi complex. Selective (and thus more precise) quantification of the investigated molecules in the specific adhesive, cytoskeletal and contractile structures could be achieved by more specialized approaches, *e.g.*, by using antibodies against phosphorylated antigens or by extraction of molecules non-bound in the membrane or cytoplasmatic cytoskeleton by detergents, such as Triton [35,36]. Nevertheless, the results of this study show that activation of PE with plasma and subsequent grafting

with bioactive molecules and atoms stimulates the molecular mechanism, leading to enhanced adhesion and maturation of vascular smooth muscle cells in cultures on these materials.

Table 2. Concentration of focal adhesion, cytoskeletal and contractile proteins in rat aortic smooth muscle cells in 7-day-old cultures on pristine PE (Pristine), PE activated with plasma (Plasma), PE grafted with glycine (Gly), polyethylene glycol (PEG), bovine serum albumin (BSA), colloidal carbon particles (C) or BSA with C (BSA + C), and tissue culture polystyrene dish (PS dish).

Protein/PE modification	Talin	Vinculin	Paxillin	α-Actinin	β-Actin	α-Actin	SM1 SM2 myosins
Pristine	100 ± 9	100 ± 14	100 ± 28	100 ± 15	100 ± 8	100 ± 4	100 ± 16
Plasma	134 ± 12	154 ± 17	98 ± 2	129 ± 28	77 ± 10	91 ± 10	69 ± 18
Gly	109 ± 12	140 ± 18	136 ± 23	50 ± 8$^{\$}$	68 ± 3	119 ± 6$^{C, *}$	78 ± 15
PEG	202 ± 16$^{\#, \$}$	123 ± 8	152 ± 30	52 ± 10$^{\$}$	107 ± 8*	123 ± 6$^{\$, C, *}$	128 ± 14
BSA	127 ± 10	151 ± 13	143 ± 27	37 ± 9$^{\$}$	95 ± 7*	115 ± 7	73 ± 17
C	112 ± 4	133 ± 9	104 ± 15	89 ± 8	111 ± 17*	87 ± 3	87 ± 16
BSA + C	201 ± 14$^{\#, *}$	185 ± 14$^{\#, *}$	114 ± 18	72 ± 12	110 ± 12*	111 ± 7	108 ± 13
PS dish	155 ± 29	113 ± 12	175 ± 37	93 ± 7	55 ± 9	89 ± 10	103 ± 16

Measured by ELISA per mg of protein. Means ± S.E.M. from three to seven experiments, each performed in duplicate or in triplicate. Absorbance values were normalized to the values obtained in cell samples from pristine PE, *i.e.*, given as a percentage of the values on pristine PE. ANOVA, Student-Newman-Keuls method. Statistical significance: $^{\#, \$, C, *}$: $p \leq 0.05$ compared to the value on pristine PE, PE irradiated with plasma, PE irradiated with plasma and exposed to colloidal C particles, and polystyrene culture dish, respectively.

Figure 9. Immunofluorescence staining of contractile protein alpha-actin in rat aortic smooth muscle cells on day 5 after seeding on pristine PE (A), reference materials represented by a microscopic glass coverslip (B), a standard cell culture polystyrene dish (C), PE irradiated with plasma (D), PE irradiated with plasma and grafted with glycine (E), polyethyleneglycol (F), bovine serum albumin (G), colloidal carbon particles (H) or bovine serum albumin and C (I).

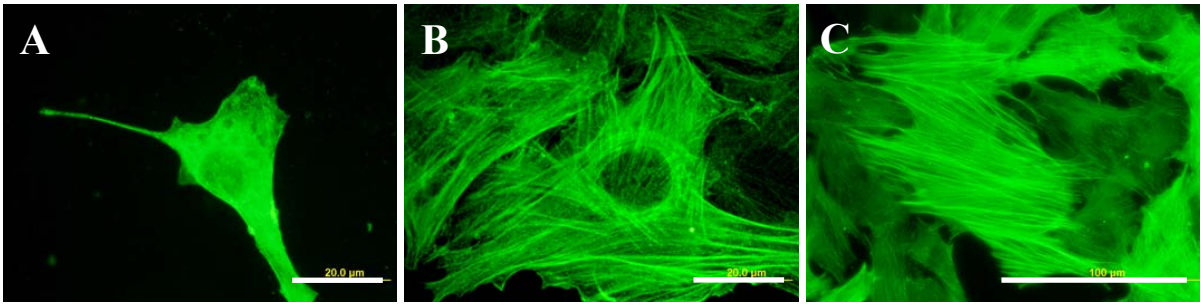

Figure 9. *Cont.*

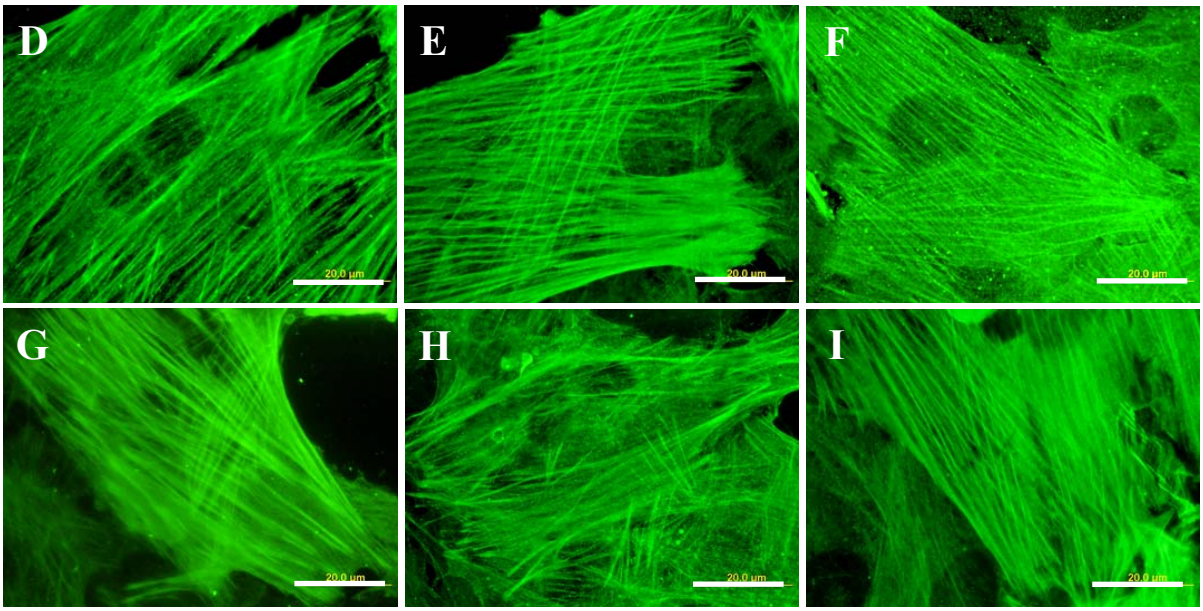

Olympus IX 51 microscope, DP 70 digital camera, obj. 100× (A, B, D-I) or 40× (C). Bar = 20 μm (A, B, D-I) or 100 μm (C).

3. Experimental Section

3.1. Preparation of the Polymer Samples

The experiments were carried out on high-density polyethylene foils (HDPE, PE) of the Microten M*S type (thickness 0.04 mm, density 0.951 g.cm^{-3}, melt flow index 0.14 g/10 minutes), purchased from Granitol a.s., Moravsky Beroun, Czech Republic. The foils were cut into circular samples (2 cm in diameter) using a metallic perforator. The samples were then modified by an Ar^+ plasma discharge (gas purity 99.997%) using a Balzers SCD 050 device. The time of exposure was 50 seconds, and the discharge power was 1.7 W. Immediately after plasma modification, the samples were immersed in water solutions of glycine (Gly; Merck, Darmstadt, Germany, product No. 104201), bovine serum albumin (BSA; Sigma-Aldrich, Germany, product No. A9418) or polyethyleneglycol (PEG; Merck, Darmstadt, Germany, product No. 817018, m.w. 20,000). Some plasma-treated samples and samples grafted with BSA were exposed to a suspension of colloidal carbon particles (C; Spezial Schwartz 4, Degussa AG, Germany) [37]. Each substance was used in a concentration of 2 wt.%, and the time of immersion was 12 hours at room temperature (RT).

3.2. Evaluation of the Physical and Chemical Properties of the Polymer Samples

Surface wettability was measured by goniometry, *i.e.*, the static (sessile) water drop contact angle method. It was shown that the contact angle of PE (exposed to plasma discharge) depends on the time elapsed from the moment of exposure [21]. Therefore, in this study, the contact angle on the plasma-modified and grafted samples was measured 20 days after the modification. The measurements of the

advancing water contact angles (error ± 5%) were performed in 10 different positions at room temperature on the Surface Energy Evaluation System (Advex Instruments, Czech Republic) [21,31].

The concentration and depth concentration profile of oxygen in the modified PE surface layer was proven by Rutherford Backscattering Spectroscopy (RBS). The RBS analysis was performed in a vacuum target chamber with 2.72 MeV He^+ ions. The elemental depth profiles in the inspected polymeric samples were determined with typical depth resolution less than 10 nm, and with an accessible depth of a few μm. The RBS spectra were evaluated by the GISA3.99 code [12]. The typical RBS detection limit is 0.1 at.% for oxygen.

The surface morphology and roughness of the pristine and modified samples were examined by the AFM technique, using a VEECO CP II device working in tapping mode. We used an RTESPA-CP Si probe, with spring constant 20-80 N/m. By repeated measurements of the same region (1 × 1 μm), it was proven that the surface morphology did not change after three consecutive scans. The mean roughness value (R_a) represents the arithmetic average of the deviations from the centre plane of the sample.

3.3. Cell Source and Culture Conditions

For an evaluation of cell number, morphology and immunofluorescence staining, each modified round sample (2 cm in diameter) was cut into four smaller samples. For semiquantification of cell adhesion and differentiation-indicating molecules by an enzyme-linked immunofluorescence assay (ELISA), the samples were used in whole. Both smaller and bigger samples were sterilized with 70% ethanol for one hour and inserted into 24-well and 6-well plates (TPP, Switzerland; well diameter 1.5 cm and 3.5 cm, respectively), and air-dried for 12 hours in a sterile environment to prevent possible negative effects of alcohol on the cells. After drying, the samples were fixed to the bottom of the culture wells by plastic rings (inner area 0.38 cm^2 and 4.91 cm^2 for smaller and bigger samples, respectively) in order to prevent the samples floating in the cell culture media. After that, the samples were seeded with smooth muscle cells derived from rat aorta by an explantation method (passage 3, 17,000 cm^2; [2,3]). The cells were cultivated in 1.5 mL Dulbecco's Modified Eagle Minimum Essential Medium (Sigma, U.S.A.) supplemented with 10% foetal bovine serum (Sebak GmbH, Aidenbach, Germany) for 1, 2, 5 or 7 days (temperature of 37 °C, humidified atmosphere of 5% of CO_2 in the air). For each experimental group and time interval, four smaller samples were used. ELISA was performed on day 7 only, and 6 samples were used for each experimental group.

3.4. Evaluation of the Cell Number and Morphology

On days 1, 2, 5 and 7 after seeding, the cells on the smaller polymer samples were rinsed in phosphate-buffered saline (PBS). The cells on one sample for each experimental group and time interval were fixed by 70% cold ethanol (−20 °C) and stained with a combination of fluorescent membrane dye Texas Red C_2-maleimide (Molecular Probes, Invitrogen, Cat. No.T6008; concentration 20 ng/mL in PBS) and a nuclear dye Hoechst # 33342 (Sigma, U.S.A.; 5 μg/mL in PBS). The number, morphology and distribution of cells on the sample surface were then evaluated on pictures taken under an Olympus IX 51 microscope using an Olympus DP 70 digital camera. The pictures taken on

days 1 and 2 after seeding were also used for measuring the size of the cell spreading area, using Atlas software (Tescan Ltd., Czech Republic).

The three remaining samples were the main material for evaluation of the cell number. The cells were rinsed by PBS, released with trypsin-EDTA solution (Sigma, Cat. No. T4174; incubation five minutes at 37 °C) and counted in a Cell Viability Analyzer (VI-cell XR, Beckman Coulter). During cell counting, this instrument performs an automatic analysis of the number of viable and dead cells, based on a trypan blue exclusion test.

3.5. Immunofluorescence Staining

On day 7 after seeding, the cells were rinsed twice in PSB, fixed with cold 70% ethanol (−20 °C, 15 min) and pre-treated with 1% bovine serum albumin in PBS containing 0.05% Triton X-100 (Sigma) for 20 minutes at room temperature in order to block non-specific binding sites and permeabilize the cell membrane. Next, the cells were incubated with primary antibodies against several molecular markers of adhesion and phenotypic maturation of VSMC, namely integrin-associated focal adhesion proteins talin, vinculin and paxillin, actin-binding protein alpha-actinin, cytoskeletal protein beta-actin and contractile proteins alpha-actin and SM1 and SM2 myosins (Table 3).

Table 3. Primary antibodies used for immunofluorescence staining (Immf.) and Enzyme-Linked Immunosorbent Assay (ELISA) of markers of adhesion and phenotypic maturation of VSMCs.

Antibody against	Developed in, type	Company, Cat. No.	Dilution	Incubation
Chicken talin	Mouse, monoclonal	Sigma [a] T 3287	Immf.: 1:200 ELISA: 1:500	Immf.: Overnight, 4 °C ELISA: 60 min, RT [c]
Human vinculin	Mouse, monoclonal	Sigma [a] V9131	Immf.: 1:200 ELISA: 1:400	Immf.: Overnight, 4 °C ELISA: 60 min, RT [c]
Recombinant human paxilin	Rabbit polyclonal	Chemicon [b] P1093	Immf.: 1:200 ELISA: 1:400	Immf.: Overnight, 4 °C ELISA: 60 min, RT [c]
Chicken α-actinin	Rabbit, polyclonal	Sigma [a] A2543	Immf.: 1:200 ELISA: 1:500	Immf.: Overnight, 4 °C ELISA: 60 min, RT [c]
Synthetic peptide of α-smooth muscle actin	Mouse, monoclonal	Sigma [a] A2547	Immf.: 1:200 ELISA: 1:400	Immf.: Overnight, 4 °C ELISA: 60 min, RT [c]
Synthetic peptide of β-actin	Mouse, monoclonal	Sigma [a] A 5441	Immf.: 1:200 ELISA: 1:400	Immf.: Overnight, 4 °C ELISA: 60 min, RT [c]
Human smooth muscle myosin SM1 and SM2	Mouse, monoclonal	Sigma [a] M7786	Immf.: 1:200 ELISA: 1:500	Immf.: Overnight, 4 °C ELISA: 60 min, RT [c]

[a] Sigma, St. Louis, MO, USA.; Czech Dealer: Sigma-Aldrich S.R.O., Prague, Czech Republic.

[b] Chemicon International Inc., Temecula, CA, USA.; Czech dealer: Scintilla S.R.O., Jihlava, Czech Republic.

[c] Room temperature (RT).

The antibodies were diluted in PBS to concentrations of 1:200 and applied overnight at 4 °C. After rinsing with PBS, the secondary antibodies (dilution 1:400) were added for 1 hour at room temperature. These antibodies were goat anti-mouse or goat anti-rabbit F(ab')2 fragments of IgG (H + L), both conjugated with Alexa Fluor® 488 and purchased from Molecular Probes, Invitrogen (Cat. No. A11017 and A11070, respectively). The cells were then rinsed twice in PBS, mounted under microscopic glass coverslips in a Gel/Mount permanent fluorescence-preserving aqueous mounting medium (Biomeda Corporation, Foster City, CA, U.S.A.), and evaluated under a Leica confocal microscope (TCS SP2, Germany; obj. HCX PL APO CS 100.0x1.40 OIL) and an Olympus IX 51 microscope (obj. 100x), using an Olympus DP 70 digital camera [2].

3.6. Enzyme-Linked Immunosorbent Assay (ELISA)

The concentration of the adhesion and differentiation molecules was measured semiquantitatively using an enzyme-linked immunosorbent assay (ELISA) in homogenized cells per mg of protein. On day 7 after seeding, the cells were rinsed with PBS, released with a trypsin-EDTA solution (Sigma, Cat. No. T4174, incubation for 5 minutes at 37 °C) and counted in a Cell Viability Analyzer (Vi-Cell XR, Beckman Coulter). Trypsinized cells were resuspended in PBS, centrifuged, resuspended in distilled and deionized water (10^6 cells in 200 μL), and kept in a freezer at −70 °C overnight. The cells were then homogenized by ultrasonication for 10 seconds in a Bandelin Sonoplus HD 3080 sonicator (BANDELIN electronic GmbH & Co.), and the total protein content was measured using a modified method originally developed by Lowry [38]; modified by [2,39]. Aliquots of the cell homogenates corresponding to 1-50 μg of protein in 50 μL of water were adsorbed on 96-well microtiter plates (Maxisorp, Nunc) at 4 °C overnight. After washing twice with PBS (100 μL/well), the non-specific binding sites were blocked by 0.02% gelatin in PBS (100 μL/well, 60 minutes) and then treated by 1% Tween (Sigma, Cat. No. P1379; 100 μL/well, 20 minutes). The primary antibodies, the same as for immunofluorescence (Table 3), were diluted in PBS (1:200 to 1:500) and applied for 60 minutes at room temperature (50 μL/well). Secondary antibodies, *i.e.,* goat anti-mouse IgG Fab specific (dilution 1:1000), or goat anti-rabbit IgG whole molecule (dilution 1:1000), both conjugated with peroxidase and purchased from Sigma (Cat. No. A3682 and A0545, respectively), were applied for 45 minutes at room temperature (50 μL/well). This step was followed by a double washing in PBS and orthophenylendiamine reaction (Sigma, Cat. No. P1526, concentration 2.76 mM) using 0.05% H_2O_2 in 0.1 M phosphate buffer (pH 6.0, dark place, 100 μL/well). The reaction was stopped after 10–30 minutes by 2M H_2SO_4 (50 μL/well), and the absorbance was measured at 490 and 690 nm by a Versa Max Microplate Reader (Molecular Devices Corporation, Sunnyvale, California, USA). The absorbance of the cell samples taken from the modified PE foils was given as a percentage of the value obtained in cells on the pure PE [2,39].

3.7. Statistics

The quantitative results were presented as mean ±S.E.M. (Standard Error of Mean). Statistical analyses were performed using SigmaStat (Jandel Corp., USA). Multiple comparison procedures were

made by the One Way Analysis of Variance (ANOVA), Student-Newman-Keuls method. *P* values equal to or less than 0.05 were considered significant.

4. Conclusions

Modifications of PE samples with a plasma discharge and subsequent grafting with biomolecules enhanced the colonization of PE with numerous and well-spread vascular smooth muscle cells with numerous talin- and vinculin-containing focal adhesion plaques. As suggested by the more numerous and thicker filaments containing a contractile protein alpha-actin, and also by the higher concentration of this protein per mg of protein, the cells on the modified polymers, particularly those grafted with PEG or Gly, also showed a higher level of phenotypic maturation. The beneficial effect of the plasma discharge could be attributed to the formation of oxygen-containing structures in the polyethylene surface layer, increased material wettability and changes in the surface morphology. Oxygen was present not only on the very surface of the sample, but also in the underlying surface layer about 50 nm in thickness. However, water-treating of plasma-irradiated PE led to a decrease in oxygen concentration in the surface layer, due to dissolution of plasma-degraded macromolecules in water. On the other hand, ablation of the surface layer by plasma-irradiation resulted in changes in the polymer surface morphology, and in an increase in the surface nanoscale roughness, which is considered to promote cell adhesion and growth. As indicated by grafting the polymer with glycine and PEG, the increase in surface roughness did not depend on the molecular weight of the grafted molecules. Grafting biomolecules (Gly, PEG, BSA) and colloidal C particles further increased the attractiveness of PE for VSMC colonization. As demonstrated on PE grafted with Gly and PEG, these biomolecules further increased the oxygen concentration in the material surface and the surface wettability. The supportive effect of biomolecules on cell colonization was most apparent on the polymer modified by PEG and BSA + C.

Acknowledgements

This study was supported by the Acad. Sci. of the Czech Republic (Grants No. 1QS500110564, KAN 400480701 and KAN 200100801), and by the Ministry of Education of the Czech Republic under Research Programs 6046137302 and LC06041. We also thank Ivana Zajanova (Inst. Physiol., Acad. Sci. CR) for her excellent technical assistance in immunofluorescence staining. Robin Healey (Czech Technical University, Prague), and Sherryl Ann Vacik (Pangrac & Associates, Port Aransas, Texas, USA), are gratefully acknowledged for his language revision of the manuscript.

References and Notes

1. Bacakova, L.; Svorcik, V.; Rybka, V.; Micek, I.; Hnatowicz, V.; Lisa, V.; Kocourek, F. Adhesion and proliferation of cultured human vascular smooth muscle cells on polystyrene implanted with N^+, F^+ and Ar^+ ions. *Biomaterials* **1996**, *17*, 1121–1126.

2. Bacakova, L.; Mares, V.; Bottone, M.G.; Pellicciari, C.; Lisa, V.; Svorcik, V. Fluorine-ion-implanted polystyrene improves growth and viability of vascular smooth muscle cells in culture. *J. Biomed. Mater. Res.* **2000**, *49*, 369–379.
3. Bacakova, L.; Walachova, K.; Svorcik, V.; Hnatowicz, V. Adhesion and proliferation of rat vascular smooth muscle cells on polyethylene implanted with O^+ and C^+ ions. *J. Biomater. Sci.—Polym. Ed*. **2001**, *12*, 817–834.
4. Bacakova, L.; Filova, E.; Rypacek, F.; Svorcik, V.; Stary, V. Cell adhesion on artificial materials for tissue engineering. *Physiol. Res.* **2004**, *53*, S35–S45.
5. Bacakova, L.; Svorcik, V. Cell colonization control by physical and chemical modification of materials. In *Cell Growth Processes: New Research*; Kimura, D., Ed.; Nova Science Publishers, Inc.: Hauppauge, NY, USA, 2008; pp. 5–56.
6. Heitz, J.; Svorcik, V.; Bacakova, L.; Rockova, K.; Ratajova, E.; Gumpenberger, T.; Bauerle, D.; Dvorankova, B.; Kahr, H.; Graz, I.; Romanin C. Cell adhesion on polytetrafluoroethylene modified by UV-irradiation in an ammonia atmosphere. *J. Biomed. Mater. Res. A* **2003**, *67*, 130–137.
7. Svorcik, V.; Rockova, K.; Ratajova, E.; Heitz, J.; Huber, N.; Bäuerle, D.; Bacakova, L.; Dvorankova, B.; Hnatowicz, V. Cell proliferation on UV-excimer lamp modified and grafted polytetrafluoroethylene. *Nucl. Instr. Meth. B* **2004**, *217*, 307–313.
8. Walachova, K.; Svorcik, V.; Bacakova, L.; Hnatowicz, V. Smooth muscle cell interaction with modified polyethylene. *Biomaterials* **2002**, *23*, 2989–2996.
9. Turos, A.; Jagielski, J.; Piatkowska, A.; Bielinski, D.; Slusarski, L.; Madi, N.K. Ion beam modification of surface properties of polyethylene. *Vacuum* **2003**, *70*, 201–206.
10. Wang, Y.; Lu, L.; Zhang, Y.; Chen, X. Improvement in hydrophilicity of PHBV films by plasma treatment. *J. Biomed. Mater. Res. A* **2006**, *76*, 589–595.
11. Kasalkova, N.; Kolarova, K.; Bacakova, L.; Parizek, M.; Svorcik, V. Cell adhesion and proliferation on modified PE. *Mater. Sci. Forum* **2007**, *567–568*, 269–272.
12. Svorcik, V.; Kasalkova, N.; Slepicka, P.; Zaruba, K.; Bacakova, L.; Parizek, M.; Lisa, V.; Ruml, T.; Gbelcova, H.; Rimpelova, S.; Mackova, A. Cytocompatibility of Ar^+ plasma-treated and Au nanoparticle-grafted PE. *Nucl. Instr. Meth. B* **2009**, *267*, 1904–1910.
13. Mikulikova, R.; Moritz, S.; Gumpenberger, T.; Olbrich, M.; Romanin, C.; Bacakova, L.; Svorcik, V.; Heitz, J. Cell microarrays on photochemically modified polytetrafluoroethylene. *Biomaterials* **2005**, *26/27*, 5572–5580.
14. Rockova K.; Svorcik V.; Bacakova L.; Dvorankova B.; Heitz J. Biocompatibility of ion beam-modified and RGD-grafted polyethylene. *Nucl. Instrum.Meth. B* **2004**, *225*, 275–279.
15. Kotal, V.; Svorcik, V.; Slepička, P.; Blahova, O.; Sutta, P.; Hnatowicz, V. Gold coating of PET modified by argon plasma. *Plasma Proc. Polym*. **2007**, *4*, 69–75.
16. Svorcik, V.; Kotal, V.; Siegel, J.; Sajdl, P.; Mackova, A.; Hnatowicz, V. Ablation and water etching of poly(ethylene) modified by Ar plasma. *Polym. Degr. Stab*. **2007**, *92*, 1645–1651.
17. Chu, P.K.; Chen, J.Y.; Wang, L.P.; Huang N. Plasma-surface modification of biomaterials. *Mater. Sci. Eng*. **2002**, *R36*, 143–206.
18. Siegel, J.; Reznickova, A.; Chaloupka, A.; Slepicka, P.; Svorcik, V. Ablation and water etching of plasma treated polymers. *Rad. Eff. Def. Sol*. **2008**, *163*, 779–785.

19. Švorčík, V.; Rybka, V.; Stibor, I.; Hnatowicz, V.; Vacik, J.; Stopka, P. Synthesis of grafted polyethylene by ion beam modification. *Polym. Deg. Stab.* **1997**, *58*, 143–147.
20. Švorčík, V.; Hnatowicz, V.; Stopka, P.; Bačáková, L.; Heitz, J.; Ochsner, R.; Ryssel, H. Aminoacids grafting of Ar ions modified PE. *Rad. Phys. Chem*. **2001**, *60*, 89–94.
21. Svorcik, V.; Kolarova, K.; Slepicka, P.; Mackova, A.; Novotna, M.; Hnatowicz, V. Modification of surface properties of high and low density PE by Ar plasma discharge. *Polym. Degr. Stab*. **2006**, *91*, 1219–1225.
22. Orlandi, A.; Ropraz, P.; Gabbiani, G. Proliferative activity and alpha-smooth muscle actin expression in cultured rat aortic smooth muscle cells are differently modulated by transforming growth factor-beta 1 and heparin. *Exp. Cell. Res*. **1994**, *214*, 528–536.
23. Webster, T.J.; Ergun, C.; Doremus, R.H.; Siegel, R.W.; Bizios, R. Specific proteins mediate enhanced osteoblast adhesion on nanophase ceramics. *J. Biomed. Mater. Res*. **2000**, *51*, 475–483.
24. Corning Cell Culture Surfaces: CorningR CellBINDR Polystyrene Surface Homepage. http://www.corning.com/lifesciences/us_canada/en/technical_resources/surfaces/culture/corning_cellbind_polystyrene.aspx (accessed July 6, 2009).
25. Bacakova, L.; Filova, E.; Kubies, D.; Machova, L.; Proks, V.; Malinova, V.; Lisa, V.; Rypacek, F. Adhesion and growth of vascular smooth muscle cells in cultures on bioactive RGD peptide-carrying polylactides. *J. Mater. Sci. Mater. Med*. **2007**, *18*, 1317–1323.
26. Filova, E.; Bacakova, L.; Lisa, V.; Kubies, D.; Machova, L.; Lapcikova, M.; Rypacek, F. Adhesion and proliferation of vascular smooth muscle cells on polylactide-polyethylene oxide copolymers with different content and length of polyethylene oxide chains. *Eng. Biomater*. **2004**, *7*, 19–21.
27. Horbett, T.A. Principles underlying the role of adsorbed plasma proteins in blood interactions with foreign materials. *Cardiovasc. Pathol*. **1993**, *2*, 137S–148S.
28. Koenig, A.L.; Gambillara, V.; Grainger, D.W. Correlating fibronectin adsorption with endothelial cell adhesion and signaling on polymer substrates. *J. Biomed. Mater. Res. A* **2003**, *64*, 20–37.
29. Koblinski, J.E.; Wu, M.; Demeler, B.; Jacob, K.; Kleinman, H.K. Matrix cell adhesion activation by non-adhesion proteins. *J. Cell Sci.* **2005**, *118*, 2965–2974.
30. Pignataro, B.; Conte, E.; Scandurra, A.; Marletta, G. Improved cell adhesion to ion beam-irradiated polymer surfaces. *Biomaterials* **1997**, *18*, 1461–1470.
31. Kubova, O.; Svorcik, V.; Heitz, J.; Moritz, S.; Romanin, C.; Matejka, P.; Mackova, A. Characterization and cytocompatibility of carbon layers prepared by photo-induced chemical vapor deposition. *Thin Solid Films* **2007**, *515*, 6765–6772.
32. Bacakova, L.; Grausova, L.; Vacik, J.; Fraczek, A.; Blazewicz, S.; Kromka, A.; Vanecek, M.; Svorcik, V. Improved adhesion and growth of human osteoblast-like MG 63 cells on biomaterials modified with carbon nanoparticles. *Diamond Relat. Mater*. **2007**, *16*, 2133–2140.
33. Lesny, P.; Pradny, M.; Jendelova, P.; Michalek, J.; Vacik, J.; Sykova, E. Macroporous hydrogels based on 2-hydroxyethyl methacrylate. Part 4: Growth of rat bone marrow stromal cells in three-dimensional hydrogels with positive and negative surface charges and in polyelectrolyte complexes. *J. Mater. Sci. Mater. Med*. **2006**, *17*, 829–833.

34. Han, M.; Wen, J.K.; Zheng, B.; Cheng, Y.; Zhang, C. Serum deprivation results in redifferentiation of human umbilical vascular smooth muscle cells. *Am. J. Physiol. Cell. Physiol.* **2006**, *J291*, C50–C58.
35. Ezzell, R.M.; Goldmann, W.H.; Wang, N.; Parashurama, N.; Ingber, D.E. Vinculin promotes cell spreading by mechanically coupling integrins to the cytoskeleton. *Exp. Cell Res*. **1997**, *231*, 14–26.
36. Sawada, Y.; Sheetz, M.P. Force transduction by Triton cytoskeletons. *J. Cell Biol*. **2002**, *156*, 609–615.
37. Van Amerongen, A.; Wichers, J.H.; Berendsen, L.B.J.M.; Timmermans, A.J.M.; Keizer, G.D.; Van Doorn, A.W.J.; Bantjes, A.; van Gelder, W.M.J. Colloidal carbon particles as a new label for rapid immunochemical test methods—Quantitative computer image-analysis of results. *J. Biotechnol*. **1993**, *30*, 185–195.
38. Lowry, O.H.; Rosebrough, N.J.; Farr, A.L.; Randall R.J. Protein measurement with the Folin phenol reagent. *J. Biol. Chem*. **1951**, *193*, 265–275.
39. Filova, E.; Brynda, E.; Riedel, T.; Bacakova, L.; Chlupac, J.; Lisa, V.; Houska, M.; Dyr, J.E. Vascular endothelial cells on two- and three-dimensional fibrin assemblies for biomaterial coatings. *J. Biomed. Mater. Res*. *A* **2009**, *90*, 55–69.

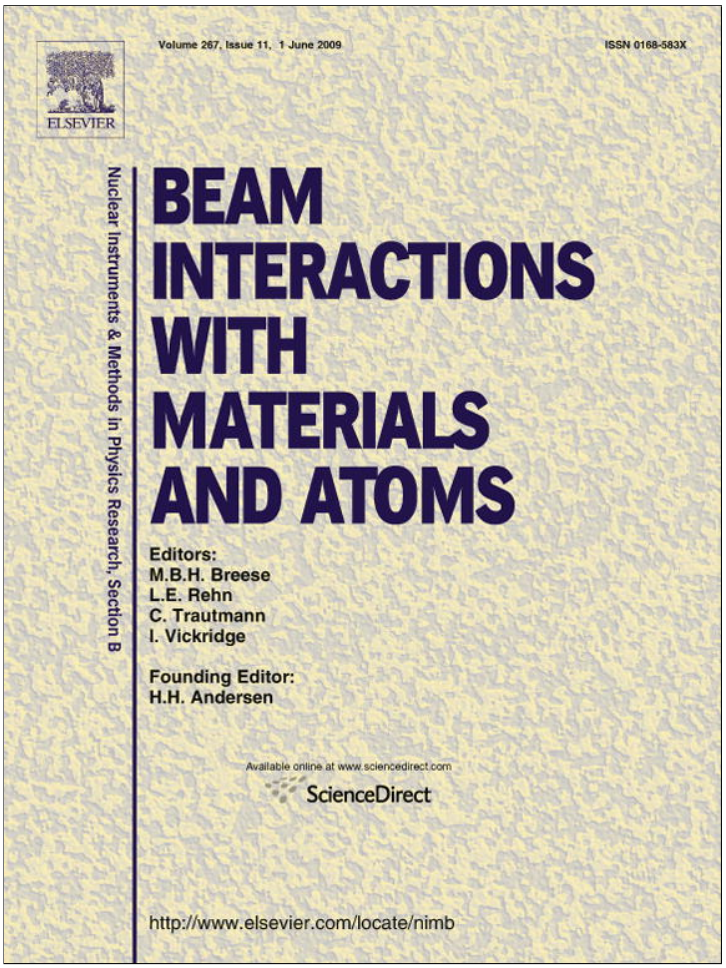

Nuclear Instruments and Methods in Physics Research B 267 (2009) 1904–1910

Contents lists available at ScienceDirect

Nuclear Instruments and Methods in Physics Research B

journal homepage: www.elsevier.com/locate/nimb

Cytocompatibility of Ar^+ plasma treated and Au nanoparticle-grafted PE

V. Švorčík [a,*], N. Kasálková [a], P. Slepička [a], K. Záruba [b], V. Král [b], L. Bačáková [c], M. Pařízek [c], V. Lisá [c], T. Ruml [d], H. Gbelcová [d], S. Rimpelová [d], A. Macková [e,f]

[a] Department of Solid State Engineering, Institute of Chemical Technology, 166 28 Prague, Czech Republic
[b] Department of Analytical Chemistry, Institute of Chemical Technology, 166 28 Prague, Czech Republic
[c] Institute of Physiology, Academy of Sciences of the Czech Republic 142 20 Prague, Czech Republic
[d] Department of Biochemistry and Microbiology, Institute of Chemical Technology, 166 28 Prague, Czech Republic
[e] Nuclear Physics Institute, Academy of Sciences of the Czech Republic, 250 68 Rez, Czech Republic
[f] Department of Physics, J.E. Purkinje University, 400 96 Ústí nad Labem, Czech Republic

ARTICLE INFO

Article history:
Received 29 January 2009
Received in revised form 20 February 2009
Available online 31 March 2009

PACS:
52.40.Hf
62.20.–x
81.65.–b

Keywords:
Polyethylene
Ar plasma discharge
Au nanoparticles grafting
Cell proliferation

ABSTRACT

Polyethylene (PE) was irradiated with inert Ar plasma, and the chemically active PE surface was grafted with Au nanoparticles. The composition and the structure of the modified PE surface were studied using X-ray photoelectron spectroscopy (XPS) and Rutherford backscattering spectroscopy (RBS). Changes in the surface wettability were determined from the contact angle measured in a reflection goniometer. The changes in the surface roughness and morphology were followed by atomic force microscopy (AFM). The modified PE samples were seeded with rat vascular smooth muscle cells (VSMC) or mouse NIH 3T3 fibroblasts, and their adhesion and proliferation were studied. We found that plasma discharge and Au grafting lead to dramatic changes in the surface morphology and roughness of PE. The Au nanoparticles were found not only on the sample surface, but also in the sample interior up to the depth of about 100 nm. In addition, plasma modification of the PE surface, followed with grafting Au-nanoparticles, significantly increased the attractiveness of the PE surface for the adhesion and growth of VSMC, and particularly for mouse embryonic 3T3 fibroblasts.

1. Introduction

Polymers have been often applied in different fields for their excellent bulk properties (e.g. low density, flexibility, mechanical and electrical strength, and chemical resistance). In some instances, however, the inert nature of most polymer surfaces creates challenges for the adjustment of their properties for a desired application. Hence, an additional modification of polymer surface is required to achieve desired surface properties (e.g. better cell adhesion, increased bioactivity), while maintaining the polymer bulk characteristics [1–3].

A common approach to tailoring surface properties of polymer materials is exposition to a plasma discharge, by which the polymer surface chemistry and morphology can be changed. Plasma treatment has become an important industrial process for the modification of polymer surfaces [3,4]. Plasma constituents, electrons, ions and radicals interact with the polymer surface and modify its chemical and physical properties. The plasma treatment of polymers leads to the creation of new chemical groups [4], branching and crosslinking of the macromolecules, and formation of low molecular weight oxidized (LMWO) structures [5–7]. The oxygen-containing groups, created by plasma treatment, render the material surface more wettable, which supports the adsorption of physiological extracellular matrix (ECM) molecules in a flexible and reorganisable form. This form enhances the accessibility of oligopeptidic ligands in these molecules for cell adhesion receptors [8–11]. Another interesting property of the modified polymers is the formation of conjugated double bonds between the carbon atoms; from this follows increasing of electrical conductivity of the material. It has been shown that this has positive effects on the adhesion, growth and maturation of various cell types, including vascular smooth muscle and endothelial cells [9,12]. Also, under some specific conditions plasma etching takes place, leading to surface ablation [1,2] and to alteration of the polymer surface morphology [13,14]. The changes in morphology and wettability of the polymer surface [13] may strongly influence the cell-substrate interaction [15]. Unsaturated chemical bonds and radicals created by plasma treatment [13,16,17] can be utilized for the grafting of new chemical functional groups, atoms and molecules [18,19] and in this way, to create nanostructured surfaces with new functionalities.

* Corresponding author. Tel.: +420 22044 5149; fax: +420 22431 0337.
E-mail address: vaclav.svorcik@vscht.cz (V. Švorčík).

0168-583X/$ - see front matter © 2009 Elsevier B.V. All rights reserved.
doi:10.1016/j.nimb.2009.03.099

The nanostructure of the material surface (irregularities smaller than 100 nm) is considered to mimic the topography of the cell membrane, as well as the architecture of ECM molecules [20]. It is known that cell adhesion to artificial materials is mediated by ECM molecules spontaneously adsorbed to the material surface from biological fluids.

Various materials have been used for constructing nanostructured surfaces (e.g. polymers [21], ceramics, metals [20,22] and combinations of these materials). However, among metallic materials, gold, including its nano-sized forms, has shown no cytotoxicity *in vitro* and *in vivo* [23]. The non-toxicity of gold is related to its well-known stability, non-reactivity and bioinertness. For example, gold nanoparticles have often been conjugated with antibodies [24].

In this work, the hypothesis is that gold nanoparticles may also serve as building blocks for creating artificial bioinspired nanostructured surfaces for tissue engineering. Thus, our newly constructed surfaces will advantageously combine several features, which will enhance synergetically the attractiveness of the material surface for cell colonization: nanostructure, appropriate chemical composition, wettability, electrical charge and conductivity. Therefore, this study was focused on the modification of polyethylene in inert Ar plasma. In addition, the possibility of grafting the chemically activated polymer surface with Au nanoparticles was investigated by the XPS and RBS methods. Changes in surface properties of the substrate, such as wettability, roughness and morphology, were also studied using goniometry and AFM, respectively. Finally, the adhesion and proliferation of VSMC in cultures derived from the rat aorta, as well as mouse fibroblasts of the line 3T3, were evaluated on the modified surfaces.

2. Experimental

2.1. Materials, plasma modification and grafting

Oriented, high density polyethylene (HDPE, density 0.951 g cm^{-3}) in the form of 40 μm thick foils (supplied by Granitol Ltd., Czech Republic) was used in the present experiments. The samples were modified in diode plasma discharge on Balzers SCD 050 device for 0–400 s, using DC Ar plasma (gas purity was 99.997%, power 1.8 W, Ar flow approx. 0.3 l s^{-1}, pressure of 10 Pa, electrode distance of 50 mm and its area 48 cm^2, chamber volume ca 1000 cm^3, plasma volume 240 cm^3). The activated surface of PE was grafted for 12 h into freshly prepared colloid solution of Au nanoparticles. The colloid solution was prepared by citrate reduction of $K[AuCl_4]$ (for detail see [25]). The average diameter of the spherically shaped nanoparticles was ca 12 nm (as determined by TEM). The decrease of Au concentration on "grafted" PE surface suspends for the samples immersed for 5 h, the Au concentration on the sample surface being constant. The excess of non-bound Au nanoparticles was removed by immersion of the sample into "fresh" water for 12 h.

2.2. Measurement techniques

Properties of the samples modified by plasma treatment and grafting with Au nanoparticles were studied using various analytical methods. The presence of Au in the modified surface layer was proved by X-ray photoelectron spectroscopy (XPS), and by Rutherford backscattering spectroscopy (RBS). An Omicron Nanotechnology ESCAProbeP spectrometer was used to measure photoelectron spectra (XPS). The exposed and analyzed area had a dimension of 2×3 mm^2. The X-ray source was monochromated at 1486.7 eV, with a step size of 0.05 eV; the take off angle was 0° with respect to surface normal. Characteristic O1s, C1s, N1s and Au4f peaks were searched. The spectra evaluation was carried out by CasaXPS software. The RBS analysis was performed in a vacuum target chamber with 2.72 MeV He^+ ions. Elemental depth profiles in the inspected polymeric samples were determined with the typical depth resolution less than 10 nm and accessible depth of a few μm. The RBS spectra were evaluated by the GISA3.99 code [26]. The typical RBS detection limit is 0.01 at.% for Au.

Surface wettability was measured by goniometry, i.e. the static (sessile) water drop contact angle method. It was shown that the contact angle of PE (exposed to plasma discharge) depends on the time elapsed from the moment of the exposure [13,27]. In this experiment, the contact angle on the plasma-modified Au-grafted samples was measured 20 days after the modification. The measurements of the advancing water contact angles (error ±5%) were performed in 10 different positions at room temperature on the Surface Energy Evaluation System (Advex Instruments, Czech Republic) [13,28].

Surface morphology and roughness of pristine and modified samples were examined by the AFM technique using a VEECO CP II device working in tapping mode. A Si probe RTESPA-CP, with the spring constant 20–80 N/m, was used. By repeated measurements of the same region (1×1 μm) it was proved that the surface morphology did not change after five consecutive scans. The mean roughness value (R_a) represents the arithmetic average of the deviations from the centre plane of the sample.

2.3. Cell culture, adhesion and proliferation

For cell culture experiments, the polymer samples were sterilized for 1 h in ethanol (70%), air-dried, inserted into 24-well plates (TPP, Switzerland; well diameter 1.5 cm) and seeded with vascular smooth muscle cells (VSMC) derived from the rat aorta by an explantation method [9,29,30]. VSMC were seeded on the samples with the density of 30.000 cells/well (i.e. 17.000 cells/cm^2) into 1.5 ml of Dulbeccós modified Eaglés Minimum Essential Medium (DMEM; Sigma, USA, Cat. No. D5648), containing 10% fetal bovine serum (FBS; Sebak GmbH, Aidenbach, Germany) and gentamicin (40 μg/ml, LEK, Ljubljana, Slovenia). Cells were cultivated at 37 °C in a humidified air atmosphere containing 5% of CO_2.

The number and morphology of initially adhered cells was evaluated 24 h after seeding. The cell proliferation activity was estimated from the increase in cell numbers achieved on the 2nd, 5th, 7th days after seeding. The cells were rinsed in phosphate-buffered saline (PBS) and fixed in 70% ethanol. The cell membranes and cytoplasmic proteins were stained with Texas Red C_2-maleimide (Molecular Probes, Invitrogen, Cat. No. T6008; 20 ng/ml), and the cell nuclei were visualized by the dye Hoechst # 33342 (Sigma, USA; 5 μg/ml). The number and morphology of cells on the sample surface were then evaluated on microphotographs taken under an Olympus IX 51 microscope (obj. 20x; visualized area of 0.136 mm^2), equipped with an Olympus DP 70 digital camera. The number of cells was determined using the image analysis software LUCIA. For each experimental group and time interval, 20 independent measurements were performed.

Mouse embryonic fibroblasts (NIH 3T3) were used as a second model cell line. Their attachment and proliferation *in vitro* was similarly evaluated as described above for VSMC. The adhered cells were counted 24 h after seeding, and the numbers of proliferating cells were determined 3 and 5 days post-inoculation. The NIH 3T3 were seeded in a density of 11,000 cells/cm^2 of polymer (sterilized as described above). Cells were cultivated in DMEM with 10% of FBS, 1% MEM vitamins solution and antibiotics (10,000 U/ml penicillin G, 10 mg/ml streptomycin sulfate, 25 μg/ml amphotericin B) at 37 °C in a humidified air atmosphere with 5% CO_2. Cells were rinsed twice with preheated phosphate-buffered saline (PBS), with a pH of 7.4, and then fixed for 20 min in 1 ml 4% formaldehyde

solution in PBS. Cell membranes were stained for 10 min with 1 μg/ml Tetramethylrhodamine isothiocyanate (TRITC) Phalloidine (Sigma, USA) solution in PBS, and the nuclei were visualized with 0.5 μg/ml DAPI (Sigma, USA) solution in PBS at room temperature (for 5 min). The unbound dye was removed by two rinses of PBS. The number and morphology of stained cells on the tested surface were then evaluated by fluorescence microscope Olympus IX 81, using a QuickPhoto digital camera 2.1. All images were acquired with 100× magnification to achieve the largest possible viewing field (0.15 × 0.20 mm). The average numbers of the cells were calculated from 20 independent measurements for each sample.

3. Results and discussion

3.1. Plasma modification and surface properties

Surface morphology of pristine PE and PE exposed to plasma discharge was examined using the AFM method (see Fig. 1). The plasma treatment led to an ablation of the PE surface layer [29]. As a result, the surface morphology was changed dramatically and surface roughness was increased. Also a lamellar structure appeared on the PE surface which could be due to the different ablation rates of amorphous and crystalline phases [13]. Observed changes might also have been due to the preferential removal of oxidized low mass degradation products from the PE surface [30,31].

Further changes in the surface morphology and a decrease in the surface roughness occured after exposure of the samples to a water environment, the changes being probably due to preferential etching of short molecular fragments formed by the plasma treatment [32]. Fig. 1 also demonstrates changes in the surface morphology and further decrease of the surface roughness after grafting the plasma-activated and water-etched polymer surface with Au nanoparticles.

The presence of oxygen and nitrogen on the surface of the plasma treated and gold grafted PE was examined using the XPS method. The presence of oxygen on the polymer surface is seen from the XPS spectrum shown in Fig. 2 (O1s peak). Obviously, the oxygen from ambient residual atmosphere interacted with the plasma-activated PE surface, and created different oxidized structures. Creation of carbonyl, carboxyl and ester groups on the plasma-treated PE was proven earlier in similar experiments [29,33]. Also, the Au4f peak was clearly seen indicating the presence of Au atoms on the surface of the gold grafted PE. The presence of gold was also proved by RBS measurement (see Fig. 3). One can see that Au particles are present not only on the very surface of the PE, but also in the near surface layer of about 100 nm thick and that the gold concentration decreases from the surface to the bulk. The presence of gold particles beneath the PE surface may indicate an inward diffusion of gold particles, which could be facilitated by the structure of the PE surface altered by the preceding plasma treatment. The penetration of Au particles could be supported by the fact, that the AFM results do not show any large Au agglomerates on the surface. The depth of Au evidence is much higher than RBS depth resolution. The simultaneously measured oxygen profiles presented in our previous work [16] exhibit the same behavior as Au profiles, oxygen decorates the plasma modified layer. The measurement of the sheet resistance proved that the grafted Au particles did not create a continuous coverage of the PE surface.

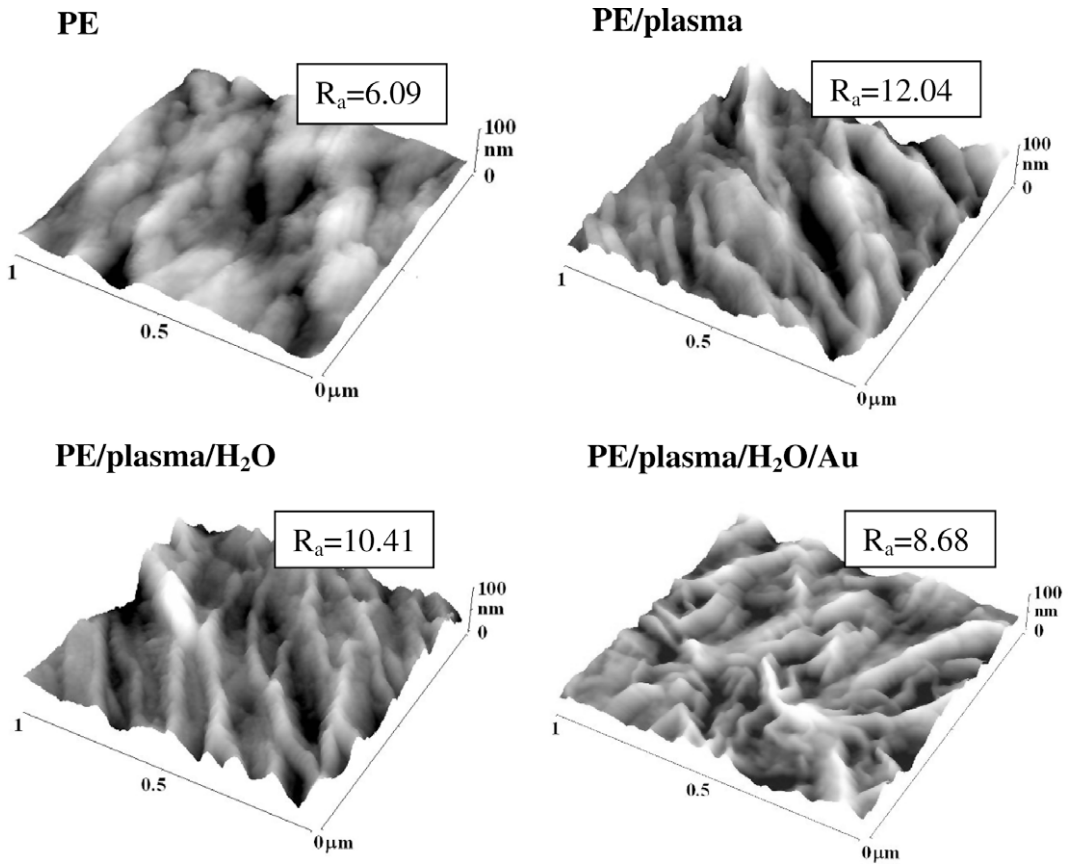

Fig. 1. AFM images of pristine PE (PE), PE treated with plasma for 150 s (PE/plasma), the same but subsequently etched by water (PE/plasma/H_2O) and grafted with Au nanoparticles (PE/plasma/H_2O/Au). R_a is the measured surface roughness in nm.

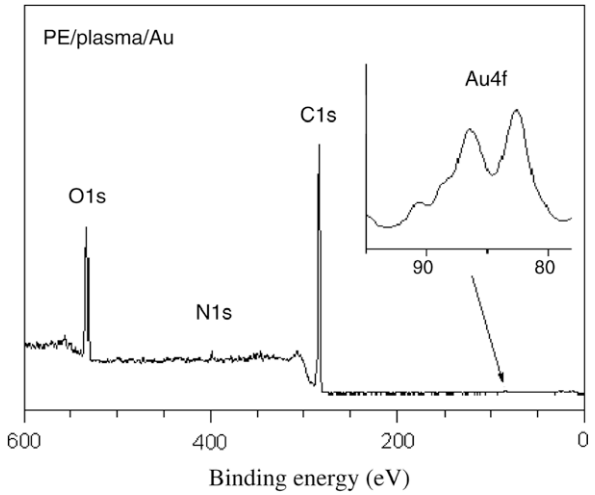

Fig. 2. XPS spectrum of the plasma treated and with Au nanoparticles grafted PE. The O1s, C1s, N1s and Au4f peaks are clearly seen. In the inset, the enlarged region of the Au4f peak is shown.

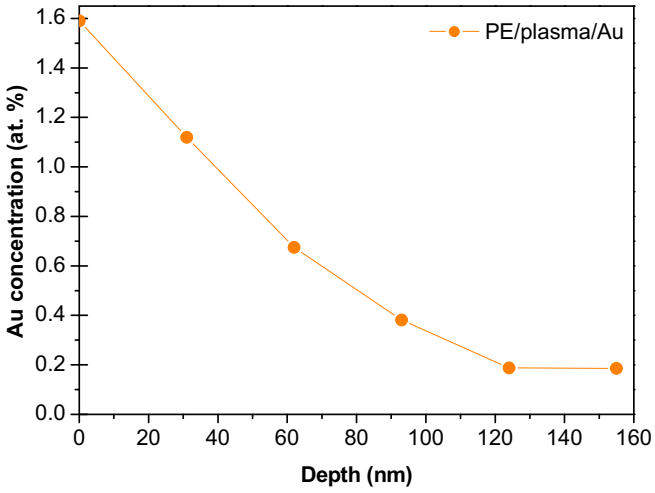

Fig. 3. Depth concentration profile of Au, determined from RBS measurement on the sample exposed to plasma discharge for 150 s and grafted with Au nanoparticles.

It is well known that chemical structure and surface morphology significantly affect surface wettability [18,19], which in turn may affect adhesion and proliferation of living cells [18,19]. The contact angle, as a measure of the surface wettability, is shown in Fig. 4 in dependence on the plasma exposure time for plasma treated and gold grafted samples. The dependence is rather complicated but similar for both sample types. For exposure times up to 50 s, the contact angle decreases from that measured on pristine PE to a minimum. Then the contact angle increases and for the samples exposed to the plasma discharge (for the times above 200 s), the contact angle exceeds that for pristine PE. A similar dependence is observed on the plasma treated and gold grafted samples, but the increase of the contact angle is slower and the contact angle remains below that on pristine PE. It may therefore be concluded that short time exposures to plasma discharge result in a rapid growth of hydrophilicity which can further be increased by the gold grafting. For longer exposure times, however, the hydrophilicity diminishes and finally the samples become hydrophobic.

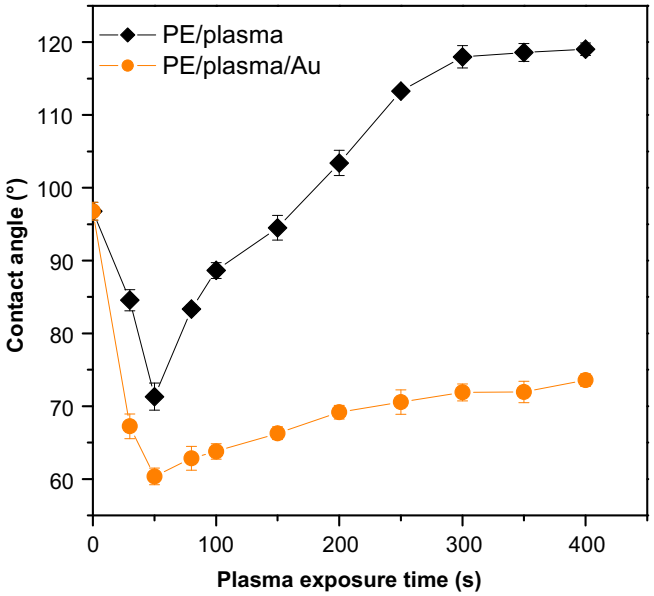

Fig. 4. Dependence of the contact angle on the plasma exposure time for plasma-treated PE (PE/plasma) and plasma treated and Au nanoparticle-grafted PE (PE/plasma/Au). The measurement was accomplished 20 days after the modification.

3.2. Cells adhesion and proliferation

The cell-material interaction was studied and compared on pristine PE, PE exposed to Ar plasma and plasma-activated samples grafted with Au nanoparticles. Fig. 5 demonstrates growth curves of VSMC in cultures on these groups of samples. It is apparent that the number of initially adhered VSMC is similar in all three groups of PE samples, i.e. this parameter is not influenced by treatment with plasma or plasma/Au grafting. However, both PE modifications enhanced the proliferation activity of VSMC. Two days after seeding, the number of VSMC on both types of modified PE samples was higher than that on pristine PE samples. This difference showed increasing tendency in the following days of cultivation. On days 5 and 7 after seeding, the cell numbers were significantly higher on modified PE samples, especially those grafted with Au nanoparticles. On the latter samples, the cell population density was approximately 4 times higher than the value on pristine PE.

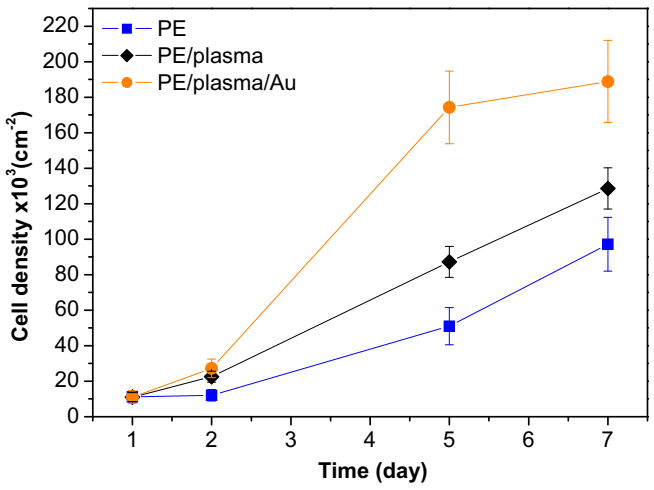

Fig. 5. Dependence of the number of VSMC cells on the cultivation time for pristine PE (PE), PE treated for 150 s with plasma (PE/plasma) and subsequently grafted with Au nanoparticles (PE/plasma/Au).

The higher proliferation activity of VSMC on modified PE samples can be explained by the oxidation of the polymer surface after the plasma treatment, resulting in the increase in the surface wettability (at least in the samples treated for 50 s). This increase was well apparent especially in samples grafted with Au nanoparticles, where the samples were wettable after all times of exposure to plasma (see Fig. 4). It is believed that hydrophilic surfaces adsorb the cell adhesion-mediating molecules (such as vitronectin or fibronectin present in the serum supplement of cell culture media) in a more physiological conformation, which supports the accessibility of specific amino acid sequences (e.g. RGD) in these molecules to cell adhesion receptors (e.g. integrins) [8–12]. Receptor-mediated adhesion and appropriate cell spreading on the adhesion substrate are prerequisites for proliferation capability in all types of anchorage-dependent cells, including VSMC (for a review, see [34,35]).

Other factors influencing the growth activity of cells is the surface roughness and morphology of the adhesion substrate. Both plasma treatment and Au grafting created nano-scale irregularities on the material surface. The surface nano-roughness acts synergetically with the surface wettability, i.e. by improving the geometrical conformation of adsorbed ECM molecules, and thus a better exposure of active sites on these molecules to the cell adhesion receptors [20–22]. Also the shape of the irregularities on the material surface is important for its colonization with cells [34,35]. After grafting with the Au nanoparticles, the surface irregularities on plasma-treated PE lost their conical shape and sharpness and become rounded and filiform (Fig. 1), which supported better spreading of cells (Fig. 6) and their subsequent proliferation activity.

As suggested above, not only the number of cells but also their spreading, shape and the homogeneity of their distribution on the material surface are important indicators of the cell growth activity. Although the numbers of VSMC on day 1 after seeding on pristine and modified PE were similar, these cells markedly differed in their morphology. As shown in Fig. 6, the cells on the pristine PE were mostly rounded, while the cells on plasma treated and especially on Au-grafted samples were spread by a significantly larger cell-material contact area, which most probably stimulated their subsequent proliferation activity. In addition, these cells were more homogeneously distributed on the material surface. On day 5 after seeding, the entire surface of the plasma-irradiated and Au-grafted PE is homogeneously covered with a confluent and dense VSMC layer, whereas the cells on the pristine PE formed islands irregularly distributed on the material surface.

In addition to VSMC, the interaction of modified PE with NIH 3T3 fibroblasts was studied. The shapes and distribution of the NIH 3T3 cells on variously treated supports are documented in Fig. 7. The obtained data strongly argues that surfaces modified either by plasma or plasma/Au are significantly more suitable for the cell adhesion than the pristine PE, as markedly higher numbers of cells were attached to the modified samples 24 h after inoculation. Moreover, they had a typically elongated shape without any

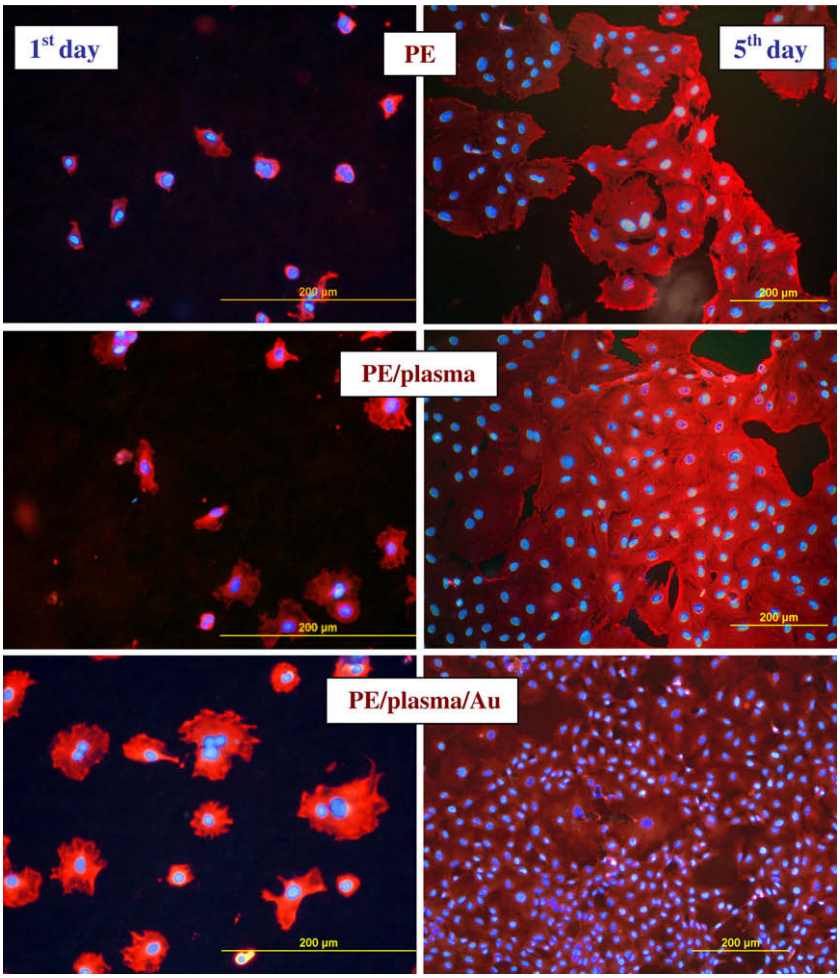

Fig. 6. The photographs of VSMC adhered (1st day) and grown (5th day) on pristine PE (PE), PE treated for 150 s with plasma (PE/plasma) and subsequently grafted with Au nanoparticles (PE/plasma/Au).

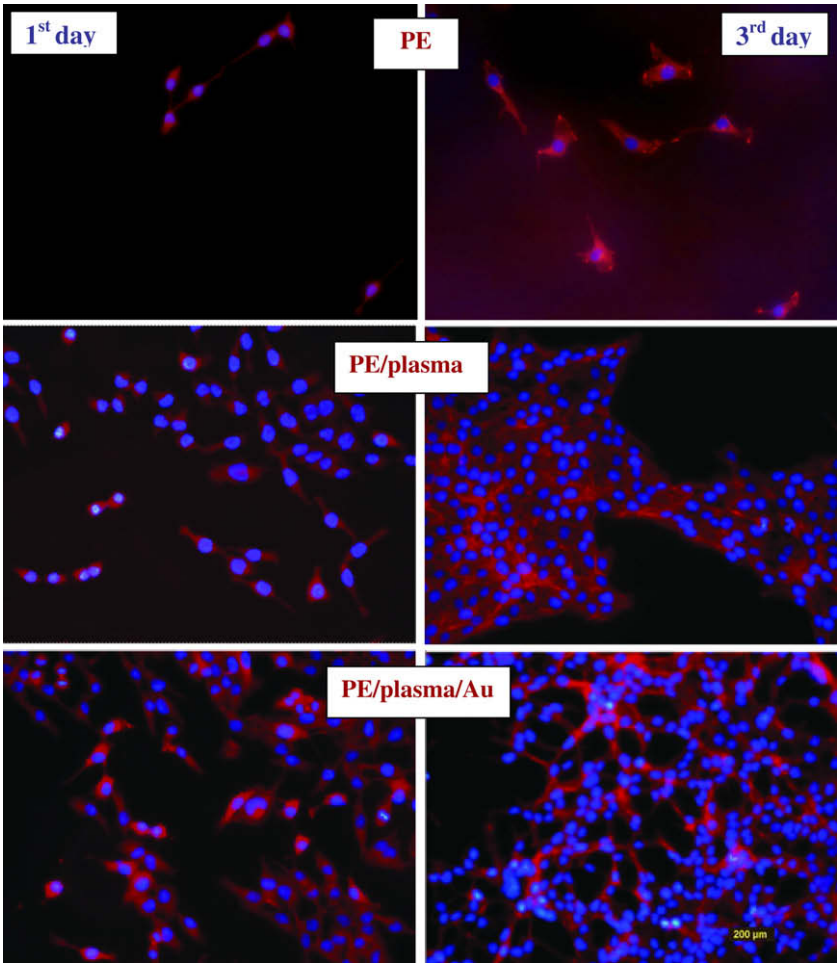

Fig. 7. The photographs of 3T3 cells adhered (1st day) and grown (3rd day) on pristine PE (PE), PE treated for 150 s with plasma (PE/plasma) and subsequently grafted with Au nanoparticles (PE/plasma /Au).

visible granulation, suggesting their good physiological state. This correlates well with their rapid proliferation on both plasma and plasma/Au treated surfaces (on day 3 after seeding). Fig. 7 also shows good homogeneity documented by the growth on the treated surfaces. The NIH 3T3 cells reached 100% confluence during four days of cultivation when seeded in suggested ratio, i.e. $\sim 10^4$ cells/cm^2 (not shown). As the NIH 3T3 cells overgrew the surface within four days, only 1 and 3 day periods were evaluated. Strikingly (and in contrast to VSMC), the pristine PE was absolutely inappropriate support material for the cultivation of NIH 3T3 cells, as they very poorly adhered to this material and exhibited very limited proliferation during the first three days (Fig. 8 - left column and Fig. 7 upper panels). Moreover, granulation of the cytoplasm and apparent loss of the cell-material contact were observed after five days of cells cultivation on the pristine PE when virtually all the cells detached into the growth medium (data not shown). In summary, the NIH 3T3 cells required plasma modification for their attachment, and application of Au slightly supported both their attachment and growth (compare columns 2 and 3 in the Fig. 8).

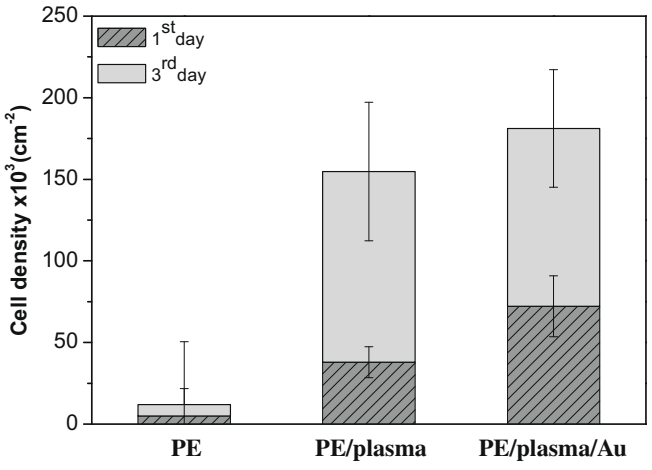

Fig. 8. Dependence of the number of 3T3 cells on the cultivation time for pristine PE (PE), PE modified 150 s by plasma treatment (PE/plasma) and subsequently grafted with Au nanoparticles (PE/plasma/Au).

It can be concluded that the plasma treatment of PE enhances the adherence of both tested cell types. However, this effect is far more dramatic for NIH 3T3 cells. On the contrary, the Au grafting exhibits a moderate positive effect on the NIH 3T3 proliferation whilst it almost doubled the proliferation capacity of VSMC.

4. Conclusion

The results can be summarized as follows:

- treatment of PE in the plasma discharge leads to dramatic changes in the surface morphology and surface roughness, further morphological changes and decrease in the surface rough-

ness occur after exposure of the sample to water, which lead to etching and removal of short polymer chains created by the material degradation in plasma;
- during interaction of plasma-activated PE with Au nanoparticles, these nanoparticles are grafted on the material surface, which is manifested by an increase in its wettability and changes in its morphology and roughness, Au nanoparticles are found not only on the material surface but also within the near surface layer (about 100 nm thick);
- the plasma treatment of the polymer, and particularly the presence of Au nanoparticles, had a positive influence on spreading, proliferation activity and homogeneity of the distribution of VSMC on the material surface;
- the positive effect of plasma treatment of PE on the adhesion of NIH 3T3 fibroblasts was even more pronounced, although their following proliferation was stimulated only moderately;
- nevertheless, as a final result, the modification of PE with plasma and grafting Au nanoparticles significantly increases the attractiveness of this polymer for colonization with VSMC and NIH 3T3 fibroblasts.

Acknowledgements

This work was supported by the Ministry of Education of the Czech Republic under programs 6046137302, 6046137305, 1M6837805002 and LC 06041, GAAS CR under the projects KAN 400480701 and KAN 200100801 and GACR under the project 106/09/0125. Mrs. Sherryl Ann Vacik, Pangrac & Associates, Port Aransas, Texas, USA is gratefully acknowledged for her language revision of the manuscript.

References

[1] R. Li, L. Ye, Y.W. Mai, Composites 28A (1997) 73.
[2] C.M. Chan, T.M. Ko, H. Hiraoka, Surf. Sci. Rep. 24 (1996) 3.
[3] J.M. Grace, L.J. Gerenser, J. Dispers. Sci. Technol. 24 (2003) 305.
[4] Y. Choi, J. Kim, K. Paek, W. Ju, Y.S. Hwang, Surf. Coat. Technol. 193 (2005) 319.
[5] M. Kuzuya, S. Kondo, M. Sugito, T. Yamashiro, Macromolecules 31 (1998) 3225.
[6] N. Inagaki, S. Tasaka, S. Shimada, J. Appl. Polym. Sci. 79 (1999) 808.
[7] V. Jones, M. Strobel, M.J. Prokosch, Plasma Proc. Polym. 2 (2005) 547.
[8] R. Tzoneva, M. Heuchel, T. Groth, G. Altankov, W. Albrecht, D. Paul, J. Biomater. Sci. Polym. Ed. 13 (2002) 1033.
[9] L. Bačáková, V. Mareš, M.G. Bottone, C. Pellicciari, V. Lisá, V. Švorčík, J. Biomed. Mater. Res. 49 (2000) 369.
[10] J. Heitz, V. Švorčík, L. Bačáková, K. Ročková, E. Ratajová, T. Gumpenberger, D. Bauerle, B. Dvořánková, H. Kahr, I. Graz, C. Romanin, J. Biomed. Mater. Res. 67A (2003) 130.
[11] R. Mikulíková, S. Moritz, T. Gumpenberger, M. Olbrich, C. Romanin, L. Bačáková, V. Švorčík, J. Heitz, Biomaterials 26 (2005) 5572.
[12] L. Bačáková, K. Walachová, V. Švorcik, V. Hnatowitz, J. Biomater. Sci. Polym. Ed. 12 (2001) 817.
[13] V. Švorčík, K. Kolářová, P. Slepička, A. Macková, M. Novotná, V. Hnatowicz, Polym. Degrad. Stab. 91 (2006) 1219.
[14] M. Tahara, N.K. Cuong, Y. Nakashima, Surf. Coat. Technol. 174 (2003) 826.
[15] V. Švorčík, K. Ročková, B. Dvořánková, V. Hnatowicz, R. Öchsner, H. Ryssel, J. Mater. Sci. 37 (2002) 1183.
[16] V. Švorčík, V. Kotál, J. Siegel, A. Macková, V. Hnatowicz, Polym. Degr. Stab. 92 (2007) 1645.
[17] V. Kotál, V. Švorčík, P. Slepička, O. Bláhová, P. Šutta, V. Hnatowicz, Plasma Proc. Polym. 4 (2007) 69.
[18] V. Švorčík, V. Hnatowicz, P. Stopka, L. Bačáková, J. Heitz, H. Ryssel, Rad. Phys. Chem. 60 (2001) 89.
[19] K. Ročková, V. Švorčík, L. Bačáková, B. Dvořánková, J. Heitz, Nucl. Instr. and Meth. B 225 (2004) 275.
[20] T.J. Webster, T.A. Smith, J. Biomed. Mater. Res. A 74 (2005) 677.
[21] D.C. Miller, A. Thapa, K.M. Haberstroh, T.J. Webster, Biomaterials 25 (2004) 53.
[22] T.J. Webster, C. Ergun, R.H. Doremus, R. Bizios, J. Biomed. Mater. Res. 51 (2000) 475.
[23] C.J. Gannon, C.R. Patra, R. Bhattacharya, P. Mukherjee, S. Curley, J. Nanobiotechnol. 6 (2008) 2.
[24] A.C. Curry, M. Crow, A. Wax, J. Biomed. Opt. 13 (2008) 014022.
[25] P. Řezanka, K. Záruba, V. Král, Tetrahedron Lett. 49 (2008) 6448.
[26] J. Saarilahti, E. Rauhala, Nucl. Instr. and Meth. B 64 (1992) 734.
[27] V. Švorčík, V. Kotál, P. Slepička, O. Bláhová, M. Špirková, P. Sajdl, V. Hnatowicz, Nucl. Instr. and Meth. B 244 (2006) 365.
[28] O. Kubová, V. Švorčík, J. Heitz, S. Moritz, C. Romanin, P. Matějka, A. Macková, Thin Solid Films 515 (2007) 6765.
[29] P.K. Chu, J.Y. Chen, L.P. Wang, N. Huang, Mater. Sci. Eng. R 36 (2002) 143.
[30] K.S. Kim, Ch.M. Ryu, Ch.S. Park, G.S. Sur, Ch.E. Park, Polymer 44 (2003) 6287.
[31] S. Guimond, M.R. Wertheimer, J. Appl. Polym. Sci. 94 (2004) 1291.
[32] J. Siegel, A. Řezníčková, A. Chaloupka, P. Slepička, V. Švorčík, Rad. Eff. Def. Sol. 163 (2008) 779.
[33] V. Švorčík, V. Hnatowicz, in: L.B. Albertov (Ed.), Polymer Degradation and Stability, Nova Sci. Publis, New York, 2008. p. 171.
[34] L. Bačáková, E. Filová, F. Rypáček, V. Švorčík, V. Starý, Physiol. Res. 53 (2004) S35.
[35] L. Bačáková, V. Švorčík, in: D. Kimura (Ed.), Cell Growth Processes: New Research, Nova Sci. Publis, New York, 2008. p. 5.

VSP

Journal of Adhesion Science and Technology 24 (2010) 743–754

Journal of ADHESION SCIENCE and TECHNOLOGY
brill.nl/jast

Cell Adhesion and Proliferation on Plasma-Treated and Poly(ethylene glycol)-Grafted Polyethylene

N. Kasálková [a,*], Z. Makajová [a], M. Pařízek [b], P. Slepička [a], K. Kolářová [a], L. Bačáková [b], V. Hnatowicz [c] and V. Švorčík [a]

[a] Department of Solid State Engineering, Institute of Chemical Technology, 166 28 Prague, Czech Republic

[b] Institute of Physiology, Academy of Sciences of the Czech Republic, 142 20 Prague, Czech Republic

[c] Nuclear Physics Institute, Academy of Sciences of the Czech Republic, 250 68 Rez, Czech Republic

Received in final form 22 October 2009

Abstract

Polyethylene (PE) was modified by an Ar plasma. The plasma-activated PE surface was grafted with poly(ethylene glycol) (PEG, molecular weight 300 and 20 000). The depth profiles of the oxygen in the modified PE samples were determined using Rutherford Backscattering Spectroscopy (RBS). The changes in the surface wettability were examined by goniometry, and Atomic Force Microscopy (AFM) was used to determine the surface roughness and morphology. The modified PE samples were seeded with rat vascular smooth muscle cells (VSMCs) and their adhesion and proliferation was studied. The plasma treatment and the subsequent PEG grafting leads to dramatic changes in the PE surface morphology, roughness and wettability. The PEG grafting of the plasma-treated PE does not increase VSMC adhesion but it results in dramatic increase of VSMC proliferation.

Keywords

Polyethylene, plasma discharge, PEG grafting, cell adhesion and proliferation

1. Introduction

The performance of polymeric materials relies largely on the properties of their surfaces. Most polymers have hydrophobic, chemically inert surface which may present a serious problem in their applications requiring adhesion, coating, etc. [1–3].

* To whom correspondence should be addressed. E-mail: nikola.kasalkova@vscht.cz

DOI:10.1163/016942409X12579497420762

For many medical and biological applications (tissue engineering, cell culture substrates and cell bio-chips) the interaction of biological cells with the substrate is of crucial importance [4]. The interaction of living cells with materials is strongly dependent on physical and chemical properties of material surface. The main properties decisive for the colonization of a material with cells are its polarity, wettability, electrical charge, roughness and topography [5–10]. Important may also be the presence of various chemical functional groups and biomolecules on the material surface [5, 6].

There are various ways of modifying the surfaces of the polymers to make them more suitable for cell cultivation. A modified polymer surface exhibits increased chemical reactivity, due to presence of free radicals and unsaturated bonds, and it can easily be grafted with suitable agents. For this purpose, the surfaces have been exposed to ultraviolet (UV) irradiation [7, 11], to beams of various ions (e.g., oxygen, nitrogen, noble gases, or halogens) for biological applications [12, 13] or to a plasma discharge [14–18]. For more pronounced changes in the physico-chemical properties of the modified surface, some of these processes are realised in a gas atmosphere, e.g., in acetylene or ammonia [7, 11]. These modifications change the stability, roughness, morphology, mechanical properties and chemical composition of the polymer surface due to creation of functional chemical groups containing oxygen or nitrogen, like carbonyl, carboxyl or amine groups, on the surface of the material [19–23]. These groups increase the surface wettability, support the adsorption of cell adhesion-mediating extracellular matrix proteins in an appropriate geometrical conformation and stimulate cell adhesion and growth [7, 12].

In this study high density polyethylene (PE) was modified by Ar plasma and subsequently grafted with poly(ethylene glycol) (PEG). The morphological, structural and compositional changes were characterized by different techniques: AFM (surface morphology, roughness), RBS (oxygen depth profile), goniometry (contact angle). The cell adhesion and proliferation on the modified polymers was studied by cultivation of rat vascular smooth muscle cells (VSMCs).

2. Experimental

2.1. Materials and Modification

Oriented high density polyethylene (PE, density 0.951 g/cm^3) in the form 40 μm thick foils (supplied by Granitol Ltd., Czech Republic) was used. The samples were modified in Ar plasma discharge in a Balzers SCD 050 device. Exposure time was 50, 150 and 400 s, discharge power was 2 W and gas purity was 99.997%. Immediately after plasma treatment, the plasma activated PE was grafted by immersion to an aqueous solution (24 h, room temperature, 2 wt%) of poly(ethylene glycol) (PEG, molecular weight (M) 300 and 20 000 g/mol). Grafting is a chemical bonding of new structures on modified polymer surface [24]. The non-bound PEG was removed by immersion of the samples into distilled water for 24 h.

2.2. Characterization of Modified PE

Surface wettability was measured by goniometry, i.e., the static (sessile) water drop contact angle method. It was shown earlier that the contact angle of PE (exposed to plasma discharge) depends on the time elapsed from the moment of exposure [19]. In this experiment, the contact angle on the plasma-modified and grafted samples was measured over 54 days. Advancing water contact angles (error ± 5%) were measured at 10 different positions at room temperature using the Surface Energy Evaluation System (Advex Instruments, Czech Republic) [19, 27].

The concentration depth profile of oxygen in the modified PE surface layer (after plasma treatment and PEG grafting) was determined by Rutherford Backscattering Spectroscopy (RBS). The RBS analysis was performed in a vacuum chamber with 2.72 MeV He^+ ions. Elemental depth profiles in the inspected samples were determined with the typical depth resolution less than 10 nm and an accessible depth of a few μm. The RBS spectra were evaluated by the GISA3.99 code [18]. The typical RBS detection limit is 0.1 at% for oxygen with an experimental error ±7%.

Surface morphology and roughness of the pristine and modified samples were determined using a VEECO CP II AFM working in the tapping mode. A Si probe, RTESPA-CP, with a spring constant 20-80 N/m was used. By repeated measurements in the same region (1 μm × 1 μm) it was shown that the surface morphology did not change after three consecutive scans. The roughness value (R_a) represents the arithmetic average of the deviations from the centre plane of the sample.

2.3. Cell Culture, Adhesion and Proliferation

The adhesion and proliferation of vascular smooth muscle cells (VSMCs) on pristine and modified PE substrates were investigated *in vitro*. Polymer samples were sterilized for 1 h in ethanol (70%) before cell cultivation. The samples were inserted into 24-well polystyrene multidishes (TPP, Switzerland; diameter 15 mm). Each sample was treated with 1.5 ml of Dulbecco's modification of Eagle's Minimum Essential Medium (DMEM, Sigma) containing 10% of fetal bovine serum (FBS, Sebak GmbH, Aidenbach, Germany) and 17 000 VSMCs per cm^{-2}. Cells were cultivated at 37°C in a humidified air atmosphere containing 5% of CO_2. The adhered cells were counted 24 hours after seeding, and cell proliferation was determined on 2nd and 7th day after seeding. Cells were rinsed in phosphate-buffered saline (PBS), fixed in 70% ethanol and colored with Texas Red C_2 maleimide, which conjugates with the cell membrane and cytoplasmatic proteins. Cell nuclei were visualized by Hoechst #33342 dye. The number and morphology of cells were then evaluated from pictures taken with an Olympus IX 51 microscope using an Olympus DP 70 digital camera.

The numbers of viable and dead cells was evaluated by automated counting in a ViCell XR analyzer (Beckman Coulter, USA) after they had been detached by a trypsin–EDTA solution (Sigma, USA, Cat. No T4174) in PBS for 10 min at 37°C. This automated analysis involved evaluation of cell viability by staining with trypan blue, which penetrated through the membrane of damaged and nonviable cells. As

revealed by trypan blue exclusion test performed automatically during cell counting in the cell viability analyser (ViCell, Beckman), the percentage of viable cells among cells detached from both PEG surfaces was relatively high, ranging from about 76 to 85%. It can be supposed that this percentage in the native culture before the cell detachment was even higher, and the cells were additionally damaged by trypsinization, resuspension in buffer and other procedures associated with the measurement in the ViCell Analyser.

3. Results and Discussion

3.1. Surface Properties of Modified PE

Treatment in the plasma discharge leads to cleavage of macromolecular chains, creation of free radicals and double bonds. Reaction with oxygen from ambient atmosphere in the reaction chamber or after exposing the samples to the atmosphere results in generation of various oxygen-containing structures which, in turn, increase surface wettability [19, 20]. The enhanced wettability is known to facilitate cell adhesion [7, 11, 18]. Contact angle as a function of time elapsed from the plasma treatment (aging) is shown in Fig. 1 for the samples exposed to the plasma discharge for 50, 150 and 400 s. Contact angle decreases dramatically after the plasma treatment and the decrease is inversely proportional to the exposure time. After about 5 days of aging the contact angle starts to increase and after some time (about 20 days) it reaches a saturated value [19]. Restoration of the contact angle is obviously connected with a rearrangement of degraded macromolecules on the plasma-treated PE surface in air [26–28]. On the contrary, contact angle measurements in water immersed samples lead to the conclusion that the surface polarity of the polymer increases continuously with time of water contact. This is attributed to the appearance at the surface of polar groups, initially 'buried' in the bulk of the polymer [29]. Reconstruction of the polymer surface may be ascribed to two stages: water adsorption, accompanied by diffusion into the bulk phase, and reorientation of the surface polar groups [30]. All biological experiments were done after sample aging time of 20 days or longer.

Dependence of the contact angle on the aging time for plasma-modified PE and plasma-modified PE and subsequently grafted with PEG (molecular weights 300 and 20 000) is shown in Fig. 2. Pronounced decrease of the contact angle after PEG grafting seen for both molecular weights indicates binding of oxygen-rich compounds onto the activated PE surface [7]. Saturated value of restored contact angle was achieved after about 25 days of aging when the reorientation of the oxygen-containing structures was completed [27, 28]. More pronounced decrease of the contact angle is observed for higher molecular weight PEG ($M = 20\,000$) due to higher oxygen content in this PEG species.

Concentration depth profiles of oxygen from plasma-treated PE, plasma-treated and immediately immersed into distilled water (water etched PE) and plasma-treated and subsequently PEG-grafted PE, obtained from RBS measurements, are

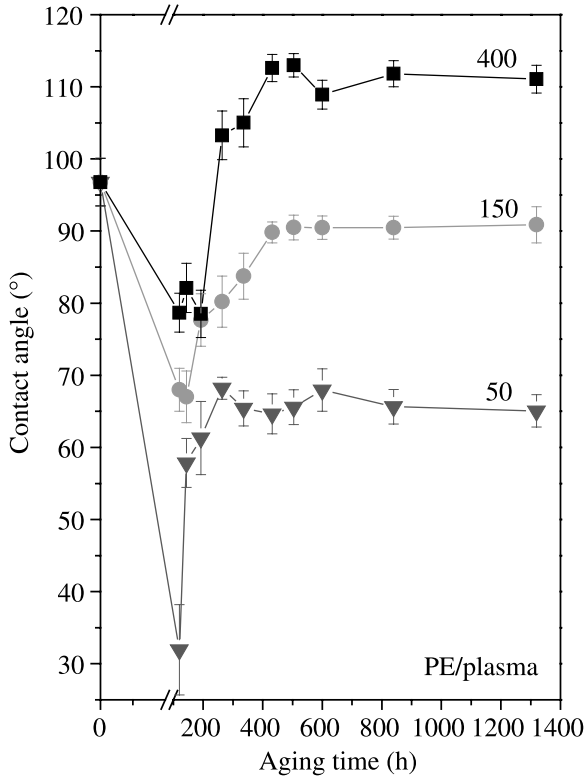

Figure 1. Dependence of the contact angle of the plasma-modified PE on the aging time. Plasma exposure times were 50, 150 and 400 s.

shown in Fig. 3. Some of the samples were etched in water since the subsequent biological experiments are carried out in a physiological solution, so that the interaction of the plasma-modified PE with water is of crucial importance. The maximum oxygen concentration is observed on the plasma-treated PE. Water etching results in a decrease of the oxygen concentration in the surface layer. This decrease indicates dissolution of a part of the oxidized structures or low molecular weight fragments [19, 26]. An increase of the oxygen concentration after the PEG grafting shows chemical binding of a part of PEG molecules on the surface of the plasma-modified PE. This increase of oxygen concentration does not explicitly prove PEG grafting on plasma-modified PE. In our previous work aminoacids were grafted onto PE degraded surface. In case of such reaction the decrease of radicals and double bonds and increase of oxygen concentration in surface layer occurred [6]. Therefore, based on our already published results we assumed that grafting occured also in case of PEG.

Surface morphology is well known to affect the interaction of cells with polymers [11, 18, 27]. AFM images of pristine, plasma-treated, plasma-treated and water-etched, and plasma-treated and subsequently grafted with PEG with differ-

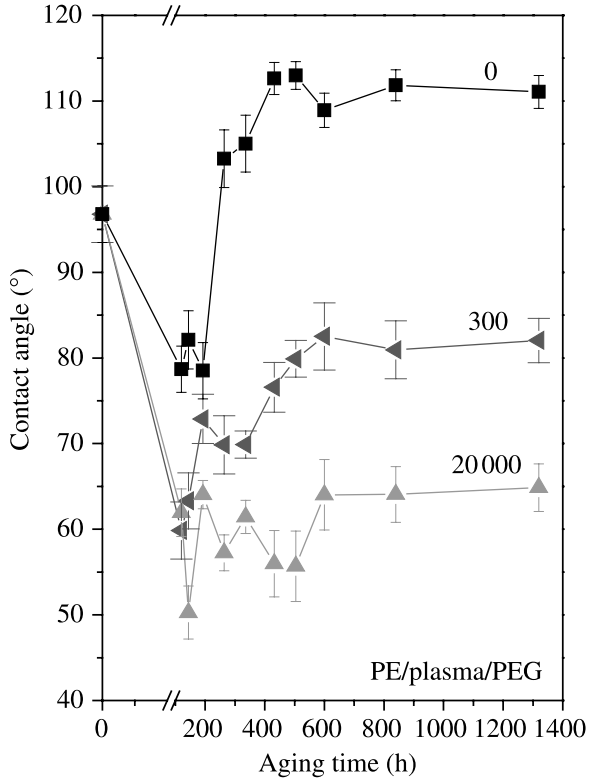

Figure 2. Dependence on the aging time of the contact angle of PE plasma modified for 400 s (0) and PE plasma modified and subsequently grafted with PEG. The molecular weights of PEG were $M = 300$ and 20 000.

ent molecular weights PE samples are shown in Fig. 4. Plasma treatment results in increased surface roughness and leads to exposure of PE lamellar structure. This phenomenon is a typical demonstration of plasma stimulated ablation of PE [9]. After water etching (Fig. 4(c)) the morphology changes due to dissolution of low molecular weight degradation products [19]. Subsequent PEG grafting leads to a change in surface roughness and, regardless of PEG molecular weight, to a decrease in surface roughness (Fig. 4(d, e)). While the grafting with PEG of molecular weight $M = 300$ preserves PE lamellar structure, the grafting with PEG of molecular weight $M = 20\,000$ results in significant change of the morphology and in creation of branched star-like formations (Fig. 4(e)). This might be a clear 2D PEG crystallization process [31].

3.2. Cell Adhesion and Proliferation

Adhesion and proliferation of rat VSMCs was studied on pristine PE, PE modified by plasma discharge for 50, 150 and 400 s and on PE modified by plasma discharge and subsequently grafted with PEG ($M = 300$ and 20 000). The anti-adhesive action of PEG is due to its very high hydrophilicity and mobility of its

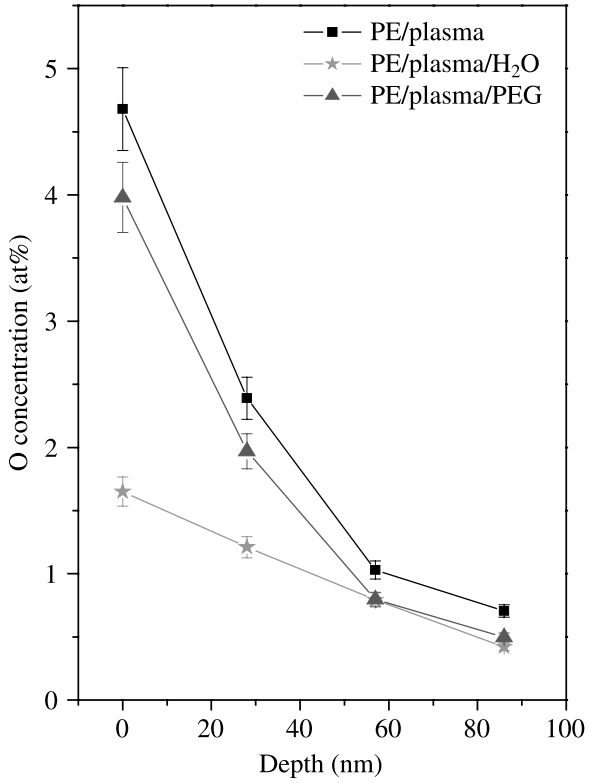

Figure 3. Oxygen concentration depth profiles of the plasma-treated PE (400 s, PE/plasma), PE plasma treated and immersed into distilled water (water etched) (PE/plasma/H_2O), PE plasma treated and subsequently grafted with PEG (molecular weight $M = 20\,000$, PE/plasma/PEG).

chains, which hamper stable adsorption of the proteins that mediate cell adhesion. However, at the same time, the anti-adhesive action of PEG is strongly dependent on its concentration on the polymer surface and on the length of its chain [32]. For comparison, the same procedures were applied to tissue culture polystyrene (TCPS). All experiments were performed *in vitro*. Total number of adhered (after 1 day cultivation) and proliferated (after 2 and 7 days of cultivation) cells is shown in Fig. 5. During the first 24 h the cells adhere very well on pristine PE and PE modified by plasma discharge. Lowest adhesion was observed on the PE grafted with PEG ($M = 300$). Higher adhesion was found on the PE grafted with PEG ($M = 20\,000$) and on the TCPS. The situation changes 2 days after seeding. While the cell proliferation on pristine and plasma-modified PE is minimal, much higher proliferation is observed on the PEG-grafted PE. Dramatic increase of proliferating cells is observed on grafted samples 7 days after seeding. Much more cells grow on the samples grafted with PEG of higher molecular weight.

In Fig. 6 are shown images of adhered and proliferated VSMCs observed after 7 days of cultivation. Cells on pristine PE and PE modifife by plasma discharge

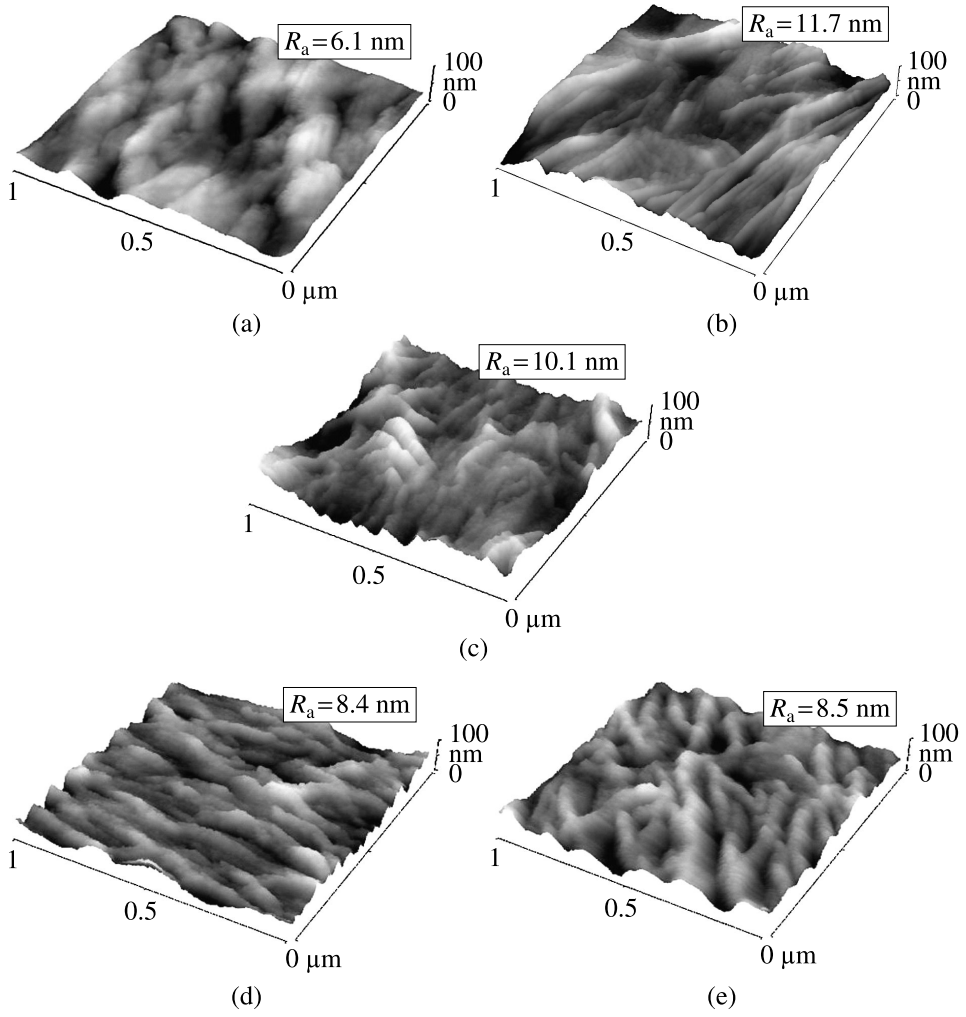

Figure 4. AFM images of pristine PE (a), plasma-treated PE (400 s) (b), PE plasma treated and immersed into distilled water (water etched) (c), PE plasma treated and subsequently grafted with PEG (molecular weight $M = 300$, d) and PEG (molecular weight $M = 20\,000$, e).

are homogeneously spread over the sample area. After 7 days, the cells are still well spread but their distribution is not homogeneous and cells agregates appear. On the contrary, on the plasma-modified and PEG-grafted PE a dense and homogeneous cell coverage is observed after 7 days of cultivation, in spite of the fact then grafting did not affect initial cell adhesion.

Similarly, the PEG chains used in the present study were either short ($M = 300$) or long ($M = 20\,000$), and good adhesion and growth of cells on the such PEG-modified surfaces were observed. In addition, the PEG chains in the present study were probably attached to the plasma-modified PE through several sites on one

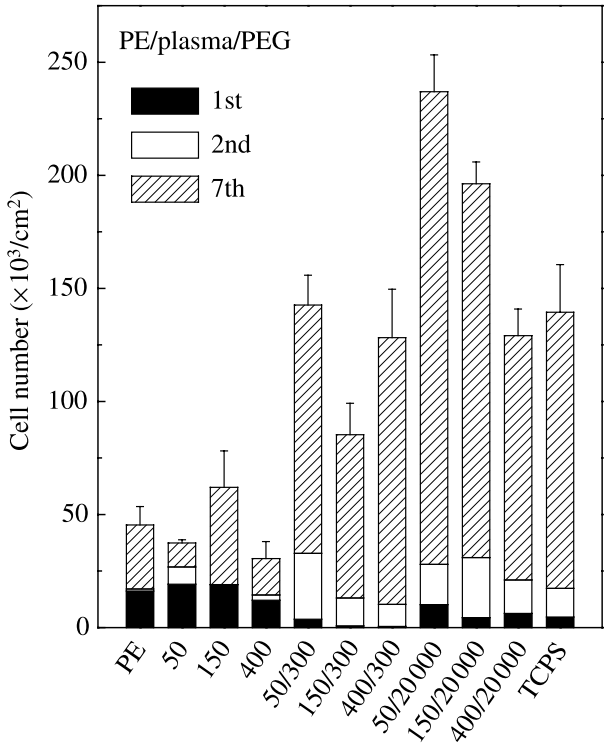

Figure 5. Dependence of the number of VSMCs on the cultivation time (1st, 2nd and 7th day) for pristine PE (PE), PE plasma modified for 50, 150 and 400 s (PE/plasma/50–400) and subsequently grafted with PEG (molecular weight $M = 300$, PE/plasma/50–400/300) and PEG (molecular weight $M = 20\,000$, PE/plasma/50–400/20 000) and tissue culture polystyrene (TCPS).

PEG chain, and not only through the chain end, which hampered mobility of the PEG chain but did not prevent the protein adsorption and cell colonization. What is more, the oxygen-containing groups present in the PEG molecules might enhance the colonization of the material by VSMCs as indicated by the highest final cell number on PEG-grafted PE on day 7 after seeding.

4. Conclusion

The properties of the plasma-modified and PEG-grafted PE were investigated and the bioactivity of modified PE was studied with VSMCs in *in vitro* experiments. Plasma treatment leads to a rapid decrease of contact angle and corresponding increase of the PE surface polarity and wettability. Sample aging results in surface relaxation and restoration of the contact angle which achieves a saturated value after about 20 days of aging when reorientation of polar structures in the modified surface layer is completed. With increasing time of exposure to the plasma discharge the wettability of the modified PE decreases. Grafting with PEG leads to additional dramatic reduction of the contact angle. With decreasing chain length of PEG the

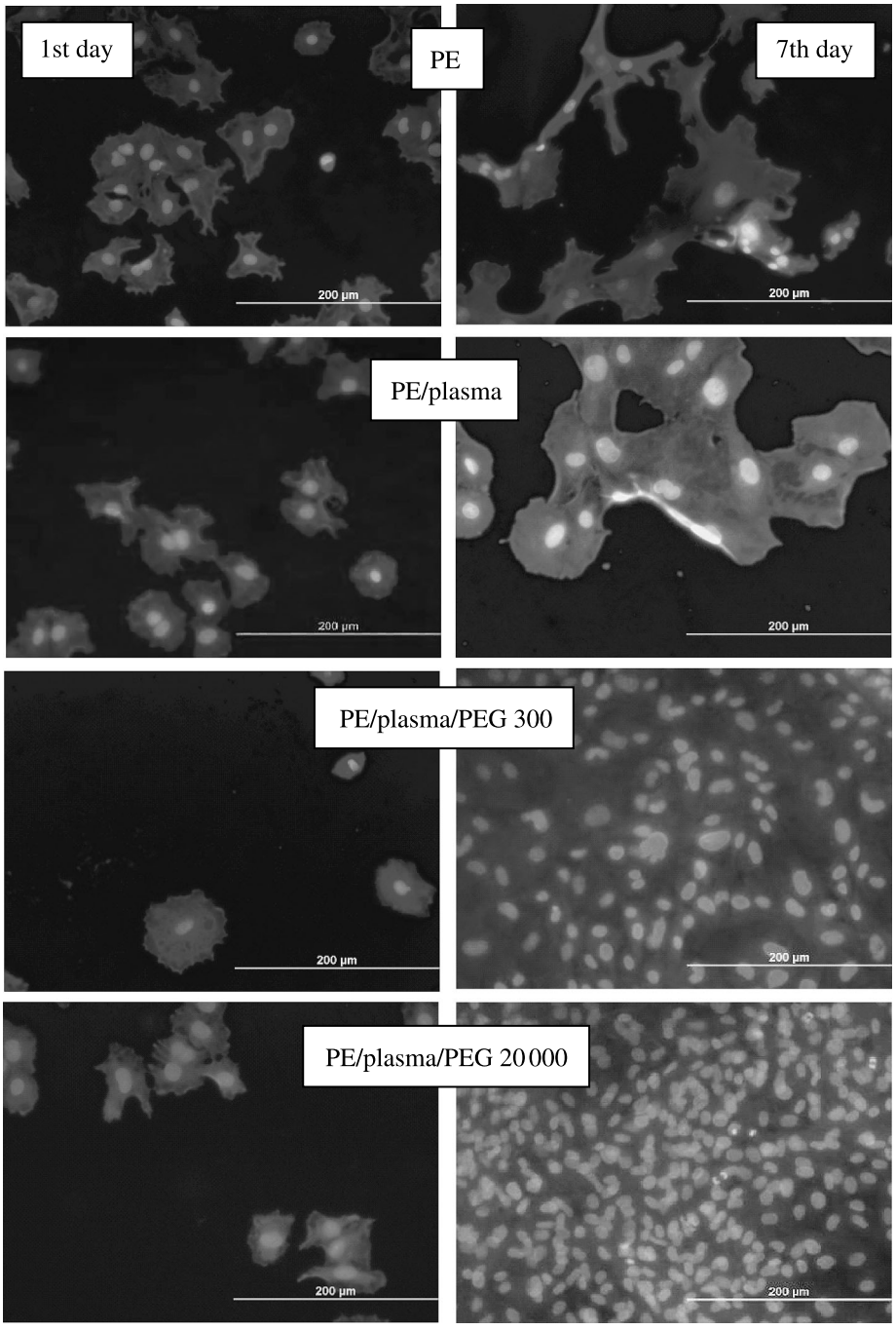

Figure 6. Photographs of VSMCs adhered (1st day) and proliferated (7th day) on pristine PE (PE), PE plasma treated for 50 s (PE/plasma) and subsequently grafted with PEG (molecular weight $M = 300$, PE/plasma/PEG 300) and PEG (molecular weight $M = 20\,000$, PE/plasma/PEG 20 000).

polarity of the grafted PE decreases. Presence of oxygen-containing groups in the surface layer of the plasma-modified PE and subsequently grafted with PEG was evidenced by the RBS technique. Plasma treatment increases surface roughness of PE and exposes its lamellar structure.

The surface roughness of the plasma-modified PE is reduced by the etching in water. Grafting with short PEG chains preserves the PE lamellar structure but grafting with longer PEG chains produces branched star-like formations on the PE surface. The biological *in vitro* experiments with VSMCs show that PEG grafting does not increase cell adhesion but it increases dramatically cell proliferation.

Acknowledgements

This work was supported by the Ministry of Education of the CR under programs LC06041 and GAASCR under projects KAN400480701 and A400500505.

References

1. P. K. Chu, J. Y. Chen, L. P. Wang and N. Juany, *Mater. Sci. Eng. R* **36**, 143 (2002).
2. K. Kato, E. Uchida, E. T. Kang, Y. Uyamaa and Y. Ikada, *Prog. Polym. Sci.* **28**, 209 (2003).
3. K. Walachová, L. Bačáková, B. Dvořánková and V. Švorčík, *Chem. Listy* **96**, 19 (2002).
4. E. Rebollar, I. Frischauf, M. Olbrich, T. Peterbauer, S. Hering, J. Preiner, P. Hinterdorfer, C. Romanin and J. Heitz, *Biomaterials* **29**, 1796 (2008).
5. L. Bačáková, E. Filová, F. Rypáček, V. Švorčík and V. Starý, *Physiol. Res.* **53**, 35 (2004).
6. L. Bačáková and V. Švorčík, in: *Cell Growth Processes: New Research*, D. Kimura (Ed.), pp. 5–56. Nova Science Publishers, Hauppauge, NY (2008).
7. V. Švorčík, K. Ročková, E. Ratajová, J. Heitz, N. Huber, D. Bäuerle, L. Bačáková, B. Dvořánková and V. Hnatowicz, *Nucl. Instrum. Meth. Phys. Res. B* **217**, 307 (2004).
8. M. Pegueroles, F. J. Gil, J. A. Planell and C. Aparicio, *Surface Coatings Technol.* **202**, 3470 (2008).
9. L. Guo, N. Kawazoe, Y. Fan, Y. Ito, J. Tanaka, T. Tateishi, X. Zhang and G. Chen, *Biomaterials* **29**, 23 (2008).
10. N. Singh, X. Cui, T. Boland and S. M. Husson, *Biomaterials* **28**, 763 (2007).
11. J. Heitz, V. Švorčík, L. Bačáková, K. Ročková, E. Ratajová, T. Gumpenberger, D. Bäuerle, B. Dvoránková, H. Kahr, I. Graz and C. Romanin, *J. Biomed. Mater. Res. A* **67**, 130 (2003).
12. L. Bačáková, K. Walachová, V. Švorčík and V. Hnatowicz, *J. Biomater. Sci. Polym. Ed.* **12**, 817 (2001).
13. K. Walachová, V. Švorčík, L. Bačáková and V. Hnatowicz, *Biomaterials* **23**, 2989 (2002).
14. Y. Choi, J. Kim, K. Paek, W. Ju and Y. S. Hwang, *Surface Coatings Technol.* **193**, 319 (2005).
15. F. Z. Cui and Z. S. Luo, *Surface Coatings Technol.* **112**, 278 (1999).
16. A. Turos, J. Jagielski, A. Piatkowska, D. Bielinski, L. Slusarski and N. K. Madi, *Vacuum* **70**, 201 (2003).
17. Y. Wang, L. Lu, Y. Zheng and X. J. Chen, *J. Biomed Mater. Res. A* **76**, 589 (2006).
18. V. Švorčík, N. Kasálková, P. Slepička, K. Záruba, L. Bačáková, M. Pařízek, V. Lisá, T. Ruml, H. Gbelcová, S. Rimpelová and A. Macková, *Nucl. Instrum. Meth. Phys. Res. B* **267**, 1904 (2009).
19. V. Švorčík, K. Kolářová, P. Slepička, A. Macková, M. Novotná and V. Hnatowicz, *Polym. Degrad. Stab.* **91**, 1219 (2006).

20. V. Švorčík, V. Kotál, P. Slepička, O. Bláhová, M. Špírková, P. Sajdl and V. Hnatowicz, *Nucl. Instrum. Meth. Phys. Res. B* **244**, 365 (2006).
21. V. Švorčík, V. Hnatowicz, P. Stopka, L. Bačáková, J. Heitz, R. Öchsner and H. Ryssel, *Radiation Phys. Chem.* **60**, 89 (2001).
22. K. L. Mittal (Ed.), *Polymer Surface Modification: Relevance to Adhesion*, Vol. 5. VSP/Brill, Leiden (2009).
23. M. Strobel, C. S. Lyons and K. L. Mittal (Eds), *Plasma Surface Modification of Polymers: Relevance to Adhesion*. VSP, Utrecht (1994).
24. K. Ročková, V. Švorčík, L. Bačáková, B. Dvořánková and J. Heitz, *Nucl. Instrum. Meth. Phys. Res. B* **225**, 275 (2004).
25. O. Kubová, V. Švorčík, J. Heitz, S. Moritz, C. Romanin, P. Matějka and A. Macková, *Thin Solid Films* **515**, 6765 (2007).
26. J. Siegel, A. Řezníčková, A. Chaloupka, P. Slepička and V. Švorčík, *Radiation Effects Defects Solids* **163**, 779 (2008).
27. K. S. Kim, C. M. Ryu, C. S. Park, G. S. Sur and C. E. Park, *Polymer* **44**, 6287 (2003).
28. V. Kotál, V. Švorčík, P. Slepička, O. Bláhová, P. Šutta and V. Hnatowicz, *Plasma Process. Polym.* **4**, 69 (2007).
29. L. Lavielle and J. Schultz, *J. Colloid Interface Sci.* **106**, 438 (1985).
30. L. Lavielle, J. Schultz and A. Sanfeld, *J. Colloid Interface Sci.* **106**, 446 (1985).
31. J. U. Sommer and G. Reiter (Eds), *Polymer Crystallization: Observation, Concepts and Interpretation*. Springer-Verlag, Berlin, Germany (2003).
32. E. Filová, L. Bačáková, V. Lisá, D. Kubies, L. Machová, M. Lapčíková and F. Rypáček, *Eng. Biomater.* **7**, 19 (2004).

Biotechnology Advances 29 (2011) 739–767

Contents lists available at ScienceDirect

Biotechnology Advances

journal homepage: www.elsevier.com/locate/biotechadv

Research review paper

Modulation of cell adhesion, proliferation and differentiation on materials designed for body implants

Lucie Bacakova [a,*], Elena Filova [a], Martin Parizek [a], Tomas Ruml [b], Vaclav Svorcik [c]

[a] Department of Growth and Differentiation of Cell Populations, Institute of Physiology, Academy of Sciences of the Czech Republic, Videnska 1082, 142 20 Prague 4-Krc, Czech Republic
[b] Department of Biochemistry and Microbiology, Institute of Chemical Technology, 166 28 Prague, Czech Republic
[c] Department of Solid State Engineering, Institute of Chemical Technology, 166 28 Prague, Czech Republic

ARTICLE INFO

Article history:
Received 15 February 2011
Received in revised form 30 May 2011
Accepted 9 June 2011
Available online 26 July 2011

Keywords:
Biomaterial
Material surface properties
Surface patterning
Bioactivity
Cell–material interaction
Tissue engineering
Bioartificial tissue
Nanotechnology
Stem cells

ABSTRACT

The interaction of cells and tissues with artificial materials designed for applications in biotechnologies and in medicine is governed by the physical and chemical properties of the material surface. There is optimal cell adhesion to moderately hydrophilic and positively charged substrates, due to the adsorption of cell adhesion-mediating molecules (e.g. vitronectin, fibronectin) in an advantageous geometrical conformation, which makes specific sites on these molecules (e.g. specific amino acid sequences) accessible to cell adhesion receptors (e.g. integrins). Highly hydrophilic surfaces prevent the adsorption of proteins, or these molecules are bound very weakly. On highly hydrophobic materials, however, proteins are adsorbed in rigid and denatured forms, hampering cell adhesion. The wettability of the material surface, particularly in synthetic polymers, can be effectively regulated by physical treatments, e.g. by irradiation with ions, plasma or UV light. The irradiation-activated material surface can be functionalized by various biomolecules and nanoparticles, and this further enhances its attractiveness for cells and its effectiveness in regulating cell functions. Another important factor for cell–material interaction is surface roughness and surface topography. Nanostructured substrates (i.e. substrates with irregularities smaller than 100 nm), are generally considered to be beneficial for cell adhesion and growth, while microstructured substrates behave more controversially (e.g. they can hamper cell spreading and proliferation but they enhance cell differentiation, particularly in osteogenic cells). A factor which has been relatively less investigated, but which is essential for cell–material interaction, is material deformability. Highly soft and deformable substrates cannot resist the tractional forces generated by cells during cell adhesion, and cells are not able to attach, spread and survive on such materials. Local variation in the physical and chemical properties of the material surface can be advantageously used for constructing patterned surfaces. Micropatterned surfaces enable regionally selective cell adhesion and directed growth, which can be utilized in tissue engineering, in constructing microarrays and in biosensorics. Nanopatterned surfaces are an effective tool for manipulating the type, number, spacing and distribution of ligands for cell adhesion receptors on the material surface. As a consequence, these surfaces are able to control the size, shape, distribution and maturity of focal adhesion plaques on cells, and thus cell adhesion, proliferation, differentiation and other cell functions.

Contents

* Corresponding author. Tel.: +420 2 9644 3743; fax: +420 2 9644 2488.
E-mail addresses: lucy@biomed.cas.cz (L. Bacakova), filova@biomed.cas.cz (E. Filova), parizek@biomed.cas.cz (M. Parizek), tomas.ruml@vscht.cz (T. Ruml), vaclav.svorcik@vscht.cz (V. Svorcik).

0734-9750/$ – see front matter © 2011 Elsevier Inc. All rights reserved.
doi:10.1016/j.biotechadv.2011.06.004

1. Introduction

In recent years, artificial materials, particularly synthetic polymers, have been of growing importance in various biomedical technologies, including tissue engineering and transplantation medicine. However, for the construction of advanced bioartificial tissues and organs, the materials should not just be passively tolerated by the cells (as often happened in the "classical" materials of earlier generations) but should actively promote specific cell responses in a controllable manner. In other words, artificial cell carriers should act as analogs of the natural extracellular matrix (ECM), i.e. they should regulate the extent and strength of cell adhesion through the binding between cell adhesion receptors (e.g. integrins) and active parts of ECM molecules (e.g. specific amino acid sequences such as Arg-Gly-Asp, Bacakova et al., 2007a).

The extent and the strength of cell adhesion then play a decisive role in regulating the subsequent cell proliferation activity and switching between the proliferation and differentiation program in the cells. Anchorage-dependent cells do not divide (and even undergo apoptosis) without previous extension on the growth substrate — cell proliferation activity is therefore usually reported to correlate positively with cell flattening. However, this is true only to a certain degree — the maximum proliferation capacity as well as maximum migration speed is achieved at the intermediate extent of cell spreading and adhesion strength. Cells with very large adhesion areas with numerous and large focal adhesion plaques, containing increased levels of specific cell adhesion molecules and associated proteins (paxillin, talin, vinculin, tensin), are usually more quiescent concerning migration and proliferation, and more active in the expression of differentiation markers (Mann and West, 2002; for a review, see Bacakova and Svorcik, 2008; Bacakova et al., 2004).

The extent and strength of cell adhesion, and subsequent cell proliferation and differentiation, depend strongly on the physical and chemical properties of the biomaterial surface. Therefore, in this review, based mainly on our results obtained in the course of more than 10 years of research on biomaterials, the effects of the following factors on the adhesion, proliferation and phenotypic maturation of cells colonizing artificial materials are discussed:

- material surface chemistry, surface energy and wettability, and changes in these parameters, e.g. on synthetic polymers modified by ion-, ultraviolet light and plasma irradiation,
- the electrical charge and conductivity of the material surface,
- surface roughness and morphology,
- rigidity and deformability of the cell adhesion substrate,
- micropatterning the material surface with cell-adhesive and non-adhesive domains,
- nanopatterning and grafting the material surface (creation of adhesive nanodomains manipulating the assembly of focal adhesion plaques on cells).

It can be supposed that in most materials currently used for constructing tissue replacements, these factors have a common (universal) influence on the cell behavior, irrespective of material type. In various cell types, some common reactions to the basic physical and chemical properties of the adhesion substrate can also be expected. This review therefore focuses on common relations between the physico-chemical properties of material surface and cell behavior. Specific materials are only used as examples to demonstrate these relations. Specific materials (e.g. natural and synthetic polymers, metals, ceramics, carbon-based materials, composite materials and their specific organic and inorganic coatings) and specific types of tissue replacements (e.g. vascular prostheses, bone implants) have been discussed in several review articles and book chapters that we have published earlier (Bacakova and Svorcik, 2008; Bacakova et al., 2004, 2008, 2011; Parizek et al., 2011; Vagaska et al., 2010; Vandrovcova and Bacakova, 2011).

2. Chemistry, energy, polarity, wettability and zeta potential of the material surface

It has been shown repeatedly that cell adhesion to an artificial material depends strongly on the physico-chemical properties of the material surface, e.g. its chemical composition, energy, polarity and wettability. The chemical composition of the material surface is an important factor determining the surface energy, polarity, wettability and zeta potential, and consequently the character of the cell–material interaction. For example, the presence of oxygen-containing chemical functional groups increases the energy, polarity and wettability of the material surface, and supports the adhesion and growth of cells on this surface (Bacakova et al., 1996; Detrait et al., 1998; Feng et al., 2003; Kubova et al., 2007; Svorcik et al., 1995a,b).

The surface energy of a material is defined as the amount of energy per area required to reversibly create an infinitesimally small unit surface (Zhuang and Hansen, 2009). Surface energy quantifies the disruption of the intermolecular bonds that occur when a surface is created. In the physics of solids, surfaces must be intrinsically less energetically favorable than the bulk of a material, otherwise there would be a driving force for surfaces to be created, removing the bulk of the material, e.g. by a sublimation process. Surface energy may therefore be defined as the excess energy at the surface of a material compared to the bulk. The surface energy which can be converted into work has been referred to as "free surface energy" (also known as "free enthalpy", "available energy" or "affinity" in chemical systems). Free surface energy can be analyzed into polar and nonpolar (i.e. dispersive) components using the Owens–Wendt–Kaeble equation:

$$W_a = \gamma_L(\cos\theta + 1) = 2\left(\gamma L^D \gamma S^D\right)^{1/2} + 2\left(\gamma L^P \gamma S^P\right)^{1/2},$$

where γL^D and γL^P are the dispersive and polar components of the liquid surface tension, and γS^D and γS^P are the dispersive and polar components of the solid surface free energy, respectively (Youssef et al., 2001).

The dispersive component of surface energy results from molecular interaction due to London forces. These forces are part of the van der Waals forces and represent the weak intermolecular forces arising from quantum-induced instantaneous polarization multipoles in molecules. These forces can therefore act between molecules without permanent multipole moments. London forces are exhibited by nonpolar molecules because of the correlated movements of the electrons in interacting molecules. *The polar component of surface energy* comprises all other interactions due to non-London forces. Polar molecules interact through dipole–dipole intermolecular forces and hydrogen bonds. Molecular polarity is dependent on the difference in electronegativity between the atoms in a compound and the asymmetry of the structure of the compound. For example, a molecule of water is polar because of the unequal sharing of its electrons in a "bent" structure, whereas methane is considered non-

polar because the carbon shares the electrons with the hydrogen atoms almost uniformly.

The material surface energy, including its polar and non-polar components, can be calculated from the contact angle measured between the material surface and liquids of various polarity, e.g. benzyl alcohol, diiodomethane, glycerol or water (Youssef et al., 2001). Polar liquids are well spread on polar surfaces, i.e. they have a low contact angle. A low contact angle between the material and water indicate good spreading of water on the material surface, i.e. *hydrophilicity* of the material, while a high water contact angle is a sign of the *hydrophobicity* of the material surface. Thus, hydrophilic surfaces are characterized by a high polar component of the surface energy.

The hydrophilicity or hydrophobicity of the material surface can be further characterized by its zeta- (ζ-) potential. The determination of the ζ-potential on planar samples is based on the measurement of the dependence of streaming current I on pressure p. The ζ-potential is calculated from the relation

$$\zeta = \frac{dI}{dp} \cdot \frac{\eta}{\varepsilon \cdot \varepsilon_0} \cdot \frac{L}{A},$$

where d*I*/d*p* is the slope of *I* vs. *p* dependence; η and ε are the viscosity and the dielectric constant of the electrolyte, respectively; ε_0 is the vacuum permittivity; *L* and *A* are the length and the cross-section of the measuring channel (Svorcik et al., 2010a). The zeta-potential has been determined for pristine thermoplastic polymers (high-density polyethylene (PE), polytetrafluoroethylene (PTFE), polystyrene (PS), polyethyleneterephthalate (PET) and polypropylene (PP) and polymers treated in plasma (Reznickova et al., 2011; Slepicka et al., 2010; Svorcik et al., 2010b). The zeta-potential of pristine polymers increases in the order PTFE<PP≈PET<PE<PS. Its value is affected by several factors, e.g. surface morphology, chemical composition and the polarity of the polymer surface. It is therefore slightly surprising that the zeta-potential of polar PET and non-polar PP are comparable. A possible explanation can be found in an earlier study (Kotal et al., 2007), where it was revealed that in pristine PET most of oxygen-containing molecular segments are oriented toward the polymer bulk, and thus the first atomic layer on the material surface is effectively depleted of oxygen. Due to this phenomenon, pristine PET with a reduced surface concentration of oxygen and PP behave in the same manner. This can also be seen from the similar contact angle values. Plasma treatment results in a dramatic increase in the zeta-potential, and its values increase in the order PTFE<PP<PS<PET<PE.

Synthetic polymers used in biotechnologies and in medicine are usually too hydrophobic in their pristine unmodified state (a water drop contact angle of about 100° or more), thus they cannot ensure sufficient cellular colonization. It is generally known that cell adhesion to artificial materials is mediated by molecules of extracellular or provisional matrix, e.g. fibronectin, vitronectin, collagen, laminin or fibrin, which are spontaneously adsorbed to the materials from the culture media, blood and other body fluids, or are deposited by the cells themselves. If the material is too hydrophobic, these molecules are adsorbed in a denatured and rigid state. Their geometrical conformation is inappropriate for binding to cells, because specific sites on these molecules (e.g. RGD-containing oligopeptides) are less accessible to cell adhesion receptors, e.g. integrins (Fig. 1). As was shown above, polymer surfaces can be efficiently rendered more wettable by physical methods, e.g. by *irradiation by ions*, *plasma* or *ultraviolet light*. These methods are safer than chemical methods, e.g. etching the polymer surface by treatment in acids or hydroxides. They are not associated with potential retention of cytotoxic chemicals and their subsequent release from the material (Bacakova et al., 2000a,b, 2001a; Heitz et al., 2003; Kasálková et al., 2007; for a review, see Bacakova and Svorcik, 2008; Bacakova et al., 2004).

For *ion irradiation*, high-energy ions are formed in an ion source, separated in a magnetic field, and accelerated in an electric field. The material is placed in an implanter chamber and is irradiated at room temperature with an ion beam of defined energy (30–150 keV), dose (10^{12}–10^{17} ions/cm^2) and current (under 50 nA/cm^2 to avoid heat degradation of polymers). For biological purposes, ions of oxygen, nitrogen, the halogens, rare (noble) gases or non-toxic metals (e.g. Ti, Au) have usually been applied. Depending on their molecular weight and energy, the ions can either be released from the material immediately after implantation, or retained in it. The polymer surface can be modified to a depth of about 10 nm–100 μm. Ion bombardment leads to cleavage of C—C and C—H bonds, which results in splitting of macromolecules and polymer dehydrogenation. Due to polymer dehydrogenation, the content of carbon in the modified layer is relatively increased, which is often reported as "carbonisation". This relative carbon-enrichment is observed especially at higher ion doses, and is accompanied by a darker color and lower transparency of the polymer. Carbon atoms form graphitic structures with conjugated double bonds, which enhance the electrical conductivity of the polymer. The degradation products of polymer macromolecules also react with the oxygen present in the ambient atmosphere in the implanter chamber and create oxidized structures, e.g. carbonyl, carboxyl and ester groups, which increase the polymer surface polarity and wettability (Bacakova et al., 1996, 2000a,b, 2001a; Svorcik et al., 1995a,b). Similar modifications of the polymer surface were also observed after it was *irradiated with ultraviolet light* generated by an excimer lamp (Heitz et al., 2003; Mikulikova et al., 2005; Svorcik et al., 2004) or irradiated with *plasma* (Kasalkova et al., 2007; Parizek et al., 2006, 2007, 2009).

Oxygen-containing groups increase the polar component of the surface free energy of the polymer surface, making this surface more wettable, stickier and more susceptible to adsorption of adhesion-mediating ECM proteins, e.g. vitronectin, fibronectin, collagen or laminin. At the same time, the adsorption of cell non-adhesive molecules, e.g. albumin, is attenuated because these molecules prefer to bind to less oxygenated and more hydrophobic surfaces (Bacakova et al., 1996; Svorcik et al., 1995a; for a review, see Bacakova et al., 2004; Lim et al., 2007a; Liu et al., 2007). In our earlier study, the intensity of fluorescence of collagen IV (i.e. an important component of cell basal laminae supporting cell adhesion) conjugated with a fluorescence marker Oregon Green 488, was increased on polyethylene samples irradiated with O or C ions (Bacakova et al., 2001a). On the other hand, on some hydrophilic materials, e.g. surfaces formed by plasma polymerization of acrylic acids, the absolute amount of cell adhesion-mediating ECM molecules was lower than on more hydrophobic surfaces created from octadiene (Filova et al., 2009a). Nevertheless, the cells adhered in higher numbers to more hydrophilic materials and were spread over a larger area. An explanation for these results may be that what is important is not only the absolute amount, but also the spatial conformation of the adsorbed molecules that mediate cell adhesion. On wettable surfaces, these molecules are adsorbed in a more flexible form, which allows them to be reorganized by the cells and thus provides access for cell adhesion receptors to the adhesion motifs on these molecules. A high amount of adsorbed protein could even be disadvantageous for cell adhesion, due to denaturing of the proteins. For example, model globular proteins (hen egg lysozyme, ribonuclease A, and insulin dimer) were adsorbed to nonpolar hydrophobic surfaces, created by functionalization of self-assembled monolayers with non-polar $-CH_3$ and $-CF_3$ groups, in higher concentrations than to polar hydrophilic surfaces with PEG, –OH, or $-CONH_2$ groups. However, the high protein concentration led to significant interprotein and protein–surface interactions. In addition, nonpolar surfaces allowed protein unfolding by reducing the unfolding free energy barriers. As a result, a rigid adsorbed layer of proteins was formed on hydrophobic surfaces. However, on polar hydrophilic surfaces, the proteins adsorb in low

concentrations, and their interprotein interactions were not significant; therefore they adsorbed in their native state (Anand et al., 2010). Corresponding results were also obtained on the cell adhesion-mediating protein fibronectin. On functionalized self-assembled monolayers, the amount of adsorbed fibronectin decreased in the following order of functionalities: $NH_2 > CH_3 > COOH > OH$, while the adhesion of MC3T3-E1 osteoblast-like cells, mediated by $\alpha_5\beta_1$ integrin adhesion receptors, increased in a similar order, i.e. $CH_3 < NH_2 = COOH < OH$, which can be

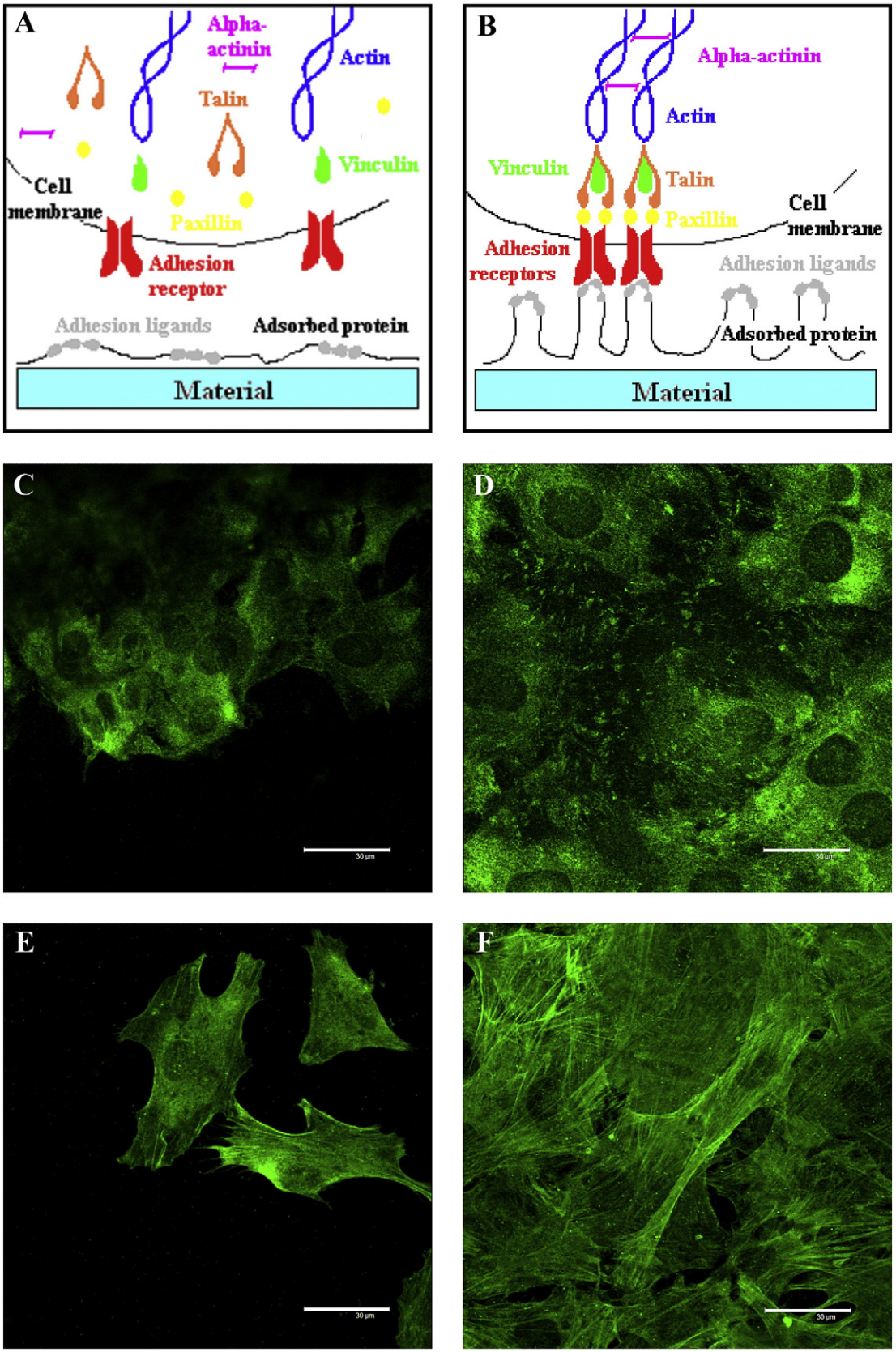

explained by changes in the geometrical conformation of fibronectin (Keselowsky et al., 2003).

However, there is optimal cell adhesion only to moderately hydrophilic surfaces. On highly hydrophilic surfaces, cell attachment and spreading is limited or completely disabled. Highly hydrophilic surfaces are known to bind the adsorbed cell adhesion-mediating molecules with relatively weak forces, which could lead to the detachment of these molecules especially at later culture intervals, when they bind a large number of cells. For example, in our studies performed on oxygen-terminated nanocrystalline diamond surfaces (contact angle about 20–35°), human osteoblast-like MG 63 cells in 5- and 7-day-old cultures, when these cells formed a confluent layer, showed a higher tendency to spontaneous detachment from the adhesion substrate (Grausova et al., 2008a, 2009a,b). However, on H-terminated nanocrystalline diamond surfaces (contact angle about 85–90°, highly confluent layers of MG 63 cells on day 7 after seeding adhered firmly without considerable cell loss (Kopecek et al., 2008). Moreover, extremely hydrophilic oxygen-terminated nanostructured diamond surfaces (contact angle <2°) almost completely resisted the adhesion of human mesenchymal stem cells derived from the bone marrow, whereas less hydrophilic nanodiamond surfaces (contact angle 86°) provided good support for the attachment, spreading and growth of these cells (Clem et al., 2008). Highly hydrophilic surfaces, made of a block copolymer of poly DL-lactide (PDLLA) and polyethylene oxide (PEO), resisted the adhesion and spreading of rat aortic smooth muscle cells in our studies, and were used as a non-adhesive background for the attachment of GRGDS sequences, i.e. synthetic fibronectin-derived ligands for integrin adhesion receptors in defined concentrations (Bacakova et al., 2007a; Fig. 2). Moreover, in this copolymer, high hydrophilicity was coupled with high mobility of PEO chains tethered from the material surface, which did not allow stable adsorption of cell adhesion-mediating ECM molecules and cell adhesion. This bioinertness of the PDLLA–PEO copolymer depended on the length and concentration of the PEO chains on the material surface, and was optimal at a molecular weight of PEO of 11,000 and at a concentration of 33% (Bacakova et al., 2007a). At both lower and higher molecular weight of PEO (5000 and 24,800), and at lower and higher concentration of PEO chains (5 to 18% and 40 to 70%), PDLLA–PEO copolymers allowed protein adsorption and cell adhesion, though the number of adhering cells, their spreading and subsequent growth were usually lower than on non-modified PDLLA (Filova et al., 2004).

3. Grafting of modified polymers

The reactive sites formed in a polymer during its irradiation (e.g. irradiation by ions, plasma or ultraviolet light), such as radicals, conjugated double bonds between carbon atoms and oxygen-containing groups, can be used for *grafting* various molecules and nanoparticles which further modulate the effects of polymer irradiation on cell adhesion, growth, phenotypic maturation and functioning (Fig. 3). These biomolecules and nanoparticles include glycine, alanine and leucine (Svorcik et al., 2004), RGD-containing adhesion oligopeptides (Rockova-Hlavackova et al., 2004), bovine serum albumin, polyethylene glycol, colloidal carbon particles (Kasalkova et al., 2010; Parizek et al., 2009) and gold nanoparticles (Svorcik et al., 2009, 2010c).

In our recent study, polyethylene (PE) and polystyrene (PS) were modified by Ar^+ plasma. The plasma is able to exert four major effects: (i) surface cleaning, (ii) surface ablation or etching, (iii) surface cross-linking, and (iv) modification of the surface chemical structure. Plasma treatment leads to cleavage of C—C and C—H bonds. This results in splitting of macromolecules, and free radicals and conjugated double bonds are generated on the polymer chain. The degradation products of macromolecules also react with the oxygen present in the ambient atmosphere in the chamber and create oxidized structures, e.g. carbonyl, carboxyl and ester groups, which increase the polarity and wettability of the polymer surface (Kasalkova et al., 2007; Parizek et al., 2009). Oxidized degradation products are produced on the polymer surface, contributing to increased hydrophilicity (wettability) of the plasma treated polymers. Faster ablation of the amorphous phase was also reported for high density PE. Preferential ablation of PE results in the creation of lamellar structures reflecting the arrangement of the molecular chains on the PE surface (Svorcik et al., 2006). In PS with a lower crystalline fraction, the tiny, sharp formations appearing after plasma treatment may represent low molecular, oxidized structures (LMWOS) (Reznickova et al., 2011). The pristine polymers that were investigated exhibit very different surface morphology and roughness. It was found that under plasma treatment the polymers are ablated and their surface morphology and roughness are changed dramatically; the zeta potential increases dramatically, too (Reznickova et al., 2011).

The surface of the plasma-activated polymers was grafted with polyethylene glycol (PEG). The changes in the surface wettability (contact angle) of the modified polymers were examined by goniometry. Atomic force microscopy (AFM) was used to determine the surface roughness and morphology, and electrokinetical analysis (zeta-potential) characterized the surface chemistry of the modified polymers. Plasma treatment and subsequent PEG grafting led to dramatic changes in the surface morphology, roughness and wettability of the polymer. The plasma-treated and PEG-grafted polymers were seeded with rat vascular smooth muscle cells (VSMC), and their adhesion and proliferation were studied. Biological tests, performed in vitro, showed increased adhesion and proliferation of cells on modified polymers. Grafting with PEG increased cell proliferation, especially on PS. Cell proliferation was shown to be an increasing function of PEG molecular weight (Svorcik et al., in press).

In another study, polyethylene was irradiated with Ar^+ plasma, and the chemically active PE surface was grafted with Au nanoparticles. The composition and the structure of the modified PE surface were studied using X-ray photoelectron spectroscopy (XPS) and Rutherford backscattering spectroscopy (RBS). The changes in surface wettability were determined from the contact angle measured in a reflection goniometer. The changes in the surface roughness and morphology were observed by AFM. The modified PE samples were seeded with VSMC or mouse NIH 3T3 fibroblasts, and their adhesion and proliferation were studied. It was found that plasma discharge and Au grafting led to dramatic changes in the surface morphology and roughness of PE. Au nanoparticles were found not only on the sample surface, but also in the sample interior up to a depth of about 100 nm. In addition, plasma modification of the PE surface, followed

Fig. 1. A: Scheme of the adsorption of a cell adhesion-mediating protein to a hydrophobic material surface. The protein is adsorbed in a denatured and rigid form, and thus specific amino acid sequences in its molecule, which serve as ligands for the adhesion receptors, are non-accessible (or only to a limited extent accessible) for these receptors. The receptors cannot then cluster into focal adhesion plaques and associate with other structural and signalling proteins, such as paxillin, talin, vinculin, alpha-actinin and actin cytoskeleton. B: On moderately hydrophilic surfaces, the protein is adsorbed in a more physiological, flexible and reorganizable form, and the oligopeptidic ligands (usually in a loop-like conformation) are well accessible by a "pocket-like" structure of adhesion receptors (integrins). The receptors then cluster into focal adhesion plaques and communicate with other focal adhesion proteins and the actin cytoskeleton. C-F: Immunofluorescence staining of talin (C, D) and alpha-actin (E, F) in rat aortic smooth muscle cells on day 5 after seeding on hydrophobic unmodified high-density polyethylene (sessile water drop contact angle almost 100°; C, E) and moderately hydrophilic polyethylene irradiated with plasma and grafted with polyethylene glycol (contact angle ~60°, D, F). Note that on hydrophobic surfaces, the cells adhere in lower numbers, are less spread and assemble only faint talin-containing focal adhesion plaques and alpha-actin-containing fibers. On hydrophilic surfaces, the cell population density is much higher, the cells are better spread and assemble well-apparent talin focal adhesion plaques and alpha-actin fibers. Leica confocal laser scanning microscope (TCS SP2, Germany), obj. 100×, bar = 30 μm (Parizek et al., 2009; Kanchanawong et al., 2010).

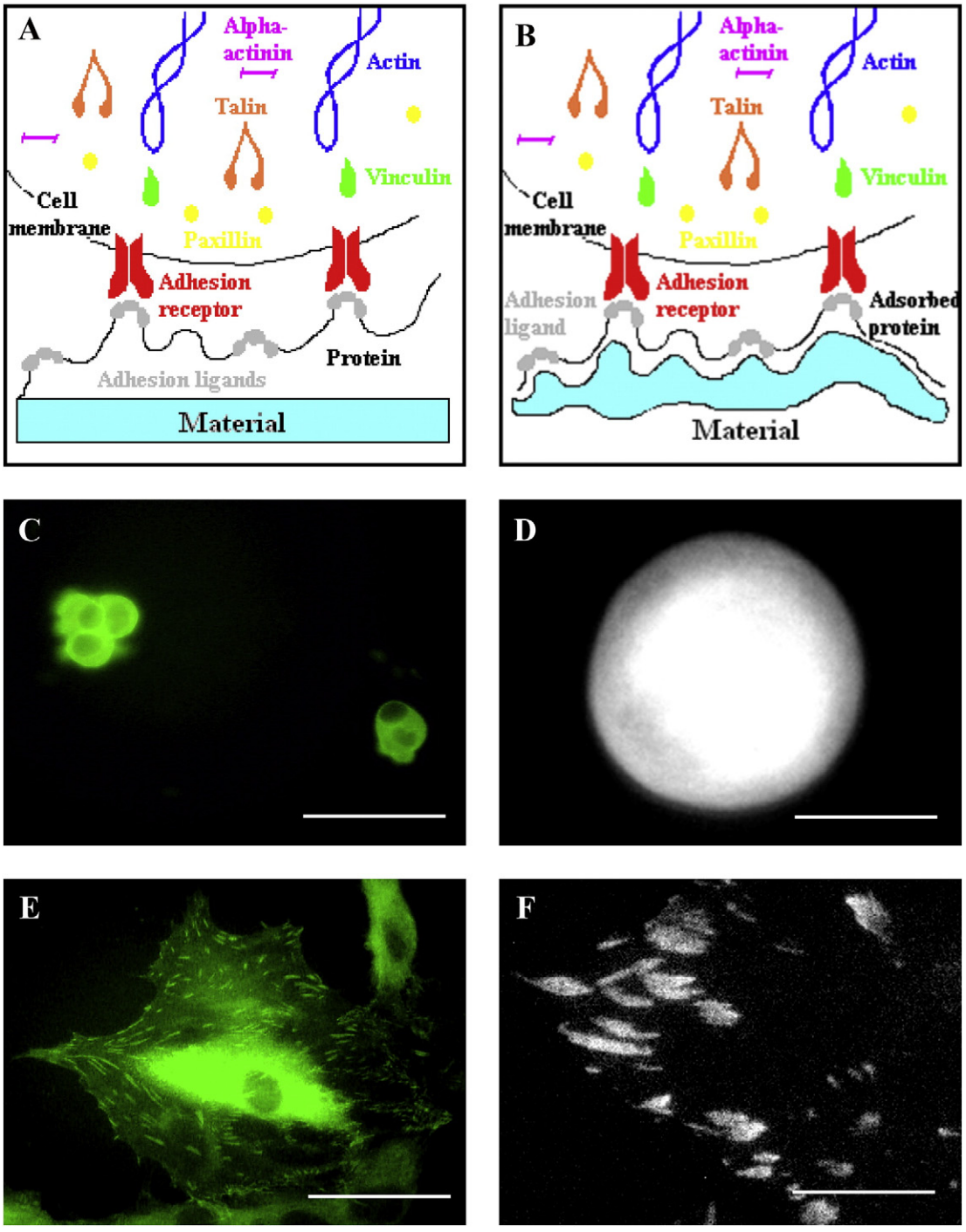

Fig. 2. A: Scheme of the adsorption of a cell adhesion-mediating protein to an extremely hydrophilic surface. This surface does not allow protein adsorption at all, or the adsorption is weak and unstable, thus the proteins cannot provide an adequately firm anchor for the adhering cells. Although the adhesion ligands in the protein molecule are accessible for cell adhesion receptors, these receptors cannot form focal adhesion plaques and associate with paxillin, talin, vinculin, alpha-actinin and actin. B: A similar situation on an extremely deformable material: although the proteins can be stably adsorbed on its surface, and the adhesion oligopeptides can be accessible for cell adhesion receptors, the material collapses under the tractional forces produced by the adhering cells. As a result, the cells are not able to assemble focal adhesion plaques and an actin cytoskeleton. C-F: Formation of focal adhesion plaques in rat aortic smooth muscle cells seeded on materials of various hydrophilicity and deformability. A PDLLA-PEO copolymer with a highly hydrophilic and mobile surface (contact angle less than 30°; C) or a soft polyacrylamide gel (modulus of elasticity 1 kPa; D) do not allow cell spreading and formation of focal adhesion plaques, even if the gel was preadsorbed with collagen. However, on pure PDLLA without hydrophilic and mobile PEO chains (contact angle ~70°; E), and also on a hard polyacrylamide gel (modulus of elasticity 40 kPa; F), the cells are well spread and assemble large and numerous focal adhesion plaques. Focal adhesion plaques were detected by immunofluorescence staining of vinculin (C, E) or by transfection of cells with a gene construct encoding paxillin and green fluorescence protein (D, F). C, E: epifluorescence Opton microscope (Axioplan, Germany) equipped with a DSC-F707 digital camera (Sony Corporation, Tokyo, Japan), bar = 100 μm. D, F: epifluorescence Nikon microscope, CCD camera, Image Pro Plus 3.0 software, bar = 20 μm (Bacakova et al., 2007a; Engler et al., 2004).

by grafting Au nanoparticles, significantly increased the attractiveness of the PE surface for the adhesion and growth of VSMC, and particularly for mouse embryonic 3T3 fibroblasts (Svorcik et al., 2009; Fig. 4).

4. Electrical charge and conductivity of the cell adhesion substrate

The electrical charge and conductivity of the material surface are also important factors for its colonization with cells. It has been shown

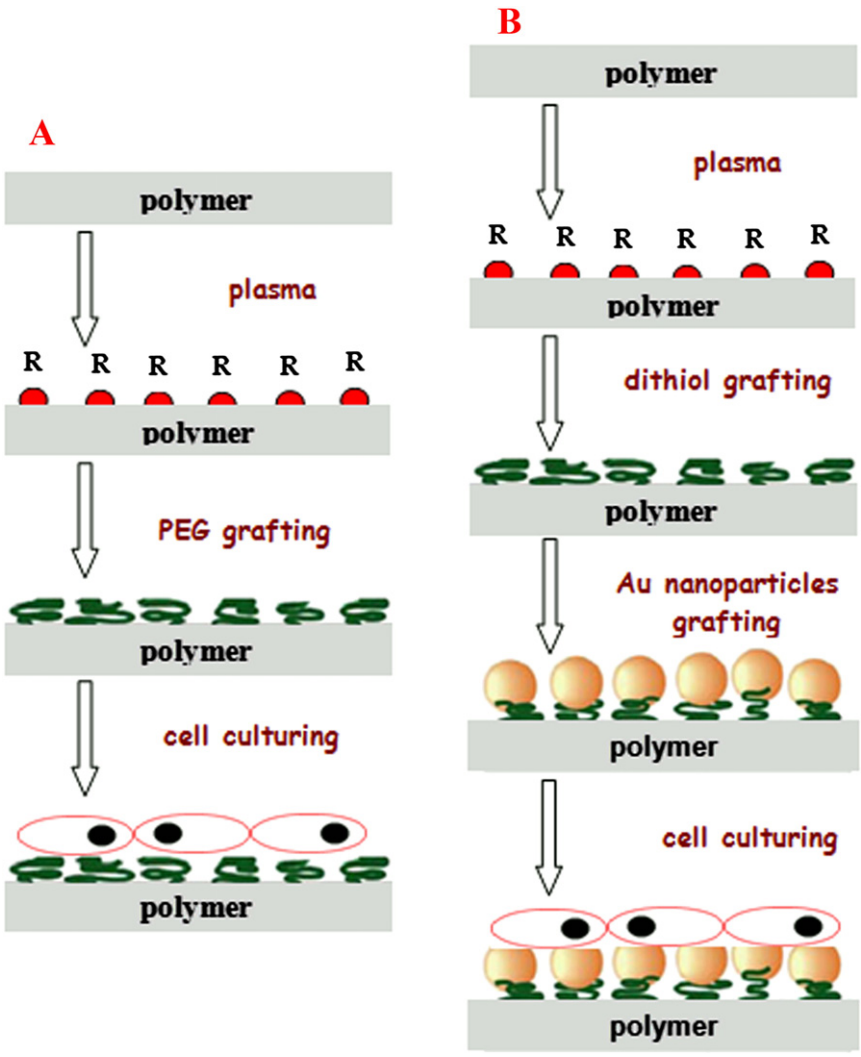

Fig. 3. Scheme of polymer surface activation (R = radical). A: the polymer was modified by plasma, the surface of the activated polymers was grafted with polyethylene glycol, and then the surface was seeded with rat vascular smooth muscle cells (VSMC; Svorcik et al., in press); B: the polymer surface was modified by plasma, grafted by dithiol and Au nanoparticles, and seeded with VSMC (Svorcik et al., 2009).

repeatedly that there is better cell adhesion to positively charged surfaces than to negatively charged surfaces. The reason is that cell adhesion-mediating ECM molecules are negatively charged, thus they adsorb preferentially to positively charged surfaces. In accordance with this idea, the stromal cells in cultures derived from rat bone marrow adhered in significantly higher densities to hydrogels based on 2-hydroxyethyl methacrylate (HEMA) bearing positively charged chemical functional groups (e.g. NH_4^+) than to negatively charged hydrogel surfaces (Lesny et al., 2006). In our earlier studies performed on polytetrafluoroethylene irradiated with ultraviolet light in a reactive NH_3 atmosphere, the positively chargeable amine groups formed on the material surface also acted synergetically with oxygen-containing groups in stimulating adhesion and growth of rat aortic smooth muscle cells, mouse 3T3 fibroblasts, human umbilical vein endothelial cells and human embryonic kidney cells (Heitz et al., 2003; Mikulikova et al., 2005; Parizek et al., 2007).

Like on surfaces with different wettability, also on surfaces with a different electrical charge, the spatial orientation and the biofunctionality of the adsorbed cell adhesion-promoting ECM proteins is more important than the absolute number of these molecules. On self-assembled monolayers of alkanethiols terminated with positively charged $–NH_2$ group or negatively charged –COOH group, the amount of ECM protein osteopontin adsorbed to both surfaces was similar, but there is a much higher number and a much greater spreading area of bovine aortic endothelial cells on the $–NH_2$ surface than on the –COOH surface. These results suggested that the orientation and the geometrical conformation of osteopontin was more favorable for cell adhesion and spreading on a positively charged $–NH_2$ surface than on a negatively charged –COOH surface (Liu et al., 2005). Similarly, on surfaces patterned with positively and negatively charged microdomains, rat calvarial osteoblasts flattened better on positively charged surfaces, and mineralized tissue was also preferentially localized on positively charged regions. This cell behavior was probably mediated by a more advantageous geometrical conformation of vitronectin and fibronectin on positively charged surfaces (for a review, see Anselme, 2000). However, the negative charge reduced the cell–material adhesion, and also the cell-to-cell adhesion, as observed in starfish embryonic cells in situ (Masui et al., 2002) or between endothelial cells and platelets (Stoltz et al., 1999).

Interestingly, negatively charged –COOH groups display a dual effect on cell–material adhesion. As relatively highly polar groups, –COOH groups can modulate the material surface wettability to values suitable for cell adhesion (Bet et al., 2003). In addition, –COOH groups allow grafting of various biomolecules supporting cell adhesion and growth, such as epidermal growth factor, collagen IV and chondroitin sulfate (von Recum et al., 1999). In our earlier studies, there was also

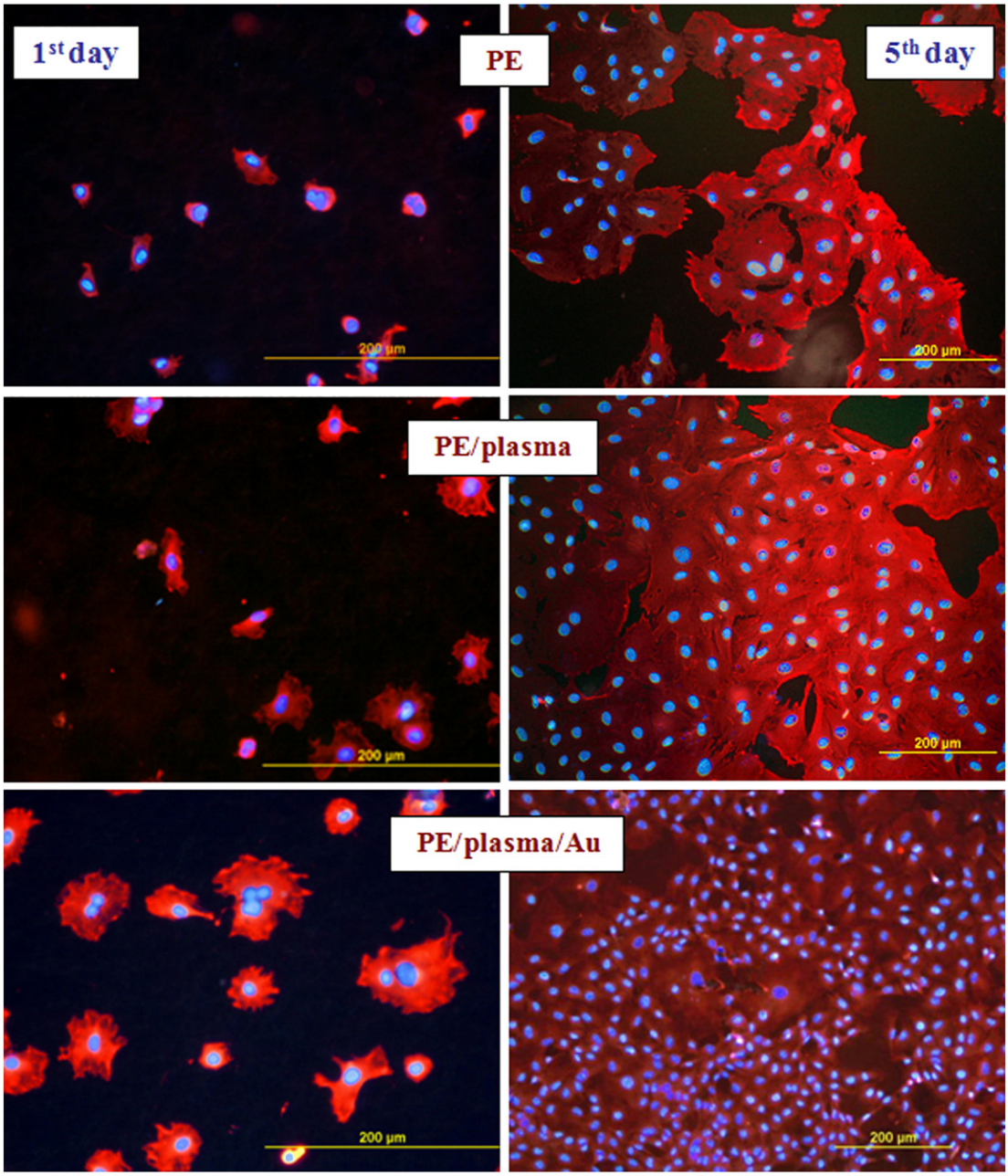

Fig. 4. Morphology of rat vascular smooth muscle cells adhered (1st day) and grown (5th day) on pristine polyethylene (PE), PE treated for 150 seconds with Ar^+ plasma (PE/plasma) and subsequently grafted with Au nanoparticles (PE/plasma/Au). Cells stained with Texas Red C_2-maleimide and Hoechst #33342. Olympus IX 51 microscope, DP 70 digital camera, obj. 20× (left column) or 10× (right column), bar = 200 μm (Svorcik et al., 2009).

higher colonization of a copolymer of poly(DL-lactic acid) and poly (ethylene oxide) with rat aortic smooth muscle cells on carboxylated PEO than on non-carboxylated PEO (Bacakova et al., 2003, 2007a). However, the introduction of negatively charged carboxyl groups to the adhesion substrate reduced the adhesion of human erythroleukemia cells on type I collagen matrices in vitro (Bet et al., 2003). Carboxyl groups on a copolymer of hydroxyethyl methacrylate and sodium methacrylate reduced the adhesion and spreading and fusion of macrophages (Smetana et al., 1993). However, in another study, a negative charge of chemically modified films of bovine collagen did not dramatically alter the attachment of endothelial cells and fibroblasts (Tiller et al., 2001).

Sulphonate groups are a more typical example than –COOH groups of negatively charged groups suppressing cell adhesion. Pendant sulphonate groups have been used for constructing anticoagulant blood-contacting surfaces repulsive for blood components (Lee et al., 2002; Park et al., 2002).

In connection with the irradiation of polymers with ions, UV light or plasma, unsaturated carbon atoms may also react with each other to form long carbon chains with conjugated double bonds which provide higher electrical conductivity of the polymer surface (Bacakova et al., 1996; Svorcik et al., 1995a). Higher electrical conductivity was also achieved on polymers chemically doped with carbon black, and this was one of the factors stimulating adhesion and growth of rat aortic smooth muscle cells on these surfaces (Svorcik et al., 1995b), on polylactide mixed with carbon nanotubes (Supronowicz et al., 2002) and on boron-doped nanocrystalline diamond films (Kromka et al., 2010). An important consideration is that electrically conductive materials improve the cell performance even without active electrical stimulation of cells. However, cell colonization and functions are further enhanced

by stimulating cells with an electrical current and an electromagnetic field in special chambers or bioreactors. This stimulation leads to the activation of phospholipase C-coupled cell surface receptors, inositol triphosphate-dependent intracellular processes and influx of Ca^{2+} ions through mechanically operated stretch-activated cationic channels in the cell membrane. The increased cytosolic Ca^{2+} is then the starting point for signaling pathways targeting specific genes regulating cell growth, differentiation and specific functions (Khatib et al., 2004; Sun et al., 2007). Cell–substrate adhesion, mediated by integrin receptors, the function of which is calcium-dependent, is also affected by electrical stimulation (Sun et al., 2007). Both electrical and electromagnetic stimulation increased the proliferation of osteoblasts, as well as switching between a proliferation program and a differentiation program in these cells, manifested by higher synthesis of ECM molecules, such as osteocalcin, collagen I and decorin, activity of alkaline phosphatase and calcium deposition (Fassina et al., 2007; Khatib et al., 2004; Sun et al., 2007; Tsai et al., 2007). Cardiomyocytes in cultures exposed to a pulsed electrical field generated by a cardiostimulator contained troponin I, a marker of differentiation of this cell type, a well developed contractile apparatus, and they contracted synchronously with the electrical pulses (Karp et al., 2006). Neuronal cells in cultures on electrically conductive substrates, e.g. layers or scaffolds containing carbon nanotubes, showed increased electrical signal transfer and synaptic stimulation, especially when stimulated by an electrical field (Lovat et al., 2005; Malarkey and Parpura, 2007; Mazzatenta et al., 2007).

5. Material surface roughness and morphology

Several degrees or grades of surface roughness can be distinguished according to the scale of the irregularities of the material surface. Surface macroroughness is characterized by irregularities distinguishable by the human eye, i.e. from at least 100 μm to millimeters or more in size. Microscale surface roughness can be defined by irregularities from 1 to 100 μm, submicron surface roughness from 100 nm to 1 μm, and nanoroughness is specified by irregularities less than 100 nm (Price et al., 2004; Webster et al., 2000a,b, for a review, see Bacakova et al., 2007b, 2008; Vagaska et al., 2010). Each type of surface roughness has a specific influence on the behavior of the implant and also on the adhering cells.

Macroroughness seems to be favorable, because the relatively large irregularities may mechanically enhance the anchorage of the implant in the surrounding bone tissue. At the same time, the irregularities are too large to be felt by the cells (i.e. the cells can have enough space to spread on the irregularities or between them; thus macroroughness usually does not restrict cell adhesion and spreading.

Surface *microroughness* is a more controversial factor affecting the behavior of cells on artificial materials. The cells typically studied on these materials, i.e. anchorage-dependent mammalian cells of various tissues and organs, including vascular tissue or bone, are usually between 10 μm and 50 μm in diameter, if they are in suspension, where they acquire a rounded shape. When adhered and spread on the material surface, their spreading area can reach from several hundreds to several thousands of μm^2. Thus, these cells are inherently sensitive to the microtopography of their environment, and many studies have reported that microroughness significantly affected the cell response to the material (for a review, see Stevens and George, 2005). Some studies have reported a positive influence of surface microroughness on cell adhesion, growth and maturation, whereas in other studies this influence has been considered negative.

As for the *positive effects*, microporous surfaces of titanium dental implants increased the spreading of rat osteoblasts in primary cultures derived from rat calvarial bones (Sammons et al., 2005). Human osteoblast-like MG 63 cells, grown on Ti substrates with microscale surface roughness, exhibited a more differentiated phenotype, characterized by increased alkaline phosphatase activity and osteocalcin, and generated an osteogenic microenvironment through higher production of prostaglandin E_2 (PGE_2) and transforming growth factor β_1 (TGF-β_1). These stimulatory effects of the surface microtopography were further enhanced by higher surface energy and wettability, as well as the addition of 1,25-dihydroxyvitamin D_3 [$1\alpha,25(OH)_2D_3$] (Zhao et al., 2005). Conversely, surface microroughness enhanced the responses of osteoblasts to 1,25-dihydroxyvitamin D_3, and 17β-estradiol, and these response were probably mediated by β_1-integrins (Boyan et al., 2003; Lohmann et al., 2000; Wang et al., 2006). The stimulatory effects of bone morphogenetic protein-2 (BMP-2) and dexamethasone on the production of mineralized bone extracellular matrix, closely resembling natural physiological bone matrix, were also enhanced on surfaces with microscale roughness, whereas on flat surfaces, represented e.g. by plastic culture dishes, the matrix mineralization exhibited a dystrophic character (Boyan et al., 2002). On Ti–6Al–4V alloy, widely used for constructing artificial joint prostheses and other bone implants, MG 63 cells showed increased expression (i.e. increased RNA synthesis) of genes for mitogen-activated kinase ERK2 and cytoskeletal protein β-actin (Kim et al., 2005). In immature preosteoblastic cells, represented by human embryonic palatal mesenchymal cells, the microtopography of the adhesion substrate induced expression of genes encoding Runx2, osteocalcin and alkaline phosphatase, which are signs of the acquisition of osteoblast phenotype by these cells (Schneider et al., 2004). At the same time, increasing surface microroughness reduced the activity of osteoclasts, and thus bone resorption (Lossdörfer et al., 2004).

There are also several examples of *negative effects* of surface microroughness on material colonization with cells. On a Ti–6Al–4V alloy, the number of MG 63 cells was significantly lower on a surface with microscale roughness than on smoother surfaces with submicron roughness. In addition, the cells on the rougher surface were incompletely spread, i.e. they adopted an irregular, elongated shape with many processes extending out, whereas the cells on smoother surfaces were well-flattened and covered the material surface homogeneously. On rough surfaces, the cells proliferated more slowly and reached lower cell population densities (Kim et al., 2005). Similarly, on alumina-blasted Ti with surface microroughness, the osteoblasts (in cultures obtained from the endosteum surface of the bone marrow cavity in mice) did not spread completely, and their proliferation rate, viability and activity of alkaline phosphatase were diminished in comparison with flatter surfaces (Sader et al., 2005). Other authors have also reported a lower cell number on microstructured surfaces than on flat surfaces (Boyan et al., 2002; Lohmann et al., 2000). Similarly, in our studies performed on composite materials containing carbon matrix reinforced with carbon fibers (so-called carbon fiber-reinforced carbon composites, CFRC), the surface microroughness, due to the prominence of the carbon fibers over the carbon matrix, decreased the number of attached MG 63 cells and vascular smooth muscle cells, their spreading and also their proliferation activity. In MG 63 cells, the formation of vinculin-containing focal adhesion plaques and the proliferation activity were also lower than on polished composites with surface roughness on the submicron scale (Bacakova et al., 2001b; Stary et al., 2003a,b).

However, the mechanism of this dual effect of surface microroughness on cell colonization still remains unclear. As several authors have pointed out, this is especially due to the lack of a systematic study of this factor (Stevens and George, 2005; Zhao et al., 2006). This problem can be directly related to the problem of defining surface roughness. The most widely used parameter for characterizing surface roughness is R_a, i.e. the average peak-to-valley height. However, this measure does not give any record of the type of surface topography, for example the spacing between the irregularities, their different shapes, e.g. pyramids, cones, ridges, grooves, round pores, the curvature of the valleys, and especially the sharpness of the peaks on the material surface, which could hamper cell adhesion and spreading (Bacakova et al., 2001b, 2004; Zhao et al., 2006). It is therefore difficult to compare the data from different research groups. The cell behavior on rough surfaces is also dependent

on other physical and chemical properties of these surfaces, e.g. surface energy and wettability. For example, on microstructured surfaces created on silicone substrates by laser irradiation, poor adhesion and spreading of NIH/3T3 fibroblasts on highly rough surfaces was improved by increasing the wettability of the material surface (Ranella et al., 2010).

Submicron-scale roughness of the material surface also exerted dual effects on cell adhesion, growth, viability and maturation, though the positive influences usually prevailed. For example, the number of MG 63 cells on titanium disks with submicron surface roughness (R_a of 700 and 400 nm) reached lower values than on the flatter nanostructures ($R_a = 60$ nm), and had a less spread, elongated morphology (Zhao et al., 2006). However, the cells on disks with submicron surface roughness produced more PGE_2 and TGF-β_1, i.e. factors promoting osteoblastic activity, and more osteocalcin, a calcium-binding ECM glycoprotein considered as an important marker of osteogenic cell differentiation (Zhao et al., 2006). In our studies performed on nanocrystalline diamond layers with a nanostructure and a hierarchically organized submicron-nanostructure, bovine pulmonary artery endothelial cells of the line CPAE reacted more sensitively to the material surface roughness than bone-derived MG 63 cells. The numbers of MG 63 cells were similar on both types of surfaces, whereas the number of CPAE cells was significantly lower on the surface with submicron scale roughness. A possible explanation is that the spreading of CPAE cells, which are relatively large and have a flat polygonal morphology, on the micro–nano NCD, and their subsequent growth, may be hampered by the micro-sized surface irregularities (Grausova et al., 2008a).

Nanoscale roughness of the material surface has been unambiguously considered as a desirable factor that has a positive influence on the adhesion, growth and maturation of cells. The reason is that the nanostructure of a material resembles the nanoarchitecture of the natural ECM, e.g. its organization into nanofibers, nanocrystals, nanosized folds of ECM molecules, etc. On nanostructured surfaces, the cell adhesion-mediating ECM molecules therefore adsorb in an appropriate geometrical orientation which gives cell adhesion receptors access to specific sites in ECM molecules, such as amino acid sequences like Arg-Gly-Asp (RGD), which serve as ligands for these receptors (Price et al., 2004; Webster et al., 2000a,b; for a review, see Bacakova et al., 2008). From this point of view, surface nanoroughness can be considered to act synergetically with the moderate hydrophilicity of the material surface described above. This also promotes the adsorption of cell adhesion-mediating molecules in bioactive physiological conformations. One of these factors can enhance or even compensate the effect of the other factor. On surfaces with the same nanoscale roughness but different wettability, the cell colonization and function was higher on more wettable surfaces. Conversely, on surfaces of the same wettability, the cell performance was better on nanostructured surfaces. For example, on three types of TiO_2 films (i.e. anatase, rutile and amorphous TiO_2) with surface irregularities of similar size (8 to 10 nm) but with different surface wettability, the adhesion, spreading, proliferation and activity of alkaline phosphatase in primary rat calvarial osteoblasts cultured on these films was higher on moderately wettable anatase surfaces (sessile water drop contact angle ~60°) than on rutile and amorphous TiO_2 surfaces with contact angle ~90° (He et al., 2008). The second example includes our earlier study performed on a terpolymer of polytetrafluoroethylene, polyvinyldifluoride and polypropylene. This material was relatively highly hydrophobic (contact angle about 100°; Table 1), and its flat surfaces allowed almost no cell adhesion and growth. However, the surface nanostructure of this substrate, obtained by mixing the terpolymer with carbon nanotubes, compensated the high hydrophobicity of this material, probably by keeping the adsorbed cell adhesion-mediating ECM molecules in a more appropriate spatial conformation for binding with the cell adhesion receptors. As a result, the terpolymer–nanotube composites markedly improved the adhesion and spreading of MG 63 cells, and increased the concentration of talin and vinculin in these cells, measured by the enzymatic immunosorbent assay (ELISA) per mg of protein (Bacakova et al., 2007b, 2008; Fig. 5). Similar behavior of MG 63 cells was observed on hydrophobic fullerene C_{60} films, which promoted the adhesion and growth of MG 63 cells in an extent similar to that observed on the control tissue culture polystyrene dishes (Grausova et al., 2008b, 2009c; Vandrovcova et al., 2008; Fig. 6).

Table 1
Sessile water drop contact angle and nanoscale surface roughness of the unmodified terpolymer of polytetrafluoroethylene, polyvinyldifluoride and polypropylene (0 wt.%) and terpolymer samples mixed with 2 wt.% or 4 wt.% of single-wall carbon nanohorns (SWCNH).

Concentration SWCNH	0 wt.%	2 wt.%	4 wt.%
Contact angle (°)	100 ± 1.6	104.5 ± 0.7 *	105.2 ± 0.7 **
R_a (nm)	30 ± 2.6	101.0 ± 8.7 **	150 ± 13.0 ***

R_a is the average deviation of the roughness profile from the mean line. Measured using the DSA 10 Mk2 automatic drop shape analysis system, Kruss, Germany (contact angle) and AFM (Ra). Mean ± SEM (Standard Error of Mean) from 6–10 measurements (contact angle) and 3 measurements (R_a). ANOVA, Student–Newman–Keuls method. Statistical significance: * $p \leq 0.05$, ** $p \leq 0.01$ and *** $p \leq 0.001$ compared to the values for the pure terpolymer.

Moreover, nanostructured surfaces are believed to promote preferential adhesion of osteoblasts over other cell types, such as fibroblasts, chondrocytes and smooth muscle cells. This has been explained by the preferential adsorption of vitronectin on nanostructured surfaces, due to its relatively small and linear molecule (15 nm in length) in comparison with other larger and more complicated ECM proteins, e.g. laminin, the configuration of which is cruciform and 70 nm both in length and in width (Price et al., 2003, 2004; Webster et al., 2000a,b). Another mechanism of the preferential adsorption of vitronectin, described on nanophase alumina, involves decreased adsorption of apolipoprotein A-I and/or increased adsorption of calcium to this material (Webster et al., 2001).

Vitronectin is then preferentially recognized by osteoblasts. This is mediated by heparan sulfate proteoglycan molecules on the cell membrane of osteoblasts, which recognize specific amino acid sequences, e.g. Lys-Arg-Ser-Arg (KRSR), in the heparin-binding domain of vitronectin. Another way is to bind RGD-containing oligopeptides in the vitronectin molecule by integrin receptors on osteoblasts (Dee et al., 1998; Webster et al., 2001). Thus, nanostructured surfaces could lower the risk of fibrous encapsulation of a bone implant and to enhance the integration of the implant with the surrounding bone tissue (Price et al., 2004). In accordance with this assumption, the adhesion, proliferation and phenotypic maturation of osteoblasts (measured by the synthesis of alkaline phosphatase and deposition of calcium-containing minerals), i.e. events which are important for the formation of regenerated bone tissue on the implant, were significantly greater on nanophase alumina, titania and hydroxyapatite (grain size less than 100 μm) than on conventional ceramics (grain size more than 100 μm; Webster et al., 2000a,b). Similarly, the osteogenic differentiation of rat bone marrow stromal cells, measured by the expression of genes for osteocalcin, osteopontin, osteonectin, collagen I and Runx2, was enhanced on nanostructured surfaces (created by the deposition of viral nanoparticles on glass slides) in comparison with conventional flat tissue culture polystyrene dishes (Kaur et al., 2008). Collagen nanofibers fabricated by electrospinning and collagen-coated P(L-lactic acid)-co-poly(ε-caprolactone) electrospun nanofibers were more efficient for adhesion of human bone marrow mesenchymal stem cells than collagen films cast on microscopic glass coverslips (Chan et al., 2009). On thin sheets of nanofibrous poly(L-lactic acid) (PLLA) matrix, mouse osteoblast MC3T3-E1 precursor cells exhibited an enhanced osteoblast differentiation phenotype, manifested by higher bone sialoprotein gene expression and significantly higher alkaline phosphatase activity than the cells on flat PLLA films (Hu et al., 2008).

Despite the preferential colonization of nanostructured surfaces by osteogenic cells, adhesion and growth was also stimulated in other cell

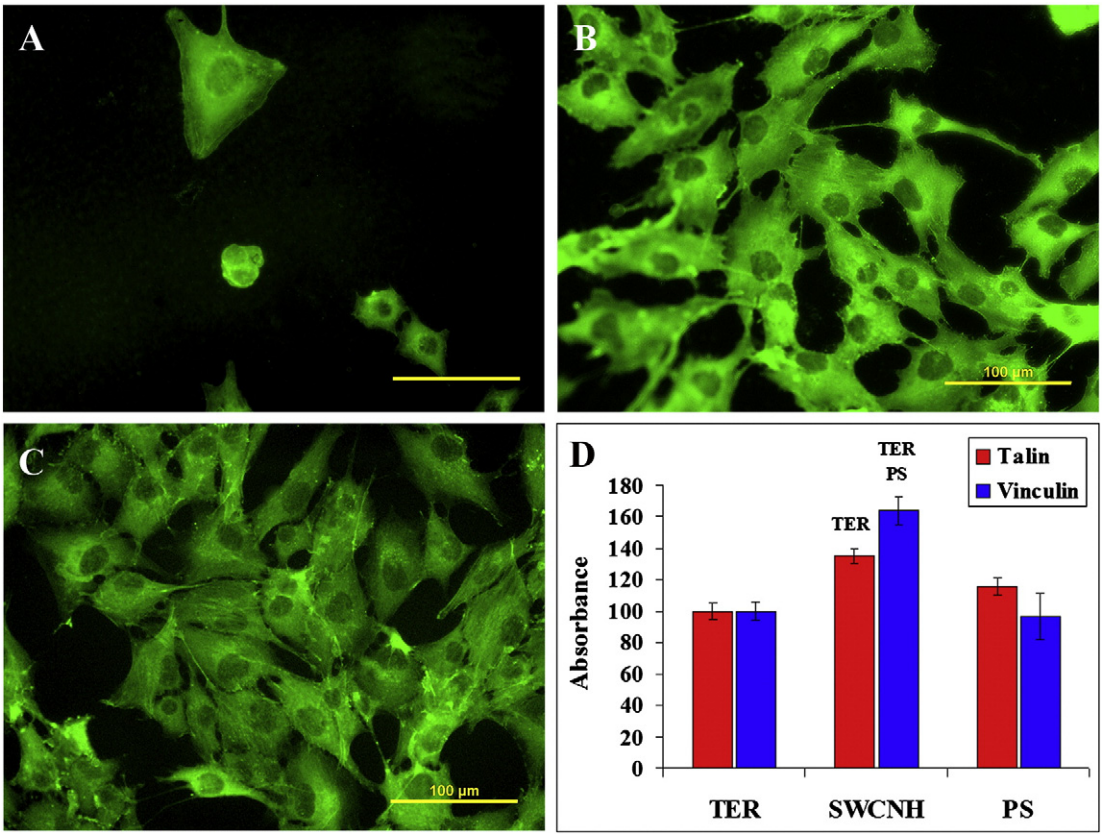

Fig. 5. Immunofluorescence staining of β-actin in human osteoblast-like MG 63 cells on day 3 after seeding on a pure terpolymer of polytetrafluoroethylene, polyvinyldifluoride and polypropylene (A), terpolymer mixed with 4 wt.% of single-wall carbon nanohorns (B) and a cell culture polystyrene dish (C). Olympus IX 51 microscope, DP 70 digital camera, obj. 20, bar = 100 μm. D: Concentration of focal adhesion proteins talin and vinculin in MG 63 cells on day 8 after seeding on pure terpolymer (TER), terpolymer mixed with 4 wt.% of single-wall carbon nanohorns (SWCNH), and a cell culture polystyrene dish (PS). Measured by ELISA per mg of protein; the absorbance values of cells from the modified terpolymers were expressed in % of the values obtained from the control cells grown on the unmodified terpolymer. Mean ± S.E.M. (Standard Error of Mean) from 4 measurements, ANOVA, Student-Newman-Keuls method. Statistical significance: $^{TER,\ PS}$: $p \leq 0.05$ compared to the corresponding values on the pure terpolymer and tissue culture polystyrene, respectively (Bacakova et al., 2007b, 2008).

types by these surfaces. On nanostructured poly(lactic-co-glycolic acid) (PLGA), designed for engineering bioartificial vascular grafts, the numbers of initially adhering rat vascular endothelial and smooth muscle cells, their proliferation activity and final population densities were higher than on conventional flat PLGA (Miller et al., 2004). Similar results were also obtained for ovine bladder smooth muscle cells (Thapa et al., 2003). This is probably because vitronectin (spontaneously adsorbed on the biomaterial surface) is bound by cells not only through the heparin-binding domain, but also through the RGD-containing oligopeptides in the vitronectin molecule, recognized by many cell types (Raimondo et al., 2010).

In addition, the material nanostructure minimizes the potential risk of the immunogenicity and inflammatory response of the material. The secretion of proinflammatory cytokines and chemokines, such as granulocyte colony stimulating factor (G-CSF), interferon gamma (INF-γ), macrophage inflammatory protein-1alpha (MIP-1α), tumor necrosis factor-alpha (TNF-α) or factor "regulated upon activation normal T cell-expressed and presumably secreted" (RANTES) was more attenuated in macrophages cultured on nanofibrous PLLA scaffolds than in cells on microfibrous PLLA scaffolds and planar PLLA films (Saino et al., 2011).

6. Rigidity and deformability of the adhesion substrate

The rigidity and flexibility of the adhesion substrate is usually taken into account to a lesser extent than the material chemistry, wettability and other physicochemical properties, though the mechanics of the adhesion substrate play a crucial role in the formation of cell–substrate adhesion complexes, assembly of the actin cytoskeleton, cell spreading, survival, growth activity and also the direction of the cell differentiation. In our earlier study (Engler et al., 2004), the behavior of rat vascular smooth muscle cells (line A7r5) differed strongly on matrices of the same chemical composition (i.e. polyacrylamide gels covalently bound with collagen) but of different elasticity. On soft polyacrylamide gels (modulus of elasticity $E = 1$ kPa), most of A7r5 smooth muscle cells were not able to form detectable cell–material adhesion complexes as well as actin cytoskeleton, and thus remained rounded, non-spread and became non-viable (Fig. 2). Similar results were also obtained on collagen gel ($E = 2.7$ kPa; Engler et al., 2004). An explanation is that extremely soft matrices do not allow a balance to be established between the cell tractional forces and the resistance of ECM to these forces, which is necessary for the assembly of functional cell–matrix adhesion complexes, actin cytoskeleton and cell spreading (Huang et al., 1998; Wang et al., 2001). Madin–Darby canine kidney (MDCK) cells in cultures on soft collagen gels down-regulated several signaling and structural proteins of focal adhesion complexes, such as focal adhesion kinase, talin, paxillin and p130Cas. This was due to the reduction of protein synthesis and the activation of proteases, such as calpain, and these processes were mediated by $alpha_2beta_1$ integrins, i.e. receptors for collagen on the cell membrane and thus the first detectors of matrix elasticity (Wang et al., 2003).

From this point of view, a certain analogy can be observed between extremely soft and extremely hydrophilic substrates for cell adhesion. Highly hydrophilic matrices do not allow stable adsorption of cell adhesion-mediating proteins, which are bound very weakly. Similar to extremely soft matrices, these proteins cannot resist the tractional forces produced by cells. They detach from the substrate and do not allow cell spreading. This effect of extreme hydrophilicity is further

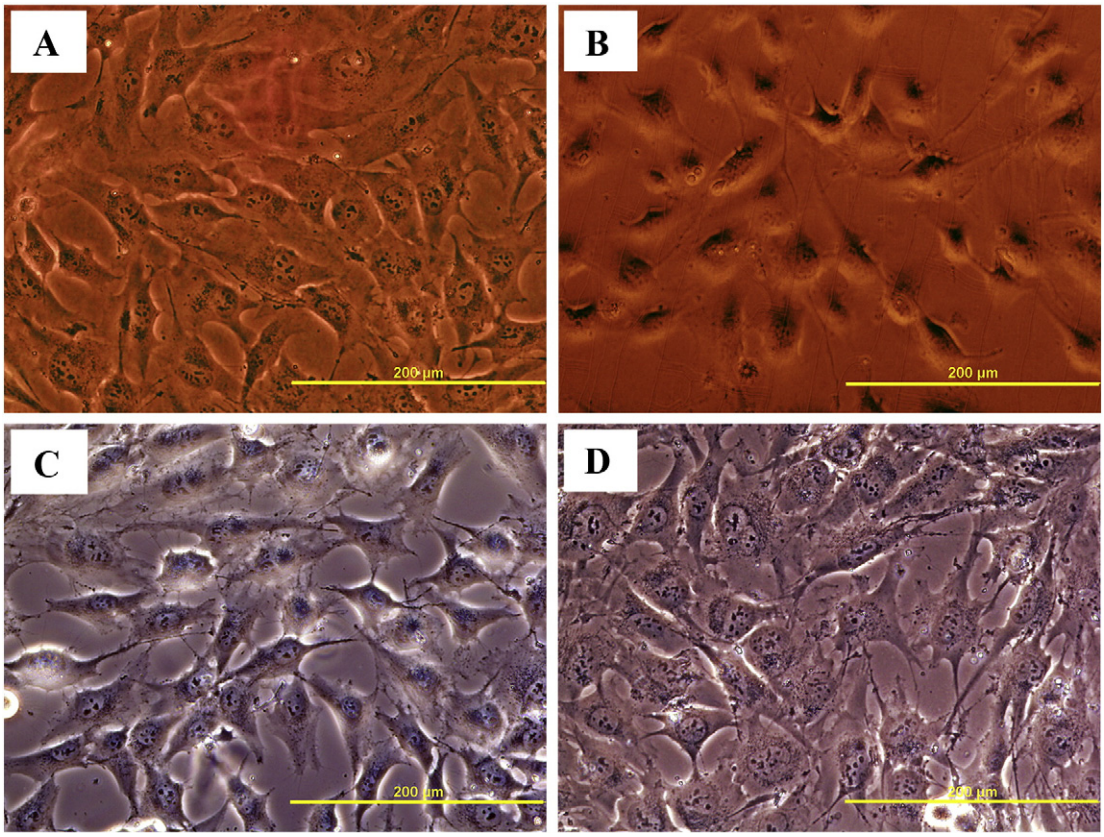

Fig. 6. Morphology of human osteoblast-like MG 63 cells in 7-day-old cultures on fullerene C_{60} layers 505 ± 43 nm in thickness (A) or 1090 ± 8 nm in thickness (B), a microscopic glass coverslip (C), which served as a substrate for fullerene deposition, and a standard cell culture polystyrene dish (D). Native cultures, Olympus IX 51 microscope, DP 70 digital camera, obj. 20×, bar = 200 µm (Grausova et al., 2009c).

potentiated by the mobility of the material surface, e.g. if this surface is formed by a brush of flexible polymeric chains, e.g. PEO chains (Bacakova et al., 2007a), which further increase the mechanical instability of the material surface (Fig. 2).

Stiffer matrices are therefore better tolerated by cells than extremely soft and irreversibly deformable substrates. Accordingly, harder polyacrylamide gels ($E = 8$ kPa) in our study promoted the assembly of focal adhesion plaques (Fig. 2), the formation of an actin cytoskeleton, and the spreading of A7r5 smooth muscle cells into a polygonal shape (Engler et al., 2004). In addition, on matrices with an elasticity gradient, the cells migrated from the softer regions to the stiffer regions, and the migration speed increased with substrate stiffness, even if the modulus of elasticity of all these matrices was in the range allowing cell spreading, i.e. from 10 to 400 kPa microelastic gradient hydrogels based on photocurable styrenated gelatin (Kidoaki and Matsuda, 2008), and from 500 to 2000 kPa in polydimethylsiloxane substrates (Tzvetkova-Chevolleau et al., 2008).

A very important finding is that the stiffness of the cell adhesion substrate is a decisive factor directing cell differentiation towards a certain phenotype. On very soft polyacrylamide gels ($E = 0.1$–1 kPa), mimicking the mechanical properties of soft brain tissue, human mesenchymal stem cells (MSCs) differentiated towards the neuronal phenotype, which was manifested by expression and upregulation of neuron-specific cytoskeletal markers such as nestin, β3 tubulin, neurofilament light chain (NFL) and an adhesion protein NCAM, as well as the formation of axon-like extensions of cells. On harder gels ($E = 8$ to 17 kPa), mimicking muscle tissue, MSCs acquired a myogenic phenotype, manifested by upregulation of myogenic factors such as MyoD. Finally, the stiffest matrices ($E = 25$ to 40 kPa) were osteogenic, as demonstrated by upregulation of the osteocalcin and transcriptional factor CBFα1 in MSC cells (Engler et al., 2006; for a review, see Rehfeldt et al., 2007).

Treatment with blebbistatin, an inhibitor of nonmuscle myosin II (NMM II) ATPase activity revealed that the lineage specification was mediated by one or all NMM II isoforms (A, B and C), involved in tensioning cortical actin structures, linked to focal adhesions. This pathway can ensure force transmission from inside the cell to the elastic matrix, as well as sensing the matrix elasticity that drives the lineage specification. It can be speculated that as the matrix stiffness increases, the cell alters its nonmuscle myosin expression in order to generate greater forces on its actin cytoskeleton, which would be necessary to deform a stiffer matrix. Accordingly, NMM II staining was diffuse on soft matrices. On moderately stiff matrices, myosin striations emerge that have an appearance described as premyofibrillar structures in cells differentiating toward myoblasts. In addition, stiff substrates promote focal adhesion growth and elongation, as well as increased expression of focal adhesion components, including paxillin, nonmuscle alpha-actinin, filamin, talin, and focal adhesion kinase. Stiffer matrices therefore produce stiffer and increasingly tensed cells (Engler et al., 2006, for a review, see Rehfeldt et al., 2007).

The stiffness of the adhesion substrate is even more important than humoral factors in driving the lineage specification. These factors, which are present e.g. in commercially available cell differentiation media, were not able to reprogram MSCs that are precommitted for weeks on a given matrix for differentiation towards a certain phenotype. However, the matrix stiffness can control the availability and the efficacy of various soluble factors regulating cell behavior. For example, transforming growth factors β (TGF-βs) are matrix-associating protein growth factors that form complexes with matrix proteins such as fibrillin, proteoglycans and fibronectin. If the cell adhesion matrix was too soft (less than 5 kPa), the tension generated by myofibroblasts resulted in deformation of the matrix without opening the TGF-β reservoir and releasing the factor. In addition, irrespective of the actual presence of TGF-β, cells on very soft matrices lost their actin fibers and thus

generated weaker forces on the matrix, which further decreased the possibility of releasing the growth factors from the matrix reservoirs. In contrast, on stiff matrices (more than 10 kPa), the cell-generated tension met resistance from the matrix, which led to deformation of the TGF-β reservoir and to the release of this factor. Both matrix stiffness and TGF-β supported the synthesis of actin in myofibroblasts, maintaining their phenotype and making them even more contractile (Wells and Discher, 2008).

The cell response to various therapeutic drugs is also dependent on matrix stiffness. MSCs adhered to moderately stiff gels (elastic modulus approx from 10 to 30 kPa) by an intermediate cell spreading area, and showed relatively high proliferation activity. Thus, these cells were more sensitive to the antiproliferative drug Mitomycin C than well-spread cells on highly stiff matrices such as glass, where the cell proliferation activity was primarily attenuated by high adhesion strength. Conversely, cycloheximide, a protein synthesis inhibitor, was more efficient on well-spread cells on very stiff matrices. These cells markedly decreased their spreading area, due to blockage of the upregulation or de novo synthesis of proteins involved in cell adhesion and spreading (for a review, see Rehfeldt et al., 2007).

Proper adjustment of rigidity and deformability is also important for creating fibrin matrices, which are widely used in tissue engineering, e.g. for coating the inner surface of synthetic polymeric vascular grafts in order to accelerate their endothelialisation, as a component of scaffolds for bone tissue engineering (for a review, see Filova et al., 2009b) or for delivering various types of cells, including mesenchymal stem cells or chondrocytes, to the sites of a tissue injury (Bensaid et al., 2003; Rampichova et al., 2010). The mechanical properties of fibrin can be controlled by the concentration of thrombin, i.e. a serine protease that converts soluble fibrinogen into insoluble strands of fibrin. The architecture of fibrin prepared from low levels of thrombin is more branched and less porous than networks from high concentrations of thrombin. Fibrin is branched through so-called trimolecular or equilateral junctions of fibrin fibrils that enhance fibrin clot elasticity. Junctions of another kind, referred to as tetramolecular or bilateral, confer strength and rigidity to network fibers (Blombäck et al., 1994; Mosesson et al., 2001). In fibrin matrices used as a delivery vehicle for human mesenchymal stem cells, satisfactory gel rigidity, good cell spreading and maximal cell proliferation were obtained when the scaffolds were prepared at a concentration of 18 mg/ml of fibrinogen and 100 IU of thrombin. A further increase in thrombin concentration decreased the viability of the cells (Bensaid et al., 2003). The mechanical properties of fibrin can be further improved by prolonging its degradation time and reducing its shrinkage. Fibrin degradation can be slowed down by adding aprotinin, an inhibitor of plasmin, or ε-aminocaproic acid, an inhibitor of fibrinolysis, into the cultivation medium (Grassl et al., 2003). Shrinkage can be reduced by chemical or mechanical fixation of the gel, e.g. using poly-L-lysine or attaching the gel to a harder material, such as a polystyrene plate. Gel fixation, on the one hand, and shrinkage forces, on the other, can lead to mechanical stress in the tissue, which may induce collagen synthesis and in turn improve the mechanical properties of the scaffold (Jockenhoevel et al., 2001).

7. Micropatterning of the material surface

Micropatterned surfaces are material surfaces containing microdomains with different chemical and physical properties, e.g. chemical composition, wettability, electrical charge or topography. These surfaces are a suitable tool for all applications in which regionally selective adhesion of cells, controlled cell spreading, directed migration and growth, specific spatial organization of cells, induction of their differentiation and functioning, preferential adhesion and growth of certain cell types, interaction and cooperation of various cell types, and also temporal control of these events are required. These applications involve tissue engineering and various other biotechnologies, such as cell microarrays for use in advanced genomics, proteomics, drug discovery or construction of biosensors (for a review, see Falconnet et al., 2006).

Micropatterned surfaces have been prepared using a wide range of methods. "Classical" approaches involve soft lithography (e.g. microcontact printing and microfluidic patterning), photolithography, plasma polymerization, photoimmobilization of photoreactive molecules, and stencil-assisted patterning, which uses flexible polymeric or stiff metal-based masks with through-holes of a desired size, shape and distribution. Interesting novel technologies make use of jet patterning, where commercially available computer printers can be adapted to create chemical patterns by jetting chemical or biological molecules or even cells on to the material surface. Another advanced technology is laser-guided writing with cells, which allows the cells to be displaced, to be propelled along a light path, and enables clusters of cells to be created on a target surface. This technology has the potential to create patterns composed of various cell types and thus to engineer heterogeneous tissues. In addition, laser-guided writing benefits from much better resolution (about 1 μm) than for the ink-jet method (about 100 μm), and thus enables a higher degree of spatial organization. This non-contact patterning method is potentially suited for building up successive layers of cells to create three-dimensional networks of cells and a new tissue (for a review, see Falconnet et al., 2006). Other high-resolution strategies include a scanning type of lithography, where the surface is directly activated through a microscope objective and a mercury lamp, e.g. using scanning near-field optical microscopy (SNOM) (H'dhili et al., 2003; Richards and Cacialli, 2004; for a review, see Falconnet et al., 2006), and maskless liquid-crystal-display projection photolithography, which enables rapid prototyping of cell micropatterning (Itoga et al., 2006).

A widely used technique is engineering micropatterned surfaces by varying the material surface roughness and topography, i.e. creating hollows and prominences of various sizes, shapes, spacing and distribution, such as grooves and ridges, pits, pillars, boxes, cylinders or honeycombs (Boateng et al., 2003; Gao et al., 2008; Hamilton and Brunette, 2007; Yamamoto et al., 2007; for a review, see Grausova et al., 2008b, 2009c).

As for the history of micropatterning, it was originally developed for applications in microelectronics, e.g. for constructing semiconductors (Britland et al., 1992; for a review, see Falconnet et al., 2006). A marked expansion of micropatterning technology into the biological disciplines started in the early 1990s, when surfaces patterned with highly hydrophilic domains non-adhesive for cells and less hydrophilic domains promoting adhesion and growth of bovine vascular endothelial cells were created by photolithography (Matsuda et al., 1990). Conversely, domains that are non-adhesive for cells can be based on highly hydrophobic polymers, whereas cell-adhesive domains are moderately hydrophilic. Patterned surfaces of this type were used for the potential construction of a bioartificial liver, where hepatocytes growing on moderately hydrophilic and collagen-functionalized rows can be sandwiched between two micropatterned surfaces, and the hydrophobic cell-free grooves would form transport channels for fluid flow and for nutrient and waste exchange (Bhatia et al., 1994).

In our studies, cell-adhesive hydrophilic microdomains were created by plasma polymerization of acrylic acid (AA), and hydrophobic cell repulsive areas were created by polymerization of 1,7 octadiene (OD; Filova et al., 2009a). The surfaces were then tested with four cell types, namely rat vascular smooth muscle cells (VSMC), bovine endothelial cells (EC), mesenchymal stem cells (MSC) derived from the pig bone marrow, and human skeletal muscle cells (HSKMC). All cell types adhered and grew preferentially on the strip-like AA domains, but the degree of this selectivity depended on cell type and on time of cultivation. On day 1 after seeding, the average percentage of cells adhering to AA domains decreased in the following order: MSC> (98.0%)>HKSMC (93.6%)>EC (85.3%)>VSMC (84.5%). However, in the following days, some cells initially adhering to the hydrophobic OD

domains were able to grow, and other cells were able to migrate to these domains and to span them. Thus, on day 7 after seeding the selectivity of the cell colonization of AA domains decreased. The most apparent decrease was observed in HKSMC and VSMC, where the cell number on AA domains was reduced to 55.0% and 63.3%, whereas in EC and especially in MSC the number of cells on AA domains still remained relatively high (73.5% and even 90.0%, respectively). Nevertheless, the VSMC and HKSMC on AA were more differentiated toward the contractile phenotype. The enzyme-linked immunosorbent assay (ELISA) revealed a significantly higher concentration (measured per mg of protein) of alpha-actin in VSMC on AA, and immunofluorescence showed a better developed alpha-actin cytoskeleton in HSKMC growing on AA. Accordingly, immunofluorescence staining of von Willebrand factor showed more apparent Weibel–Palade bodies in EC on AA domains (Fig. 7), which can be considered as a sign of endothelial cell maturation. Similarly, the MSC growing on AA had a better developed beta-actin cytoskeleton, i.e. an important structure participating in cell adhesion, spreading, migration and growth, and contained a higher concentration of this protein. Conversely, the adhesion and spreading of MSC on hydrophobic OD surfaces was very low, and these cells contained a higher concentration of the hyaluronan receptor CD44, i.e. a molecule mediating cell–cell adhesion, which was probably a mechanism compensating the low cell–material adhesion (Filová et al., 2009a).

Another approach for creating cell–adhesive microdomains with appropriate hydrophilicity, used in our earlier studies, was irradiation of synthetic polymers with ions or ultraviolet light through metallic contact masks with circular openings (Mikulikova et al., 2005; Parizek et al., 2006). For ion irradiation, Ar^+ ions were used, and adhesive domains 25, 50, 75 or 100 μm in diameter (center-to-center distance of 200 μm) were created. The selectivity of the adhesion of vascular smooth muscle cells (VSMC) derived from rat aorta depended on the *size of the domain*, being most apparent on microdomains with the highest diameter, i.e. 100 μm. This selectivity also depended on the *intensity of modification*, i.e. a combination of the Ar^+ ion energy (15 or 150 keV) and the ion dose (from 3×10^{12} to 10^{15} ions/cm^2).

At lower energy of 15 keV, the selectivity of cell adhesion was greatest at higher ion doses. For example, at an ion dose of 3×10^{14} ions/cm^2, the percentage of VSMC adhering to the microdomains (100 μm in diameter) on day 2 after seeding reached the highest value of 76% (though these microdomains occupied less than 20% of the polymer surface). Conversely, at a higher ion energy of 150 keV, the selectivity of cell adhesion reached its maximum at the lowest ion dose (80% at a dose of 3×10^{12} Ar^+ ions/cm^2) (Fig. 8). As mentioned above, cell adhesion to irradiated polymers is supported by the oxygen-containing chemical functional groups that appear on these surfaces. At lower ion energies, polymer degradation and the subsequent formation of oxygenated groups requires more ions, whereas at higher ion energies higher ion doses may cause a secondary degradation of these groups (Bacakova et al., 1996, 2000a,b, 2001a; Parizek et al., 2006).

In addition, the behavior of VSMC on polyethylene micropatterned using irradiation with Ar ions in our studies depended on the *cell seeding density*. At *lower densities*, ranging from 2500 to 10,000 cells/cm^2, the domains had a theoretical chance to be occupied by at most 1 to 4 cells, because 1 cm^2 of the polymer surface contained 2500 microdomains, irrespective of their diameter. Under these conditions, the cells on the microdomains were well-spread and polygonal, whereas the cells on the adjacent non-modified polymer were often rounded or spindle-shaped. In addition, the VSMC on ion-irradiated domains displayed well-developed focal adhesion plaques containing $beta_1$ and $alpha_v$ integrins, talin and vinculin, and were filled with a rich filamentous alpha-actin cytoskeleton (alpha-actin is a marker of VSMC differentiation towards

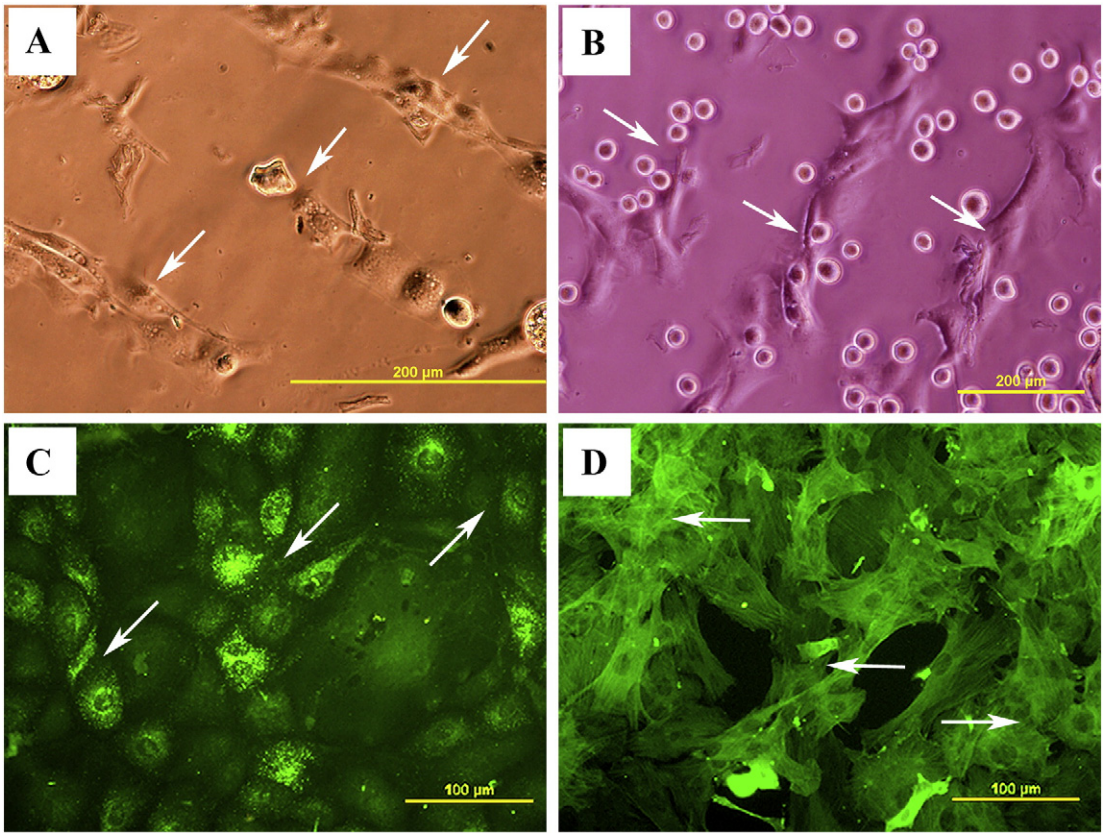

Fig. 7. Bovine pulmonary artery endothelial cells (line CPAE) and rat aortic smooth muscle cells (VSMC) in cultures on surfaces micropatterned with stripe-like domains of hydrophilic acrylic acid and hydrophobic 1,7-octadiene. A, B: native cultures of CPAE (A) and VSMC (B) 6 hours after seeding; C, D: Immunofluorescence staining of cell differentiation markers on day 5 after seeding, i.e. von Willebrand factor in endothelial cells (C) and alpha-actin in smooth muscle cells (D). Note that both cell types adhere and differentiate preferentially on acrylic acid domains (arrows). Olympus IX 51 microscope, DP 70 digital camera. Bar = 200 μm (A, B) or 100 μm (C, D) (Filova et al., 2009a).

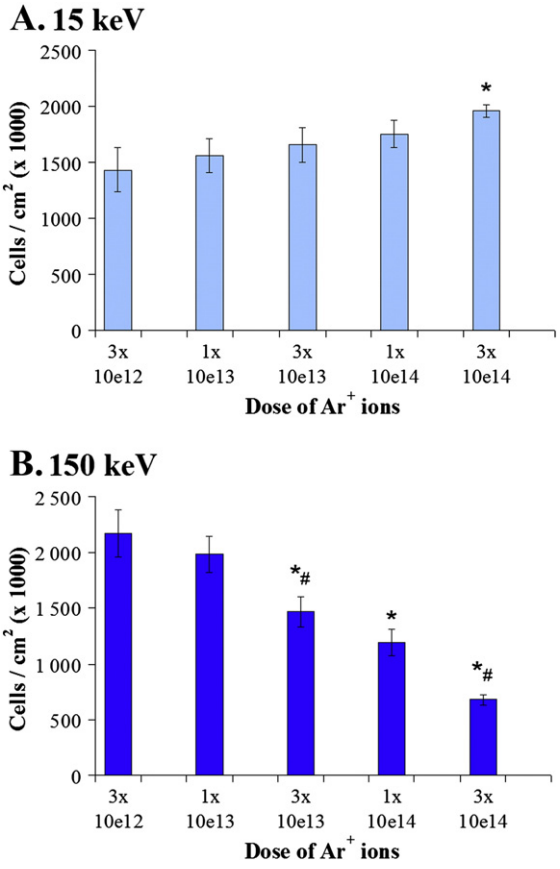

Fig. 8. Number of rat aortic smooth muscle cells on adhesive domains created in polyethylene by irradiation with Ar^+ ions of energy 15 keV (A) or 150 keV (B). Doses from 3×10^{12} to 3×10^{14} ions/cm^2, day 5 after seeding. Mean ± S.E.M. (Standard Error of Mean) from 5 to 8 independent samples for each experimental group and ion dose. Student-Newman-Keuls method. Statistical significance: *, #: $p \le 0.05$ compared to the group irradiated with the lowest dose of 3×10^{14} ions/cm^2 and compared to the previous group, respectively (Parizek et al., 2006).

the contractile phenotype). On the non-irradiated part of the polymers, all mentioned molecules were usually distributed homogeneously, i.e. they did not form well-apparent specific assemblies. These differences increased with increasing size of the domain. However, at *higher seeding densities* of 15,000 to 30,000 cells/cm^2, each domain could receive 6 to 12 cells, and this number was in reality even higher, because the cells tried to adhere preferentially to the domains. As a result, the domains were relatively "crowded", and the cell spreading area was smaller than the cell spreading area on the all-surface-modified polymer, or even smaller than on the non-modified polymer among the microdomains. On the microdomains, the VSMC often formed multilayers already on day 2 after seeding, and this tendency increased with the time of cultivation. Probably for this reason, the concentration of molecules engaged in cell–matrix adhesion, such as integrins alpha$_v$ and beta$_1$, as well as the integrin-associated protein talin, did not increase significantly in these cells (measured on days 4 to 7 after seeding by ELISA per mg of protein) in comparison with VSMC on the fully modified or even non-modified polyethylene. On the other hand, the concentration of VE-cadherins, i.e. molecules mediating intercellular contacts, as well as vinculin, associated with both types of receptors mediating cell–cell and cell–matrix adhesion, was increased in the cells on microdomains. Nevertheless, the concentrations of alpha-actin as well as SM$_1$ and SM$_2$ myosins, important markers of VSMC differentiation, were increased in these cells. Immunofluorescence showed that the cells in the upper layer of the multilayered regions contained the best developed and brightest alpha-actin and myosin-containing filaments.

In addition, the clusters of VSMC were not only confined to the modified spots but were extended for relatively long distances to the neighborhood, and were able to span the unmodified polymer regions between the domains. Similar behavior was also observed in human umbilical endothelial cells (HUVECs, Fig. 9), human embryonic kidney cells (HEK) and VSMC cultured on domains created on polytetrafluoroethylene by ultraviolet light in a reactive NH_3 atmosphere (Mikulikova et al., 2005; Parizek et al., 2006).

As was suggested above, preferential colonization of the domains by cells also depended on the *cultivation time*. Immediately after seeding, due to gravitation, the cells were randomly distributed and covered the entire surface of the polymer homogeneously. However, during the 1st day after seeding, cell spreading was observed preferentially on the irradiated domains. Among the domains, the cells often remained rounded, weakly attached to the material surface and prone to spontaneous detachment, especially while the culture was being handled (mild shaking, medium removal, rinsing and staining cells, etc.) In the case of VSMC, preferential cell adhesion and growth on ion-irradiated domains usually increased during the 1st week of cultivation, whereas at later culture intervals the cells showed a great tendency to span the domains and to colonize the entire polymer surface homogeneously (Parizek et al., 2006; Fig. 10).

Finally, preferential colonization of the irradiated domains depended on the *cell type*. VSMC reacted more sensitively than bovine pulmonary artery endothelial cells of the line CPAE to the ion-irradiated domains. This may be due to higher adaptation of the highly passaged line cells (more than 100 passages) to the in vitro condition than in low-passaged VSMC (passage 3), and thus their lower sensitivity to the physical and chemical properties of the cultivation substrate. On the other hand, other cell lines, derived from humans, i.e. HUVEC and HEK, showed higher selectivity of adhesion to UV-irradiated microdomains than rat VSMC, which were more prone to extend from the microdomains and to span the non-irradiated regions between them (Fig. 11). On microdomains created on polyethylene terephthalate by UV irradiation in an acetylene atmosphere, HUVEC cells showed a strong preference for colonizing these domains, whereas VSMC were homogeneously distributed over the entire polymer surface (Kubova et al., 2007; Parizek et al., 2006). Different responses of various cell types were also shown on surfaces patterned by manipulating the surface roughness and topography, e.g. on polydimethylsiloxane substrates patterned with grooves with lateral dimensions of 2–10 μm and depths of 50–200 nm. Three cell types, namely human foreskin fibroblasts (FCs), human coronary artery endothelial cells (ECs) and human coronary artery smooth muscle cells (SMCs) in cultures on these substrates were elongated in parallel to the grooves and migrated along them, but this behavior was most pronounced in FCs. For these cells, the minimum groove depth to induce the orientation response and change in cell shape was 50 nm, while for ECs and SMCs, about two times deeper grooves were required (Biela et al., 2009).

Another interesting and novel generation of patterned surfaces, based on changes between surface hydrophobia and hydrophilicity, is formed by thermoresponsive polymers. These "smart" polymers, based e.g. on a poly(N-isopropylacrylamide) backbone with n-butyl methacrylate side chains, are capable of a reversible transition from hydrophilicity to hydrophobia when their temperature is lowered by a few degrees, and thus they can temporally control their colonization with cells. In the form of continuous surfaces, thermoresponsive polymers can be used for engineering and harvesting cell sheets to treat a wide range of diseases, from corneal dysfunction to oesophageal cancer, tracheal resection, and cardiac failure (Yang et al., 2007). Surfaces patterned with thermoresponsive polymers can be used for engineering spatially more complicated tissues, such as vascular networks (Hatakeyama et al., 2007; for a review, see Falconnet et al., 2006).

In other patterned surfaces developed in our studies, surface hydrophobicity was combined with engineering the surface roughness

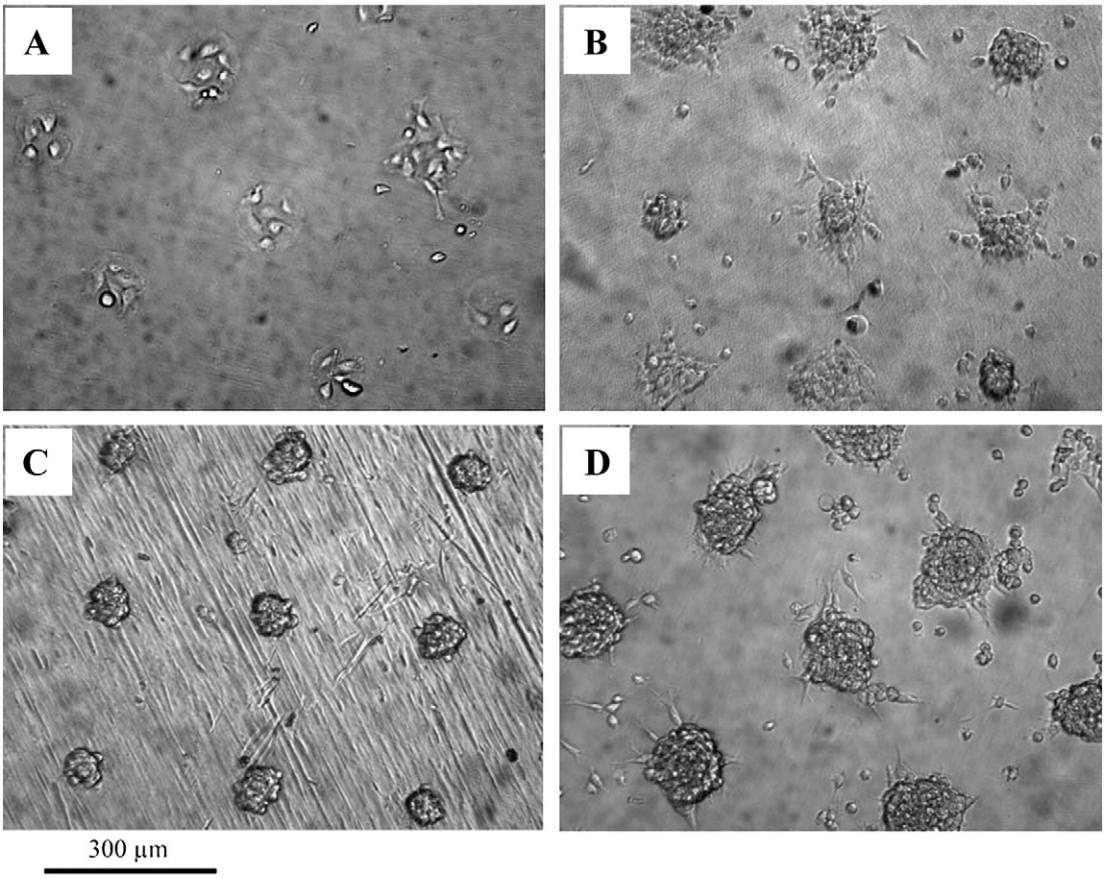

Fig. 9. The effect of cell seeding density on the selectivity of adhesion of human umbilical vein endothelial cells (HUVEC, line EA.hy926) to spots at the PTFE surface created by 20 min exposure to irradiation with a 172 nm X_{e_2}*-lamp through a metallic mask (diameter of holes 100 μm, centre-to-centre distance 300 μm) in 5 mbar NH_3. The images were taken 3 days after cell seeding with an initial density of 6 500 cells/cm^2 (A), 13 000 cells/cm^2 (B), 21 000 cells/cm^2 (C) and 32 000 cells/cm^2 (D). Inverted phase-contrast microscope (Zeiss, Germany) equipped with a CCD-camera (PCO-sensicam, Kelheim, Germany); bar = 300μm (Mikulikova et al., 2005).

and topography. These surfaces were created by depositing fullerenes C_{60} on microscopic glass coverslips through metallic masks with rectangular openings (128 μm per 98 μm). Depending on the temperature and the time of the deposition, the fullerenes formed bulge-like prominences of various heights. When seeded with human osteoblast-like MG 63 cells, the surfaces with lower prominences (128 ± 8 nm and 238 ± 3 nm) were almost homogeneously covered with cells. On surfaces with higher prominences of 326 ± 5 nm, the cells tended to adhere and grow preferentially in the grooves among the prominences. This selectivity became fully apparent on surfaces with the highest prominences of 1043 ± 57 nm, and increased further with time of cultivation. Although the grooves among the prominences occupied only approximately 41% of the surface, they contained from 80% to 98% of the cells on surfaces with the highest prominences, and the cell population density in the grooves was about 5 to 57 times higher than on the bulges (Bacakova et al., 2008; Grausova et al., 2008b, 2009c; Fig. 12). In other studies, preferential growth of bone-derived cells has been observed in grooves, pits and other types of hollows created on various polymeric and metallic materials applicable for constructing bone and dental implants (Hamilton and Brunette, 2007; for a review, see Grausova et al., 2008b, 2009c). However, the cells were also able to colonize the prominences on these surfaces, represented e.g. by ridges or pillars, although these prominences were usually much higher (i.e. several micrometers or even tens of μm) than those on the thick micropatterned fullerene layers in our present study (only about 1 μm). On our fullerene C_{60} layers, the MG 63 cells were not able to "climb up" relatively low prominences only about 1 μm in height, even at a relatively late culture interval of 7 day after seeding. This may be due to a synergetic action of hydrophobia and other physicochemical properties of the fullerene bulges less appropriate for cell adhesion, such as their steep rise and the tendency of spherical ball-like fullerene C_{60} molecules to diffuse out of the prominences towards the grooves (Grausova et al., 2008b, 2009c). Preferential growth of MG 63 cells in the grooves among the prominences was also observed on microstructured hybrid Ti/C_{60} films, as well as on pure Ti films (Vacik et al., 2010; Vandrovcova et al., 2008).

An interesting feature of micropatterned surfaces is that the cell functions on them are often enhanced in comparison with flat non-patterned materials. For example, vascular endothelial cells were more active in cell–material adhesion. Porcine aortic endothelial cells 1 h after seeding on poly(epsilon-caprolactone) films micropatterned with honeycomb-shaped pores showed three times higher expression of focal adhesion kinase autophosphorylated at the tyrosine residue (pFAK) than cells on a corresponding unpatterned film. This indicates that the signaling mediated by the binding between fibronectin (adsorbed preferentially on the pore edges) and the integrin adhesion receptors on cells was more highly activated on the patterned film than on the control flat film (Yamamoto et al., 2007).

There was also higher retention of endothelial cells subjected to shear stress on micropatterned surfaces. On surfaces microstructured with hollows and prominences, e.g. grooves and ridges, the EC were hidden in the hollows; in addition, the microroughness of these surfaces changed the hydrodynamics on the surface and thus decreased the local shear stress. When polyurethane, i.e. a polymer suitable for construction of vascular prostheses, was microtextured with arrays of parallel channels 95 μm in width and 32 μm in depth, the average local shear stress in the channels was significantly lowered, and the retention of endothelial cells was markedly improved from 58% on non-patterned

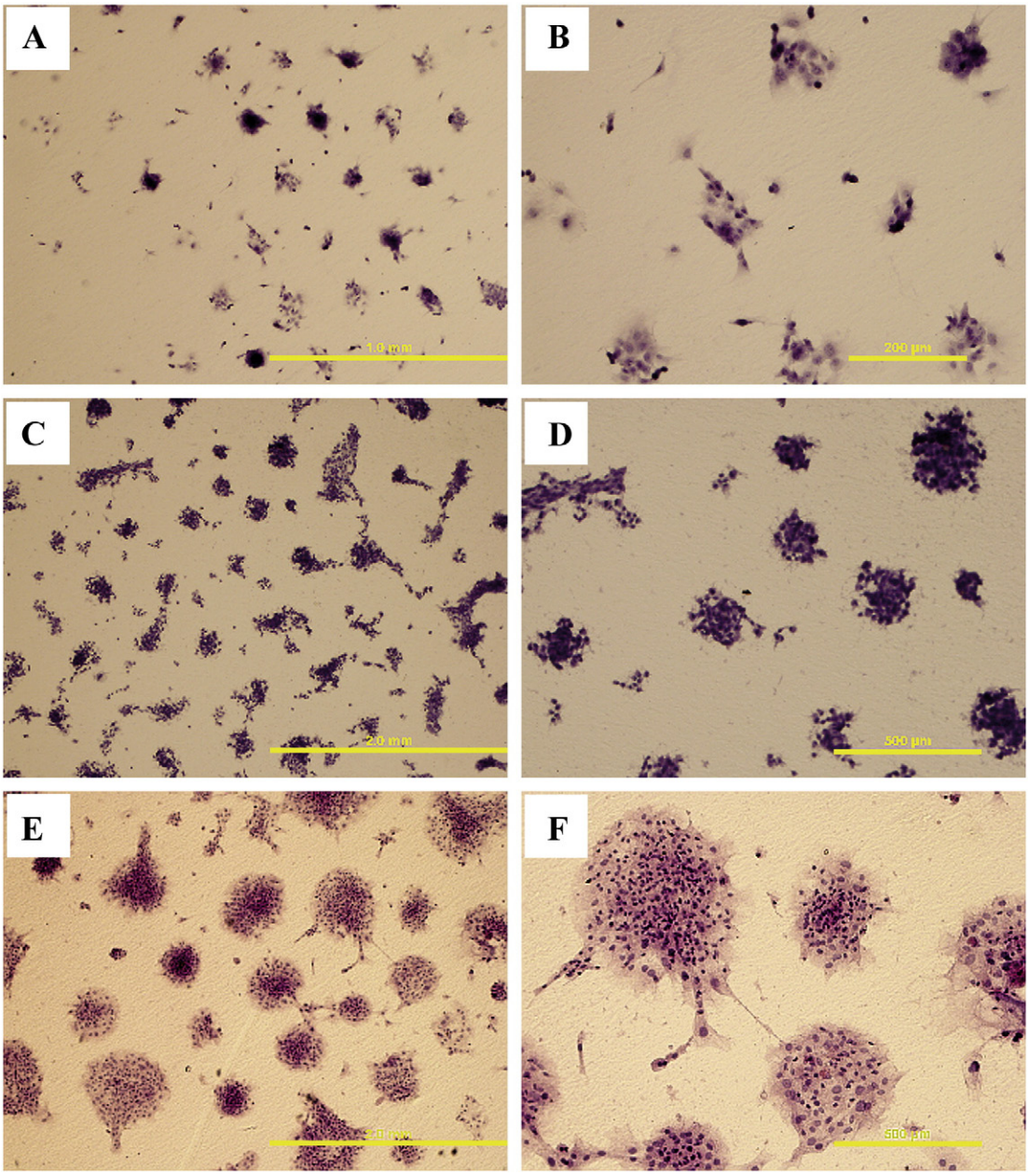

Fig. 10. The effect of cultivation time on the selectivity of adhesion of rat aortic smooth muscle cells to spots at the surface of polyethylene foils, created by irradiation with Ar^+ ions (energy 150 keV, dose 10^{13} ions/cm^2) through a metallic mask with holes 100 μm in diameter and center-to-center distance 200 μm. The cell seeding density was 17,000 cells/cm^2. A, B: day 1 after seeding; C, D: day 5 after seeding, E, F: day 7 after seeding. Stained with hematoxylin-eosin, Olympus IX 51 microscope, DP 70 digital camera. A, C, E: Obj. 4×, bar 1 mm (A), 2 mm (C, E); B, D, F: obj. 10×, bar 200 μm (A), 500 μm (D, F) (Parizek et al., 2006).

surfaces to 92% (Daxini et al., 2006). In addition, studies combining surfaces patterned with stripes bearing endothelial cells and unidirectional shear stress (acting in parallel or perpendicular to these stripes) showed that the surface pattern is more important for the shape, orientation, direction of migration and cytoskeletal organization than exogenous mechanical stimulation (Lin and Helmke, 2008; Vartanian et al., 2008). Similar results were also obtained in endothelial cells (lines HUVEC and CPAE) on PLLA surfaces patterned with grooves and submicron- and micron-scale ridges from 350 nm to 1750 nm in width. The highest cell adhesion strength (measured by the resistance of the cells to detachment by shear stress) was found on the surface of ridges 700 nm in width and grooves 350 nm in width for both HUVEC and CPAE cells. This was attributed to (i) contact guidance along the groove direction, which lowered the shear stress applied to the cell surface, and (ii) clustered focal adhesions, which increased the strength of the cell–substrate binding (Hwang et al., 2010).

Preferential adhesion of a certain cell type over other types can also be induced by micropatterned surfaces. For example, a major drawback in culturing cardiac myocytes is overproliferation of fibroblasts, present physiologically in the cardiac tissue, and thus contaminating the isolated myocyte suspension. Patterning of silicone surfaces with vertically oriented cylindrical prominences attenuated the attachment and growth of fibroblasts, while the proportion of cardiomyocytes was increased. This approach made it possible to avoid pharmacological intervention with cytostatins, such as cytosine β-D-arabino-furanoside, which can induce apoptosis in many cell types. At the same time, the physiological cooperation between the myocytes and fibroblasts necessary for the appropriate development, maturation and function of cardiomyocytes was preserved (Boateng et al., 2003).

Micropatterned surfaces can also help to establish communication and cooperation between different cell types, which is necessary for

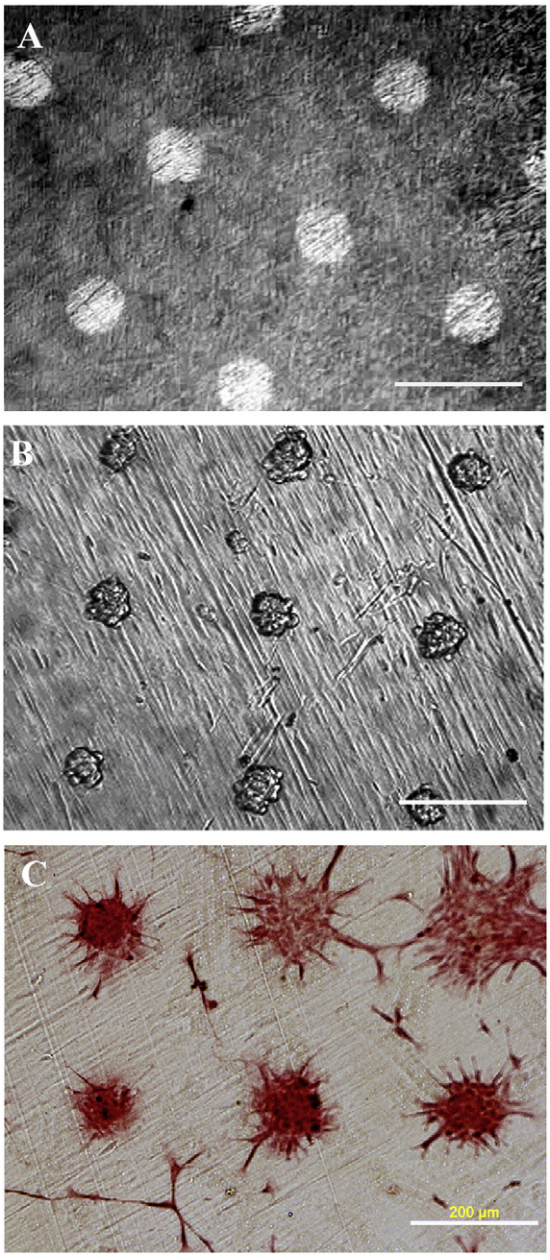

Fig. 11. The effect of cell type on the selectivity of cell to spots at the PTFE surface created by 20 min exposure to irradiation with a 172 nm $X_{e_2}^*$-lamp in 5 mbar NH_3. The modification was performed through a metallic mask with holes 100 μm in diameter and centre-to-centre distance 300 μm (A). The material was seeded with human umbilical vein endothelial cells (HUVEC, line EA.hy926; B) or rat aortic smooth muscle cells (C) at similar seeding densities (21 000 and 17 000 cells/cm^2, respectively). Day 3 after seeding. Note that the endothelial cells grow almost selectively on the domains, while the smooth muscle cells overlap the domains and span the unmodified regions among them. A: Fluorescence microscopic image of the modified spots at the PTFE surface (excitation wavelength 513 nm, exposure 3 s); B: Inverted phase-contrast microscope (Zeiss, Germany) equipped with a CCD-camera (PCO-sensicam, Kelheim, Germany), C: cells stained with hematoxylin-eosin, Olympus IX 51 microscope, DP 70 digital camera. Bar = 300 μm (Mikulikova et al., 2005; Parizek et al., 2006).

successful construction of all bioartificial tissues and organs. For example, the interaction between hepatocytes and Kupffer cells needed for the construction of a bioartificial liver was established on polystyrene culture plates coated with bovine serum albumin and patterned with collagen islands through polydimethylsiloxane stencils (Zinchenko and Coger, 2005).

An interesting issue is the use of surfaces micropatterned with adhesive islands of various sizes for switching between proliferation/apoptosis and proliferation/differentiation programs by variations in the size of the cell spreading area. For example, human capillary endothelial cells cultured on fibronectin-coated islands larger than 1500 μm^2 spread and progressed through the cell cycle, whereas cells restricted to areas smaller than 500 μm^2 failed to extend and underwent apoptosis. The cells that were prevented from spreading were grown in a medium containing soluble growth factors and exhibited normal activation of the mitogen-activated kinase (ERK1/ERK2) growth signaling pathway. However, these cells failed to increase cyclin D1 protein levels, to progress through the G1 phase of the cell cycle and enter the S phase (Huang et al., 1998). Conversely, if the vascular endothelial cells were extended for some minimum time (approx. 12–15 h) on the adhesion substrate, and then trypsinised, they synthesized DNA even if they were round and in suspension. This was because the extension on the adhesion substrate enabled them to pass the restriction point between the G1 and S phases of the cell cycle (Ingber et al., 1995). These results suggested that geometrical control of the cell cycle progression is more important than biochemical control, which alone is not sufficient. During cell spreading, the actin cytoskeleton (which associates the integrin receptors, clustered in focal adhesion plaques, with the nuclear membrane) generates tension, leading to enlargement of the nuclear volume, chromatin decondensation and thus increased accessibility of DNA to the replication machinery (Dike et al., 1999; Huang et al., 1998; Roca-Cusachs et al., 2008).

The formation of capillary-like structures, which can be considered as a specific form of the endothelial cell differentiation and vascular tissue formation, was also induced by the size of the adhesive domains. Human microvascular endothelial cells cultured on substrates micropatterned with 10-μm-wide lines of fibronectin formed extensive cell–cell contacts and spread to approximately 1000 μm^2. Within 72 h, the cells shut off both growth and apoptosis programs and formed tubular structures containing a central lumen. At the same time, the cells cultured on wider (30 μm) lines also formed cell–cell contacts and aligned their actin cytoskeleton, but these cells spread to larger areas (2200 μm^2), proliferated, and did not form tubes (Dike et al., 1999). Similarly, endothelial cells isolated from bovine aorta were induced to form tubular capillary-like structures on 50-μm-wide stripes functionalized with the oligopeptide Arg-Gly-Asp-Ser (RGDS), a ligand for integrin cell adhesion receptors, but not on wider stripes (Moon et al., 2009). The formation of capillary-like structures was also induced on gelatin or chitosan patterned with grooves, in which the selective adhesion and growth of human microvascular endothelial cells was ensured by microcontact printing the plateau regions between the grooves with cell adhesion-resistant polyethyleneglycol-L-polylactic acid (PEG/PLA) (Gao et al., 2008). As mentioned above, the use of surfaces patterned with domains made of thermoresponsive polymers would enable the release of capillary-like structures from the material and their use for engineering three-dimensional tissues (Hatakeyama et al., 2007).

8. Nanopatterning of the material surface

The physicochemical properties of the material surface, e.g. its chemical composition, wettability, electrical charge or topography, can be varied not only on a microscale level but also on a nanoscale level. The principles for creating nanopatterned surfaces are similar to those used for surface micropatterning — lithographical methods (e.g. scanning probe, electron beam, ion beam, colloidal and imprint lithography), self-assembly of molecules (for a review, see Kim et al., 2010; Schmidt and Healy, 2009), stencil-assisted patterning (Sanz et al., 2010), deposition of nanoparticles or grafting biomolecules, particularly oligopeptidic ligands for cell adhesion receptors (Bacakova et al., 2007a; Cavalcanti-Adam et al., 2007; Maheshwari et al., 2000; Mann and West, 2002).

Nanopatterned surfaces have been designed for several biomedical applications, e.g. construction of biosensors (Schmidt and Healy, 2009), controlled drug delivery (Stern et al., 2009) and for capturing

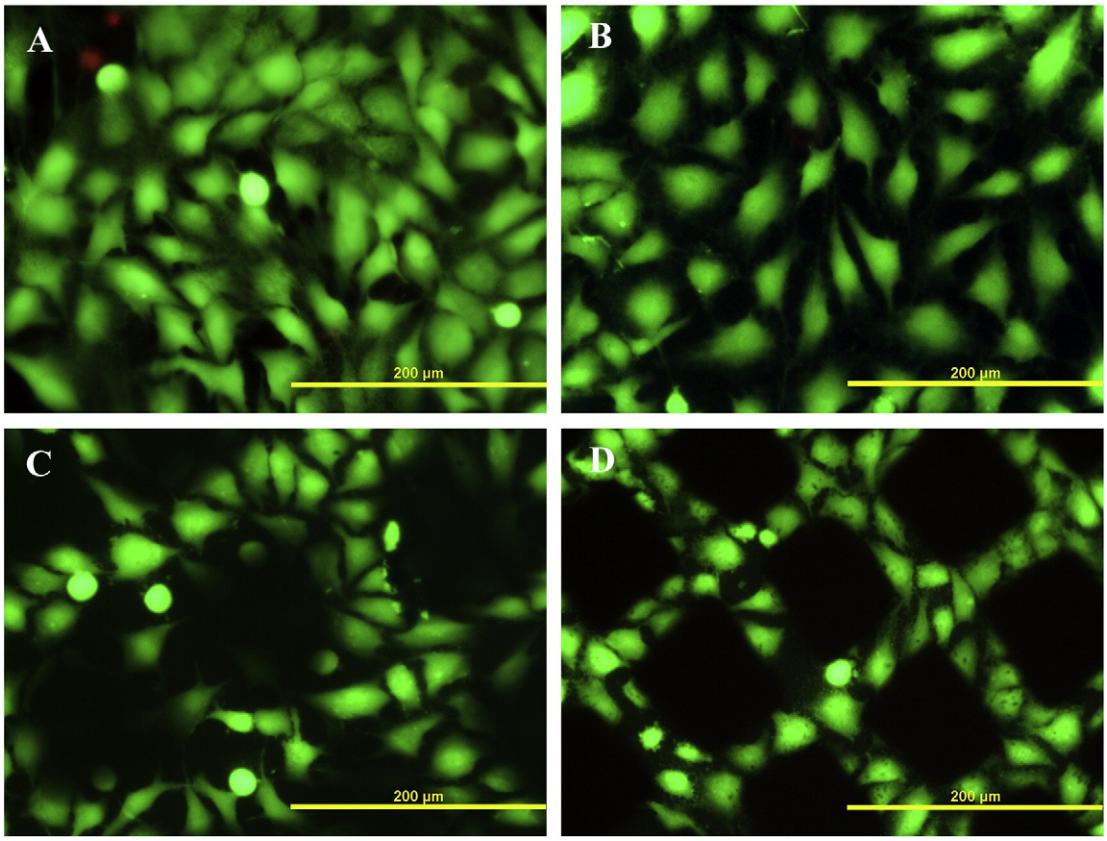

Fig. 12. Human osteoblast-like MG 63 cells on day 7 after seeding on fullerene layers micropatterned with prominences 128 ± 8 nm in height (A), 238 ± 3 nm in height (B), 326 ± 5 nm in height (C) or 1043 ± 57 nm in height (D). Stained with LIVE/DEAD viability/cytotoxicity kit. Olympus IX 51 microscope, DP 70 digital camera, obj. 20×, bar = 200 μm (Bacakova et al., 2008b; Grausova et al., 2008b, 2009b).

endothelial progenitor cells (EPCs) in order to endothelialise vascular prostheses (Alobaid et al., 2006). Another broad and important application is for controlling cell behavior, e.g. regionally-selective adhesion of various cell types, spreading, survival, proliferation activity and differentiation of cells. This cell behavior can be regulated by manipulating the *type*, *number*, *spacing* and *distribution* of ligands for cell adhesion receptors on the material surface. As for the *type*, some oligopeptidic ligands for cell adhesion receptors are preferentially or specifically recognized by certain cell types. For example, the amino acid sequence REDV is preferentially recognized by vascular endothelial cells, while the sequences VAPG and KRSR are bound specifically by vascular smooth muscle cells and osteoblasts, respectively (for a review, see Bacakova and Svorcik, 2008; Bacakova et al., 2004). As for the *number* of adhesion ligands, in a study by Mann and West (2002), performed on glass slides grafted with adhesion peptides RGDS, KQAGDV and VAPG, the migration and proliferation activity of vascular smooth muscle cells decreased with increasing concentration of the adhesion ligands, which ranged from 0.2 nmol/cm^2 to 2 nmol/cm^2. For optimum migration and proliferation activity of VSMC, much lower concentrations were probably needed. For example, on surfaces modified with a related RGD-containing adhesion oligopeptide, i.e. GRGDSY, the maximum proliferation activity of fibroblasts was achieved at a ligand concentration of approx. 1.33 pmol/cm^2 (Neff et al., 1999). As for the *spacing* of the adhesion ligands, a minimum distance of 58 nm between RGD peptides (bound via thiol group and an alkane spacer on gold nanoparticles deposited on glass coverslips) was required for full spreading of rat REF 52 fibroblasts, including stability and maturation of focal adhesion plaques on these cells (Cavalcanti-Adam et al., 2007). A key role in controlling the cell behavior on material surfaces is played by the spatial *distribution* of the adhesion ligands. For example, on surfaces endowed with oligopeptide YGRGD (tethered from glass coverslips via polyethylene oxide chains against a cell non-adhesive background), clustering of these ligands was required for complete spreading and migration of murine NR6 fibroblasts, including the formation of focal adhesion plaques and the assembly of an actin cytoskeleton in these cells. In addition, all these events, and also the adhesion strength (measured by the resistance of the cell to detachment from the adhesion substrate by centrifugation) correlated positively with the number of oligopeptides per cluster, which was 5 and 9 (Maheshwari et al., 2000).

Nanopatterned surfaces can also regulate the maturity of cell–matrix adhesions. On the above-mentioned surfaces with non-clustered YGRGD ligands, the focal adhesions almost completely lacked vinculin, i.e. a structural protein stabilizing focal adhesions (Maheshwari et al., 2000). A similar result was obtained on surfaces with a relatively long spacing between RGD ligands, i.e. 108 nm, compared to surfaces with interligand distances of 58 nm (Cavalcanti-Adam et al., 2007). In addition, the focal adhesions in cells on a 108-nm-spaced pattern contained lower levels of zyxin, i.e. another marker of more mature focal adhesions, which is recruited to these sites when mechanical stress is applied to the cells (Cavalcanti-Adam et al., 2007). Another interesting example is provided by polycarbonate disks with highly ordered nanopits homogeneously distributed over the material surface in a square or hexagonal configuration. On these substrates, the number and the length of the fibrillar adhesions, i.e. the most mature stage of focal adhesion plaques (see paragraph 9) on primary human osteoblasts (HOB) was significantly reduced in comparison with surfaces with a slightly disordered (near-square) distribution of the nanopits. Ordered arrays of nanopits reduced cellular spreading and induced an elongated cellular phenotype, indicative of increased motility, while a near-square nanopit configuration induced HOB spreading and more mature organization of the actin cytoskeleton (Biggs et al., 2007). Further studies by this

group of authors revealed that a near-square distribution of the nanopits is also capable of inducing osteogenic differentiation in human osteoprogenitor cells with similar efficiency as dexamethasone and ascorbate treatment. The switch from proliferation to differentiation in osteoprogenitor cells is most probably driven by signaling through the extracellular signal-regulated kinase (ERK1/2). This pathway is related to cell adhesion, includes the focal adhesion kinase, and is involved in mechanotransduction via integrin signaling (Kantawong et al., 2009).

In general, the cell behavior on nanopatterned surfaces can be regulated by the orientation, and also by the shape and size of the nanoscale irregularities on the material surface. The orientation of the nanofibers in nanofibrous scaffolds, i.e. random or aligned, modulated the adhesion, spreading, shape and cytoskeletal organization of various cell types (Lim et al., 2010; Meng et al., 2010). For example, in our experiments focused on constructing bioartificial heart valves, the valve interstitial cells (VIC) cultured on randomly oriented polyamid nanofibers were flat and polygonal, and their alpha-actin-containing filaments were arranged randomly, forming a mesh-like structure. However, on nanofibers aligned in parallel, the cells were spindle-shaped, oriented along the fibers, and their alpha-actin-containing filaments were arranged in parallel with the long axis of the cells (Filova et al., 2009c; Fig. 13A and B).

The cell proliferation, differentiation, phenotypic maturation and functioning were usually better on aligned nanofibers than on randomly oriented nanofibers or on unpatterned flat surfaces. Composite nanofibers of multiwalled carbon nanotubes and polyurethane aligned in parallel stimulated proliferation and collagen secretion in human umbilical vein endothelial cells (HUVECs). At the same time, they preserved the anticoagulant function of HUVECs, manifested by a low secretion of plasminogen activator inhibitor-1 (PAI-1) and tissue factor (Meng et al., 2010). In cultures of rat bone marrow stromal cells on PLLA nanofibers, the calcium content on fibers aligned in parallel was significantly higher than that of randomly oriented fibers (Ma et al., 2011). Collagen I secreted by dural fibroblasts cultured on poly(ε-caprolactone) nanofibrous scaffolds exhibited a high degree of organization on radially aligned fibers and a haphazard distribution on scaffolds of random fibers (Xie et al., 2010). In neural stem cells derived from rat hippocampus and cultured on aligned polycaprolactone fibers, a higher fraction of cells exhibited markers of neuronal differentiation (e.g. neuron-specific class III beta-tubulin Tuj 1) after stimulation with retinoic acid than cells on randomly distributed fibers (Lim et al., 2010). Primary hepatocytes in cultures on type-I collagen-coated PLLA aligned nanofibers developed multicellular aggregates more quickly than on tissue culture plastic with type-I collagen, and also on meshes of type-I collagen-coated PLLA random nanofibers. On aligned nanofibers, the cells also showed a higher functional expression in terms of albumin secretion, urea synthesis and phase I and II (CYP1A and UGT) metabolic enzyme activity (Feng et al., 2010).

The better performance of cells on aligned nanofibers is a typical example of morphological and then biochemical control of the cell behavior by the adhesion substrate. Aligned nanofibers guide the cells to be elongated along the major fiber axis. The elongated cell shape then stimulates specific biochemical pathways of extracellular signal transduction, such as the canonical Wnt/β-catenin pathway or

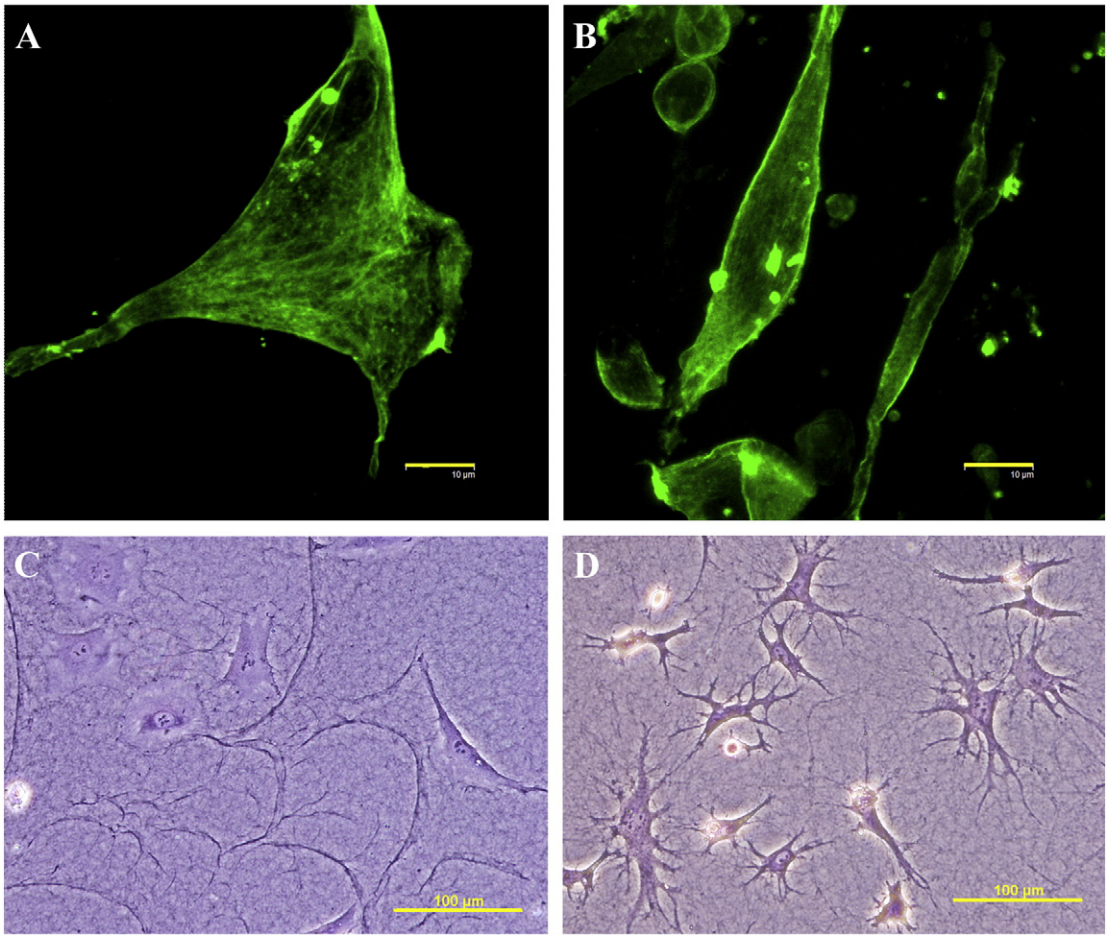

Fig. 13. Morphology of valve interstitial cells (VIC) in cultures on polyamide nanofibers oriented randomly (A) or in parallel (B), and bovine pulmonary artery endothelial cells of the line CPAE in cultures on fibrin coated with laminin (C), or on fibrin coated with collagen I (D). A, B: immunofluorescence of alpha-actin, day 3 after seeding; C, D: staining with hematoxylin and eosin, day 1 after seeding. A, B: Leica SP2 confocal microscope, obj. ×63, zoom × 3, scale bar = 10 µm; C, D: Olympus IX 51 microscope, DP 70 digital camera, obj. ×20, scale bar = 100 µm.

activation of Rho and Rac/Cdc42. In the canonical Wnt/β-catenin pathway, the extracellular signal is transmited to the cell nucleus by β-catenin, which is able to enter the nucleus and interact with TCF/LEF family transcription factors (i.e. transcription factors TCF7, TCF7L1, TCF7L2 and lymphoid enhancer-binding factor-1, LEF1) to promote specific gene expression (Lim et al., 2010). After activation of Rho and Rac/Cdc42 (which are small GTPases regulating gene transcription, actin reorganization, cell migration and growth in response to various extracellular signals, such as growth factors, hormones and chemoattractants in the ECM), the signal is relayed to the nucleus by the MAP kinase pathway (Meng et al., 2010).

Other interesting results on cell guidance by nanofibrous structures were obtained on fibrin nanofibers, prepared on polystyrene dishes by in vitro simulation of the physiological hemocoagulation process (Filova et al., 2009b) and seeded with rat aortic smooth muscle cells. On fibrin coated with laminin, where the nanofibrous network was relatively fine, the cells were polygonal or spindle-shaped, while on fibrin coated with collagen I, where the nanofibers were relatively thick and formed a 3D-like network, the cells developed abundant extensions which were arborised in the direction of the fibers (Fig. 13C and D).

Generally, the nanofibrous shape of nanoscale irregularities on the material surface is considered to be more advantageous for cell performance than other types of irregularities. On composite films produced from chitosan/poly-L-lysine blend solutions with fiber-like surface morphologies, the spreading, assembly of actin cytoskeleton, proliferation, expression of osteocalcin and mineralization of MC3T3-E1 cells were more pronounced than in cells on chitosan/poly-L-lysine films with particle- or granule-like irregularities (Zheng et al., 2009). An explanation is that nanofibrous structures bear a better resemblance than other types of nanoscale irregularities to the natural ECM, which is often fibrous in character, e.g. collagen. A possible mechanism through which the nanofibers promote osteogenic cell differentiation is the RhoA-Rock signaling pathway (Hu et al., 2008).

The size of the nanoscale irregularities on the material surface can also manipulate cell behavior. For example, the attachment and spreading of human fetal osteoblastic cells (hFOB), the expression of α_v-integrins in these cells, the synthesis of focal adhesion protein paxillin, as well as the colocalization of paxillin with cytoskeletal actin stress fibers, focal adhesion kinase (FAK) and phosphorylated FAK (pY397), were greater on polymeric surfaces with shallower pits (14 and 29 nm) than on surfaces with deeper pits (45 nm) (Lim et al., 2007a). Similarly, in an older study performed by the same group on polymeric surfaces with nanoislands 11, 38 and 85 nm in height, the proliferation of hFOB cells and also their osteogenic differentiation, measured by the activity of alkaline phosphatase, correlated inversely with the height of the nanoisland (Lim et al., 2005). On the other hand, the metabolic activity of human osteoblast-like SAOS-2 cells in cultures on nanocrystalline diamond films, measured by the activity of cellular dehydrogenases, increased with increasing surface roughness (the root mean square roughness, *RMS*, i.e. a parameter measured by atomic force microscopy and similar to R_a, was in the range from 11 nm to 39 nm; Kalbacova et al., 2007).

Specific cell behavior on nanopatterned surfaces was also induced by the surface chemistry of the nanodomains. Planar gold surfaces were patterned by dip pen nanolithography to produce arrays of nanodots (diameter 70 nm, spacing from 140 to 1000 nm) terminated with methyl, hydroxyl, carboxyl and amino groups. Human mesenchymal stem cells (MSCs) in cultures on $-CH_3$-terminated nanodots maintained an undifferentiated phenotype, whereas on nanoarrays functionalized with –OH and –COOH groups, MSCs differentiated toward a chondrogenic phenotype (manifested by the production of collagen II and aggrecan), and on nanoarrays functionalized with $-NH_2$ groups, the cells differentiated into osteoblasts (manifested by positive immunocytochemical staining for osteocalcin, osteoblast-specific transcription factor CBFA1, and positive von Kossa staining for mineralized tissue). The mechanisms for regulating these differentiation pathways by surface chemistry have not yet been fully elucidated, but they probably involve differences in the material surface energy, in protein adsorption and in the formation and morphology of focal adhesion plaques in the adhering cells (Curran et al., 2010).

9. Correlation between cell adhesion, proliferation and differentiation

It is well known that anchorage-dependent cells do not divide without previous extension on the growth substrate, and can even undergo anoikis, i.e. a specific type of apoptosis caused by adhesion deprivation (Straface et al., 1999). Therefore, in the first phase of cell spreading, the size of the spreading area correlates positively with the cell proliferation activity (Chen et al., 1997, 1998, 1999; Dike et al., 1999; Huang and Ingber, 2000; Huang et al., 1998; Ingber et al., 1995; Thomas et al., 1999; for a review, see Bacakova and Svorcik, 2008; Bacakova et al., 2004).

Cell spreading stimulates cell proliferation by at least two mechanisms, i.e. *biochemical* and *mechanical* pathways (Chen et al., 1998; Huang et al., 1998; Huang and Ingber, 2000; Ingber et al., 1995). Both mechanisms start by adsorbing cell adhesion-mediating molecules from biological fluids to the material surface and binding the active sites in these molecules with cell adhesion receptors, which involve integrin and non-integrin (e.g. proteoglycan-based) adhesion molecules. Occupation of adhesion receptors by their ligands leads to clustering of these receptors into specific domains called “adhesion plaques” or “adhesion sites”, where the receptors communicate with numerous structural and signaling proteins, through which they are associated with the actin cytoskeleton (Bacakova et al., 2004).

The *biochemical* mechanism then continues by activating the signaling component of the adhesion plaques, e.g. focal adhesion kinase (FAK) and other tyrosine kinases (Src, PYK2, Csk, Abl) as well as other intracellular signaling pathways also used by growth factor receptors, e.g. mitogen-activated protein (MAP) kinases, such as ERK 1 and 2, or serine/threonine kinases, such as ILK or PKC (Avraham et al., 2003; Dwivedi et al., 2008; Huang et al., 1998; Katz et al., 2000; Liu et al., 2002; Zaidel-Bar et al., 2007; Zamir and Geiger, 2001; Zhao et al., 2001). These events result in transition of the cell from the G0 phase to the G1 phase and from the G1 phase to the S phase of the cell cycle, DNA synthesis and cell division. The *mechanical* cell growth control mechanism is based on changes in the tension of the actin cytoskeleton. The actin fibers are anchored to the structural component of the adhesion sites (e.g. talin, vinculin, paxillin, alpha-actinin, tensin), also called “the membrane cytoskeleton”. At the same time, these fibers are associated with the nuclear membrane, the membranes of the cellular organelles, and also with various enzymes (Ingber et al., 1995). The increasing tension of the cytoskeletal fibers during cell spreading can stimulate cell proliferation by nuclear expansion, enlarging the nuclear pores, increasing the nuclear export and DNA synthesis, and also by changes in the synthesis and transportation of various extranuclear cell cycle-regulating factors (Assoian and Klein, 2008; Huang et al., 1998; Huang and Ingber, 2000; Ingber et al., 1995). In addition, the expansion of the nuclear volume leads to chromatin decondensation, and thus increased accessibility of DNA to the replication machinery (Dike et al., 1999; Huang et al., 1998; Roca-Cusachs et al., 2008).

The dependence between cell spreading and cell proliferation, described above, is not linear. The increased spreading, formation of adhesion plaques and assembly of the actin cytoskeleton stimulates cell proliferation only to a certain degree. In our earlier studies performed on rat aortic smooth muscle cells cultured on ion-implanted polymers, a large cell spreading area, large and numerous adhesion plaques, a higher concentration of integrin receptors and structural proteins of the adhesion plaques, e.g. paxillin, talin and vinculin, higher resistance of cells to both spontaneous and proteolytic enzyme-mediated detachment from the adhesion

Table 2
Types and characteristics of cell-matrix adhesion structures.

Parameter /adhesion type	Phosphorylation (Pax)	FAK content	Turnover	Localization and relation to actin and myosin fibres	Presence of other molecules
Focal complex				Periphery	$\alpha_v\beta_3$
•	↑	↑	↑		
Focal adhesion				Towards central part	$\alpha_v\beta_3$ Talin Vinculin Zyxin
⬭	↑	↑	↑		
Fibrillar adhesion				Central part	$\alpha_5\beta_1$ Tensin Fibrillar fibronectin
———	↓	↓	↓	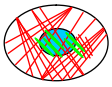	

substrate and well-developed actin cytoskeleton was often associated with slower cell proliferation (measured by doubling time, ^{3}H thymidine and bromodeoxyuridine incorporation) in comparison with cells on pristine polymers. At the same time, these cells contained a higher concentration of alpha-actin as well as SM1 and SM2 myosins, i.e. important markers of the maturation of vascular smooth muscle cells toward the contractile phenotype (Bacakova et al., 1996, 2000a, 2001a). Similar results were also obtained in rat aortic smooth muscle cells of the line A7r5 in cultures on polyacrylamide gels of various elasticity and collagen concentrations (Engler et al., 2004). Data from some other authors also suggests that the proliferation capacity and migration speed of various cell types, e.g. smooth muscle cells, endothelial cells, fibroblasts and mesenchymal stem cells, grown on various substrates, is highest at intermediate adhesion strength, while high adhesion capacity is associated rather with quiescence and maturation of cells (DiMilla et al., 1993; Fernandez et al., 1993; Lesny et al., 2006; Mann and West, 2002; Mann et al., 2001; Palecek et al., 1997; Podesta et al., 1997; for a review, see Bacakova and Svorcik, 2008; Bacakova et al., 2004). In addition, the induction of a larger cell spreading area, increased number and size of adhesion plaques, increased concentration of integrins and structural proteins, e.g. paxillin, talin, vinculin and alpha-actinin, at these sites, accompanied by the formation of thick bundles of actin fibers, is the basic mechanism of the action of a wide spectrum of antiproliferative, antimigratory and cell differentiation-inducing drugs and natural molecules, such as dimethyl sulphoxide (Lampugnani et al., 1987), retinoic acid and synthetic retinoid mofarotene (Helige et al., 2004; Leung et al., 1992), lipoxygenase inhibitor baicalein (Hsieh et al., 2007), nerve growth factor (Rhee et al., 2000) and transforming growth factor β_1 (Tian and Philips, 2003). The tumor suppressor p16/CDKN2A/INK4a gene, frequently mutated in high-grade gliomas, suppresses cell proliferation primarily through inhibition of cell-cycle progression in the G1 phase, which is associated with large and flattened cytoplasm, increased formation of cytoplasmic actin-stress fibers and vinculin accumulation in the adhesion plaques (Noguchi et al., 2001).

In other words, mitotically active cells typically lack well-formed adhesion plaques as well as long, thick and numerous actin fibers, because these structures would hamper the partial detachment of the cells from their adhesion substrate and the reorganization of the cytoskeleton required for mitosis (Yamaguchi et al., 1997; for a review, see Bacakova et al., 2004).

An interesting issue which remains to be fully and systematically elucidated is the correlation of the switch between the proliferation and differentiation programs and the maturation status of the adhesion plaques. Zaidel-Bar et al. (2007) systemized the cell–matrix adhesion structures into the following three types: less mature “focal complexes”, which drive cell spreading and migration, more mature “focal adhesions”, mediating robust adhesion of the cell to the extracellular matrix, and the most mature structures called “fibrillar adhesions”, which are involved in matrix remodeling (Table 2, Fig. 14). These adhesion types differ in their morphology, chemical

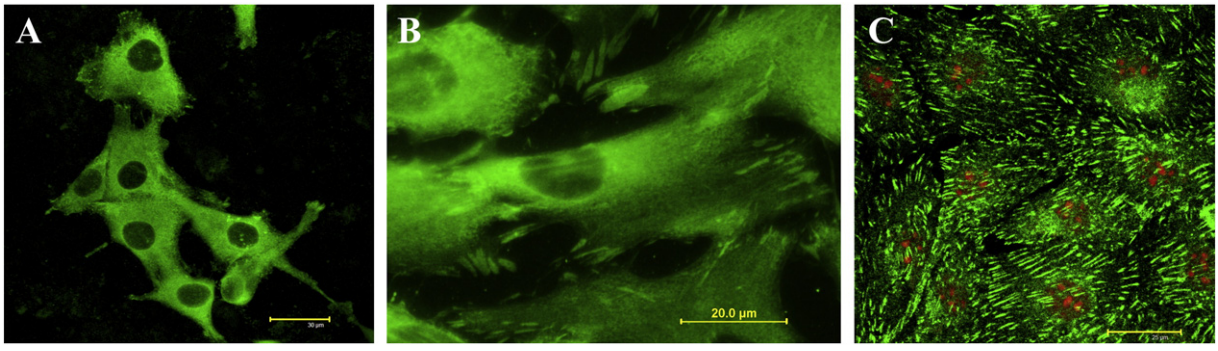

Fig. 14. Examples of various maturation stages of cell–matrix adhesions: focal complexes (A), focal adhesions (B) and fibrillar adhesions (C) in human osteoblast-like MG 63 cells cultured on a composite material containing 15 wt.% of hydroxyapatite nanoparticles (A), porcine valve interstitial cells cultured on microscopic glass coverslips (B) and bovine pulmonary artery endothelial cells of the line CPAE grown on fibrin gel (C). Immunofluorescence staining against vinculin (A, C) and talin (B), day 3 after seeding. Pictures were taken in a Leica SP2 confocal microscope, obj. 20×, water immersion (A, C); zoom ×4 (A) and zoom ×6 (C), or an Olympus IX 51 microscope with a DP 70 digital camera, obj. ×100, oil immersion (B). Scale bar: 30 µm (A), 20 µm (B) or 25 µm (C).

composition, localization on the cell membrane, turnover and also their association with specific ECM and cytoskeletal molecules.

Focal complexes are dot-like in shape, localized on the periphery (often on the lamellipodia) of cells which are starting to spread and migrate on their adhesion substrate. They contain relatively high levels of focal adhesion kinase (FAK) and other tyrosine kinases, such as Src, and phosphorylated paxillin. Similar phosphorylation of paxillin on both tyrosine and serine residues also occurs after stimulation of cells with growth factors (Zaidel-Bar et al., 2007). In vascular endothelial cells or mouse embryonic fibroblasts growing on fibronectin substrates, these complexes contained preferentially integrin $\alpha_v\beta_3$ rather than other integrin types involved in cell-fibronectin adhesion (Zaidel-Bar et al., 2007). In murine osteoblastic MC3T3-E1 cells, overexpression of $\alpha_v\beta_3$-integrin increased the proliferation of these cells, whereas their differentiation was retarded, as indicated by lower activity of alkaline phosphatase, lower expression of osteocalcin, type I collagen, bone sialoprotein as well as lower matrix mineralization (Cheng et al., 2001). In vascular smooth muscle cells, the $\alpha_v\beta_3$-integrin adhesion molecule was associated with their proliferative, atherogenic and less differentiated phenotype (Hoshiga et al., 1995; Sajid et al., 2003; Srivatsa et al., 1997; Stoufer et al., 1998). The fibrilogenesis of fibrinogen localized beneath these sites is impaired. Intracellularly, the focal complexes are in connection with newly forming short actin and myosin fibers localized at the cell periphery. The turnover of the focal complexes is very quick; the duration of these structures is less than one minute (Zaidel-Bar et al., 2007; Table 2, Fig. 14).

Focal adhesions are localized not only at the cell periphery. They also move towards the central part of the cells. They are larger than focal adhesion complexes, and are shaped in the form of short and thick streaks. The phosphorylation status of paxillin and the recruitment of FAK in these structures are still high, but lower than in focal complexes. Focal adhesions associate with considerably longer actin and myosin fibers localized not only peripherally, but also close to the perinuclear region of cells. Focal adhesions still contain integrin $\alpha_v\beta_3$, associated with cell proliferation, and the cells are active in migration. However, these adhesions have a relatively high content of talin and vinculin, and fibronectin fibrillogenesis starts below these sites. The turnover of focal adhesions is slower than in focal complexes, taking about 8.5 min (Zamir and Geiger, 2001; Zamir et al., 1999, 2000; Zaidel-Bar et al., 2007). The formation of focal adhesions was also supported by disruption of microtubules. In Swiss 3T3 cells, the disruption of microtubules by nocodazole or vinblastine induced a rapid assembly of focal adhesions and microfilament bundles, tyrosine phosphorylation of FAK and paxillin, and subsequent enhancement of DNA synthesis without the addition of external growth factors (Bershadsky et al., 1996) (Table 2, Fig. 14).

Fibrillar adhesions have the morphology of long thin streaks and are localized in the central region of cells. The paxillin in these sites is not phosphorylated, and the content of FAK is very low. In comparison with focal complexes and focal adhesions, the content of paxillin, talin and vinculin in these sites is relatively low, and the sites contain predominantly tensin. Cells with fibrillar adhesions contain thick bundles of actin and myosin fibers filling the entire volume of the cells, but these adhesions colocalize rather with thinner fibers crossing the actin and myosin bundles in the central parts of the cells. In cells adhering to fibronectin substrates, the fibrillar adhesions contain predominantly integrin $\alpha_5\beta_1$. Integrins with a β_1 chain (including integrin $\alpha_v\beta_1$), have often been reported to be associated with lower proliferation activity and cell maturation (Dahm and Bowers, 1998; Lourenço et al., 2007; Wilson, 2007). In addition, the fibrillogenesis in the fibronectin matrix located beneath fibrillar adhesions is very high. The turnover of fibrillar adhesions is relatively slow, and they are stable for 42 min. The development of fibrillar adhesions is supported by 3D matrices and dynamic cell cultivation. These properties of these adhesions are close to those of cell–matrix adhesions under physiological in vivo conditions, while focal complexes and focal adhesions are typical features for the classical static two-dimensional cell culture system (Danen et al., 2002; Esteban-Barragan et al., 2002; Katz et al., 2000; Zamir and Geiger, 2001; Zamir et al., 1999, 2000; Zaidel-Bar et al., 2007; Table 2, Fig. 14).

10. Control of cell proliferation and differentiation in tissue engineering

The switch between proliferation and differentiation and its precise control and timing are desirable in tissue engineering applications. In these applications, the construction of vascular replacements deserves special attention, especially if vascular smooth muscle cells are introduced in these grafts. Excessive migratory and proliferation activity of vascular smooth muscle cells (VSMC) can result in stenosis and occlusion of the lumen of vascular prostheses, especially those of small caliber (Bordenave et al., 2005; Heise et al., 2006; Ishii et al., 2008; Zilla et al., 2007). In addition, the proliferating VSMC usually express a higher number of surface adhesion molecules of the immunoglobulin and selectin superfamilies, which bind platelets and cells of the immune systems, such as leucocytes, lymphocytes, monocytes and macrophages (Bacakova et al., 2001a,b, 2002). VSMC have therefore often been considered an undesirable component of these prostheses, which should be excluded from artificial vascular

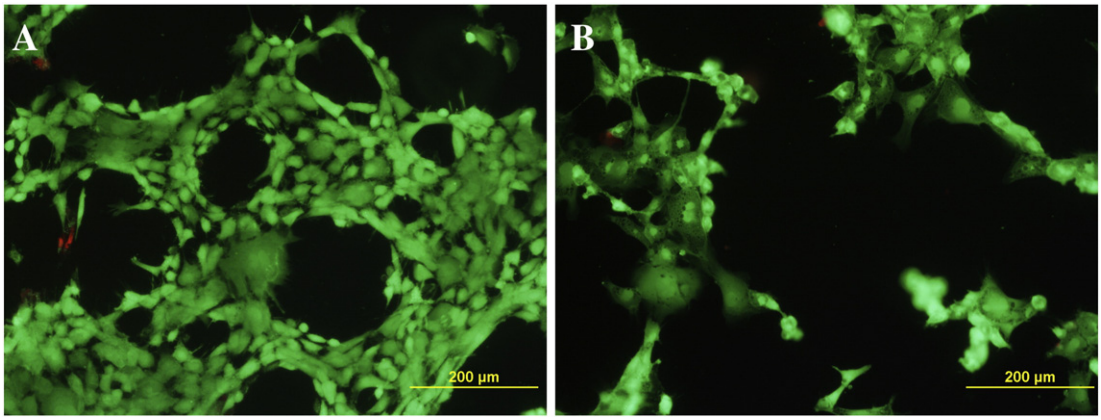

Fig. 15. Rat aortic smooth muscle cells in cultures on tissue culture polystyrene in the presence of a pure polyester mesh (A) and a sirolimus-releasing polyester mesh (B) on day 2 after adding the meshes. Stained with a LIVE/DEAD viability/cytotoxicity kit (Invitrogen). Living cells with active esterases are stained in green, while dead cells with permeable cytoplasmic membrane are stained in red. Olympus microscope IX 51, DP 70 digital camera, obj. ×20, scale bar = 200 µm. Note that in the presence of sirolimus, the cells are alive but they are apparently less numerous, i.e., they are less active in proliferation (Filova et al., 2011).

grafts. There have been several approaches to achieve this goal. The first was to create a bioinert surface not allowing attachment, spreading and subsequent growth of cells, such as VSMC, or adhesion and activation of thrombocytes and immunocompetent cells. However, in this case, the artificial blood vessel replacements act as passive, non-living and thus non-physiological conduits for blood. In addition, these conduits gradually lose their bioinertness with time, and thus their durability in the patient's organism. The inertness of clinically used vascular prostheses toward cell adhesion is usually based on high hydrophobia of the material used for their construction, e.g. polyethylene terephthalate or polytetrafluoroethylene (Bordenave et al., 2005; Chlupac et al., 2009; Deutsch et al., 1997). However, these materials adsorb proteins, though in a less appropriate spectrum and spatial orientation, and thus they can support some minimal cell adhesion, which could increase with time due to biochemically active biological environments, the mechanical stress provided by blood flow, and, in the case of knitted or woven prostheses, also the penetration of blood material inside the graft wall. Similarly, extremely hydrophilic surfaces, also used in vascular tissue engineering, such as surfaces based on polyethylene oxide (PEO), polyethylene glycol (PEG), triblock copolymer of PEG-b-poly(propylene glycol) (PPG)-b-PEG triblock copolymer (Pluronic) or polyrotaxanes (Ko et al., 2001; Lee et al., 2002; Park et al., 2002), could undergo wear and increase their permissiveness for protein adsorption and cell adhesion. Other approaches used for inhibiting adhesion and growth of VSMC and adhesion and activation of platelets involved modifying the prostheses with albumin, i.e. a serum protein non-adhesive for cells (Kang et al., 1997), heparin and heparin-like molecules (Lee et al., 2002) or other drugs exerting anticoagulant effects and/or antimigratory and antiproliferative effects on VSMC. These drugs include hirudin (Heise et al., 2006), dipyridamole (Aldenhoff et al., 2001), antiangiogenic agents (Shigematsu et al., 2001), inhibitors of CDK2 kinase (Brooks et al., 1997), sirolimus (Filova et al., 2011; Ishii et al., 2008) and paclitaxel (Lim et al., 2007b). These drugs can be incorporated directly into the prosthesis wall or can be delivered through drug-eluting stents (Lee et al., 2008), catheters and perivascular collars (Filova et al., 2011; for a review, see Sriram and Patterson, 2001). Systemic administration of antiproliferative drugs (Ilkay et al., 2006; for a review, see Sriram and Patterson, 2001), radiation therapy (Tepe et al., 2005; Zhang et al., 2007), photodynamic therapy (Heckenkamp et al., 2007) and gene therapy (Hayashi et al., 2000; Qian et al., 2006) have also been used or developed to suppress VSMC proliferation on artificial vascular replacements (Fig. 15).

A more physiological approach to the prevention of restenosis of artificial vascular prostheses involves lining the inner surface of these grafts with a confluent, mature, semipermeable and quiescent endothelial cell layer. A layer of this type is considered the best way of preventing thrombus formation as well as the adhesion and activation of immunocompetent cells. Mature endothelial cells also synthesize heparin-like glycosaminoglycans, preventing excessive proliferation of VSMC and maintaining these cells in a quiescent, differentiated and contractile state. Because of these beneficial effects of endothelium, the artificial materials for potential use in vascular transplantation are developed to be attractive mainly for endothelial cells, and a lot of work has been done to understand the mechanisms that control the adhesion, growth and function of this cell type, as well as ways to obtain it by differentiation of progenitor stem cells (Alobaid et al., 2006; Bacakova et al., 2000b; Bordenave et al., 2005; Chlupac et al., 2009; Deutsch et al., 1997; Greisler et al., 1991; Meinhart et al., 2005; Punshon et al., 2008; Zilla et al., 2007).

Under certain conditions, which promote cell maturation and differentiated function, VSMC could also act beneficially in vascular prostheses, and there is no need to exclude them from the list of artificial vascular replacements. VSMC are physiological, and are the most numerous component of the natural vascular wall, thus their presence in an advanced bioartificial vascular wall is reasonable and necessary.

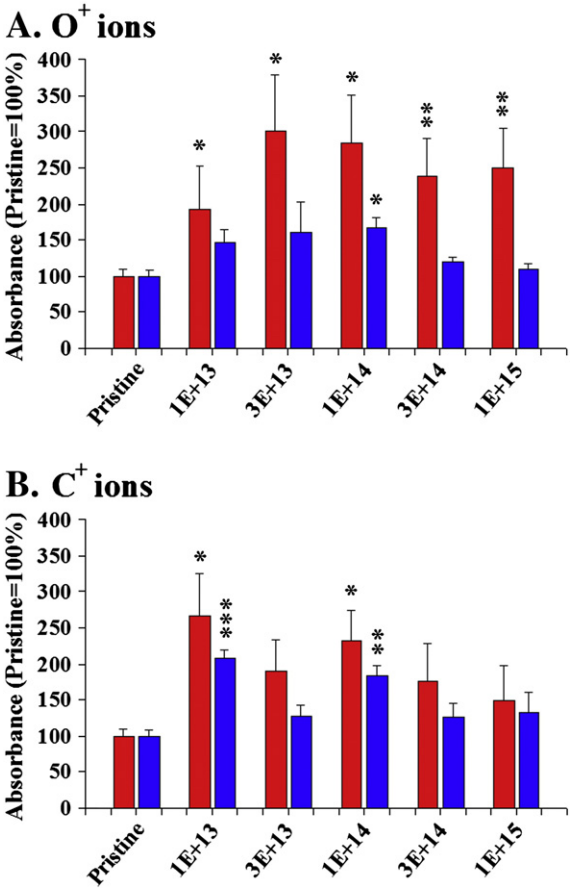

Fig. 16. Concentration of alpha-actin (A) and SM1 and SM2 myosins (B), i.e. markers of vascular smooth muscle cell differentiation towards the contractile phenotype, in rat aortic smooth muscle cells in 4-day-old cultures on pristine polyethylene and polyethylene modified by irradiation with O^+ or C^+ ions (energy 30 keV, doses from 10^{13} to 10^{15} ions/cm^2). Measured by enzymatic immunosorbent assay (ELISA) per mg of protein, absorbances expressed as a % of the values obtained on pristine non-modified PE. Mean ± SEM from 4 to 6 experiments, Student *t*-test for unpaired data, $^*p<0.05$, $^{**}p<0.01$, $^{***}p<0.001$ compared to the values on pristine polyethylene.

Quiescent and highly differentiated VSMC with a contractile phenotype support the endothelialisation of artificial vascular prostheses and can also perform their contractile function. VSMC could also participate in the gradual removal of bioresorbable components of artificial vascular prostheses, replacing these molecules with natural ECM (Campbell and Campbell, 1995; Deutsch et al., 1997; for a review, see Bacakova et al., 2001a, 2004). Therefore, from this point of view, the goal of vascular tissue engineering should lie in reconstructing both the *tunica intima* and the *media* on an artificial growth support (polymeric carrier). These autologous VSMC could be derived e.g. from subcutaneous veins, expanded in cell culture conditions and seeded on the prostheses before a planned surgery. The VSMC could be also differentiated from mesenchymal stem cells, e.g. those taken from the bone marrow, or other progenitor cells.

A cardinal question is: How to differentiate the VSMC and keep them in a non-proliferative, contractile phenotype? Physiological control of cell growth and differentiation involves the following considerations: *soluble factors* physiologically present in the blood (or in the serum supplement of the culture medium) or synthesized in an autocrine manner in the cells of the vascular wall (e.g. growth factors like PDGF, EGF, FGF, various hormones such as steroids, catecholamines, angiotensin, heparin). The second consideration is the regulation of growth and differentiation by *intercellular contacts*. If the physicochemical surface properties of ion-implanted and other modified polymers in our experiments enabled the

attachment of VSMC at high initial densities near confluence, i.e. if the intercellular contacts were established very soon, the cells then proliferated only moderately and contained a higher concentration of markers of VSMC differentiation, such as alpha-actin and SM myosins (Bacakova et al., 2000a, 2001a; Fig. 16). Similarly, in vascular endothelial cells, the establishment of intercellular contacts, mediated by VE-cadherin, between a cell and two or more of its neighboring cells decreased the cell proliferation (Gray et al., 2008).

The third important approach for inducing a switch from proliferation to a differentiation program involves manipulating the *cell–matrix adhesion*. This involves cell adhesion with many integrin or other adhesion receptors of an appropriate type, associated with cell differentiation, and also the formation of a large number of mature cell–matrix adhesion sites. This intensive cell–matrix interaction requires the engagement of a large portion of the cell membrane, which can be achieved not only by extensive cell spreading on 2D surfaces but mainly in a 3D culture system. The differentiation program induced by the intensive cell–matrix contact in a 3D environment can be further potentiated by dynamic cultivation conditions, namely mechanical stimulation of VSMC by cyclic strain (Cevallos et al., 2006; Riha et al., 2007; Shimizu et al., 2008).

11. Conclusion

Artificial materials have become more and more important cell carriers for tissue engineering and tissue replacement. Like natural ECM, they regulate the gene expression in cells, and as a consequence, the adhesion, viability, proliferation and differentiation of the cells. Cell attachment and spreading is strongly influenced by the physicochemical properties of the material surface, namely its chemical composition, surface energy, polarity, wettability, roughness, topography and mechanical properties. The extent and the strength of the cell adhesion then control further cell behavior, such as the decision between apoptosis and survival or a switch between a proliferation program and a differentiation program. Cell adhesion to artificial materials is usually mediated by spontaneous adsorption of ECM molecules, and the spectrum, the amount and the geometrical conformation of these molecules depend on the physical and chemical properties of the material surface. However, in more advanced cell carriers, the surface can be endowed with synthetic ECM-derived ligands for cell adhesion receptors of defined types, concentration, spacing and distribution, which regulate the formation, character and maturation of cell–material contacts and the further cell performance. In addition, the cell behavior in bioartificial tissue replacements can be further modulated by loading the material with various drugs, which can be released under control, and also by exposing the cell–material construct to dynamic conditions and appropriate mechanical stress.

Acknowledgments

This work has been supported by the Grant Agency of the Czech Republic (Grants No. P108/10/1106 and P108/10/1858), by the Academy of Sciences of the Czech Republic (Grants No. KAN400480701, KAN101120701, KAN200100801, IAA400320901 and IAAX00100902), and by Czech Ministry of Education (Grant No. 6046137305). We thank Mrs. Jana Vobornikova (Inst. Physiol., Acad. Sci. CR) for her excellent technical assistance in preparing the manuscript. Mr. Robin Healey (Czech Technical University in Prague) is gratefully acknowledged for his language revision of the manuscript.

References

Aldenhoff YB, van Der Veen FH, ter Woorst J, Habets J, Poole-Warren LA, Koole LH. Performance of a polyurethane vascular prosthesis carrying a dipyridamole (Persantin) coating on its lumenal surface. Biomed Mater Res 2001;54(2):224–33.

Alobaid N, Salacinski HJ, Sales KM, Ramesh B, Kannan RY, Hamilton G, et al. Nanocomposite containing bioactive peptides promote endothelialisation by circulating progenitor cells: an in vitro evaluation. Eur J Vasc Endovasc Surg 2006;32(1):76–83.

Anand G, Sharma S, Dutta AK, Kumar SK, Belfort G. Conformational transitions of adsorbed proteins on surfaces of varying polarity. Langmuir 2010;26(13):10803–11.

Anselme K. Osteoblast adhesion on biomaterials. Biomaterials 2000;21(7):667–81.

Assoian RK, Klein EA. Growth control by intracellular tension and extracellular stiffness. Trends Cell Biol 2008;18(7):347–52.

Avraham HK, Lee TH, Koh Y, Kim TA, Jiang S, Sussman M, et al. Vascular endothelial growth factor regulates focal adhesion assembly in human brain microvascular endothelial cells through activation of the focal adhesion kinase and related adhesion focal tyrosine kinase. J Biol Chem 2003;278(38):36661–8.

Bacakova L, Svorcik V. Cell colonization control by physical and chemical modification of materials. In: Kimura D, editor. Cell growth processes: new research. New York: Nova Science Publishers Inc; 2008. p. 5–56.

Bacakova L, Svorcik V, Rybka V, Micek I, Hnatowicz V, Lisá V, et al. Adhesion and proliferation of cultured human vascular smooth muscle cells on polystyrene implanted with N^+, F^+ and Ar^+ ions. Biomaterials 1996;17(11):1121–6.

Bacakova L, Mares V, Bottone MG, Pellicciari C, Lisa V, Svorcik V. Fluorine-ion-implanted polystyrene improves growth and viability of vascular smooth muscle cells in culture. J Biomed Mater Res 2000a;49(3):369–79.

Bacakova L, Mares V, Lisa V, Svorcik V. Molecular mechanisms of improved adhesion and growth of an endothelial cell line cultured on polystyrene implanted with fluorine ions. Biomaterials 2000b;21(11):1173–9.

Bacakova L, Walachova K, Svorcik V, Hnatowicz V. Adhesion and proliferation of rat vascular smooth muscle cells on polyethylene implanted with O^+ and C^+ ions. J Biomater Sci Polym Ed 2001a;12(7):817–34.

Bacakova L, Stary V, Kofronova O, Lisa V. Polishing and coating carbon fibre-reinforced carbon composites with a carbon–titanium layer enhances adhesion and growth of osteoblast-like MG63 cells and vascular smooth muscle cells *in vitro*. J Biomed Mater Res 2001b;54(4):567–78.

Bacakova L, Lisa V, Kubinova L, Wilhelm J, Novotna J, Eckhardt A, et al. Ultraviolet light-irradiated collagen III modulates expression of cytoskeletal and surface adhesion molecules in rat aortic smooth muscle cells in vitro. Virchows Arch 2002;440(1):50–62.

Bacakova L, Lapcikova M, Kubies D, Rypacek F. Adhesion and growth of rat aortic smooth muscle cells on lactide-based polymers. Adv Exp Med Biol 2003;534:179–89.

Bacakova L, Filova E, Rypacek F, Svorcik V, Stary V. Cell adhesion on artificial materials for tissue engineering. Physiol Res 2004;53(Suppl 1):S35–45.

Bacakova L, Filova E, Kubies D, Machova L, Proks V, Malinova V, et al. Adhesion and growth of vascular smooth muscle cells in cultures on bioactive RGD peptide-carrying polylactides. J Mater Sci Mater Med 2007a;18(7):1317–23.

Bacakova L, Grausova L, Vacik J, Fraczek A, Blazewicz S, Kromka A, et al. Improved adhesion and growth of human osteoblast-like MG 63cells on biomaterials modified with carbon nanoparticles. Diamond Relat Mater 2007b;16(12):2133–40.

Bacakova L, Grausova L, Vandrovcova M, Vacik J, Frazcek A, Blazewicz S, et al. Carbon nanoparticles as substrates for cell adhesion and growth. In: Lombardi SL, editor. Nanoparticles: new research. New York: Nova Science Publishers Inc; 2008. p. 39–107.

Bacakova L, Grausova L, Vacik J, Kromka A, Biederman H, Choukourov A, et al. Nanocomposite and nanostructured carbon-based films as growth substrates for bone cells. In: Reddy B, editor. Advances in diverse industrial applications of nanocomposites. Intech: Open Access Publisher; 2011. p. 399–435.

Bensaid W, Triffitt JT, Blanchat C, Oudina K, Sedel L, Petite H. A biodegradable fibrin scaffold for mesenchymal stem cell transplantation. Biomaterials 2003;24(14):2497–502.

Bershadsky A, Chausovsky A, Becker E, Lyubimova A, Geiger B. Involvement of microtubules in the control of adhesion-dependent signal transduction. Curr Biol 1996;6(10):1279–89.

Bet MR, Goissis G, Vargas S, Selistre-de-Araujo HS. Cell adhesion and cytotoxicity studies over polyanionic collagen surfaces with variable negative charge and wettability. Biomaterials 2003;24(1):131–7.

Bhatia SN, Toner M, Tompkins RG, Yarmush ML. Selective adhesion of hepatocytes on patterned surfaces. Ann N Y Acad Sci 1994;745:187–209.

Biela SA, Su Y, Spatz JP, Kemkemer R. Different sensitivity of human endothelial cells, smooth muscle cells and fibroblasts to topography in the nano-micro range. Acta Biomater 2009;5(7):2460–6.

Biggs MJ, Richards RG, Gadegaard N, Wilkinson CD, Dalby MJ. Regulation of implant surface cell adhesion: characterization and quantification of S-phase primary osteoblast adhesions on biomimetic nanoscale substrates. J Orthop Res 2007;25(2):273–82.

Blombäck B, Carlsson K, Fatah K. Fibrin in human plasma: gel architectures governed by rate and nature of fibrinogen activation. Thromb Res 1994;75(5):521–38.

Boateng SY, Hartman TJ, Ahluwalia N, Vidula H, Desai TA, Russell B. Inhibition of fibroblast proliferation in cardiac myocyte cultures by surface microtopography. Am J Physiol Cell Physiol 2003;285(1):C171–82.

Bordenave L, Fernandez P, Rémy-Zolghadri M, Villars S, Daculsi R, Midy D. In vitro endothelialized ePTFE prostheses: clinical update 20 years after the first realization. Clin Hemorheol Microcirc 2005;33(3):227–34.

Boyan BD, Bonewald LF, Paschalis EP, Lohmann CH, Rosser J, Cochran DL. Osteoblast-mediated mineral deposition in culture is dependent on surface microtopography. Calcif Tissue Int 2002;71(6):519–29.

Boyan BD, Lossdörfer S, Wang L, Zhao G, Lohmann CH, Cochran DL, et al. Osteoblasts generate an osteogenic microenvironment when grown on surfaces with rough microtopographies. Eur Cell Mater 2003;6:22–7.

Britland S, Perez-Arnaud E, Clark P, McGinn B, Connolly P, Moores G. Micropatterning proteins and synthetic peptides on solid supports: a novel application for microelectronics fabrication technology. Biotechnol Prog 1992;8(2):155–60.
Brooks EE, Gray NS, Joly A, Kerwar SS, Lum R, Mackman RL, et al. CVT-313, a specific and potent inhibitor of CDK2 that prevents neointimal proliferation. J Biol Chem 1997;272(46):29207–11.
Campbell GR, Campbell JH. Molecular and biological responses to the extracellular matrix. In: Schwartz SM, Mecham RP, editors. The vascular smooth muscle cell. San Diego, New York, Boston: Acad. Press; 1995. p. 1–15.
Cavalcanti-Adam EA, Volberg T, Micoulet A, Kessler H, Geiger B, Spatz JP. Cell spreading and focal adhesion dynamics are regulated by spacing of integrin ligands. Biophys J 2007;92(8):2964–74.
Cevallos M, Riha GM, Wang X, Yang H, Yan S, Li M, et al. Cyclic strain induces expression of specific smooth muscle cell markers in human endothelial cells. Differentiation 2006;74(9–10):552–61.
Chan CK, Liao S, Li B, Lareu RR, Larrick JW, Ramakrishna S, et al. Early adhesive behavior of bone-marrow-derived mesenchymal stem cells on collagen electrospun fibers. Biomed Mater 2009;4(3):035006.
Chen CS, Mrksich M, Huang S, Whitesides GM, Ingber DE. Geometric control of cell life and death. Science 1997;276(5317):1425–8.
Chen CS, Mrksich M, Huang S, Whitesides GM, Ingber DE. Micropatterned surfaces for control of cell shape, position, and function. Biotechnol Prog 1998;14(3):356–63.
Chen CS, Brangwynne C, Ingber DE. Pictures in cell biology: squaring up to the cell-shape debate. Trends Cell Biol 1999;9(7):283.
Cheng SL, Lai CF, Blystone SD, Avioli LV. Bone mineralization and osteoblast differentiation are negatively modulated by integrin alpha(v)beta3. J Bone Miner Res 2001;16(2):277–88.
Chlupac J, Filova E, Bacakova L. Blood vessel replacement: 50 years of development and tissue engineering paradigms in vascular surgery. Physiol Res 2009;58(Suppl 2): S119–39.
Clem WC, Chowdhury S, Catledge SA, Weimer JJ, Shaikh FM, Hennessy KM, et al. Mesenchymal stem cell interaction with ultra-smooth nanostructured diamond for wear-resistant orthopaedic implants. Biomaterials 2008;29(24–25):3461–8.
Curran JM, Stokes R, Irvine E, Graham D, Amro NA, Sanedrin RG, et al. Introducing dip pen nanolithography as a tool for controlling stem cell behaviour: unlocking the potential of the next generation of smart materials in regenerative medicine. Lab Chip 2010;10(13):1662–70.
Dahm LM, Bowers CW. Vitronectin regulates smooth muscle contractility via alphav and beta1 integrin. J Cell Sci 1998;111(Pt 9):1175–83.
Danen EH, Sonneveld P, Brakebusch C, Fassler R, Sonnenberg A. The fibronectin-binding integrins alpha5beta1 and alphavbeta3 differentially modulate RhoA-GTP loading, organization of cell matrix adhesions, and fibronectin fibrillogenesis. J Cell Biol 2002;159(6):1071–86.
Daxini SC, Nichol JW, Sieminski AL, Smith G, Gooch KJ, Shastri VP. Micropatterned polymer surfaces improve retention of endothelial cells exposed to flow-induced shear stress. Biorheology 2006;43(1):45–55.
Dee KC, Andersen TT, Bizios R. Design and function of novel osteoblast-adhesive peptides for chemical modification of biomaterials. J Biomed Mater Res 1998;40(3):371–7.
Detrait E, Lhoest JB, Knoops B, Bertrand P, van den Bosch de Aguilar P. Orientation of cell adhesion and growth on patterned heterogeneous polystyrene surface. J Neurosci Methods 1998;84(1–2):193–204.
Deutsch M, Meinhart J, Vesely M, Fischlein T, Groscurth P, von Oppell U, et al. In vitro endothelialization of expanded polytetrafluoroethylene grafts: a clinical case report after 41 months of implantation. J Vasc Surg 1997;25(4):757–63.
Dike LE, Chen CS, Mrksich M, Tien J, Whitesides GM, Ingber DE. Geometric control of switching between growth, apoptosis, and differentiation during angiogenesis using micropatterned substrates. In Vitro Cell Dev Biol Anim 1999;35(8): 441–8.
DiMillia PA, Stone JA, Quinn JA, Albelda SM, Lauffenburger DA. Maximal migration of human smooth muscle cells on fibronectin and type IV collagen occurs at an intermediate attachment strength. J Cell Biol 1993;122(3):729–37.
Dwivedi A, Sala-Newby GB, George SJ. Regulation of cell–matrix contacts and beta-catenin signaling in VSMC by integrin-linked kinase: implications for intimal thickening. Basic Res Cardiol 2008;103(3):244–56.
Engler A, Bacakova L, Newman C, Hategan A, Griffin M, Discher D. Substrate compliance versus ligand density in cell on gel responses. Biophys J 2004;86(1 Pt 1):617–28.
Engler AJ, Sen S, Sweeney HL, Discher DE. Matrix elasticity directs stem cell lineage specification. Cell 2006;126(4):677–89.
Esteban-Barragán MA, Avila P, Alvarez-Tejado M, Gutiérrez MD, García-Pardo A, Sánchez-Madrid F, et al. Role of the von Hippel–Lindau tumor suppressor gene in the formation of beta1-integrin fibrillar adhesions. Cancer Res 2002;62(10): 2929–36.
Falconnet D, Csucs G, Grandin HM, Textor M. Surface engineering approaches to micropattern surfaces for cell-based assays. Biomaterials 2006;27(16):3044–63.
Fassina L, Visai L, De Angelis MG, Benazzo F, Magenes G. Surface modification of a porous polyurethane through a culture of human osteoblasts and an electromagnetic bioreactor. Technol Health Care 2007;15(1):33–45.
Feng B, Weng J, Yang BC, Qu SX, Zhang XD. Characterization of surface oxide films on titanium and adhesion of osteoblast. Biomaterials 2003;24(25):4663–70.
Feng ZQ, Chu XH, Huang NP, Leach MK, Wang G, Wang YC, et al. Rat hepatocyte aggregate formation on discrete aligned nanofibers of type-I collagen-coated poly (L-lactic acid). Biomaterials 2010;31(13):3604–12.
Fernandez JL, Geiger B, Salomon D, Ben-Ze'ev A. Suppression of vinculin expression by antisense transfection confers changes in cell morphology, motility, and anchorage-dependent growth of 3T3 cells. J Cell Biol 1993;122(3):1285–94.
Filova E, Bacakova L, Lisa V, Kubies D, Machova L, Lapcikova M, et al. Adhesion and proliferation of vascular smooth muscle cells on polylactide–polyethylene oxide copolymers with different content and length of polyethylene oxide chains. Inz Biomater Eng Biomater 2004;7(38–42):19–21.
Filova E, Bullett NA, Bacakova L, Grausova L, Haycock JW, Hlucilova J, et al. Regionally-selective cell colonization of micropatterned surfaces prepared by plasma polymerization of acrylic acid and 1,7-octadiene. Physiol Res 2009a;58(5): 669–84.
Filova E, Brynda E, Riedel T, Bacakova L, Chlupac J, Lisa V, et al. Vascular endothelial cells on two- and three-dimensional fibrin assemblies for biomaterial coatings. J Biomed Mater Res A 2009b;90(1):55–69.
Filova E, Straka F, Bacakova L, Munzarova M, Svobodova J. Growth of valve interstitial cells on aligned and randomly oriented electrospun nanofibres. Abstract No. P155, the 5th Biennial Meeting of the SHVD, Berlin, Germany, June 27–30; 2009c http://www.shvd.org/documents/BERLIN%20POSTERS/P155.pdf.
Filova E, Parizek M, Olsovska J, Kamenik Z, Brynda E, Riedel T, et al. Perivascular sirolimus-delivery system. Int J Pharm 2011;404(1–2):94–101.
Gao D, Kumar G, Co C, Ho CC. Formation of capillary tube-like structures on micropatterned biomaterials. Adv Exp Med Biol 2008;614:199–205.
Grassl E, Oegema TR, Tranquillo RT. A fibrin-based arterial media equivalent. J Biomed Mater Res 2003;66A(3):550–61.
Grausova L, Kromka A, Bacakova L, Potocky S, Vanecek M, Lisa V. Bone and vascular endothelial cells in cultures on nanocrystalline diamond films. Diamond Relat Mater 2008a;17(7–10):1405–9.
Grausova L, Vacik J, Bilkova P, Vorlicek V, Svorcik V, Soukup D, et al. Regionally-selective adhesion and growth of human osteoblast-like MG 63 cells on micropatterned fullerene C60 layers. J Optoelectron Adv Mater 2008b;10(8):2071–6.
Grausova L, Bacakova L, Kromka A, Vanecek M, Lisa V. Molecular markers of adhesion, maturation and immune activation of human osteoblast-like MG 63 cells on nanocrystalline diamond films. Diamond Relat Mater 2009a;18(2–3): 258–63.
Grausova L, Bacakova L, Kromka A, Potocky S, Vanecek M, Nesladek M, et al. Nanodiamond as a promising material for bone tissue engineering. J Nanosci Nanotechnol 2009b;9(6): 3524–34.
Grausova L, Vacik J, Vorlicek V, Svorcik V, Slepicka P, Bilkova P, et al. Fullerene C60 films of continuous and micropatterned morphology as substrates for adhesion and growth of bone cells. Diamond Relat Mater 2009c;18(2–3):578–86.
Gray DS, Liu WF, Shen CJ, Bhadriraju K, Nelson CM, Chen CS. Engineering amount of cell–cell contact demonstrates biphasic proliferative regulation through RhoA and the actin cytoskeleton. Exp Cell Res 2008;314(15):2846–54.
Greisler HP, Tattersall CW, Klosak JJ, Cabusao EA, Garfield JD, Kim DU. Partially bioresorbable vascular grafts in dogs. Surgery 1991;110(4):645–54.
Hamilton DW, Brunette DM. The effect of substratum topography on osteoblast adhesion mediated signal transduction and phosphorylation. Biomaterials 2007;28(10): 1806–19.
Hatakeyama H, Kikuchi A, Yamato M, Okano T. Patterned biofunctional designs of thermoresponsive surfaces for spatiotemporally controlled cell adhesion, growth, and thermally induced detachment. Biomaterials 2007;28(25): 3632–43.
Hayashi K, Nakamura S, Morishita R, Moriguchi A, Aoki M, Matsumoto K, et al. In vivo transfer of human hepatocyte growth factor gene accelerates re-endothelialization and inhibits neointimal formation after balloon injury in rat model. Gene Ther 2000;7(19):1664–71.
H'dhili F, Bachelot R, Rumyantseva A, Lerondel G, Royer P. Nano-patterning photosensitive polymers using local field enhancement at the end of apertureless SNOM tips. J Microsc 2003;209(Pt 3):214–22.
He J, Zhou W, Zhou X, Zhong X, Zhang X, Wan P, et al. The anatase phase of nanotopography titania plays an important role on osteoblast cell morphology and proliferation. J Mater Sci Mater Med 2008;19(11):3465–72.
Heckenkamp J, Mellander S, Fogelstrand P, Breuer S, Brunkwall J, Mattsson E. Photodynamic therapy reduces intimal hyperplasia in prosthetic vascular bypass grafts in a pig model. Eur J Vasc Endovasc Surg 2007;34(3):333–9.
Heise M, Schmidmaier G, Husmann I, Heidenhain C, Schmidt J, Neuhaus P, et al. PEG-hirudin/iloprost coating of small diameter ePTFE grafts effectively prevents pseudointima and intimal hyperplasia development. Eur J Vasc Endovasc Surg 2006;32(4):418–24.
Heitz J, Svorcik V, Bacakova L, Rockova K, Ratajová E, Gumpenberger T, et al. Cell adhesion on polytetrafluoroethylene modified by UV-irradiation in an ammonia atmosphere. J Biomed Mater Res 2003;67A(1):130–7.
Helige C, Hofmann-Wellenhof R, Fink-Puches R, Smolle J. Mofarotene-induced inhibition of melanoma cell motility by increasing vinculin-containing focal contacts. Melanoma Res 2004;14(6):547–54.
Hoshiga M, Alpers CE, Smith LL, Giachelli CM, Schwartz SM. Alpha-v beta-3 integrin expression in normal and atherosclerotic artery. Circ Res 1995;77(6): 1129–35.
Hsieh YC, Hsieh SJ, Chang YS, Hsueh CM, Hsu SL. The lipoxygenase inhibitor, baicalein, modulates cell adhesion and migration by up-regulation of integrins and vinculin in rat heart endothelial cells. Br J Pharmacol 2007;151(8):1235–45.
Hu J, Liu X, Ma PX. Induction of osteoblast differentiation phenotype on poly(L-lactic acid) nanofibrous matrix. Biomaterials 2008;29(28):3815–21.
Huang S, Ingber DE. Shape-dependent control of cell growth, differentiation, and apoptosis: switching between attractors in cell regulatory networks. Exp Cell Res 2000;261(1):91–103.
Huang S, Chen CS, Ingber DE. Control of cyclin D1, p27(Kip1), and cell cycle progression in human capillary endothelial cells by cell shape and cytoskeletal tension. Mol Biol Cell 1998;9(11):3179–93.

Hwang SY, Kwon KW, Jang KJ, Park MC, Lee JS, Suh KY. Adhesion assays of endothelial cells on nanopatterned surfaces within a microfluidic channel. Anal Chem 2010;82 (7):3016–22.
Ilkay E, Tirikli L, Ozercan I, Yavuzkir M, Karaca I, Rahman A, et al. Oral mycophenolate mofetil prevents in-stent intimal hyperplasia without edge effect. Angiology 2006;57(5):577–84.
Ingber DE, Prusty D, Sun Z, Betensky H, Wang N. Cell shape, cytoskeletal mechanics, and cell cycle control in angiogenesis. J Biomech 1995;28(12):1471–84.
Ishii Y, Sakamoto S, Kronengold RT, Virmani R, Rivera EA, Goldman SM, et al. A novel bioengineered small-caliber vascular graft incorporating heparin and sirolimus: excellent 6-month patency. J Thorac Cardiovasc Surg 2008;135(6):1237–45. discussion 1245-6.
Itoga K, Kobayashi J, Yamato M, Kikuchi A, Okano T. Maskless liquid-crystal-display projection photolithography for improved design flexibility of cellular micropatterns. Biomaterials 2006;27(15):3005–9.
Jockenhoevel S, Zund G, Hoerstrup SP, Chalabi K, Sachweh JS, Demircan L, et al. Fibrin gel — advantages of a new scaffold in cardiovascular tissue engineering. Eur J Cardiothorac Surg 2001;19(4):424–30.
Kalbacova M, Kalbac M, Dunsch L, Kromka A, Vanecek M, Rezek B, et al. The effect of SWCNT and nano-diamond films on human osteoblast cells. Phys Stat Sol (b) 2007;244(11): 4356–9.
Kanchanawong P, Shtengel G, Pasapera AM, Ramko EB, Davidson MW, Hess HF, et al. Nanoscale architecture of integrin-based cell adhesions. Nature 2010;468(7323): 580–4.
Kang SS, Petsikas D, Murchan P, Cziperle DJ, Ren D, Kim DU, et al. Effects of albumin coating of knitted Dacron grafts on transinterstitial blood loss and tissue ingrowth and incorporation. Cardiovasc Surg 1997;5(2):184–9.
Kantawong F, Burgess KE, Jayawardena K, Hart A, Burchmore RJ, Gadegaard N, et al. Whole proteome analysis of osteoprogenitor differentiation induced by disordered nanotopography and mediated by ERK signalling. Biomaterials 2009;30(27): 4723–31.
Karp JM, Yeo Y, Geng W, Cannizarro C, Yan K, Kohane DS, et al. A photolithographic method to create cellular micropatterns. Biomaterials 2006;27(27): 4755–64.
Kasalkova N, Kolarova K, Bacakova L, Parizek M, Svorcik V. Cell adhesion and proliferation on modified polyethylene. Mater Sci Forum 2007;567–568:269–72.
Kasalkova N, Makajova Z, Parizek M, Slepicka P, Kolarova K, Bacakova L, et al. Cell adhesion and proliferation on plasma-treated and poly(ethylene glycol)-grafted polyethylene. J Adhes Sci Technol 2010;24(4):743–54.
Katz BZ, Zamir E, Bershadsky A, Kam Z, Yamada KM, Geiger B. Physical state of the extracellular matrix regulates the structure and molecular composition of cell–matrix adhesions. Mol Biol Cell 2000;11(3):1047–60.
Kaur G, Valarmathi MT, Potts JD, Wang Q. The promotion of osteoblastic differentiation of rat bone marrow stromal cells by a polyvalent plant mosaic virus. Biomaterials 2008;29(30):4074–81.
Keselowsky BG, Collard DM, García AJ. Surface chemistry modulates fibronectin conformation and directs integrin binding and specificity to control cell adhesion. Biomed Mater Res A 2003;66(2):247–59.
Khatib L, Golan DE, Cho M. Physiologic electrical stimulation provokes intracellular calcium increase mediated by phospholipase C activation in human osteoblasts. FASEB J 2004;18(15):1903–5.
Kidoaki S, Matsuda T. Microelastic gradient gelatinous gels to induce cellular mechanotaxis. J Biotechnol 2008;133(2):225–30.
Kim HJ, Kim SH, Kim MS, Lee EJ, Oh HG, Oh WM, et al. Varying Ti–6Al–4V surface roughness induces different early morphologic and molecular responses in MG63 osteoblast-like cells. J Biomed Mater Res 2005;74(3):366–73.
Kim DH, Lee H, Lee YK, Nam JM, Levchenko A. Biomimetic nanopatterns as enabling tools for analysis and control of live cells. Adv Mater 2010;22(41):4551–66.
Ko YG, Kim YH, Park KD, Lee HJ, Lee WK, Park HD, et al. Immobilization of poly(ethylene glycol) or its sulfonate onto polymer surfaces by ozone oxidation. Biomaterials 2001;22(15):2115–23.
Kopecek M, Bacakova L, Vacik J, Fendrych F, Vorlicek V, Kratochvilova I, et al. Improved adhesion, growth and maturation of human bone-derived cells on manocrystalline diamond films. Phys Stat Sol (a) 2008;205(9):2146–53.
Kotal V, Svorcik V, Slepicka P, Blahova O, Sutta P, Hnatowicz V. Gold coating of poly (ethylene terephthalate) modified by argon plasma. Plasma Process Polym 2007;4(1): 69–76.
Kromka A, Grausova L, Bacakova L, Vacik J, Rezek B, Vanecek M, et al. Semiconducting to metallic-like boron doping of nanocrystalline diamond films and its effect on osteoblastic cells. Diamond Relat Mater 2010;19(2–3):190–5.
Kubova O, Svorcik V, Heitz J, Moritz S, Romanin C, Matejka P, et al. Characterization and cytocompatibility of carbon layers prepared by photo-induced chemical vapor deposition. Thin Solid Films 2007;515(17):6765–72.
Lampugnani MG, Pedenovi M, Niewiarowski A, Casali B, Donati MB, Corbascio GC, et al. Effects of dimethyl sulfoxide (DMSO) on microfilament organization, cellular adhesion, and growth of cultured mouse B16 melanoma cells. Exp Cell Res 1987;172(2):385–96.
Lee HJ, Hong JK, Goo HC, Lee WK, Park KD, Kim SH, et al. Improved blood compatibility and decreased VSMC proliferation of surface-modified metal grafted with sulfonated PEG or heparin. J Biomater Sci Polym Ed 2002;13(8):939–52.
Lee SW, Park SW, Kim YH, Yun SC, Park DW, Lee CW, et al. A randomized comparison of sirolimus- versus Paclitaxel-eluting stent implantation in patients with diabetes mellitus. J Am Coll Cardiol 2008;52(9):727–33.
Lesny P, Pradny M, Jendelova P, Michalek J, Vacik J, Sykova E. Macroporous hydrogels based on 2-hydroxyethyl methacrylate. Part 4: growth of rat bone marrow stromal cells in three-dimensional hydrogels with positive and negative surface charges and in polyelectrolyte complexes. J Mater Sci Mater Med 2006;17(9):829–33.
Leung MF, Lin TS, Sartorelli AC. Changes in actin and actin-binding proteins during the differentiation of HL-60 leukemia cells. Cancer Res 1992;52(11):3063–6.
Lim JY, Hansen JC, Siedlecki CA, Runt J, Donahue HJ. Human foetal osteoblastic cell response to polymer-demixed nanotopographic interfaces. J R Soc Interface 2005;2 (2):97–108.
Lim JY, Dreiss AD, Zhou Z, Hansen JC, Siedlecki CA, Hengstebeck RW, et al. The regulation of integrin-mediated osteoblast focal adhesion and focal adhesion kinase expression by nanoscale topography. Biomaterials 2007a;28(10):1787–97.
Lim HJ, Nam HY, Lee BH, Kim DJ, Ko JY, Park JS. A novel technique for loading of paclitaxel-PLGA nanoparticles onto ePTFE vascular grafts. Biotechnol Prog 2007b;23(3):693–7.
Lim SH, Liu XY, Song H, Yarema KJ, Mao HQ. The effect of nanofiber-guided cell alignment on the preferential differentiation of neural stem cells. Biomaterials 2010;31(34):9031–9.
Lin X, Helmke BP. Micropatterned structural control suppresses mechanotaxis of endothelial cells. Biophys J 2008;95(6):3066–78.
Liu ZX, Yu CF, Nickel C, Thomas S, Cantley LG. Hepatocyte growth factor induces ERK-dependent paxillin phosphorylation and regulates paxillin-focal adhesion kinase association. J Biol Chem 2002;277(12):10452–8.
Liu L, Chen S, Giachelli CM, Ratner BD, Jiang S. Controlling osteopontin orientation on surfaces to modulate endothelial cell adhesion. J Biomed Mater Res A 2005;74(1): 23–31.
Liu X, Lim JY, Donahue HJ, Dhurjati R, Mastro AM, Vogler EA. Influence of substratum surface chemistry/energy and topography on the human fetal osteoblastic cell line hFOB 1.19: phenotypic and genotypic responses observed in vitro. Biomaterials 2007;28(31):4535–50.
Lohmann CH, Bonewald LF, Sisk MA, Sylvia VL, Cochran DL, Dean DD. Maturation state determines the response of osteogenic cells to surface roughness and 1,25-dihydroxyvitamin D3. J Bone Miner Res 2000;15(6):1169–80.
Lossdörfer S, Schwartz Z, Wang L, Lohmann CH, Turner JD, Wieland M. Microrough implant surface topographies increase osteogenesis by reducing osteoclast formation and activity. J Biomed Mater Res A 2004;70(3):361–9.
Lourenço SV, Lima DM, Uyekita SH, Schultz R, de Brito T. Expression of beta-1 integrin in human developing salivary glands and its parallel relation with maturation markers: in situ hybridisation and immunofluorescence study. Arch Oral Biol 2007;52(11):1064–71.
Lovat V, Pantarotto D, Lagostena L, Cacciari B, Grandolfo M, Righi M. Carbon nanotube substrates boost neuronal electrical signaling. Nano Lett 2005;5(6):1107–10.
Ma J, He X, Jabbari E. Osteogenic differentiation of marrow stromal cells on random and aligned electrospun poly(L-lactide) nanofibers. Ann Biomed Eng 2011;39(1): 14–25.
Maheshwari G, Brown G, Lauffenburger DA, Wells A, Griffith LG. Cell adhesion and motility depend on nanoscale RGD clustering. J Cell Sci 2000;113(Pt 10): 1677–86.
Malarkey EB, Parpura V. Applications of carbon nanotubes in neurobiology. Neurodegener Dis 2007;4(4):292–9.
Mann BK, West JL. Cell adhesion peptides alter smooth muscle cell adhesion, proliferation, migration, and matrix protein synthesis on modified surfaces and in polymer scaffolds. J Biomed Mater Res 2002;60(1):86–93.
Mann BK, Gobin AS, Tsai AT, Schmedlen RH, West JL. Smooth muscle cell growth in photopolymerized hydrogels with cell adhesive and proteolytically degradable domains: synthetic ECM analogs for tissue engineering. Biomaterials 2001;22(22): 3045–51.
Masui M, Takata H, Kominami T. Cell adhesion and the negative cell surface charges in embryonic cells of the starfish *Asterina pectinifera*. Electrophoresis 2002;23(13): 2087–95.
Matsuda T, Inoue K, Sugawara T. Development of micropatterning technology for cultured cells. ASAIO Trans 1990;36(3):M559–62.
Mazzatenta A, Giugliano M, Campidelli S, Gambazzi L, Businaro L, Markram H, et al. Interfacing neurons with carbon nanotubes: electrical signal transfer and synaptic stimulation in cultured brain circuits. J Neurosci 2007;27(26):6931–6.
Meinhart JG, Schense JC, Schima H, Gorlitzer M, Hubbell JA, Deutsch M, et al. Enhanced endothelial cell retention on shear-stressed synthetic vascular grafts precoated with RGD-cross-linked fibrin. Tissue Eng 2005;11(5–6):887–95.
Meng J, Han Z, Kong H, Qi X, Wang C, Xie S, et al. Electrospun aligned nanofibrous composite of MWCNT/polyurethane to enhance vascular endothelium cells proliferation and function. J Biomed Mater Res A 2010;95(1):312–20.
Mikulikova R, Moritz S, Gumpenberger T, Olbrich M, Romanin C, Bacakova L, et al. Cell microarrays on photochemically modified polytetrafluoroethylene. Biomaterials 2005;26(27):5572–80.
Miller DC, Thapa A, Haberstroh KM, Webster TJ. Endothelial and vascular smooth muscle cell function on poly(lactic-co-glycolic acid) with nano-structured surface features. Biomaterials 2004;25(1):53–61.
Moon JJ, Hahn MS, Kim I, Nsiah BA, West JL. Micropatterning of poly(ethylene glycol) diacrylate hydrogels with biomolecules to regulate and guide endothelial morphogenesis. Tissue Eng Part A 2009;15(3):579–85.
Mosesson MW, Siebenlist KR, Meh DA. The structure and biological features of fibrinogen and fibrin. Ann N Y Acad Sci 2001;936:11–30.
Neff JA, Tresco PA, Caldwell KD. Surface modification for controlled studies of cell–ligand interactions. Biomaterials 1999;20(23–24):2377–93.
Noguchi A, Ito N, Sawa H, Nagane M, Hara M, Saito I. Phenotypic changes associated with exogenous expression of p16INK4a in human glioma cells. Brain Tumor Pathol 2001;18(2):73–81.
Palecek SP, Loftus JC, Ginsberg MH, Lauffenburger DA, Horwitz AF. Integrin–ligand binding properties govern cell migration speed through cell–substratum adhesiveness. Nature 1997;385(6616):537–40.

Parizek M, Bacakova L, Lisa V, Kubova O, Svorcik V, Heitz J. Vascular smooth muscle cells in cultures on synthetic polymers with adhesive microdomains. Inz Biomater (Eng Biomater) 2006;IX(58–60):7–10.
Parizek M, Bacakova L, Kasalkova N, Svorcik V, Kolarova K. Improved adhesion and growth of vascular smooth muscle cells in cultures on polyethylene modified by plasma discharge. Inz Biomater (Eng Biomater) 2007;X(67–68):1–4.
Parizek M, Kasalkova N, Bacakova L, Slepicka P, Lisa V, Blazkova M, et al. Improved adhesion, growth and maturation of vascular smooth muscle cells on polyethylene grafted with bioactive molecules and carbon particles. Int J Mol Sci 2009;10(10): 4352–74.
Parizek M, Novotna K, Bacakova L. The role of smooth muscle cells in vessel wall pathophysiology and reconstruction using bioactive synthetic polymers. A review. Physiol Res 2011;60(3):419–37.
Park HD, Lee WK, Ooya T, Park KD, Kim YH, Yui N. Anticoagulant activity of sulfonated polyrotaxanes as blood-compatible materials. J Biomed Mater Res 2002;60(1): 186–90.
Podestá D, Roth T, Ferrara F, Cagliero E, Lorenzi M. Cytoskeletal changes induced by excess extracellular matrix impair endothelial cell replication. Diabetologia 1997;40(8): 879–86.
Price RL, Waid MC, Haberstroh KM, Webster TJ. Selective bone cell adhesion on formulations containing carbon nanofibers. Biomaterials 2003;24(11):1877–87.
Price RL, Ellison K, Haberstroh KM, Webster TJ. Nanometer surface roughness increases select osteoblast adhesion on carbon nanofiber compacts. J Biomed Mater Res A 2004;70(1):129–38.
Punshon G, Sales KM, Vara DS, Hamilton G, Seifalian AM. Assessment of the potential of progenitor stem cells extracted from human peripheral blood for seeding a novel vascular graft material. Cell Prolif 2008;41(2):321–35.
Qian Z, Haessler M, Lemos JA, Arsenault JR, Aguirre JE, Gilbert JR. Targeting vascular injury using Hantavirus-pseudotyped lentiviral vectors. Mol Ther 2006;13(4): 694–704.
Rampichova M, Filova E, Varga F, Lytvynets A, Prosecka E, Kolacna L, et al. Fibrin/hyaluronic acid composite hydrogels as appropriate scaffolds for in vivo artificial cartilage implantation. ASAIO J 2010;56(6):563–8.
Raimondo T, Puckett S, Webster TJ. Greater osteoblast and endothelial cell adhesion on nanostructured polyethylene and titanium. Int J Nanomedicine 2010;5:647–52.
Ranella A, Barberoglou M, Bakogianni S, Fotakis C, Stratakis E. Tuning cell adhesion by controlling the roughness and wettability of 3D micro/nano silicon structures. Acta Biomater 2010;6(7):2711–20.
Rehfeldt F, Engler AJ, Eckhardt A, Ahmed F, Discher DE. Cell responses to the mechanochemical microenvironment — implications for regenerative medicine and drug delivery. Adv Drug Deliv Rev 2007;59(13):1329–39.
Reznickova A, Kolska Z, Hnatowicz V, Stopka P, Svorcik V. Comparison of glow argon plasma-induced surface changes of thermoplastic polymers. Nucl Instrum Methods Phys Res B 2011;269(2):83–8.
Rhee S, Lee KH, Kim D, Kwon YK, Kang MS, Kwon H. Sustained formation of focal adhesions with paxillin in morphological differentiation of PC12 cells. Mol Cells 2000;10(2):169–79.
Richards D, Cacialli F. Near-field microscopy and lithography of light-emitting polymers. Philos Transact A Math Phys Eng Sci 2004;362(1817):771–86.
Riha GM, Wang X, Wang H, Chai H, Mu H, Lin PH, et al. Cyclic strain induces vascular smooth muscle cell differentiation from murine embryonic mesenchymal progenitor cells. Surgery 2007;141(3):394–402.
Roca-Cusachs P, Alcaraz J, Sunyer R, Samitier J, Farré R, Navajas D. Micropatterning of single endothelial cell shape reveals a tight coupling between nuclear volume in G1 and proliferation. Biophys J 2008;94(12):4984–95.
Rockova-Hlavackova K, Svorcik V, Bacakova L, Dvorankova B, Heitz J, Hnatowicz V. Biocompatibility of ion beam-modified and RGD-grafted polyethylene. Nucl Instr Meth Phys Res B 2004;225(3):275–82.
Sader MS, Balduino A, de Soares A, Borojevic R. Effect of three distinct treatments of titanium surface on osteoblast attachment, proliferation, and differentiation. Clin Oral Implants Res 2005;16(6):667–75.
Saino E, Focarete ML, Gualandi C, Emanuele E, Cornaglia AI, Imbriani M, et al. Effect of electrospun fiber diameter and alignment on macrophage activation and secretion of proinflammatory cytokines and chemokines. Biomacromolecules 2011;12(5): 1900–11.
Sajid M, Zhao R, Pathak A, Smyth SS, Stouffer GA. Alphavbeta3-integrin antagonists inhibit thrombin-induced proliferation and focal adhesion formation in smooth muscle cells. Am J Physiol Cell Physiol 2003;285(5):C1330–8.
Sammons RL, Lumbikanonda N, Gross M, Cantzler P. Comparison of osteoblast spreading on microstructured dental implant surfaces and cell behaviour in an explant model of osseointegration. A scanning electron microscopic study. Clin Oral Implants Res 2005;16(6):657–66.
Sanz R, Jaafar M, Hernández-Vélez M, Asenjo A, Vázquez M, Jensen J. Patterning of rutile TiO_2 surface by ion beam lithography through full-solid masks. Nanotechnology 2010;21(23):235301.
Schmidt RC, Healy KE. Controlling biological interfaces on the nanometer length scale. J Biomed Mater Res A 2009;90(4):1252–61.
Schneider GB, Zaharias R, Seabold D, Keller J, Stanford C. Differentiation of preosteoblasts is affected by implant surface microtopographies. J Biomed Mater Res A 2004;69(3):462–8.
Shigematsu K, Yasuhara H, Shigematsu H. Topical application of antiangiogenic agent AGM-1470 suppresses anastomotic intimal hyperplasia after ePTFE grafting in a rabbit model. Surgery 2001;129(2):220–30.
Shimizu N, Yamamoto K, Obi S, Kumagaya S, Masumura T, Shimano Y, et al. Cyclic strain induces mouse embryonic stem cell differentiation into vascular smooth muscle cells by activating PDGF receptor beta. J Appl Physiol 2008;104(3):766–72.
Slepicka P, Vasina A, Kolska Z, Luxbacher T, Mackova A, Svorcik V. Argon plasma irradiation of polypropylene. Nucl Instr Meth Phys Res B 2010;268(11–12):2111–4.
Smetana K, Vacik J, Houska M, Souckova D, Lukas J. Macrophage recognition of polymers: effect of carboxylate groups. J Mater Sci Mater Med 1993;4(5):526–9.
Sriram V, Patterson C. Cell cycle in vasculoproliferative diseases: potential interventions and routes of delivery. Circulation 2001;103(19):2414–9.
Srivatsa SS, Fitzpatrick LA, Tsao PW, Reilly TM, Holmes Jr DR, Schwartz RS, et al. Selective alpha v beta 3 integrin blockade potently limits neointimal hyperplasia and lumen stenosis following deep coronary arterial stent injury: evidence for the functional importance of integrin alpha v beta 3 and osteopontin expression during neointima formation. Cardiovasc Res 1997;36(3):408–28.
Stary V, Bacakova L, Hornik J, Chmelik V. Bio-compatibility of the surface layer of pyrolytic graphite. Thin Solid Films 2003a;433(1–2):191–8.
Stary V, Glogar P, Bacakova L, Hnilica F, Chmelik V, Korinek Z, et al. A study of surface properties of composite materials and their influence on the biocompatibility. Acta Montana AB 2003b;11(128):19–36.
Stern E, Jay SM, Demento SL, Murelli RP, Reed MA, Malinski T, et al. Spatiotemporal control over molecular delivery and cellular encapsulation from electropolymerized micro- and nanopatterned surfaces. Adv Funct Mater 2009;19(18):2888–95.
Stevens MM, George JH. Exploring and engineering the cell surface interface. Science 2005;310(5751):1135–8.
Stoltz JF, Boisseau M, Muller S, Wang X, Legrand S, Labrador MV. Hemorheology and vascular endothelial cells. J Mal Vasc 1999;24(2):99–109.
Stouffer GA, Hu Z, Sajid M, Li H, Jin G, Nakada MT, et al. Beta3 integrins are upregulated after vascular injury and modulate thrombospondin- and thrombin-induced proliferation of cultured smooth muscle cells. Circulation 1998;97 (9):907–15.
Straface E, Natalini B, Monti D, Franceschi C, Schettini G, Bisaglia M, et al. C3-fullero-tris-methanodicarboxylic acid protects epithelial cells from radiation-induced anoikia by influencing cell adhesion ability. FEBS Lett 1999;454(3):335–40.
Sun S, Liu Y, Lipsky S, Cho M. Physical manipulation of calcium oscillations facilitates osteodifferentiation of human mesenchymal stem cells. FASEB J 2007;21(7):1472–80.
Supronowicz PR, Ajayan PM, Ullmann KR, Arulanandam BP, Metzger DW, Bizios R. Novel current-conducting composite substrates for exposing osteoblasts to alternating current stimulation. J Biomed Mater Res 2002;59(3):499–506.
Svorcik V, Rybka V, Hnatowicz V, Bacakova L, Lisa V, Kocourek F. Surface properties and biocompatibility of ion implanted polymers. J Mater Chem 1995a;5(1):27–30.
Svorcik V, Rybka V, Hnatowicz V, Bacakova L. Polarity, resistivity and biocompatibility of polyethylene doped with carbon black. J Mater Sci Lett 1995b;14(24):1723–4.
Svorcik V, Rockova K, Ratajova E, Heitz J, Huber N, Bäuerle D, et al. Cell proliferation on UV-excimer lamp modified and grafted polytetrafluoroethylene. Nucl Instr Meth Phys Res B 2004;217(2):307–13.
Svorcik V, Kolarova K, Slepicka P, Mackova A, Novotna M, Hnatowicz V. Modification of surface properties of high and low density PE by Ar plasma discharge. Polym Degrad Stab 2006;91(6):1219–25.
Svorcik V, Kasalkova N, Slepicka P, Zaruba K, Kral V, Bacakova L, et al. Cytocompatibility of Ar^+ plasma treated and Au nanoparticle-grafted PE. Nucl Instr Meth Phys Res B 2009;267(11):1904–10.
Svorcik V, Kolska Z, Luxbacher T, Mistrik J. Properties of Au nano-layer sputtered on PE. Mater Lett 2010a;64(5):611–3.
Svorcik V, Reznickova A, Kolska Z, Slepička P. Variable surface properties of PTFE foils. e-Polymers 2010b;133:1–6.
Svorcik V, Chaloupka A, Rezanka P, Slepicka P, Kolska Z, Kasalkova N, et al. Au-nanoparticles grafted on plasma treated PE. Rad Phys Chem 2010c;79(3):315–7.
Svorcik V, Makajova Z, Kasalkova N, Kolska Z, Bacakova L. Plasma-modified and polyethylene glycol-grafted polymers for potential tissue engineering applications. J Nanosci Nanotechnol in press.
Tepe G, Dietrich T, Grafen F, Brehme U, Muschick P, Dinkelborg LM, et al. Reduction of intimal hyperplasia with Re-188-labeled stents in a rabbit model at 7 and 26 weeks: an experimental study. Cardiovasc Intervent Radiol 2005;28(5):632–7.
Thapa A, Miller DC, Webster TJ, Haberstroh KM. Nano-structured polymers enhance bladder smooth muscle cell function. Biomaterials 2003;24(17):2915–26.
Thomas CH, Lhoest JB, Castner DG, McFarland CD, Healy KE. Surfaces designed to control the projected area and shape of individual cells. J Biomech Eng 1999;121(1):40–8.
Tian YC, Phillips AO. TGF-beta1-mediated inhibition of HK-2 cell migration. J Am Soc Nephrol 2003;14(3):631–40.
Tiller JC, Bonner G, Pan LC, Klibanov AM. Improving biomaterial properties of collagen films by chemical modification. Biotechnol Bioeng 2001;73(3):246–52.
Tsai MT, Chang WH, Chang K, Hou RJ, Wu TW. Pulsed electromagnetic fields affect osteoblast proliferation and differentiation in bone tissue engineering. Bioelectromagnetics 2007;28(7):519–28.
Tzvetkova-Chevolleau T, Stéphanou A, Fuard D, Ohayon J, Schiavone P, Tracqui P. The motility of normal and cancer cells in response to the combined influence of the substrate rigidity and anisotropic microstructure. 1. Biomaterials 2008;29(10): 1541–51.
Vacik J, Lavrentiev V, Novotna K, Bacakova L, Lisa V, Vorlicek V, et al. Fullerene (C60)–transitional metal (Ti) composites: structural and biological properties of the thin films. Diamond Relat Mater 2010;19(2–3):242–6.
Vagaska B, Bacakova L, Filova E, Balik K. Osteogenic cells on bio-inspired materials for bone tissue engineering. Physiol Res 2010;59(3):309–22.
Vandrovcova M, Bacakova L. Adhesion, growth and differentiation of osteoblasts on surface-modified materials developed for bone implants. Physiol Res 2011;60(3): 403–17.
Vandrovcova M, Vacik J, Svorcik V, Slepicka P, Kasalkova N, Vorlicek V, et al. Fullerene C60 and hybrid C60/Ti films as substrates for adhesion and growth of bone cells. Phys Stat Sol (a) 2008;205(9):2252–61.

Vartanian KB, Kirkpatrick SJ, Hanson SR, Hinds MT. Endothelial cell cytoskeletal alignment independent of fluid shear stress on micropatterned surfaces. Biochem Biophys Res Commun 2008;371(4):787–92.
vonRecum H, Kikuchi A, Yamato M, Sakurai Y, Okano T, Kim SW. Growth factor and matrix molecules preserve cell function on thermally responsive culture surfaces. Tissue Eng 1999;5(3):251–65.
Wang N, Naruse K, Stamenovic D, Fredberg JJ, Mijailovich SM, Tolic-Norrelykke IM, et al. Mechanical behavior in living cells consistent with the tensegrity model. Proc Natl Acad Sci USA 2001;98(14):7765–70.
Wang YK, Wang YH, Wang CZ, Sung JM, Chiu WT, Lin SH, et al. Rigidity of collagen fibrils controls collagen gel-induced down-regulation of focal adhesion complex proteins mediated by alpha2beta1 integrin. J Biol Chem 2003;278(24):21886–92.
Wang L, Zhao G, Olivares-Navarrete R, Bell BF, Wieland M, Cochran DL. Integrin beta$_1$ silencing in osteoblasts alters substrate-dependent responses to 1,25-dihydroxy vitamin D3. Biomaterials 2006;27(20):3716–25.
Webster TJ, Ergun C, Doremus RH, Siegel RW, Bizios R. Specific proteins mediate enhanced osteoblast adhesion on nanophase ceramics. J Biomed Mater Res 2000a;51(3):475–83.
Webster TJ, Ergun C, Doremus RH, Siegel RW, Bizios R. Enhanced functions of osteoblasts on nanophase ceramics. Biomaterials 2000b;21(17):1803–10.
Webster TJ, Schadler LS, Siegel RW, Bizios R. Mechanisms of enhanced osteoblast adhesion on nanophase alumina involve vitronectin. Tissue Eng 2001;7(3):291–301.
Wells RG, Discher DE. Matrix elasticity, cytoskeletal tension, and TGF-beta: the insoluble and soluble meet. Sci Signal 2008;1(10):pe13.
Wilson E. Alpha 7 beta 1 integrin: putting the brakes on smooth muscle cell proliferation. Circ Res 2007;101(7):651–3.
Xie J, Macewan MR, Ray WZ, Liu W, Siewe DY, Xia Y. Radially aligned, electrospun nanofibers as dural substitutes for wound closure and tissue regeneration applications. ACS Nano 2010;4(9):5027–36.
Yamaguchi R, Mazaki Y, Hirota K, Hashimoto S, Sabe H. Mitosis specific serine phosphorylation and downregulation of one of the focal adhesion protein, paxillin. Oncogene 1997;15(15):1753–61.
Yamamoto S, Tanaka M, Sunami H, Ito E, Yamashita S, Morita Y, et al. Effect of honeycomb-patterned surface topography on the adhesion and signal transduction of porcine aortic endothelial cells. Langmuir 2007;23(15):8114–20.
Yang J, Yamato M, Shimizu T, Sekine H, Ohashi K, Kanzaki M, et al. Reconstruction of functional tissues with cell sheet engineering. 1. Biomaterials 2007;28(34):5033–43.
Youssef W, Wickett RR, Hoath SB. Surface free energy characterization of vernix caseosa. Potential role in waterproofing the newborn infant. Skin Res Technol 2001;7(1):10–7.
Zaidel-Bar R, Milo R, Kam Z, Geiger B. A paxillin tyrosine phosphorylation switch regulates the assembly and form of cell-matrix adhesions. J Cell Sci 2007;120(Pt 1):137–48.
Zamir E, Geiger B. Molecular complexity and dynamics of cell–matrix adhesions. J Cell Sci 2001;114(Pt 20):3583–90.
Zamir E, Katz BZ, Aota S, Yamada KM, Geiger B, Kam Z. Molecular diversity of cell–matrix adhesions. J Cell Sci 1999;112(Pt 11):1655–69.
Zamir E, Katz M, Posen Y, Erez N, Yamada KM, Katz BZ, et al. Dynamics and segregation of cell–matrix adhesions in cultured fibroblasts. Nat Cell Biol 2000;2(4):191–6.
Zhang J, Melhem M, Kassing W, Kelly B, Wang Y, Krishnamoorthy M, et al. In vitro paclitaxel and radiation effects on the cell types responsible for vascular stenosis: a preliminary analysis. Blood Purif 2007;25(2):155–60.
Zhao J, Pestell R, Guan JL. Transcriptional activation of cyclin D1 promoter by FAK contributes to cell cycle progression. Mol Biol Cell 2001;12(12):4066–77.
Zhao G, Schwartz Z, Wieland M, Rupp F, Geis-Gerstorfer J, Cochran DL, et al. High surface energy enhances cell response to titanium substrate microstructure. J Biomed Mater Res A 2005;74(1):49–58.
Zhao G, Zinger O, Schwartz Z, Wieland M, Landolt D, Boyan BD. Osteoblast-like cells are sensitive to submicron-scale surface structure. Clin Oral Implants Res 2006;17(3):258–64.
Zheng Z, Zhang L, Kong L, Wang A, Gong Y, Zhang X. The behavior of MC3T3-E1 cells on chitosan/poly-L-lysine composite films: effect of nanotopography, surface chemistry, and wettability. J Biomed Mater Res A 2009;89(2):453–65.
Zhuang YX, Hansen O. Correlation of effective dispersive and polar surface energies in heterogeneous self-assembled monolayer coatings. Langmuir 2009;25(10):5437–41.
Zilla P, Bezuidenhout D, Human P. Prosthetic vascular grafts: wrong models, wrong questions and no healing. Biomaterials 2007;28(34):5009–27.
Zinchenko YS, Coger RN. Engineering micropatterned surfaces for the coculture of hepatocytes and Kupffer cells. J Biomed Mater Res 2005;75A(1):242–8.

International Journal of Pharmaceutics 404 (2011) 94–101

Contents lists available at ScienceDirect

International Journal of Pharmaceutics

journal homepage: www.elsevier.com/locate/ijpharm

Perivascular sirolimus-delivery system

Elena Filova[a,*], Martin Parizek[a], Jana Olsovska[b], Zdenek Kamenik[b], Eduard Brynda[c], Tomas Riedel[c], Marta Vandrovcova[a], Vera Lisa[a], Ludka Machova[c], Ivo Skalsky[d], Ondrej Szarszoi[d], Tomas Suchy[e], Lucie Bacakova[a]

[a] Institute of Physiology, Academy of Sciences of the Czech Republic, v.v.i., Videnska 1083, 142 20 Prague 4, Czech Republic
[b] Institute of Microbiology, Academy of Sciences of the Czech Republic, v.v.i., Videnska 1083, 142 20 Prague 4, Czech Republic
[c] Institute of Macromolecular Chemistry, Academy of Sciences of the Czech Republic, v.v.i., Heyrovsky Sq. 2, 162 06 Prague 6, Czech Republic
[d] Institute for Clinical and Experimental Medicine, Videnská 1958/9, 140 21 Prague 4, Czech Republic
[e] Institute of Rock Structure and Mechanics, Academy of Sciences of the Czech Republic, v.v.i., V Holešovičkách 41, 182 09 Prague 8, Czech Republic

ARTICLE INFO

Article history:
Received 24 August 2010
Received in revised form 27 October 2010
Accepted 6 November 2010
Available online 12 November 2010

Keywords:
Drug delivery
Rapamycin
Sustained release
Restenosis
Vascular smooth muscle cells
Periadventitial wrap

ABSTRACT

Autologous vein grafts are often used for treating damaged vessels, e.g. arteriovenous fistulas or arterial bypass conduits. Veins have a different histological structure from arteries, which often leads to intimal hyperplasia and graft restenosis. The aim of this study was to develop a perivascular sirolimus-delivery system that would release the antiproliferative drug sirolimus in a controlled manner. Polyester Mesh I was coated with purasorb, i.e. a copolymer of L-lactide and ε-caprolactone, with dissolved sirolimus; Mesh II was coated with two copolymer layers; the layer with dissolved sirolimus was overlaid with pure purasorb. This arrangement allowed sirolimus to be released for 6 and 4 weeks, for Mesh I and Mesh II, respectively. Mesh II released sirolimus more homogeneously, without the initial burst effect during the first week. However, the cumulative release curve was steeper at later time points than the curve for Mesh I. Both meshes inhibited proliferation of rat vascular smooth muscle cells during 14-day culture *in vitro* and preserved excellent cell viability. Newly developed sirolimus-releasing perivascular meshes are promising devices for preventing autologous graft restenosis.

1. Introduction

Damage or stenosis of a vessel caused either by injury or by some pathological processes, e.g. atherosclerosis and thrombosis, must often be treated by replacing the vessel with an autologous graft, mostly vein. Four-year patency of an autologous saphenous vein was achieved in 40–70% of treated patients (Taylor et al., 1990; Conklin et al., 2002). Intimal thickening, however, often occurs in veins used as arteriovenous fistulas or arterial bypass conduits, due to the different structure of the vein wall and the arterial wall. In addition, the layer of endothelial cells (EC) in the autologous graft is often damaged during surgery. The restoration of a new EC lining usually lasts several weeks, which results in relatively long-term direct exposure of vascular smooth muscle cells (VSMC) to the blood stream. Platelets and macrophages from the blood start to adhere to the denuded luminal surface of the graft, which is followed by platelet aggregation and release of growth and migratory-promoting factors from these cells (Liuzzo et al., 2005). Growth factors released from platelets, EC, and VSMC, e.g. PDGF, stimulate phenotypic modulation of VSMC from contractile to synthetic phenotype, which is characterised by excessive proliferation and migration of VSMC, and their extracellular matrix production. This results in intimal hyperplasia and graft stenosis (Liuzzo et al., 2005).

Drug-eluting stents were the first local anti-proliferative drug-delivery systems introduced in interventional cardiology. Commercially available stents (e.g. BX Velocity™, Cypher™, Cordis, Johnson & Johnson) and also newly developed sirolimus-eluting stents have been proved to reduce neo-intimal formation in vessels (Mehilli et al., 2008). The restenosis rate was reduced from 20–30% to 1–3% after 1 year (Morice et al., 2002). Drug-eluting stents, however, cause increased mechanical strain on a vessel or damage to the endothelium and thrombosis (Colombo and Iakovou,

* Corresponding author at: Department of Growth and Differentiation of Cell Populations (#11), Institute of Physiology, Academy of Sciences of the Czech Republic, v.v.i., Videnska 1083, 142 20 Prague 4-Krc, Czech Republic. Tel.: +42 0 296443742; fax: +42 0 241062488.
E-mail addresses: filova@biomed.cas.cz (E. Filova), parizek@biomed.cas.cz (M. Parizek), olsovska@beerresearch.cz (J. Olsovska), kamenik@biomed.cas.cz (Z. Kamenik), brynda@imc.cas.cz (E. Brynda), riedel@imc.cas.cz (T. Riedel), vandrovcova@biomed.cas.cz (M. Vandrovcova), machova@imc.cas.cz (L. Machova), ivo.skalsky@ikem.cz (I. Skalsky), ondrej.szarszoi@ikem.cz (O. Szarszoi), suchyt@irsm.cas.cz (T. Suchy), lucy@biomed.cas.cz (L. Bacakova).

0378-5173/$ – see front matter © 2010 Elsevier B.V. All rights reserved.
doi:10.1016/j.ijpharm.2010.11.005

2004). The damaged vein graft is re-endothelialized within several weeks after implantation. During this time an antiproliferative drug should be released from a suitable drug delivery system.

Mechanical strain on the endothelium can be avoided by stent-free drug-delivery systems, e.g. periadventitial or perivascular films, gels, or cuffs. These systems can be advantageously based on a degradable synthetic polymer loaded with a drug, which is continuously released during the polymer degradation. This degradation is usually hydrolytic and not mediated by cells, thus the system can be spontaneously removed from the patient's organism. However, the kinetics of both polymer degradation and drug release should be adjusted to the period necessary for regeneration of endothelial cell layer damaged by the surgery; i.e. at least a few weeks. From this point of view, promising results have been obtained with PEG-Cys-NO hydrogels loaded with S-nitrosothiols, i.e. nitric oxide precursors. When applied perivascularly, these hydrogels generated NO for up to 50 days and inhibited VSMC proliferation, while the proliferation of endothelial cells was increased. This system also inhibited platelet adhesion *in vitro* and reduced neointima formation in a rat carotid balloon injury model at 14 days by approximately 80% compared to controls (Lipke and West, 2005). However, nitric oxide precursors, although some of them occur naturally *in vivo*, have not yet been approved for clinical use.

Another drug with antiproliferative effects, which is widely used in current clinical practice, is sirolimus, also known as rapamycin. Sirolimus is a macrocyclic lactone antibiotic produced by *Streptomyces hygroscopicus*, often used as an antiproliferative agent in drug-eluting intravascular stents. Sirolimus binds to the FK binding protein complex (FKBP12), which subsequently binds to the mammalian target of rapamycin (mTOR) (Daemen and Serruys, 2007). Interaction with mTOR prevents phosphorylation of p70S6 kinase, 4E-BP1, and indirectly also of other proteins involved in transcription, translation, and cell cycle control and progression (Vignot et al., 2005). Sirolimus exhibited a dose-dependent reduction in intimal hyperplasia using 60–200 μg sirolimus-coated stents in the rabbit model. In the porcine model, sirolimus-eluting stents, and stents releasing both sirolimus and dexamethasone reduced the neointimal area compared to bare metal stents after 28 days. This resulted in a 50% decrease of in-stent restenosis (Suzuki et al., 2001).

Sirolimus has also been tested for its potential use in a perivascular drug delivery system. Non-constrictive perivascular poly(ε-caprolactone) (PCL) cuffs releasing paclitaxel or rapamycin allowed dose-dependent sustained drug release for 3 weeks. Their application reduced intimal thickening of the treated femoral arteries by 75% and 76%, respectively (Pires et al., 2005). Pluronic gel containing 200 μg of sirolimus reduced intimal hyperplasia by 41% after 6 weeks (Schachner et al., 2004). Films made of poly(lactic-co-glycolic acid) (PLGA) and PLGA blended with methoxypolyethylene glycol (MePEG) loaded with paclitaxel and wrapped around the injured carotid artery degraded after 28 days in rats (Jackson et al., 2004). Owen et al. (2010) investigated injectable terpolymer ReGel made of, i.e. poly(lactic-co-glycolic acid)–polyethylene glycol–poly(lactic-co-glycolic acid) (PLGA–PEG–PLGA) containing sirolimus (2.5 mg/ml in 2 ml of gel) either in the form of a suspension or a solution *in vivo* on pigs. However, in this case, the gel had to be replenished with the drug at 1, 2, and 3 weeks post-operatively. In addition, most of the above-mentioned systems were based on materials with relatively weak mechanical properties, requiring special handling (manipulation) during the surgical procedure or prone to move away from the desired therapeutic position.

The aim of the study was to develop a periadventitial drug delivery system consisting of a polyester silk mesh, coated with a degradable copolymer purasorb loaded with sirolimus. The polyester mesh was expected to give a stable mechanical support to the sirolimus-releasing system, to facilitate and accelerate wrapping the system around the vascular graft, and to prevent migration of the system out of the periadventitial position. The release of sirolimus onto aqueous and non-aqueous media was then measured by UHPLC, and the antiproliferative effects of the system were tested in cultures of rat aortic smooth muscle cells.

2. Materials and methods

2.1. Materials

A knitted polyester silk mesh (CHS 50, PES Mesh) was obtained from VUP Joint-Stock Company, Brno, CR. Purasorb PLC 7015, a grade copolymer of L-lactide and ε-caprolactone (70/30 molar ratio, inherent viscosity midpoint of 1.5 dl/g; semicrystalline, without residual monomers) was purchased from PURAC Biomaterials. Acetonitrile (ACN; 99.95%, Biosolve), methanol (99.95%, Chromapur GG) and dichlormethane (min. 99%, Chromapur GG) were purchased from Chromservis (Prague, Czech Republic). HPLC grade water was prepared by Milli-Q reverse osmosis Millipore (USA). Sirolimus (Rapamycin from Streptomyces, Cat. No. R0395) was obtained from Sigma–Aldrich (Germany).

2.2. Sample preparation

2.2.1. Mesh impregnation

The mesh is made from yarns. A yarn of about 90 μm across is formed by polyester fibres 17.5 μm in diameter. Purasorb penetrated into the gaps among the fibres in the yarn during mesh coating. The solutions used for the coating were as follows: *solution 1*: 5.2 mg of sirolimus, 36.4 mg of purasorb in 1 ml of chlorbenzen–ethanol (1.75:1 v/v); *solution 2*: 10.4 mg of sirolimus, 36.4 mg of purasorb in 1 ml of chlorbenzen–ethanol (1.75:1 v/v); *solution 3*: 36.4 mg of purasorb in 1 ml chlorbenzen–ethanol (1.75:1 v/v).

2.2.2. Homogeneous coating of Mesh I

The mesh was dip-coated with solution 1 and dried (30 min), and then coated quantitatively (i.e. with the whole remaining amount of the solution) for the second time with solution 1 and then dried. The impregnated mesh contained 0.14 mg sirolimus homogeneously distributed in 0.98 mg purasorb per 1 cm^2.

2.2.3. Gradient coating of Mesh II

The polyester mesh was dip-coated with solution 2 and dried (30 min), and then quantitatively overlaid with solution 3 and dried. The total amount of 0.14 mg sirolimus in 0.98 mg purasorb per 1 cm^2 in the impregnated mesh was the same as that after homogeneous coating; however, the sirolimus concentration was expected to be higher inside the yarns than near their surface.

2.2.4. Purasorb Mesh

The polyester mesh was coated with solution 3 and dried, and then overlaid with solution 3 and dried. This mesh was coated with sirolimus-free purasorb, and served as a reference sample.

2.3. Sample incubation

Mesh I and Mesh II were cut into pieces 0.5 cm^2 and 1 cm^2 in area, and were incubated in 5 ml of phosphate-buffered saline (PBS) per cm^2 of the mesh at 37 °C on a shaker. The PBS was changed daily. For the analyses, the samples were removed after 0, 1, 4, 7, 9, 11, 14, 17, 21, 28, 35, and 42 days of incubation in PBS. For each time interval, 3–8 samples of the mesh were used.

2.4. Stability of sirolimus

The stability of sirolimus in PBS was assessed at 37 °C, −20 °C, and −75 °C at two concentrations of 50 and 750 ng/ml after 0, 24, 48 and 168 h. The samples were 100 times pre-concentrated by extraction to methanol using solid phase extraction (HLB OASIS 3cc, Waters) and were analyzed by Ultra High Performance Liquid Chromatography (UHPLC).

The stability of sirolimus in methanol was assessed at 25 °C and −75 °C at three concentration levels 0.125, 5.0, and 75.0 μg/ml. The samples stored at 25 °C and −20 °C were analyzed after 0, 2, 24, and 48 h, whereas the samples stored at −75 °C were analyzed after 0, 2, 24, 48 h, and 5, 15, 30, and 60 days.

The stability of sirolimus in dichlormethane was assessed at 25 °C at three concentration levels 0.125, 5.0, and 75.0 μg/ml after 0, 5, 10, and 30 min.

2.5. Sirolimus extraction and UHPLC analysis

After incubation of Mesh I and Mesh II in PBS buffer, the meshes were removed and dried at room temperature. Three mililiters of dichlormethane were added to the mesh for 10 min in order to wash purasorb and sirolimus out of the mesh. The mesh was removed and dichlormethane was evaporated to dryness. Sirolimus was then reconstituted in 1 ml of methanol, centrifuged 5 min at 13,000 rpm in order to eliminate undissolved purasorb, and the supernatant was immediately analyzed. If the sirolimus concentration during the incubation experiment reached a limit of quantification (LOQ), sirolimus was reconstituted in 0.1 ml of methanol, and the obtained amount of sirolimus was divided by 10. Analyses were performed on the Acquity UHPLC system (Waters) equipped with a 2996 PDA detector operating in the range from 194 to 600 nm. Chromatograms of sirolimus analyses were extracted and subsequently quantified at 278 nm. The data was processed using Empower 2 software (Waters).

Samples were injected on a Waters BEH C18 column (50 mm × 2.1 mm I.D., particle size 1.7 μm); the mobile phase consisted of solvent A, 10% ACN, and solvent B, ACN; linear gradient elution (min/%B): 0/60, 1.5/100, 2/100; flow rate, 0.4 ml min^{-1}; column temperature, 50 °C; injection volume, 5 μl. Each analysis was followed by an equilibration step (0.5 min).

2.6. Calculation of the remaining weight of sirolimus

The remaining weight of sirolimus on meshes X (μg/cm^2) was calculated as follows:

$$X = C_{UHPLC} \times \frac{3.97}{m} \quad (1)$$

where C_{UHPLC} (μg ml^{-1}) represents the concentration of sirolimus extracted from one piece of mesh and measured by UHPLC, m represents the weight of analyzed piece of sirolimus and purasorb-free mesh measured after extraction (see Section 2.5), and constant 3.97 represents the weight of 1 cm^2 of sirolimus and purasorb-free mesh.

2.7. Partial validation of the sirolimus UHPLC method

The sirolimus quantification method was partially validated. The calibration curve over the linear range from 3.125 to 100 μg ml^{-1} was determined using methanol solutions of sirolimus at concentration levels of 100.0, 50.0, 25.0, 12.5, 6.3, and 3.1 μg ml^{-1}. LOQ was determined as the lowest point of the calibration curves with precision (expressed as relative standard deviation, RSD%) less than 20% and accuracy of 80–120% in six replicates.

2.8. Scanning electron microscopy

The pure PES Mesh and Mesh I were used without any processing and after 2 and 6 weeks of incubation in PBS at 37 °C and drying in a vacuum oven. The samples coated with 2 nm platinum in an SCD 050 Sputter Coater (Balzers Union AG, Balzers, Liechtenstein) were observed using a Quanta™ Scanning Electron Microscope 200F (FEI Czech Republic, s.r.o.).

2.9. Size-exclusion chromatography

The samples of Purasorb Mesh were incubated in PBS at 37 °C for 0, 2, 4, and 6 weeks. In addition, the originally purchased polymer purasorb was evaluated without any incubation. The molar mass distribution of purasorb dissolved at a concentration of 2 mg/ml in tetrahydrofuran (THF) and dimethylformamid (DMF) (10:1) was measured by size-exclusion chromatography (SEC) in THF/DMF carried out on a Waters SEC modular system using coupled PLgel 10^3 Å, 10 μm (7.5 mm × 600 mm), and PLgel MIXED C (7.5 mm × 600 mm) columns (Polymer Laboratories, Ltd.) with a Waters 410 RI detector.

2.10. Cells and culture conditions

Polyester meshes (PES Mesh), meshes coated with purasorb (Purasorb Mesh) and meshes coated with purasorb mixed with sirolimus (Mesh I and Mesh II) were sterilized by ethylene oxide. After sterilization, the samples were stored in a vacuum oven at 35 °C for 4 weeks in order to remove the rest of organic solvents used during preparation. Polystyrene dishes (24-well test plate, TPP, Switzerland; well diameter 1.5 cm) were seeded with VSMC derived from the intima-media complex of the thoracic aorta of 8-week-old male Wistar SPF rats by the explantation method (Bačáková et al., 2002), and were used in passage 5–10. VSMC were seeded at an initial number of 16,000 cells/well (i.e. population density of about 9000 cells/cm^2) into 1.5 ml Dulbecco-modified Eagle Minimum Essential Medium (DMEM; Sigma, St. Louis, MO, U.S.A.; Cat. No. D5648), supplemented with 10% of fetal bovine serum (FBS; Sebak GmbH, Aidenbach, Germany) and 40 μg/ml of gentamicin (LEK, Ljubljana, Slovenia). Twenty-four hours after cell seeding, the samples (PES Mesh or Purasorb Mesh or Mesh I or Mesh II, each 1 cm^2) were added into the wells of the culture plates. Pure polystyrene (PS) without added meshes was used as a control. The cells were cultured for zero, two, seven and 14 days after adding the meshes at 37 °C in a humidified air atmosphere containing 5% of CO_2. For each experimental group and time interval, 3 samples were used.

2.11. Cell viability and number

Cell viability was measured using a LIVE-DEAD Viability/Cytotoxicity Kit (Invitrogen). VSMC were washed with PBS, and incubated with calcein AM (1 μM) and ethidium homodimer-1 (2 μM) for 15 min. The number of living cells (stained green) and dead cells (stained red) were counted from micrographs that were taken under an Olympus IX 71 epifluorescence microscope with a DP 71 digital camera. For each sample and time interval, 30–45 homogenously distributed microscopic fields were used.

2.12. Statistical analysis

The quantitative data was presented as mean ± SEM (standard error of mean) or mean ± RSD (relative standard deviation, Table 1). The statistical analyses were performed using SigmaStat (Jandel Corporation, U.S.A.). Multiple comparison procedures were made by the ANOVA, Student–Newman–Keuls method. The value $p \leq 0.05$

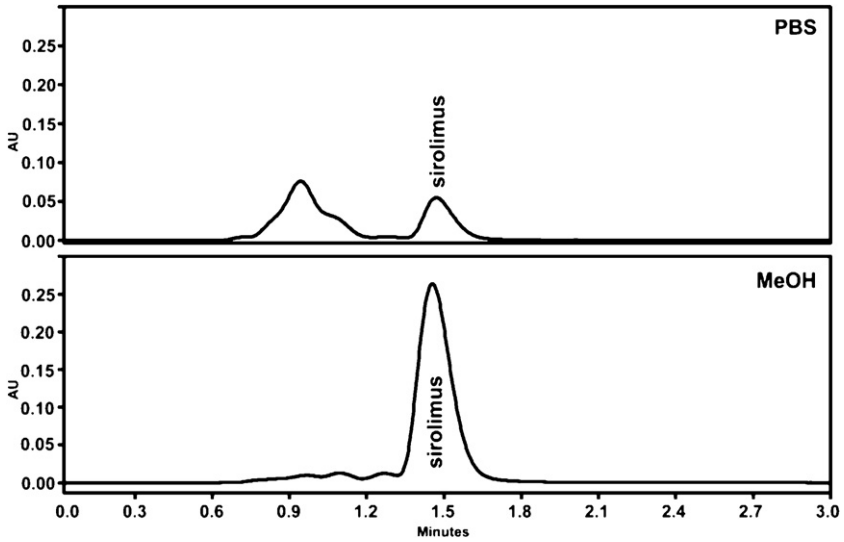

Fig. 1. Chromatogram of sirolimus after incubation at 37 °C for 24 h in PBS and methanol (the concentration of sirolimus was 25 μg/ml). Chromatographic conditions: UPLC column Acquity BEH C18 (50 mm × 2.1 mm I.D., particle size 1.7 μm); mobile phase A, 10% acetonitrile, and B, acetonitrile; linear gradient elution (min/%B): 0/60, 1.5/100, 2/100; flow rate 0.4 ml min^{-1}; column temperature, 50 °C; injection volume, 5 μl; UV max 278 nm; retention time of sirolimus 1.48 min.

was considered significant. For statistical evaluation of the cumulative release of sirolimus we used STATGRAPHICS Centurion XV software (StatPoint, U.S.A.) and the statistical literature (ČSN ISO 2602). The confidence intervals for the estimated mean values and the confidence limits for the plot of the fitted models were calculated at a confidence level of 95%.

3. Results

3.1. Partial validation of the sirolimus UHPLC method

The original rapid UHPLC method for determining sirolimus was developed; for the parameters, see Section 2.5. Under the conditions that were developed, baseline separation of sirolimus without any interference was obtained. The sirolimus peak retention time was 1.48 min (see Fig. 1). The calibration curve was linear with regression equations of $y = 3.32 \times 10^4 + 3.49 \times 10^4$ and determination coefficient of 0.999. LOQ was determined as 3.125 with μg ml^{-1} with precision (RSD) of 2.2% and accuracy of 102.4% ($n = 6$). The recovery of the extraction method was 101.1% with RSD of 8.6%.

Table 1
Stability of sirolimus dissolved in PBS at 37 °C, −20 °C, and −75 °C. Residues of sirolimus (%) are presented as the mean of the measured concentrations ± L; where L represents the confidence interval (95%) and was calculated as follows: $L = R \times K_n$, where R is the difference between the lowest and highest measured concentration, K_n is constant for n replicates at a confidence level of 95%; $n = 4$ and $K_4 = 0.72$.

Temperature	Time (h)	Residue of sirolimus (%) for relevant concentrations	
		50 (ng/ml)	750 (ng/ml)
	0	100 (%)	100 (%)
37 °C	24	20.9 ± 7.5	26.5 ± 4.1
	48	12.5 ± 5.2	8.5 ± 2.6
	168	(Under detection limit)	(Under detection limit)
−20 °C	24	45.6 ± 4.8	67.8 ± 5.2
	48	21.0 ± 8.2	39.1 ± 4.8
	168	(Under detection limit)	(Under detection limit)
−75 °C	24	44.6 ± 4.7	72.2 ± 5.6
	48	27.0 ± 6.5	71.5 ± 5.3
	168	26.8 ± 6.6	69.2 ± 5.1

3.2. Stability of sirolimus in water and methanol

It was found out that sirolimus is not stable in aqueous media including PBS (Fig. 1 and Table 1). Table 1 shows that after 24 h in PBS, sirolimus degraded by more than 70%. It was therefore

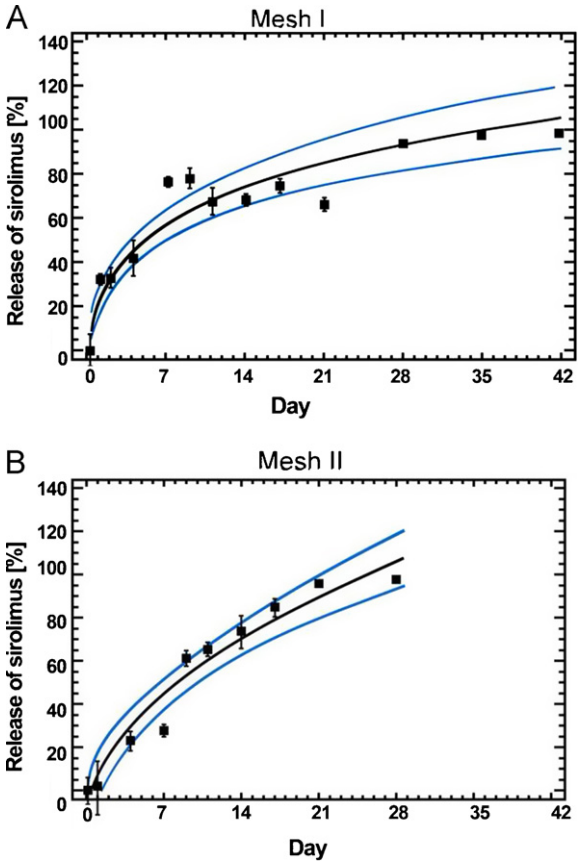

Fig. 2. Accumulated release of sirolimus from the coated polyester meshes, i.e. Mesh I and Mesh II. The data is presented as the means ± SEM, blue curves represent two-sided confidence intervals (at a confidence level of 95%). (For interpretation of the references to color in this figure legend, the reader is referred to the web version of this article.)

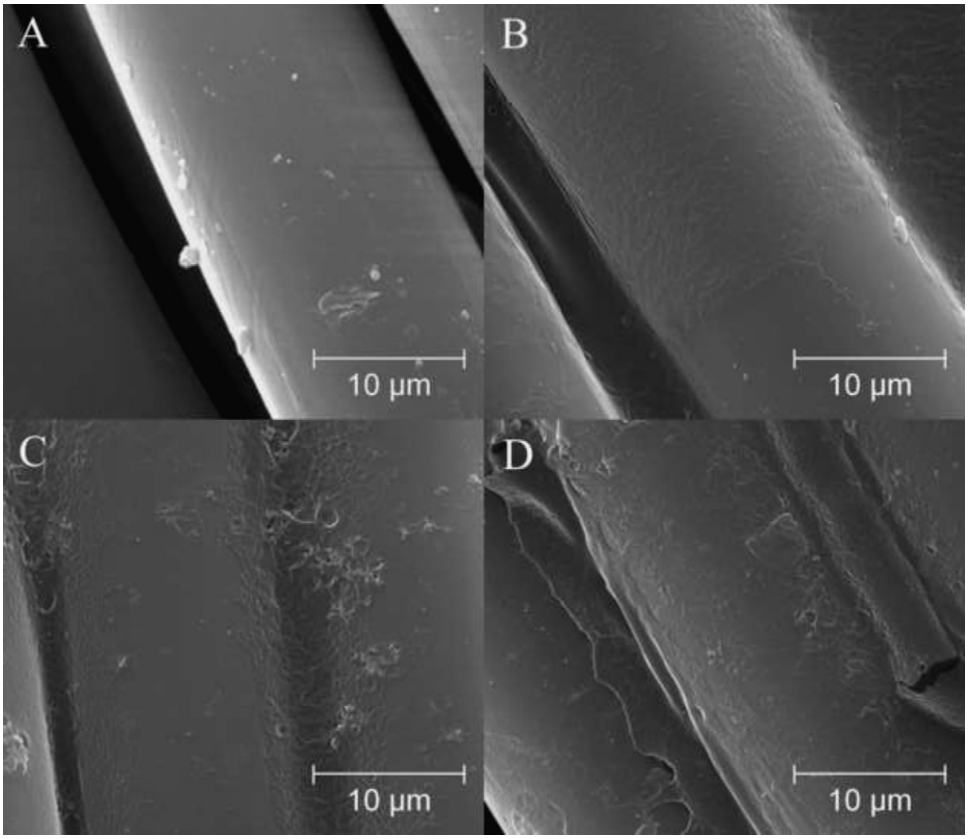

Fig. 3. Micrographs of the PES Mesh (A), Mesh I before incubation in PBS (B), Mesh I after 2 weeks (C), and 6 weeks (D) of incubation in PBS, taken under scanning electron microscopy, magn. 2000×, 30.0 kV.

not possible to determine sirolimus released into PBS directly. Instead, the sirolimus retained in the mesh was assayed, and the amount of released sirolimus was calculated. For this purpose, an investigation was made of the stability of methanol and dichlormethane, which were used for extracting sirolimus from the meshes. The methanol solution of sirolimus at 25 °C is stable for 2 days, which is sufficient for the sample preparation and analysis. This solution is stable at −75 °C for 60 days, which enables storage of sirolimus stock solutions (data not shown). Dichlormethane was found to be suitable for extraction of sirolimus, because sirolimus in dichlormethane is stable for at least 30 min (data not shown).

3.3. Cumulative release of sirolimus from Mesh I and Mesh II

Mesh I consisted of PES Mesh coated with purasorb layer with homogenously dissolved sirolimus. Mesh II was PES Mesh coated with sirolimus-containing purasorb with a higher concentration of sirolimus, and on top there was a layer of pure purasorb. This arrangement of the drug-delivery systems substantially influenced the sirolimus release. Mesh I released the entire amount of sirolimus after 6 weeks, Mesh II after 4 weeks of incubation in PBS (Fig. 2). As regression models, Square root-*Y* logarithmic-*X* $[4.57331 + 1.52937 \times \ln(\text{day})]^2$ and Square root-*X* $[-16.4822 + 23.2462 \times \text{sqrt}(\text{day})]$ were used for Mesh I and Mesh II, respectively; the correlations obtained were 0.9627 and 0.9712 for Mesh I and Mesh II, respectively. An initial burst of sirolimus release from Mesh I was observed during the first week of its incubation. On day 11, however, the percentage of released sirolimus was equal for both meshes, i.e. 67.7% and 65.5% for Meshes I and II, respectively. Mesh II released sirolimus more homogeneously, without the initial burst effect during the first week, but the curve was steeper at later time points than for Mesh I. This shortened the time needed for total sirolimus release from Mesh II to 4 weeks.

3.4. Scanning electron microscopy

A copolymer film was found on the surface of the fibres, and it also bridges gaps between the fibres. Erosion of the film was visible after 2 weeks of incubation with PBS. A broken film was observed after 6 weeks.

3.5. Molecular weight

The molecular weight of purasorb from the Purasorb Meshes after 2, 4, and 6 weeks of incubation in PBS was similar to its weight before incubation (Fig. 4). The values of M_w 117,250 and M_n 85,000 were determined for the original polymer supplied by PURAC. Pura-

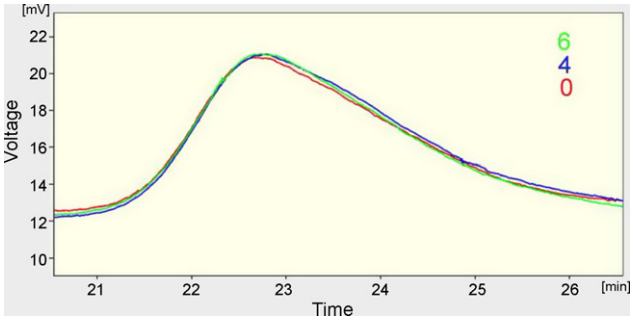

Fig. 4. Chromatogram of purasorb after 0 (red), 4 (blue) and 6 (green) weeks of incubation in phosphate-buffered saline at 37 °C. (For interpretation of the references to color in this figure legend, the reader is referred to the web version of this article.)

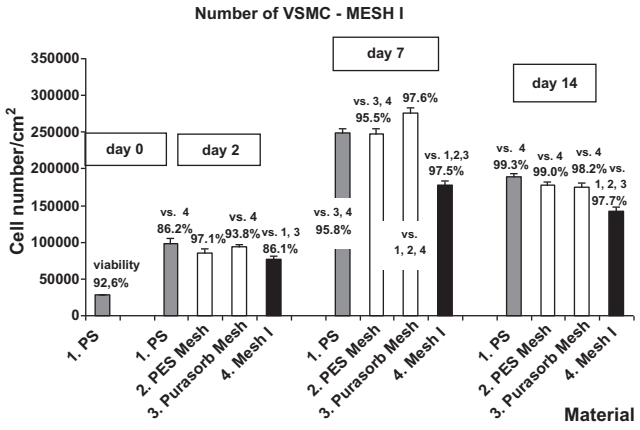

Fig. 5. Number and viability of vascular smooth muscle cells on a pure polystyrene culture dish (PS), on PS with a polyester mesh (PES Mesh), a purasorb-coated PES Mesh (Purasorb Mesh) or a sirolimus-containing PES Mesh (Mesh I) on day 0, 2, 7 and 14 after adding the meshes into the cultures. p-Value <0.05 is considered significant in comparison with the sample of the same number and the day of culture.

sorb solutions obtained by soaking coated meshes in THF/DMF were analyzed in the same way by SEC. No differences in the molecular mass distribution were observed in the samples of originally supplied purasorb, polymer dissolved from intact coated meshes, and polymer dissolved from coated meshes incubated with PBS for 1, 2, 4, and 6 weeks in PBS and then dried.

3.6. Cell number and viability

The viability of VSMC was in the range of 86.2–99.4%, and this viability was similar on Mesh I and Mesh II and on the control samples (Figs. 5 and 6). Sirolimus eluted from Mesh I in an *in vitro* experiment significantly reduced the VSMC number on day 2, 7, and 14. The reduction in the VSMC number was by 21.8%, 28.7%, and 24.8% compared to PS on day 2, 7, and 14, respectively. For Mesh II, VSMC proliferation was reduced by 67.6%, 76.1%, and 60.1% compared to PS on day 2, 7, and 14 after adding the meshes, respectively.

4. Discussion

Local drug delivery is assumed to have a substantial effect on preventing vascular restenosis without causing systemic adverse reactions (Pires et al., 2005). It prevents drug degradation before reaching the target, and assures excellent uptake of the drug by the tissue (Golomb et al., 1996). However, a long-term follow-up of antiproliferative drug-eluting intravascular stents, containing, e.g. paclitaxel, sirolimus, or tacrolimus, revealed a wide range of adverse reactions, caused by mechanical and biochemical damage to the vascular wall by the stent. These reactions involved particularly damage to the endothelium, increased platelet aggregation and a thrombogenic response, the presence of focal remnants of residual fibrin deposition, induced apoptosis of VSMC, and insufficient reduction of neointimal hyperplasia at 90 and 180 days in animals, when the drug was completely eluted from the stent (Suzuki et al., 2001). Other important complications are inflammation of the vessel wall and local hypersensitivity reaction against the polymer coating the stent. High-molecular weight PLLA (320,000 Da) used as a coating of the tantalum stent caused lower neo-intimal inflammatory response compared to the low-molecular weight PLLA (80,000 Da) coating (Lincoff et al., 1997). The presence of stents in the vascular lumen often leads to impaired healing of endothelium accompanied by an excessive risk of late thrombosis.

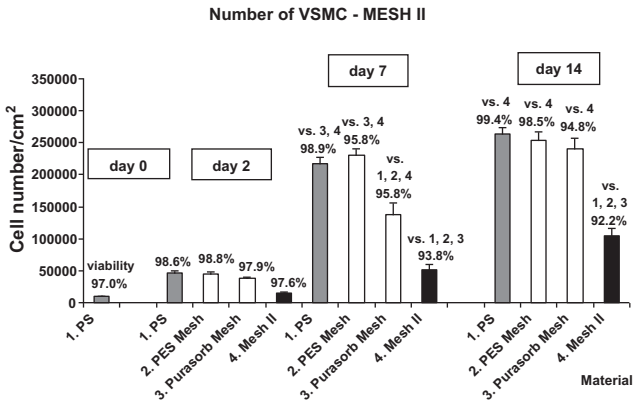

Fig. 6. Number and viability of vascular smooth muscle cells on a pure polystyrene culture dish (PS), on PS with a polyester mesh (PES Mesh), a purasorb-coated PES Mesh (Purasorb Mesh) or a sirolimus-containing PES Mesh (Mesh II) on day 0, 2, 7 and 14 after adding the meshes into the culture. p-Value <0.05 is considered significant in comparison with the sample of the same number and the day of culture.

On the other hand, a perivascular wrap prevents mechanical damage to the endothelium layer. The risk of late thrombosis caused by sirolimus released from the perivascular delivery system can be minimized by the distance of the sirolimus source from the endothelial cell layer, and by limiting the time of sirolimus release to the several weeks that are needed for re-endothelialization of the graft. However, in earlier studies, the drug carriers for the perivascular drug delivery system were often constructed in the form of a gel, which allowed them to move (migrate) away from the desired therapeutic position (Owen et al., 2010).

We have developed a perivascular drug delivery system based on a relatively mechanically strong polyester mesh, which is expected to be stably wrapped around the vascular graft. In addition, the mechanical support provided by the meshes can prevent distension of the autologous vein graft placed into arterial position, reduces the increased vessel wall stress and in turn leads to inhibition of VSMC proliferation (Mehta et al., 1998).

This mesh is coated with a degradable copolymer of L-lactide and ε-caprolactone (i.e. purasorb) containing sirolimus. Release from degradable matrices is usually triphasic, contains an initial burst release, a diffusional phase, and a degradation-controlled phase (Venkatraman and Boey, 2007). The kinetics of the drug release depends on the physical and chemical properties of the drug, the choice of a degradable polymer or copolymer, and their arrangement into polymer bilayers or multilayers with and without the drug, and also barriers (Finkelstein et al., 2003).

The degradation of polycaprolactone is within the order of 2–3 years, which is a much slower rate than that of PLA (Gunatillake and Adhikari, 2003). The rate of degradation of polyesters, such as polyglycolide, polylactide, and polycaprolactone, is preferably caused by access of water to the ester bond. Water rapidly plasticizes these polymers, and this in turn leads to mechanical distortion, cracking, pitting and fissure of the polymer in an uncontrolled way (Vert et al., 1994). Paclitaxel release from PLGA/methoxypolyethylene glycol (PLGA/MePEG) films was very slow, with less than 5% of the encapsulated drug being released over 2 weeks. The addition of 30% diblock copolymer composed of PDLLA-block-MePEG to paclitaxel-loaded PLGA films caused a substantial increase (five- to eight-fold) in the release rate of paclitaxel. The water soluble diblock copolymer seemed to enhance the hydrophilicity of the matrix, water uptake, the formation of water-filled channels throughout the matrix, and greatly increased the paclitaxel release rates (Jackson et al., 2004).

The copolymer used in the study, i.e. copolymer of L-lactide and ε-caprolactone (70/30) was of a relatively high M_w, i.e.

117,250 g/mol. After 2 weeks (Fig. 3) and 4 weeks (not shown) of incubation in PBS, we observed only small erosion changes in the copolymer coating; cracks appeared after 6 weeks. No changes in molar mass distribution observable by SEC indicated that there was no hydrolytic degradation of the purasorb polymer chains. Thus, sirolimus was released from the polymer matrix by diffusion rather than by polymer degradation. Mesh I released the total amount of sirolimus after 6 weeks, and Mesh II after 4 weeks. From Mesh I, there was substantial release of the drug in the first week of incubation, while the sirolimus release from Mesh II was more homogenous, without an initial burst release of the drug (Fig. 2). The difference in the kinetics of sirolimus release was caused by the different coating of the two meshes. Mesh I was coated with a homogeneous layer containing sirolimus. Mesh II contained the first layer which was twice as concentrated as that in the Mesh I, and the second upper layer composed of pure copolymer. The upper layer prevented an initial burst effect of sirolimus from Mesh II, due to gradual sirolimus diffusion through the pure copolymer. A similar arrangement, which prevented an initial burst drug release, was used in a study on bilayer rapamycin-eluting stents, coated with two different PLGA layers (Pan et al., 2009). The first PLGA layer (95 kDa, 85/15) contained a substantial amount of the drug (316 μg), while the upper layer was composed of PLGA of low M_w (20 kDa, 75/25) and contained only a small portion of rapamycin (30 μg).

The release of sirolimus differed according to the composition and arrangement of the two matrices. The sirolimus release from Mesh II, being completed after 4 weeks, was faster than the 6-week release from Mesh I. This may have been caused by a higher concentration of sirolimus in the first (i.e. bottom) layer of the Mesh II coating, which may have created a high concentration gradient of sirolimus, supporting drug diffusion into the upper layer and its release. In other studies, the complete drug release has varied, being observed after 15, 28, or even 90 days (Venkatraman and Boey, 2007; Hausleiter et al., 2005; Pires et al., 2005). Perivascular poly(ε-caprolactone) (PCL) cuff released all paclitaxel or rapamycin after 3 weeks (Pires et al., 2005). Films made of poly(lactic-co-glycolic acid) (PLGA) and PLGA blended with methoxypolyethylene glycol (MePEG) loaded with paclitaxel used as perivascular wraps released only 5–20% of the drug after 30 days (Jackson et al., 2004).

Both Mesh I and Mesh II inhibited growth of VSMC in culture for 14 days, although the Mesh II reduced VSMC proliferation more apparently (Figs. 4 and 5). This correlates positively on with the kinetics of sirolimus release, as the same amount of drug (140 μg/cm^2) in the Mesh II is released in a shorter time interval of 4 weeks. However, the Mesh I has been releasing sirolimus for 6 weeks which can be useful for *in vivo* studies in the future. In addition, as indicated by staining of VSMC by LIVE-DEAD Viability/Cytotoxicity Kit, the growth of VSMC was inhibited without significant death of these cells, which can be considered as a favourable effect preserving the physiological functions of VSMC, particularly their contractility. On the contrary, treatment with the rapamycin-eluting Pluronic gel, applied into the perivascular spaces of the grafted vein in mice, was associated with an increased apoptosis rate in the vascular wall, including the tunica media (Schachner et al., 2004). However, in this case, the dose of rapamycin was higher than in our system (i.e. 140 μg/cm^2 of the mesh), amounting to 200 μg per 0.1 ml of the gel.

In clinically used Cypher^{TM} stents, the total load of sirolimus is in the range of 70–300 μg (Venkatraman and Boey, 2007). Two profiles of drug release from stents have been prepared: fast release profile released the total amount of sirolimus (i.e. 140 μg/cm^2) in 15 days, and slow release that needed 90 days for the release of the drug. In our study, we used the same concentration of sirolimus per cm^2 in both Mesh I and Mesh II). Bare microporous metal stents without polymer coating were loaded with three concentrations of sirolimus, i.e. 138, 313, and 479 μg/mm^2. Complete release was found after 4 weeks with 66% of drug released in the first week (Hausleiter et al., 2005).

A significantly higher amount of sirolimus (2.5 mg/ml in 2 ml of gel) was used in the injectable terpolymer ReGel made of poly(lactic-co-glycolic acid)–polyethylene glycol–poly(lactic-co-glycolic acid) (PLGA–PEG–PLGA) (Owen et al., 2010). An *in vitro* study showed that 65–80% of the drug was released by day 14. For *in vivo* application, the gel should be replenished at 1, 2, and 3 weeks post-operatively. Mean sirolimus concentrations in all tissue sections analyzed at 1 week were found to be below 3 ng/mg of tissue, and were lower at this early time point than the experimentally determined concentration that was required to inhibit the proliferation of cultured smooth muscle cells by 50% (IC_{50} = 5 ng/ml).

5. Conclusions

We developed a perivacular system for controlled delivery of antiproliferative drug sirolimus. The perivascular delivery system is intended for wrapping a vein graft after its implantation into an arterial position. The system is based on polyester mesh coated with copolymer of L-lactide and ε-caprolactone with dissolved sirolimus. Two similar formulations of the system were able to release sirolimus within 4 or 6 weeks. The concentrations of sirolimus released from both meshes inhibited proliferation of smooth muscle cells in culture for 14 days. The perivascular sirolimus-delivery system seems to be promising for prevention of intimal hyperplasia and graft restenosis.

Acknowledgements

This study was supported by the Grant Agency of the Ministry of Health (Project No. NR9358), Centre for Cardiovascular Research (Project No. 1M6798582302) and Research Project AV0Z50110509. We also thank to Mr. Zdeněk Plichta for mesh coating and Mr. Robin Healey (Czech Technical University, Prague) for the language revision of the manuscript.

References

Bačáková, L., Lisá, V., Kubínová, L., Wilhelm, J., Novotná, J., Eckhart, A., Herget, J., 2002. UV light – irradiated collagen III modulates expression of cytoskeletal and surface adhesion molecules in rat aortic smooth muscle cells *in vitro*. Virchows Arch. 440, 50–62.

Colombo, A., Iakovou, I., 2004. Drug-eluting stents: the new gold standard for percutaneous coronary revascularisation. Eur. Heart J. 25, 895–897.

Conklin, B.S., Richter, E.R., Kreutziger, K.L., Zhong, D.-S., Chen, C., 2002. Development and evaluation of a novel decellularized vascular xenograft. Med. Eng. Phys. 24, 173–183.

ČSN ISO 2602 (010231), 1993. Statistical interpretation of tests results. Estimation of mean. Confidence intervals.

Daemen, J., Serruys, P.W., 2007. Drug-eluting stent update 2007: part I: a survey of current and future generation drug-eluting stents: meaningful advances or more of the same? Circulation 116, 316–328.

Finkelstein, A., McClean, D., Kar, S., Takizawa, K., Varghese, K., Baek, N., Park, K., Fishbein, M.C., Maškar, R., Litvack, F., Eigler, N.L., 2003. Local drug delivery via a coronary stent with programmable release pharmacokinetics. Circulation 107, 777–784.

Golomb, G., Fishbein, I., Banai, S., Mishaly, D., Moscovitz, D., Gertz, S.D., Gazit, A., Poradosu, E., Levitzki, A., 1996. Controlled delivery of a tyrphostin inhibits intimal hyperplasia in a rat carotid artery injury model. Atherosclerosis 125, 171–182.

Gunatillake, P.A., Adhikari, R., 2003. Biodegradable synthetic polymers for tissue engineering. Eur. Cell Mater. 5, 1–16.

Hausleiter, J., Kastrati, A., Wessely, R., Dibra, A., Mehilli, J., Schratzenstaller, T., Graf, I., Renke-Gluszko, M., Behnisch, B., Dirschinger, J., Wintermantel, E., Schömig, A., Investigators of the individualizable drug-eluting stent system to abrogate restenosis project, 2005. Prevention of restenosis by a novel drug-eluting stent system with a dose-adjustable, polymer-free, on-site stent coating. Eur. Heart J. 25, 1475–1481.

Jackson, J.K., Smith, J., Letchford, K., Babiuk, K.A., Machan, L., Signore, P., Hunter, W.L., Wang, K., Burt, H.M., 2004. Characterization of perivascular poly(lactic-co-glycolic acid) films containing paclitaxel. Int. J. Pharm. 283, 97–109.

Lincoff, M.A., Furst, J.G., Ellis, S.G., Tuch, R.J., Topol, E.J., 1997. Sustained local delivery of dexamethasone by a novel intravascular eluting stent to prevent restenosis in the porcine coronary injury model. J. Am. Coll. Cardiol. 29, 808–816.

Lipke, E.A., West, J.L., 2005. Localized delivery of nitric oxide from hydrogels inhibits neointima formation in a rat carotid balloon injury model. Acta Biomater. 1, 597–606.

Liuzzo, J.P., Ambrose, J.A., Coppola, J.T., 2005. Sirolimus- and taxol-eluting stents differ towards intimal hyperplasia and re-endothelialization. J. Invasive Cardiol. 17, 497–502.

Mehilli, J., Byrne, R.A., Wieczorek, A., Iijima, R., Schulz, S., Bruskina, O., Pache, J., Wessely, R., Schömig, A., Kastrati, A., 2008. Intracoronary stenting and angiographic restenosis investigators—test efficacy of rapamycin-eluting stents with different polymer coating strategies (ISAR-TEST-3). Randomized trial of three rapamycin-eluting stents with different coating strategies for the reduction of coronary restenosis. Eur. Heart J. 29, 1975–1982.

Mehta, D., George, S.J., Jeremy, J.Y., Izzat, M.B., Southgate, K.M., Bryan, A.J., Newby, A.C., Angelini, G.D., 1998. External stenting reduces long-term medial and neointimal thickening and platelet derived growth factor expressionin space a pig model of arteriovenous bypass grafting. Nat. Med. 4, 235–239.

Morice, M.C., Serruys, P.W., Sousa, J.E., Fajadet, J., Ban Hayashi, E., Perin, M., Colombo, A., Schuler, G., Barragan, P., Guagliumi, G., Molnar, F., Falotico, R., RAVEL Study Group, 2002. Randomized study with the sirolimus-coated Bx velocity balloon-expandable stent in the treatment of patients with de novo native coronary artery lesions. A randomized comparison of a sirolimus-eluting stent with a standard stent for coronary revascularization. New Engl. J. Med. 346, 1773–1780.

Owen, S.C., Li, H., Sanders, W.G., Cheung, A.K., Terry, C.M., 2010. Correlation of tissue drug concentrations with in vivo magnetic resonance images of polymer drug depot around arteriovenous graft. J. Control. Release 146, 23–30.

Pan, C.J., Tang, J.J., Weng, Y.J., Wang, J., Huang, N., 2009. Preparation and in vitro release profiles of drug-eluting controlled biodegradable polymer coating stents. Colloids Surf. B. Biointerfaces 73, 199–206.

Pires, N.M., van der Hoeven, B.L., de Vries, M.R., Havekes, L.M., van Vlijmen, B.J., Hennink, W.E., Quax, P.H., Jukema, J.W., 2005. Local perivascular delivery of anti-restenotic agents from a drug-eluting poly(epsilon-caprolactone) stent cuff. Biomaterials 26, 5386–5394.

Schachner, T., Zou, Y., Oberhuber, A., Tzankov, A., Mairinger, T., Laufer, G., Bonatti, J.O., 2004. Local application of rapamycin inhibits neointimal hyperplasia in experimental vein grafts. Ann. Thorac. Surg. 77, 1580–1585.

Suzuki, T., Kopia, G., Hayashi, S., Bailey, L.R., Llanos, G., Wilensky, R., Klugherz, B.D., Papandreou, G., Narayan, P., Leon, M.B., Yeung, A.C., Tio, F., Tsao, P.S., Falotico, R., Carter, A.J., 2001. Stent-based delivery of sirolimus reduced neointimal formation in a porcine coronary model. Circulation 104, 1188–1193.

Taylor Jr., L.M., Edwards, J.M., Porter, J.M., 1990. Present status of reversed vein bypass grafting: five-year results of a modern series. J. Vasc. Surg. 11, 193–206.

Venkatraman, S., Boey, F., 2007. Release profiles in drug eluting stents: issues and uncertainties. J. Control. Release 120, 149–160.

Vert, M., Mauduit, J., Li, S., 1994. Biodegradation of PLA/GA polymers: increasing complexity. Biomaterials 15, 1209–1213.

Vignot, S., Faivre, S., Aguirre, D., Raymond, E., 2005. mTtor-targeted therapy of cancer with rapamycin derivates. Ann. Oncol. 16, 525–537.

Physiol. Res. 60: 585-588, 2011

RAPID COMMUNICATION

A Periadventitial Sirolimus-Releasing Mesh Decreased Intimal Hyperplasia in a Rabbit Model

I. SKALSKÝ[1], E. FILOVÁ[2,3], O. SZÁRSZOI[1,3], M. PAŘÍZEK[2,3], A. LYTVYNETS[2], J. MALUŠKOVÁ[1], A. LODEREROVÁ[1], E. BRYNDA[4], V. LISÁ[2], Z. BURDÍKOVÁ[2], M. ČAPEK[2], J. PIRK[1,3], L. BAČÁKOVÁ[2,3]

[1]Institute for Clinical and Experimental Medicine, Prague, Czech Republic, [2]Institute of Physiology, Academy of Sciences of the Czech Republic, v.v.i., Prague, Czech Republic, [3]Centre for Cardiovascular Research, Prague, Czech Republic, [4]Institute of Macromolecular Chemistry, Academy of Sciences of the Czech Republic, v.v.i., Prague, Czech Republic

Received October 27, 2010
Accepted May 31, 2011

Summary

Autologous vein grafts used as aortocoronary bypasses are often prone to intimal hyperplasia, which results in stenosis and occlusion of the vein. The aim of this study was to prevent intimal hyperplasia using a newly developed perivascular system with sustained release of sirolimus. This system of controlled drug release consists of a polyester mesh coated with a copolymer of L-lactic acid and ε-caprolactone that releases sirolimus. The mesh is intended for wrapping around the vein graft during surgery. The mesh releasing sirolimus was implanted in periadventitial position onto arteria carotis communis of rabbits, and neointimal hyperplasia was then assessed. We found that implanted sirolimus-releasing meshes reduced intima thickness by 47±10 % compared to a vein graft after 3 weeks. The pure polyester mesh decreased vein intima thickness by 35±9 %. Thus, our periadventitial system for controlled release of sirolimus prevented the development of intimal hyperplasia in autologous vein grafts *in vivo* in rabbits. A perivascularly applied mesh releasing sirolimus is a promising device for preventing stenosis of autologous vein grafts.

Key words

Stenosis • Intimal hyperplasia • Controlled drug release • Perivascular mesh • Rapamycin

Corresponding author

Elena Filová, Dept. of Growth and Differentiation of Cell Populations, Institute of Physiology, Academy of Sciences of the Czech Republic, Videnska 1083, CZ-142 20 Prague 4 – Krc, Czech Republic. Fax: +420 2 4106 2488. E-mail: filova@biomed.cas.cz

Autologous saphenous vein is widely used as a conduit to solve the problem of stenosis or occlusion of the coronary and femoral arteries due to atherosclerotic lesions. The surgical outcome of these procedures has improved remarkably thanks to the use of alternative conduits (e.g. autologous arterial grafts, artificial synthetic grafts), but the saphenous vein is still used in coronary artery bypass grafting (CABG) and infrainguinal bypass graft surgery (Motwani and Topol 1998). The long-term patency of the vein graft likely depends on adequate adaptation into the arterial vascular system as well as relative moderation in the development of intimal hyperplasia. Neointimal hyperplasia, which develops immediately after grafting, is the most important early change in the grafted vein. Remodelling of autologous vessels after bypass surgery is characterised by damage to the endothelial cell layer and exposure of vascular smooth muscle cells (VSMC) on the luminal surface, which causes adhesion and aggregation of platelets, adhesion of monocytes, activation of migration and proliferation of VSMC, and also the attachment of regenerating endothelial cells (EC). In order to prevent autologous vascular graft remodelling, it is essential to support the endothelialization process, and to reduce the proliferation of VSMC.

Endothelialization of the graft is completed within several weeks after surgery (Liuzzo *et al*. 2005). Stents are usually inserted into autologous graft stenosis

to solve the graft lumen patency. In order to prevent VSMC proliferation and graft restenosis, antiproliferative drug-eluting stents have been developed, such as sirolimus-eluting stents (CypherTM, Cordis J&J, NJ), and paclitaxel-eluting stents (Colombo and Iakovou 2004).

Another way to influence neointimal formation is by an access from the adventitial surface of the grafted vessel. Periadventitial delivery of drugs from matrices placed adjacent to implanted grafts has been successfully used in animal models. Sirolimus was selected because previous studies had confirmed the ability of the drug to prevent neointimal hyperplasia with respect to its release kinetics, effective dosage, and safety in clinical practice (Schachner *et al.* 2004, Suzuki *et al.* 2001).

In our previous *in vitro* study, a periadventitial system of sustained release of sirolimus was developed (Filova *et al.* 2011). The system was constructed in the form of a polyester mesh (PES mesh) coated with copolymer of poly(L-lactic acid) and poly(ε-caprolactone) with dissolved sirolimus (Fig. 1). We observed relatively quick release of sirolimus from the mesh into the phosphate-buffered saline; 68±6 % of sirolimus was released within 11 days (Filova *et al.* 2011). Both the mesh and the copolymer ensured appropriate mechanical properties of the sheet, especially its strength, firmness, and the flexibility necessary for handling and the ability to be sutured. The results showed that the periadventitial copolymer-based system assured sustained release of antiproliferative drug sirolimus for 6 weeks. Sustained release of sirolimus suppresses VSMC proliferation for the time necessary for re-endothelialisation of the graft. This should reduce autologous graft remodelling and the need for subsequent treatment.

Wrapping the autologous graft with our polymeric sirolimus-releasing system ensures that the endothelial cell layer will be affected less than in the case of intravascular stents tightly touching the endothelium. Wrapping the vessel also can prevent mechanical strain on the graft induced by the stent (Jeremy *et al.* 2004). In addition, positive effects of external wall support on reducing vessel wall stress and inhibition of neointimal proliferation can be expected (Krejca *et al.* 2002).

The aim of this study was to evaluate the dynamics of the intimal changes in interposed external jugular vein grafts after three weeks. We hypothesize that this periadventitial sirolimus-releasing system wrapped around the autotransplanted vein will be a suitable option for positively influencing intimal hyperplasia and the patency of the vein graft.

A polyester mesh (PES mesh) (CHS 50, VUP Joint-Stock Company, Brno, bursting strength 138.0 N, EN 12332-1 standard) was coated with a solution containing 5.2 mg of sirolimus (Rapamycin, Sigma-Aldrich, Germany), 36.4 mg of purasorb (Purasorb PLC 7015, a copolymer of L-lactic acid and ε-caprolactone, PURAC biomaterials) in 1 ml of chlorbenzen – ethanol (1.75:1 v/v); and dried. Then it was coated for a second time with the same solution and dried. The resulting impregnated mesh contained 0.14 mg sirolimus per cm^2. The dry mesh was sterilised with ethylene oxide.

Eighteen male Giant Chinchilla rabbits (3.0-3.5 kg) were used in the experiments. Each experimental group included 4 to 8 animals, and the following experimental groups were tested: animals with an autologous graft (6 animals), animals with an autologous graft wrapped with a pure polyester mesh (4 animals), and animals with an autologous graft wrapped with the sirolimus-releasing mesh (8 animals). A rabbit model was used in the study as the mesh structure and mesh density were appropriate for the size of a rabbit jugular vein. Before surgery, the animals were anaesthetized using an intramuscular injection with ketamine hydrochloride (30.0 mg/kg). Anaesthesia was maintained with a mask and inhaled isoflurane (2.5-3.0 %). Heparin (300 IU/kg) was administered intravenously to the animals. The operative procedure was performed using an aseptic technique. The right external jugular vein and the right common carotid artery were exposed. The vein bypass grafts were constructed using an anastomotic cuff technique and were implanted to the common carotid artery (Jiang *et al.* 2004). Finally, either a pure PES mesh or a sirolimus-releasing mesh was wrapped around the vein graft and fixed by polypropylene suture 8/0 on the side. Non-wrapped autologous grafts were used as control samples. The animals were euthanized 3 weeks after implantation.

The explanted grafts were fixed in 10 % formalin, embedded in paraffin, cut into 3-4 μm sections and stained with Van Gieson with elastica. The thickness of the intima was calculated from 32-84 measurements per rabbit using the MeasureStackLines plug-in module of Ellipse Software (ViDiTo Systems, Slovakia). The data is presented as mean ± S.E.M. (Standard Error of Mean). One-way ANOVA and Scheffe's method of multiple comparison were used for the statistical analysis; the effect of drug presence was tested. A value of $p<0.05$ was considered to be significant.

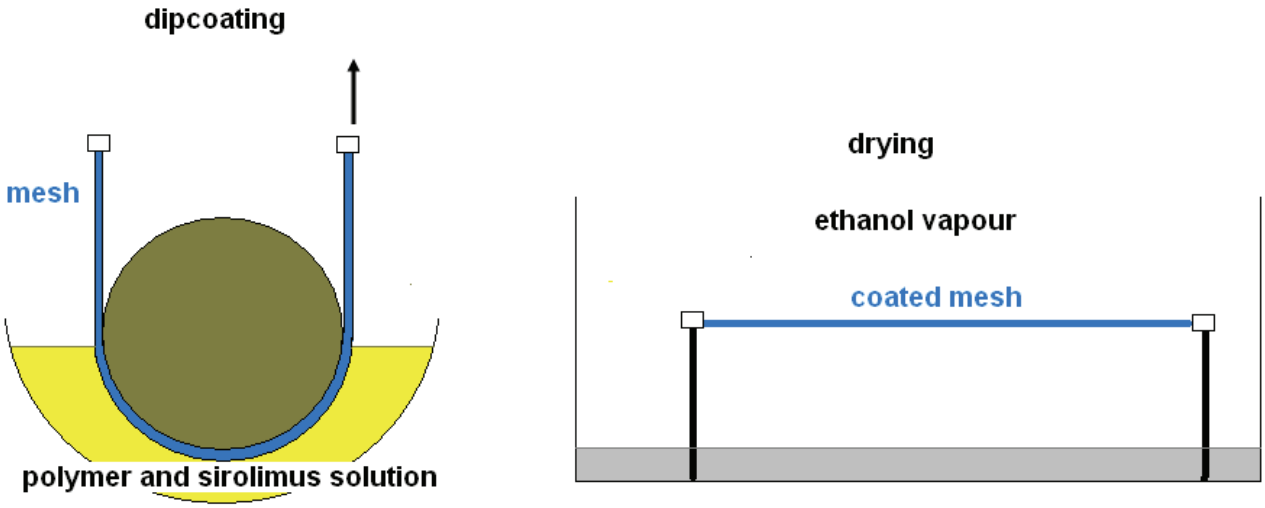

Fig. 1. The polyester mesh was passed through a solution of sirolimus, 5.2 mg, and purasorb, 36.4 mg, in 1 ml chlorbenzen – ethanol (1.75:1 v/v) and slowly dried in ethanol vapours.

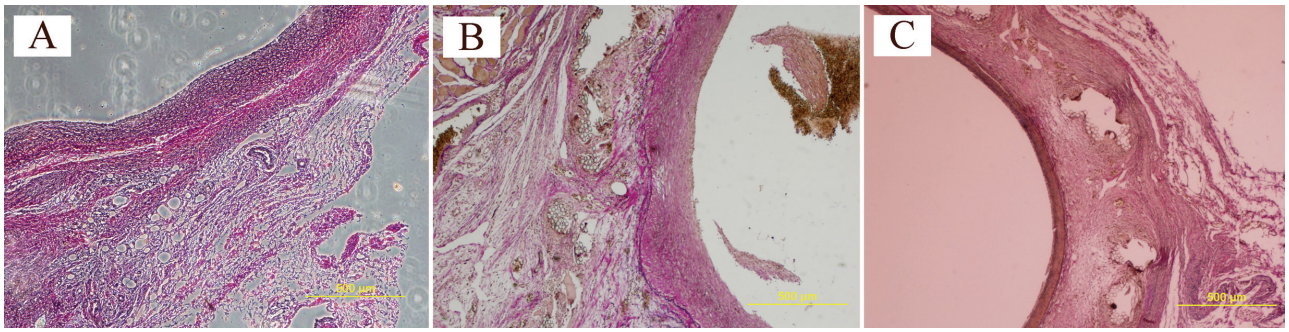

Fig. 2. An autologous vein graft (**A**), an autologous vein graft wrapped with a PES mesh (**B**), and an autologous vein graft wrapped with a PES mesh releasing sirolimus (**C**) after 3 weeks of implantation in rabbits, staining van Gieson and elastica, Olympus IX 51 microscope, objective × 4, DP 70 digital camera, scale bar = 500 µm.

Histological staining revealed the presence of either a PES mesh or a sirolimus-releasing mesh in vein adventitia (Fig. 2), probably due to the graft expansion. The intima thickness in the controlled autologous grafts was 16.8±0.9 µm, in the autologous grafts wrapped with the pure PES mesh it was 11.0±0.4 µm, and in the autologous grafts wrapped with sirolimus-releasing mesh it was 8.9±0.2 µm. The decrease in intima thickness when the vein graft was wrapped with a pure PES mesh or a sirolimus-releasing mesh was by 35±10 % or 47±9 %, respectively, compared to the autologous vein graft after three weeks; the difference was significant with a value of $p<0.001$ (Fig. 2). Sirolimus-releasing meshes had a significantly ($p<0.05$) stronger effect on reducing intimal hyperplasia than a pure PES mesh. No oblitering thrombi were found in any of the animals.

The copolymer purasorb loaded with sirolimus released sirolimus for several weeks to the vein graft tissue. We assume that the thickness of the vessel wall was low enough to enable diffusion of sirolimus into the tunica media to inhibit VSMC proliferation. Sirolimus penetration may also be supported by its hydrophobicity. A reduction of intimal hyperplasia dependent on the sirolimus dose was observed for stents containing 60-200 µg of sirolimus (Suzuki *et al.* 2001). The effective concentration of sirolimus necessary for inhibiting VSMC proliferation is relatively low (from ng/ml to µg/ml, Owen *et al.* 2010), allowing us to load the polymer with an amount of the drug sufficient for long-term release.

Our present study confirmed the hypothesis about the synergistic effect of a PES mesh and sirolimus on vein wall remodelling. The polyester periadventitial mesh probably worked in the same way as the external elastic membrane of the native arterial vessels, allowing them to withstand higher pressures in arterial circulation. While the release of sirolimus reduces intimal hyperplasia for a period of several weeks after implantation of the

sirolimus-releasing PES mesh, the favourable elastic effect of the PES mesh itself can proceed even after the entire sirolimus load has been released.

It can be concluded that we created a unique periadventitial system with controlled release of antiproliferative drug sirolimus that reduced intimal hyperplasia in a rabbit model. This sirolimus-delivery system combines the positive effect of mechanical support from the wrap with the effect of the antiproliferative action of sirolimus. This system therefore represents a promising approach for preventing neointimal hyperplasia of vein grafts interposed into the arterial bed.

Conflict of Interest

There is no conflict of interest.

Acknowledgements

This study was supported by the Grant Agency of the Czech Ministry of Health (project No. NR9358), the Czech Science Foundation (projects No. 102/08/0691 and P108/11/0794), the Centre for Cardiovascular Research (project No. 1M6798582302) and research project AV0Z50110509. We also thank Mr. Zdeněk Plichta for mesh coating, Dr. V. Lánská for statistical analyses and Mr. Robin Healey (Czech Technical University in Prague) for his language revision of the manuscript.

References

COLOMBO A, IAKOVOU I: Drug-eluting stents: the new gold standard for percutaneous coronary revascularisation. *Eur Heart J* **25**: 895-897, 2004.

EN 12332-1 (804629) Rubber- or plastics-coated fabrics. Determination of bursting strength. Steel ball method British-Adopted European Standard / 15-Feb-1999 / 8 pages.

FILOVÁ E, PAŘÍZEK M, OLŠOVSKÁ J, KAMENÍK Z, BRYNDA E, RIEDEL T, VANDROVCOVÁ M, LISÁ V, MACHOVÁ L, SKALSKÝ I, SZÁRSZOI O, SUCHÝ T, BAČÁKOVÁ L: Perivascular sirolimus-delivery system. *Int J Pharm* **404**: 94-101, 2011.

JEREMY JY, BULBULIA R, JOHNSON JL, GADSDON P, VIJAYAN V, SHUKLA N, SMITH FCT, ANGELINI GD: A bioabsorbable (polyglactin), nonrestrictive, external sheath inhibits porcine saphenous vein graft thickening. *J Thorac Cardiovasc Surg* **127**: 1766-1772, 2004.

JIANG Z, WU L, MILLER BL, GOLDMAN DR, FERNANDEZ CM, ABOUHAMZE ZS, OZAKI CK, BERCELI SA: A novel vein graft model: adaptation to differential flow environments. *Am J Physiol Heart Circ Physiol* **286**: H240-H245, 2004.

KREJCA M, SKARYSZ J, SZMAGALA P, PLEWKA D, NOWACZYK G, PLEWKA A, BOCHENEK A: A new outside stent – does it prevent vein graft intimal proliferation? *Eur J Cardiothorac Surg* **22**: 898-903, 2002.

LIUZZO JP, AMBROSE JA, COPPOLA JT: Sirolimus- and taxol-eluting stents differ towards intimal hyperplasia and re-endothelialization. *J Invasive Cardiol* **17**: 497-502, 2005.

MOTWANI JG, TOPOL EJ: Aortocoronary saphenous vein graft disease: pathogenesis, predisposition, and prevention. *Circulation* **97**: 916-931, 1998.

OWEN SC, LI H, SANDERS WG, CHEUNG AK, TERRY CM: Correlation of tissue drug concentrations with in vivo magnetic resonance images of polymer drug depot around arteriovenous graft. *J Control Release* **146**: 23-30, 2010.

SCHACHNER T, ZOU Y, OBERHUBER A, TZANKOV A, MAIRINGER T, LAUFER G, BONATTI JO: Local application of rapamycin inhibits neointimal hyperplasia in experimental vein grafts. *Ann Thorac Surg* **77**: 1580-1585, 2004.

SUZUKI T, KOPIA G, HAYASHI S, BAILEY LR, LLANOS G, WILENSKY R, KLUGHERZ BD, PAPANDREOU G, NARAYAN P, LEON MB, YEUNG AC, TIO F, TSAO PS, FALOTICO R, CARTER AJ: Stent-based delivery of sirolimus reduced neointimal formation in a porcine coronary model. *Circulation* **104**: 1188-1193, 2001.

Physiol. Res. 60: 419-437, 2011

REVIEW

The Role of Smooth Muscle Cells in Vessel Wall Pathophysiology and Reconstruction Using Bioactive Synthetic Polymers

M. PAŘÍZEK[1], K. NOVOTNÁ[1], L. BAČÁKOVÁ[1,2]

[1]Department of Growth and Differentiation of Cell Populations and [2]Center for Cardiovascular Research, Institute of Physiology, Academy of Sciences of the Czech Republic, Prague, Czech Republic

Received May 28, 2010
Accepted September 10, 2010
On-line March 14, 2011

Summary

This review summarizes recent trends in the construction of bioartificial vascular replacements, i.e. hybrid grafts containing synthetic polymeric scaffolds and cells. In these advanced replacements, vascular smooth muscle cells (VSMC) should be considered as a physiological component, although it is known that activation of the migration and proliferation of VSMC plays an important role in the onset and development of vascular diseases, and also in restenosis of currently used vascular grafts. Therefore, in novel bioartificial vascular grafts, VSMCs should be kept in quiescent mature contractile phenotype. This can be achieved by (1) appropriate physical and chemical properties of the material, such as its chemical composition, polarity, wettability, surface roughness and topography, electrical charge and conductivity, functionalization with biomolecules and mechanical properties, (2) appropriate cell culture conditions, such as composition of cell culture media and dynamic load, namely cyclic strain, and (3) the presence of a confluent, mature, semipermeable, non-thrombogenic and non-immunogenic endothelial cell (EC) barrier, covering the luminal surface of the graft and separating the VSMCs from the blood. Both VSMCs and ECs can also be differentiated from stem and progenitor cells of various sources. In the case of degradable scaffolds, the material will gradually be removed by the cells and will be replaced by their own new extracellular matrix. Thus, the material component in advanced blood vessel substitutes acts as a temporary scaffold that promotes regeneration of the damaged vascular tissue.

Key words

Tissue engineering • Bioartificial vascular grafts • Polymer irradiation • Wettability • Nanostructure • Dynamic bioreactor

Corresponding author

L. Bačáková, Dept. of Growth and Differentiation of Cell Populations, Institute of Physiology, Academy of Sciences of the Czech Republic, Vídeňská 1083, 142 20 Prague 4 – Krc, Czech Republic. Fax: +420 2 4106 2488. E-mail: lucy@biomed.cas.cz

Introduction

Aim of the review

This review article summarizes our 20-year experience in studying the role of vascular smooth muscle cells in physiology and pathophysiology of blood vessels, and also the interaction of these cells with materials developed for constructing bioartificial vascular replacements. The main mechanisms of blood vessel damage, especially those related to VSMC, are briefly explained, and then the review concentrates on current and future ways of replacing irreversibly damaged blood vessels. As bioartificial vascular grafts contain material and cellular components, both these components, i.e. synthetic polymeric materials (including their surface modifications) and potential cell sources are observed. Mechanisms of the cell-material interaction and methods for studying these processes are also analyzed.

Blood vessel damage

Cardiovascular diseases, such as atherosclerosis and hypertension, are often associated with irreversible damage of the vessel and loss of its function. These diseases are relatively widespread in our population, and

are serious risk factors with a marked influence on length and quality of life. Vascular smooth muscle cells (VSMC) play an important role in the mechanism of atherosclerotic plaque formation and in vessel thickening during hypertension. These disorders are initiated through mechanical damage to the endothelial cell lining of blood vessels, evoked mainly by non-physiologically high blood pressure, and also through biochemical damage to the endothelial cell layer due to civilization stress (e.g., increased level of cholesterol or glucose, smoking, etc.). The permeability of the endothelial cell layer then increases, and molecules not occurring inside the vessel under physiological conditions penetrate inside it. These molecules include particularly the platelet-derived growth factor (PDGF), which is chemotactic and mitogenic for VSMCs. PDGF-like molecules can be produced by VSMCs by an autocrine manner under pathological conditions (Bačáková-Řeřábková 1990). Other proteins present in the blood, such as albumin, fibronectin and vitronectin, can also permeate to the vessel wall and change the qualitative composition of the vascular extracellular matrix (ECM). Both endothelium and VSMCs respond to vessel wall damage by immune activation, manifested by synthesis of imunoglobulin and selectin adhesion molecules, such as intercellular adhesion molecule-1 (ICAM-1), vascular adhesion molecule-1 (VCAM-1) or endothelial-leukocyte adhesion molecule-1 (ELAM-1), and by the presence of these molecules on the cell surface (Bačáková *et al*. 2000a,b, 2002). These molecules act as receptors for cells of the immune system, such as leukocytes, lymphocytes, macrophages and mast cells. The role of mast cells in pathology of the vessel wall has often been underestimated, although it has been reported that in a pathologically changed vessel wall the ratio between mast cells and VSMC, i.e. the most numerous cell component of the vascular wall, can reach 1:5 (Rohatgi *et al*. 2009, Maxová *et al*. 2010). Inflammatory cells then penetrate into the vessel wall, release proteolytic enzymes, disrupt and oxidize the ECM, and thus activate migration and growth of VSMCs (Bačáková *et al*. 1997, 1999, 2002). In addition, the inflammatory cells produce cytokines, for example interleukins or tumor necrosis factors (TNF). Similarly to PDGF, these agents stimulate the VSMCs to change their phenotype from contractile to synthetic, which is referred to as phenotypic modulation (Hedin and Thyberg 1987, Campbell and Campbell 1995, Orr *et al*. 2009). This modulation is characterized particularly by loss of specific isoforms of contractile proteins, such as alpha-actin and SM1- and SM2-myosins, and accumulation of cell organelles involved in proteosynthesis, such as endoplasmic reticulum, ribosomes or Golgi complex (Fager *et al.* 1989, Suzuki *et al*. 2010). Phenotypically modulated VSMCs are prone to hyperplastic and hypertrophic cell growth, migration into the *tunica intima*, production of osteopontin, i.e. a calcium-binding glycoprotein (Orr *et al.* 2009). They thus markedly participate in remodeling the vessel wall and in the creation of atherosclerotic plaques. Atherosclerosis is treated conservatively by a specific low-fat diet, following a healthy life style and the use of medicines, e.g. statins. However, severely and irreversibly damaged vessels must be replaced with autologous or artificial substitutes (for a review, see Chlupáč *et al*. 2009).

Bioartificial vascular substitutes

In modern tissue engineering, perfect blood vessel replacements can be based either completely on biological material, i.e. extracellular matrix and cells (totally-engineered blood vessels; for a review, see Chlupáč *et al*. 2009), or can be characterized as bioartificial, i.e. consisting of synthetic scaffolds and cells. Optimal artificial scaffolds are constructed as a three-dimensional porous or fibrous tubular structure. The wall of this tubular scaffold is assigned for ingrowth of VSMCs, which will form a contractile multilayer, and also for ingrowth of nourishing capillaries (i.e., *vasa vasorum*) and nerve fibres. The luminal surface of the tubular construct is designed to be colonized by endothelial cells, which are expected to form a continuous, phenotypically mature, and thus semipermeable, non-imunnogenic and non-thrombogenic layer. This layer also helps to maintain the underlying VSMCs in quiescent contractile phenotype, e.g. by synthesis of sulfated and heparin-like glycosaminoglycans (Bačáková *et al*. 2000b, 2004*,* Filová *et al*. 2009a, Bačáková and Švorčík 2008).

An important characteristic of artificial scaffolds in advanced bioartificial vessel substitutes is that they are not only passively tolerated by cells (as was the case for earlier generations of vessel and other tissue replacements), but that they mimic functions of the natural ECM. This means that the synthetic material regulates the extent and the strength of cell adhesion, cell growth activity, cell differentiation and maturation to a desired phenotype. Resorbable materials (often synthetic polymers) have been considered as ideal substrates for scaffold fabrication, because these matrices can gradually

be replaced by cells and their newly formed natural extracellular matrix. In other words, in the concept of advanced tissue engineering, synthetic materials do not act as permanent vascular substitutes, but as temporary supportive structures stimulating regeneration of a defective vessel (Bačáková *et al.* 2004, 2007, Bačáková and Švorčík 2008).

However, experiments in laboratory animals have shown that degradable synthetic polymers often have insufficient mechanical qualities (Greisler *et al*. 1991), which can lead to the formation of an aneurysm on the vascular replacements or a rupture of the replacement. Relatively fast degradation of the polymer and slow regeneration of new vascular tissue also contribute to the insufficiency of the mechanical properties of vascular replacements based on degradable polymers. Resorbable polymers often used in tissue engineering, such as polylactides, polyglycolides, polycaprolactones and their copolymers, usually degrade within weeks or months, whereas for human vessel reconstruction, especially for older people with other intercurrent diseases, the degradation time should rather be several years. Therefore, even in advanced tissue engineering approaches, there has been a certain "renaissance" of biostable polymers in vascular wall reconstruction, or semi-degradable materials containing both resorbable and biostable polymeric components have been considered for this purpose (Greisler *et al.* 1991, Xue and Greisler 2003).

Differentiated autologous endothelial and smooth muscle cells, isolated from the patient's subcutaneous veins before the planned surgery, have usually been considered for use as the cell component of blood vessel replacements. These cells can be further expanded under *in vitro* conditions and seeded on to synthetic scaffolds. After phenotypic maturation of the cells, which can achieved in a dynamic cultivation system, this construct can be implanted into the patient's organism. Ideally, it can be expected that the synthetic scaffold will gradually be resorbed and replaced by newly regenerated functional vascular tissue (Bačáková *et al*. 2003, 2004, 2007, Bačáková and Švorčík 2008). However, differentiated cells may be available in limited quantities, and their growth activity can also be low. For these cases, attempts have been made to differentiate vascular cells from stem or progenitor cells, e.g. those present in bone marrow, blood, fat tissue, or skeletal muscle satellite cells are used (for a review, see Chlupáč *et al.* 2009, Filová *et al.* 2009b, Suzuki *et al*. 2010). The desirable cell phenotype can be achieved by an appropriate composition of the culture medium, and also by the physicochemical properties and the bioactivity of the synthetic scaffolds.

Currently used vascular substitutes

The tissue engineering approaches mentioned above, although promising for the future, still remain rather on a theoretical level, i.e., they have been applied in experiments *in vitro* or on laboratory animals. Autologous vessels are still considered as vascular substitutes of the highest quality – a classic example is an aortocoronary bypass created from subcutaneous veins of the lower limbs or from *a. thoracica interna*. However, this approach also has some limits, such as the availability of an appropriate healthy vessel for creating the substitute. As mentioned above, in our civilized society there are considerable numbers of people, especially those of older age, who suffer from vascular diseases including atherosclerosis. In addition, even healthy vessels are usually available only in limited quantities (for a review, see Chlupáč *et al.* 2009). Other serious problems are the burden to the patient due to additional surgery, donor site morbidity, and in the case of implantation of a vein into an arterial position, also limited adaptation of the vein tissue to higher mechanic requirements. This maladaptation is often manifested by activated migration, proliferation and synthesis activity of smooth muscle cells, i.e. effects that, together with endothelial layer damage and thrombus formation, lead to restenosis and failure of autologous vessel substitutes. It is also possible to use allogenous or even xenogenous substitutes from healthy donor organisms, but this approach is associated with the risk of immune rejection of the implant, and also the risk of pathogen transmission (Kakikis *et al*. 2005).

In the case of damaged vessels larger than 6 mm in diameter, artificial substitutes created from routinely available synthetic polymers, such as polyethylene terephthalate (PET) or expanded polytetrafluoroethylene (ePTFE), are currently used in clinical practice. These substitutes have relatively good mechanical properties and are resistant to stress due to the bloodstream. However, their potential for long-term durability and physiological function in the patient's organism is limited (Xue and Geisler 2003). These replacements have physical and chemical properties that are less appropriate for colonization with cells. Firstly, they are hydrophobic. This is the main factor limiting cell adhesion and thus

hampering the desired reconstruction of a continuous and mature endothelial cell layer, which is considered to be the best anti-thrombogenic surface. In large diameter vascular replacements, a missing endothelial cell layer is not a factor markedly limiting long-term patency, because quick blood flow prevents the adhesion of thrombocytes and other blood cells to the prosthesis (for a review, see Chlupáč *et al*. 2009). However, in small diameter vessel replacements, the blood flow is slower, and thus thrombocytes and other blood components, including the cells of the immune system, can be accumulated here, and this can lead to stenosis or total obliteration of the artificial vessel. After implantation of the prosthesis the patients are therefore reliant for the rest of their lives on anticoagulant treatment, which can have negative side effects on their organism (for a review, see Chlupáč *et al*. 2009). Thus, in the case of small-diameter vascular replacements, there is a particularly important need for bioartificial vascular prostheses with a mature continuous layer of anti-thrombogenic endothelium.

Reconstruction of the endothelial cell layer has been at the centre of interest in all innovations of polymeric vascular replacements, while VSMCs have usually been excluded from these replacements due to the risk of their excessive proliferation and vessel restenosis (Chlupáč *et al*. 2009). However, VSMCs are the most numerous cell types in the natural vessel wall, and a contractile layer of these cells is a physiological component of this wall. For this reason, the *tunica media* containing VSMCs should also be reconstructed in advanced vascular replacements. The character of the synthetic material in these replacements, and also the cell culture environment used for preparing the cell-material construct, should direct VSMCs from the synthetic phenotype, which is usual in conventional cell culture systems, to maturation towards quiescent contractile phenotype (Bačáková *et al*. 2004, Bačáková and Švorčík 2008, Chlupáč *et al*. 2009).

Synthetic polymers for reconstructing blood vessels

Polymers for clinically and experimentally used vascular replacements

The vascular replacements used in current clinical practice are based on polyethylene terephthalate (PET) or polytetrafluoroethylene (PTFE). Polyurethane has been applied for constructing hemodialysis access grafts (for a review, see Chlupáč *et al.* 2009). In the experimental field, biostable polymers, such as polypropylene and polyethylene (PE), and also degradable polymers, such as polylactides, polyglycolides, polycaprolactone and their copolymers, have been used for creating cell carriers or prostheses tested *in vitro* or in laboratory animals (Bačáková *et al.* 1996, 2001a, 2004, 2007, Chlupáč *et al.* 2009).

Our studies have usually focused on the interaction of vascular endothelial and smooth muscle cells with PET, PTFE or PE. PET, also known under the trade name Dacron, is a thermoplastic polymer belonging to the polyester group, developed by polycondensation, where the catalyst is phthalic acid. This polymer is hydrophobic (advancing water drop contact angle about 90°; van Bilsen *et al*. 2008). For vascular replacement construction purposes it is used mostly in fibrous form (knitted or woven), mimicking the architecture of the natural vessel. This fibrous structure can serve as a scaffold for colonization with cells (endothelial cells on the luminal surface of the prosthesis and VSMCs inside its wall), and will allow a certain degree of transmural tissue ingrowth, such as capillaries and connective tissue. A disadvantage of this type of vascular prosthesis, particularly if knitted, is its permeability for blood, which has been prevented by impregnation with proteins such as albumin, collagen or gelatine (Marois *et al*. 1996; for a review, see Chlupáč *et al*. 2009). Glutaraldehyde or formaldehyde used for crosslinking these proteins may persist in the prosthesis and have cytotoxic effects (You *et al*. 2010, for a review, see Filová *et al.* 2009b). Therefore, in our studies, knitted PET prostheses have been impregnated with a copolymer poly(glycolide–L–lactide) or with a terpolymer poly(glycolide–L–lactide–(ε)caprolactone). This approach has not only reduced their permeability, but has also enhanced their attractiveness for endothelial cells by flattening the relatively rough inner surface and increasing its wettability. Cell colonization has further been supported by coating the luminal surface of PET prostheses with fibrin, laminin and collagen type I in combination with laminin, fibronectin or fibrin (Chlupáč *et al*. 2006, 2008).

PTFE is known under the trade names Teflon or Goretex. It is a thermoplastic fluorinated polymer with a high oxygen index (i.e., a parameter of the flammability of the material), which means that this material is relatively resistant to fire and high temperatures (Cullis and Hirschler 1983). From a clinical point of view, PTFE is a more biostable material than PET, i.e. it is less prone to deterioration in biological environments, and has low

reactivity towards blood elements. For fabricating vascular prostheses, expanded PTFE is used, i.e. with a porous structure created by a special manufacture technology based on heating, stretching and extruding the material. The mechanical properties of PTFE are highly suitable for constructing vascular replacements (Guidoin *et al*. 1993). However, similarly to PET, PTFE in its unmodified state is also highly hydrophobic, and this is a limiting factor for cell adhesion and for potential construction of bioartificial vascular prostheses based on PTFE scaffolds (Heitz *et al*. 2003, Chlupáč *et al*. 2009).

Polyethylene (PE) has been used as a model material because of its good availability, low cost and relatively easy processing by methods commonly used for polymer surface modification. It is biostable and resistant to deterioration by water, frost and various chemicals. PE has been classified into several different categories based mostly on its density and branching. The most frequently-used types of PE are ultra-high molecular weight polyethylene (UHMWPE), used as a component for total joint replacements and spine implants, low density polyethylene (LDPE, density 0.922 g/cm^3), and high density polyethylene (HDPE, density 0.951 g/cm^3) (Švorčík *et al*. 2006).

Concerning its physical and chemical properties, LDPE has a slightly lower water drop contact angle of 98°, while HDPE has a contact angle of 102°. This difference in the contact angles between LDPE and HDPE is relatively small; thus both polymers are considered to be highly hydrophobic. However the two polymers differ from each other more markedly in their structure. HDPE has linear chains, whereas LDPE is branched (Hameed and Hussain 2004, Ducháček 2006). These differences could explain, at least partly, the higher adhesion and growth of VSMCs on LDPE observed in our studies, although the cell colonization was relatively low on both types of PE. Similarly to PET and PTFE, PE in its pristine unmodified state is not optimal for scaffolds for vascular tissue engineering, due to its bioinertness (Švorčík *et al.* 1995, 2006, 2009*,* Bačáková *et al*. 2001a, Walachová *et al*. 2002, Kasálková *et al*. 2008, 2010*,* Pařízek *et al*. 2009).

Polymer modification methodology

Modifications are made to the polymers used in our studies in order to change their physical and chemical surface properties, such as polarity, wettability, chemical composition (presence of oxygen-containing chemical functional groups, free radicals, carbon content, etc.), surface roughness and topography. These characteristics of the polymer surface are the key factors controlling spontaneous adsorption of extracellular matrix (ECM) molecules from biological fluids such as culture medium or blood. These characteristics determine the type of adsorbed molecules – for example, vitronectin, fibronectin and collagen are adsorbed preferentially on wettable surfaces, while albumin is absorbed preferentially on hydrophobic surfaces. The quantity, geometrical conformation and flexibility of cell adhesion-mediating molecules are also influenced by the physical and chemical properties of the material surface, and by the consequent availability of specific sites on ECM molecules for cell adhesion receptors, which direct the subsequent cell behavior, e.g. their adhesion, spreading, migration, proliferation, differentiation, viability and other cell functions (Bačáková *et al.* 2004, Bačáková and Švorčík 2008).

A range of physical and chemical modifications have been used to create a bioactive surface attractive for cell colonization. For example, in our earlier studies, polymers were irradiated with ultraviolet light (UV), ions or plasma irradiation, and some of them were subsequently grafted with various biomolecules or nanoparticles attached to newly-developed binding sites on the activated polymer.

UV light irradiation is a relatively simple and easily available method for changing the physical and chemical surface properties of synthetic polymers in order to enhance their bioactivity. In our studies performed in collaboration with the Department of Applied Physics, Institute of Experimental Physics, Johannes-Kepler-University, Linz, UV light was generated using a Heraeus-Noblelight Xe_2 lamp (Hanau, Germany; centre wavelength of 172 nm, spectral bandwidth about 16 nm, intensity about 22 mW/cm^2). The exposure time ranged from 5 to 30 min (Heitz *et al*. 2003, Mikulíková *et al*. 2005, Bačáková and Švorčík 2008). In our earlier studies, this method was used to modify the surfaces of PTFE (Heitz *et al.* 2003, Mikulíková *et al.* 2005) or PET foils (Kubová *et al.* 2007). Polymer modification by UV light has usually been performed homogeneously on the entire polymer surface. However, it is also possible to achieve irradiated micro-domains of various sizes, shapes, distances and distributions on the polymer surface in order to guide regionally-selective cell adhesion and growth. For this purpose, we used metallic (e.g. nickel) contact masks with gaps ranging in diameter from several micrometres

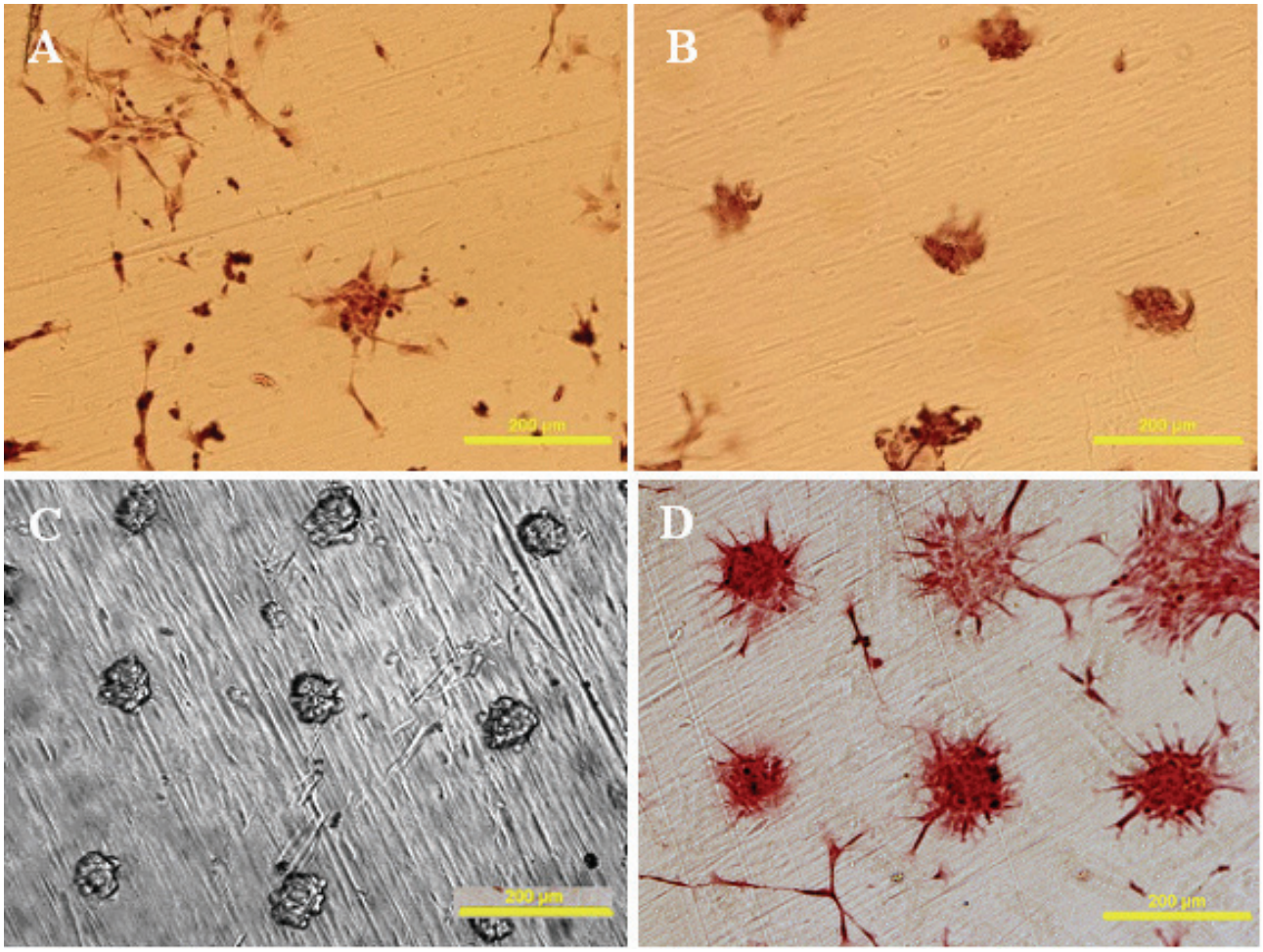

Fig. 1. Effects of time of exposure to UV light, cell type, and time of cultivation on cell adhesion to UV-irradiated domains created on PTFE through a nickel mask with round openings (diameter 100 µm, center-to-center distance 300 µm) in an ammonia atmosphere. **A, B**: Rat aortic smooth muscle cells on day 1 after seeding on PTFE irradiated for 10 min and 20 min, respectively. **C, D**: Human umbilical vein endothelial EA.hy926 cells and rat aortic smooth muscle cells, respectively, on day 3 after seeding on PTFE irradiated by UV light for 20 min. **B, D**: Rat aortic smooth muscle cells on PTFE irradiated for 20 min on day 1 and day 3 after seeding, respectively. The cells were stained with hematoxylin-eosin and photographed under an Olympus IX 50 microscope using a DP 70 digital camera, except in the case of B, where the cells are native and are photographed using a phase-contrast microscope (Zeiss, Germany) with a CCD-camera (PCO-Sensicam, Kelheim, Germany). Bar = 200 µm.

to hundreds of micrometres. The spacing between the gaps was usually hundreds of micrometres or even millimetres, in order to avoid possible bridging of the unexposed regions by cells, especially by VSMCs. Compared to other cell types, such as the vascular endothelial cells or human embryonic kidney (HEK) cells also used in our studies, VSMCs were more active in migration and growth, and thus also in overlapping the irradiated domains and spanning the unmodified polymer regions. The selectivity of cell adhesion on the irradiated domains was also influenced by the time of exposure to UV light, cell seeding density and the time of cell cultivation (Mikulíková *et al.* 2005, Pařízek *et al.* 2009, Bačáková *et al*. 2009; Fig. 1).

As mentioned above, the purpose of irradiating synthetic polymers is to convert their surfaces, which are rather bioinert in their pristine unmodified state, to bioactive surfaces promoting cell colonization. UV light irradiation induces degradation of polymer chains and the release of some atoms, namely hydrogen or fluorine in PTFE, from the polymer, and the creation of radicals. These radicals react with air oxygen, leading to the formation of oxygen-containing functional chemical groups on the polymer surface (Heitz *et al*. 2003, Mikulíková *et al*. 2005, Bačáková and Švorčík 2008). Afterwards these groups enhance the polymer polarity and wettability, and in this way they have a favorable influence on the adsorption of cell adhesion-mediating ECM molecules. These molecules, including particularly fibronectin, vitronectin, collagen or laminin, are present in biological fluids such as standard serum-supplemented cell culture media, blood or extracellular fluid, and are

also synthesized and deposited by cells colonizing the polymer (for a review, see Bačáková *et al.* 2001a, 2004, Bačáková and Švorčík 2008).

Changes in the polymers induced by UV irradiation can be further intensified by irradiation in reactive atmospheres, such as NH_3 (Heitz *et al.* 2003, Mikulíková *et al.* 2005) or acetylene (Kubová *et al.* 2007). In our experiments, the most positive effect on cell adhesion was observed when the polymers were irradiated in an NH_3 atmosphere. When PTFE was irradiated with UV light in this atmosphere, fluorine atoms were substituted with C-H, C=O and particularly C-NH_2 groups. It is well known that amino groups not only enhance the wettability of a material but also provide its positive charge. This has favorable effects on the adsorption of cell adhesion mediating proteins (Heitz *et al.* 2003, Mikulíková *et al.* 2005, Liu *et al.* 2007; for a review, see Bačáková and Švorčík 2008).

Ion irradiation of polymers, also known as ion implantation, is based on similar principles as UV light irradiation. This method was originally developed for technical purposes, for example for incorporating metal ions into materials designed for electronics (Fink *et al.* 2004, Macková *et al.* 2006, Švorčík and Hnatowicz 2007). Using this method, various materials can also be enriched with various ions for biological purposes; for example, calcium can be implanted into materials for bone replacements (Nayab *et al.* 2007). In our studies, we have focused on modifying synthetic polymers, such as polyethylene, polystyrene and polypropylene, with gas ions considered as biocompatible, namely oxygen and carbon ions, halogens, such as fluorine, or inert gases, such as argon (Švorčík *et al.* 1993, 1995, Bačáková *et al*. 1996, 2000a,b, 2001a, Walachová *et al*. 2002, Švorčík and Hnatowicz 2007). During ion bombardment of the polymer, these ions are not retained in the polymer structure (or only minimally, usually below the limit detectable by available methods; Bačáková *et al*. 2000a, 2001a). However, the ions cause changes in the polymer leading to its oxidation and subsequent enhancement of its polarity and wettability. As in the case of UV light irradiation, the polymer chains are degraded, various atoms are released, radicals are formed and they react with oxygen. These processes take place already in the implantation chamber, where the vacuum is not absolute (the pressure of the residual air is about 10^{-4} Pa), and continue after exposition of the irradiated material to the air atmosphere. Chemical functional groups containing oxygen (i.e., carbonyl, carboxyl, hydroxyl, ether or ester groups) are exposed on the polymer surface, enhance its polarity and wettability and promote the adsorption of cell adhesion-mediating molecules in appropriate geometrical conformations, which enable the specific amino acid sequences in the molecules to be reached by cell adhesion receptors (Bačáková *et al.* 2000a,b, 2001a).

As for the energy and dosage of ions, the surface of the samples used in our experiments was bombarded by ions of energies from 15 to 150 keV and of doses from 10^{12} to 10^{15} ions/cm^2. Higher ion energies and doses in this range (i.e., 150 keV combined with $5x10^{14}$ or 10^{15} ions/cm^2) resulted in an interesting effect, referred to as "relative carbonization" of the polymer. This means that during intensive irradiation of the polymer, the release of non-carbon atoms from the polymer prevailed over binding new atoms from the ambient atmosphere. As a result, the content of non-carbon atoms in the polymer decreased markedly and carbon relatively outweighed the other atoms, although its absolute content remained unchanged. In addition, conjugated double bonds arose between carbon atoms, and the polymer became electrically conductive – its electrical resistivity was able to decrease by as many as 15 orders of magnitude. This newly established electrical conductivity also significantly supported colonization of the polymer with cells (Švorčík *et al*. 1995, Bačáková *et al*. 1996, 2000a,b, 2001a). It is known that the electrical conductivity of other types of materials, too, enhances cell adhesion and growth, even without active electrical stimulation of the cells (Jeong *et al*. 2008, Mihardja *et al.* 2008, Bettinger *et al*. 2009).

Similarly as in the case of UV light irradiation, ion irradiation can also be performed through contact metal masks in order to create microdomains adhesive for cells (Pařízek *et al.* 2009).

Plasma irradiation of polymers is another important technology for changing the physicochemical properties of the polymer surface in a similar way as by the use of UV light irradiation or ion irradiation. In our studies we used a Balzer SCD 050 device, where the polymers, mainly polyethylene, were irradiated with Ar^+ plasma for various time intervals ranging from tens to hundreds of seconds (usually 50-400 s). The Ar^+ plasma discharge activated the polymer surface by creating reactive radicals, oxygen-containing chemical functional groups and groups with double bonds (Kasálková *et al*. 2008, 2010, Švorčík and Hnatowicz 2008). These active sites were grafted with various biologically active molecules, such as amino acids (glycine, arginine),

proteins (albumin, fibronectin), other synthetic polymers (polyethylene glycol), and even carbon or gold (Pařízek *et al.* 2009, Švorčík *et al*. 2009, Kasálková *et al*. 2010). These elements can be grafted to the activated polymer surface in the form of nanoparticles from a colloidal suspension of these elements in water (Pařízek *et al.* 2009, Švorčík *et al*. 2009). The nanostructure of the polymer, created by partial polymer degradation during irradiation and further enhanced by the attachment of nanoparticles, is supportive for cell adhesion by a mechanism synergistic with that on moderately wettable surfaces, i.e. adsorption of cell adhesion-mediating proteins in an appropriate geometrical conformation for binding them with cell adhesion receptors (Miller *et al*. 2007).

Mechanism of cell-material interaction

As mentioned above, the cells adhere to conventional biomaterials (i.e. those not endowed with ligands for cell adhesion receptors, e.g. RGD-containing oligopeptides) through ECM proteins, spontaneously adsorbed on the material surface exposed to biological environments. Under *in vivo* conditions, these proteins are adsorbed from body fluids, and under *in vitro* conditions they are adsorbed from the serum in the culture medium, and also after synthesis and secretion by cells colonizing the material.

The cells can also be attached to the material surface without adsorbed proteins, i.e. through weak chemical bonds between molecules of the cell membrane and the material surface. However, these bonds are nonspecific, i.e. not mediated by cell adhesion receptors, and thus they cannot transfer adequate signals into the cells ensuring their viability, growth, differentiation and other specific functions (for a review, see Bačáková *et al.* 2004, Bačáková and Švorčík 2008).

Proteins mediating cell-material adhesion

ECM proteins that which mediate the cell-material adhesion and markedly influence the subsequent cell behavior, such as cell spreading and shape, migration, proliferation, metabolic activity, viability, differentiation and phenotypic maturation, include particularly collagen, elastin, fibronectin, vitronectin and laminin. Most of these proteins are important components of vascular ECM *in vivo*, and therefore they play a significant role in blood vessel reconstruction and regeneration.

Collagen is a widespread protein in mammalian tissues, where it represents 25-30 % of all proteins in mammalian organisms. Its molecule consists of three polypeptide strands (called alpha chains), each possessing the conformation of a left-handed helix. These three left-handed helices are twisted together into a right-handed coil, also referred to as a triple helix or a "super helix", which is a cooperative quaternary structure stabilized by numerous hydrogen bonds. The collagen molecule, i.e. tropocollagen, is approximately 300 nm in length and 1.5 nm in diameter, and is a subunit of larger collagen aggregates, namely fibrils. The fibrils are interconnected through covalent bonds, which provide large mechanical stability to the whole collagen network (Abraham *et al.* 2008). Nowadays, 29 various types of collagen have been described. The most common is the type I, which represents 90 % of collagen in a living organism and is contained mainly in the epidermis, ligaments, bones and teeth, and it is also an important component of the vascular ECM. Type II occurs in cartilages. Type III is collagen of embryonic development, and it is later replaced by collagen I. However, its content increases in the vascular wall under pathological conditions, which can be due to a dedifferentiated synthetic phenotype of VSMC, which is in some aspects similar to the embryonic and fetal VSMC phenotype (Bačáková *et al.* 1997, 2002). Type IV occurs together with laminin in cell basal laminae, and together with laminin it maintains the VSMCs in the differentiated contractile phenotype (Roy *et al*. 2002). VSMCs bind collagen through β_1-integrin adhesion molecules, especially through $\alpha_1\beta_1$, $\alpha_2\beta_1$, $\alpha_3\beta_1$ integrins, which are referred to as “collagen receptors” (Glukhova and Koteliansky 1995).

Elastin is defined as an insoluble scleroprotein, and is the main component of elastic fibers in animal tissues (ligaments, bronchi, lungs and vessel wall tissues). It contains a large amount of glycine, proline and aliphatic amino acids (alanine, valine, leucine and isoleucine), and also relatively numerous basic lysine residues. As for the vascular wall, high quantities of elastin occur in large vessels near the heart, such as thoracic aorta or carotid arteries. VSMCs are attached to elastin through a non-integrin adhesion receptor, which recognizes the amino acid sequence VAPG (Val-Ala-Pro-Gly) in the elastin molecule (Gobin and West 2003). As elastin maintains VSMCs in a quiescent differentiated contractile phase (Karnik *et al.* 2003), recombinant elastin-like proteins with VAPG sequences are considered to be suitable for constructing bioartificial

blood vessel replacements (Bandiera *et al.* 2005).

Fibronectin belongs to the family of dimeric glycoproteins (molecular weight about 600 kDa). It has binding sites for other ECM molecules, such as collagen, heparan sulfate proteoglycans and also fibrin, a provisional matrix molecule taking part in wound healing, including repairs to vascular damage. Fibronectin can connect many ECM molecules into a continuous network. It is also an important component of blood serum, which is commonly used as a supplement for the cell culture media (Bačáková and Švorčík 2008). The cells adhere to fibronectin through integrin receptors, particularly integrin $\alpha_5\beta_1$, referred to as a "fibronectin receptor". Another important receptor for fibronectin on the cell membrane is the $\alpha_v\beta_3$ integrin. Both $\alpha_5\beta_1$ and $\alpha_v\beta_3$ integrins bind fibronectin through the RGD (Arg–Gly–Asp) sequence in its molecule (Glukhova and Koteliansky 1995). Fibronectin can alternatively be spliced in three regions, namely extradomains EIIIA, EIIIB, and a variable segment V, potentially giving rise to functionally distinct variants of the molecule (Barnes *et al.* 1995). When differentiated mature VSMCs, freshly isolated from the rat aorta, were seeded on fibronectin substrates, fibronectin induced their phenotypic modulation to synthetic phenotype, and, in the presence of growth factors, also their migration and proliferation (Roy *et al.* 2002). Moreover, in the presence of a special osteogenic cell culture medium, fibronectin induced osteogenic differentiation of VSMCs, manifested by expression of osteocalcin, i.e. a calcium-binding ECM glycoprotein, activity of alkaline phosphatase and tissue calcification (Ding *et al.* 2006).

Similar effects were also observed in the presence of serum fibronectin in the culture medium (Hedin and Thyberg 1987). Also in experiments performed *in vivo* on mice with partial ligation of the carotid arteries, infusion of pUR4, i.e. a fibronectin polymerization inhibitor, reduced carotid intima, media and adventitial thickening, leukocyte infiltration into the vessel wall, ICAM-1 and VCAM-1 levels, cell proliferation and VSMC phenotypic modulation (Chiang *et al.* 2009). On the other hand, in non-differentiated progenitor cells, and also in other cell types than VSMC, such as mesangial cells, fibronectin is capable of inducing differentiation towards VSMC phenotype, manifested by synthesis of alpha-actin (Costa-Silva *et al.* 2009).

Vitronectin is a 75 kDa glycoprotein consisting of 459 amino acid residues. It is plasmatic glycoprotein circulating in blood in a concentration of 200-400 mg/ml, present in the serum supplement of the cell culture medium and in the extracellular matrix. It is one of the principal glycoproteins enabling cell adhesion and spreading, and the main ligand for vitronectin cell receptors, such as $\alpha_v\beta_3$, $\alpha_{IIb}\beta_3$, $\alpha_v\beta_1$, $\alpha_v\beta_5$. Other molecules bound by vitronectin are heparin and collagen. In cell cultures, vitronectin induces migration, proliferation and synthetic phenotype of VSMCs (Dufourcq *et al*. 2002).

Laminins are high molecular multidomain heterotrimer proteins (850 kDa), composed of α-, β- and γ-chains, and these chains occur in five, three and three genetic variants, respectively. Laminins are major proteins of the cellular basal lamina. In the vascular wall, laminin together collagen IV, elastin and sulfated and heparin-like glycosaminoglycans maintains VSMCs in a quiescent differentiated contractile state. Sixteen laminin isoforms have been described in mammals. The cellular receptors for laminin are integrins $\alpha_1\beta_1$, $\alpha_2\beta_1$, $\alpha_6\beta_1$, $\alpha_7\beta_1$, $\alpha_9\beta_1$ (Bačáková-Řeřábková 1990, Glukhova and Koteliansky 1995, Roy *et al*. 2002, Suzuki *et al*. 2010).

In addition to proteins and glycoproteins, cells can also adhere to the growth surface through ECM molecules based mainly on saccharides, for example proteoglycans. These molecules are formed by a polypeptide chain, to which glycosaminoglycans (i.e., polysaccharides containing glucosamin) are bound. Polysaccharide chains are hydrophilic and bind a relatively high amount of water, i.e., they form gels (Nečas *et al*. 2000). A cell binds proteoglycans through non-integrin adhesion receptors, which also are saccharide-based molecules (for a review, see Bačáková *et al.* 2004, Bačáková and Švorčík 2008).

Mechanism of ECM-material and ECM-cell binding

Binding between cells and ECM molecules through adhesion receptors, especially binding between protein molecules and integrins, has been intensively investigated in many studies (for a review, see Bačáková *et al.* 2004, Bačáková and Švorčík 2008). However, less is known about bonding between ECM molecules, spontaneously adsorbed on an artificial material, and the material. It is usually the result of weak chemical bonding, such as hydrogen bonds, van der Waals forces, polar or electrostatic interactions. Protein molecules are more weakly bound to the material surface with increased hydrophilicity. The hydrophilicity of the material provides flexibility of these molecules, easier remodeling and availability of specific bioactive sites (e.g., adhesion oligopeptides) in these molecules for cell adhesion

receptors. On the other hand, extremely hydrophilic surfaces inhibit stable adsorption of proteins, and thus adhesion of cells. Cell adhesion is therefore highest on moderately hydrophilic surfaces, i.e. usually surfaces with a water drop contact angle between 50-80°. Highly hydrophobic surfaces (contact angle more than 100°) adsorb ECM molecules in rigid and denaturated forms, which hamper or even disable the binding of cell adhesion receptors to the ECM molecules (for a review, see Bačáková *et al.* 2004, 2007, Bačáková and Švorčík 2008). On the other hand, when the ECM molecules were bound covalently in a controllable manner to hydrophobic surfaces, they resembled the physiological ECM and promoted cell adhesion (Brynda *et al.* 2005, Filová *et al.* 2009a).

As indicated above, the cells do not bind the entire protein or glycoprotein macromolecules, but only their specific amino acid sequences, which are typical for a specific protein or which are preferred by a certain cell type for binding. For example, typical sequences are YIGSR and IKVAV for laminin, REDV for fibronectin, DGEA for collagen, VAPG for elastin, and RGD and KQAGDV for both vitronectin and fibronectin sequences (for a review, see Bačáková *et al.* 2004, Bačáková and Švorčík 2008).

Concerning the amino acid sequences preferred by certain cell types, KQAGDV and VAPG sequences are preferred for adhesion by vascular smooth muscle cells, REDV by endothelial cells, KRSR are bound by osteoblasts, and YIGSR and IKVAV by nerve cells. Sequences like RGD or DGEA have no significant preference for specific cell types (Nečas *et al.* 2000, Bačáková *et al.* 2003, 2004, 2007, Bačáková and Švorčík 2008).

Cells bind the amino acid sequences of adsorbed proteins with adhesion receptors located on the cell membrane. The most intensively investigated and systematized type of adhesion receptors are integrins. Integrins are heterodimeric transmembrane glycoproteins with binding sites for ECM molecules located on their extracellular part. The intracellular part of integrins is associated with several structural and signaling proteins, such as paxillin, talin, vinculin and focal adhesion kinase. These proteins further communicate with the actin cytoskeleton, which crosses the entire cell and is also connected to the nuclear membrane. The sub-membrane actin cytoskeleton is thus structurally associated with the exoskeleton (in our case represented by the ECM-material complex), through integrins. This feature has been referred to as the transmembrane skeleton. This skeleton limits the fluidity of the proteins, determines the functional differentiation of specific parts of the cell membrane, for example establishing the apical and basal part of the membrane in epithelial cells, and thus their polarity. The transmembrane character of the cell membrane skeleton enables exogenous factors to interact with the interior of the cell, and also enables signaling in the inside-out direction. In this way, the signal provided by the artificial cell carrier can influence the gene expression and proteosynthesis in the adhering cells, and thus their behavior, such as spreading, migration, viability or death, switching between proliferation and differentiation, and also remodeling or degradation of the artificial growth support by cells (Nečas *et al.* 2000, Bačáková *et al.* 2004, 2007, Ochsenhirt 2006, Bačáková and Švorčík 2008).

Methods for studying the cell-material interaction

Conditions of cell cultivation on artificial materials

Our earlier studies focused mainly on monitoring the interaction between cells and materials *in vitro*. For this purpose, anchorage-dependent cells were used, i.e. cells whose survival and functions are dependent on specific receptor-mediated adhesion to a growth substrate. This substrate has to be stable in order to resist the tractional forces produced by the actin cytoskeleton during cell spreading. If the material is too weak, it does not allow the assembly of the actin cytoskeleton and focal adhesions, i.e. domains on the cell membrane where integrins cluster together and communicate with structural and signal proteins of the cell membrane and cytoplasm, such as paxillin, talin, vinculin, focal adhesion kinase and the actin cytoskeleton. The creation, maturation and function of focal adhesions is necessary for future viability, division and phenotypic maturation of all types of anchorage-dependent cells. In other words, not only wettability or surface topography, i.e. commonly studied properties of a material, but also its mechanical properties play a decisive role in the cell-material interaction (Engler *et al.* 2004, Bačáková *et al.* 2004, Zaidel-Bar *et al.* 2007, Bačáková and Švorčík 2008).

The classical static cell culture system has usually been applied for studying cell-material interaction *in vitro*. In this system, the material samples, usually of planar "two-dimensional" character, are inserted into

plastic culture dishes, seeded with cells, immersed in a culture medium and incubated at 37 °C in a humidified air atmosphere with 5 % CO_2. For standard cultivation of cells, the medium is supplemented with 5-20 % blood serum (usually fetal bovine serum), which contains growth factors (e.g., platelet-derived growth factor), proteins mediating cell adhesion (vitronectin, fibronectin) and also albumin, which is non-adhesive for cells. In special cases, a serum-free medium can be used, for example a medium supplemented with essential growth factors, hormones etc., in order to evaluate the ability of the cells to bind the material without the cell adhesion-mediating proteins adsorbed from the serum. This approach is used particularly when the material surface is functionalized with oligopeptidic and other ligands for cell adhesion receptors (Bačáková *et al.* 2007). Another important application of serum-free media is for inducing cell differentiation, particularly VSMC. For example, differentiation of VSMCs can be induced using SMC D-STIM™ Differentiation Medium, supplemented with insulin, transferrin, selenous acid, linoleic acid and bovine serum albumin. This medium is optimized for use with BD BioCoat™ Growth Factor Reduced Matrigel (BD Biosciences), i.e. a mixture of ECM molecules imitating the basal lamina and containing predominantly laminin (www.bdbiosciences.com).

Disadvantages of the static cultivation system are a relatively low level of oxygen and nutrition delivery to the cells and slow waste removal, which has a negative influence especially on cells colonizing the inside of three-dimensionally constructed materials. In addition, there is usually no mechanical stimulation of the cells, which is necessary for their proper phenotypic maturation. On the other hand, the cells are less subjected to rinsing out from the material surface, and they have enough time to adhere and grow on the surface of the investigated sample. Static cultivation is often used prior to dynamic cultivation in order to achieve adhesion of cells in high initial numbers (near confluence) and through a large cell spreading area, which is desirable particularly in vascular smooth muscle cells. Numerous and large cell-cell and cell-material contacts shorten the proliferative phase and accelerate entry into the differentiation program (Bačáková *et al.* 2004, Bačáková and Švorčík 2008).

For more sophisticated studies requiring better imitation of the conditions in the living organism, the use of dynamic cultivation systems is more convenient. These systems are also more appropriate for testing and finishing new bioartificial tissue or organ replacements developed by tissue engineering methods. Dynamic perfusion systems, which enable the application of laminar shear stress and cyclic strain stress to the cell-material construct, are needed for constructing bioartificial vascular replacements. Laminar shear stress is necessary for phenotypic maturation of endothelial cells, manifested by the development of a confluent, semipermeable, non-immunogenic and non-thrombogenic endothelial cell monolayer (Wang *et al.* 2005). Strain stress is necessary for the development of contractile phenotype in VSMCs (Shimizu *et al.* 2008).

Perfusion bioreactors for the creation of bioartificial vascular grafts usually consist of a tubular cultivation chamber for inserting a tubular material construct, a reservoir of cell culture medium, a pump generating flow of the medium and pulsation in a controllable manner, and tubing that enables the medium to flow through the cultivation chamber (Fig. 2A-C). Prior to exposure to the flow of the medium, the cells are seeded on the tubular construct fixed in the tube chamber slowly rotating along its long axis (about 3-5 rounds per hour). The perfusion system can also be adapted for porous sponge-like or fibrous 3D scaffolds (e.g., for bone tissue engineering) by changing the tubular cultivation chamber for a perfusion chamber (Fig. 2 D, E). Perfusion of 3D cell-material constructs with the culture medium can be also achieved in a bioreactor with a rotating cultivation chamber (Fig. 2F). These systems ensure better accessibility of fresh culture medium to the cells, waste removal and appropriate mechanical stimulation of the cells. Some systems also enable continuous saturation of the culture medium with oxygen. Dynamic cultivation systems accelerate cell differentiation, phenotypic maturation and induce cell functions typical for a certain cell type (Bačáková and Švorčík 2008).

Cell types used for studying cell-material interaction

Testing the biocompatibility and bioactivity of an artificial material usually starts with the use of commercially available cell lines. These cells provide relatively well-growing and easily cultivable cell populations (for example, the life expectancy can reach several tens or even hundreds of population doublings). These cell populations are relatively homogeneous, with stable phenotypic characteristics, and are able to give reproducible results. Despite long-term cultivation and repeated passaging, many cell lines retained important markers of a given cell phenotype. For example, the

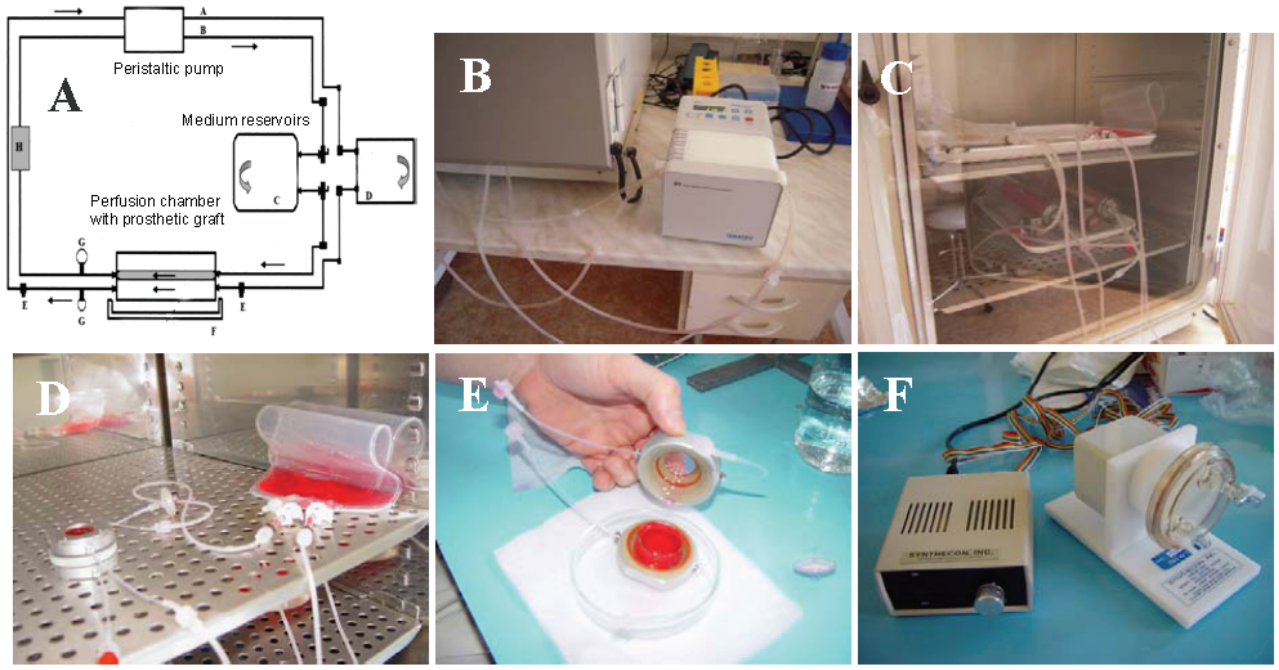

Fig. 2. **A-E**: Dynamic perfusion cell culture system (Provitro GmbH, Berlin, Germany). **A**: Scheme of the system with a peristaltic pump (above), medium reservoirs (centre) and a perfusion chamber with a prosthetic graft (below). **B**: Peristaltic pump with silicon tubing conducting the culture medium into a cell incubator. **C**: The interior of the cell incubator with medium reservoirs (upper shelf) and perfusion chambers with endothelializing vascular prostheses (lower shelf). **D, E**: Perfusion chamber for 3D porous or fibrous scaffolds. **F**: Dynamic rotary cell culture system (Cellon, Synthecon, Luxembourg).

VSMC line A7r5 derived from rat aorta (ATCC CRL-1444, Rockville, MD, U.S.A.), used in our earlier study for an investigation of the effects of material compliance on cell adhesion and spreading (Engler *et al.* 2004), retained the main VSMC differentiation markers, such as SM-alpha actin, SM-calponin and SM-myosins (Graves and Yablonka-Reuveni 2000). Bovine pulmonary artery endothelial cells of the line CPAE, used in our earlier studies on ion-implanted polymers, micropatterned surfaces created by plasma polymerization of acrylic acid and octadiene and fibrin nanostructures for potential construction of a bioarteficial vascular wall, maintain a "cobblestone-like" morphology of the cells and can form a semipermeable confluent monolayer expressing the von Willebrand factor (vWf) and angiotensin-converting enzyme, characteristic for normal endothelium *in situ* (Bačáková *et al*. 2000b, Filová *et al.* 2009a,c). Lines established from human umbilical vein endothelial cells (HUVEC) provide a good model of physiological endothelial cells. For example, the line HUVEC-CS (ATCC CRL-2873) exhibits positive acetylated low-density lipoprotein (AcLDL) uptake and expresses endothelial nitric oxide synthase (eNOS), platelet-endothelial cell adhesion molecule-1 (PECAM-1, also known as CD 31) and VE-cadherin (CD144), which, in addition to vWf, are classical markers of endothelial cell phenotype). Moreover, HUVEC-CS cells spontaneously form capillary-like structures when grown on Matrigel. Receptors for angiotensin II (AII), bradykinin and ATP were also detected on these cells (Gifford *et al*. 2004). However, commercially available frozen lots of HUVEC-CS cells have a relatively low doubling potential - from 5 to 8 population doubling times only. Therefore, in order to establish permanent and immortalized HUVEC cells, these cells were fused with A549 cells derived from a human lung carcinoma, and formed hybrid cells referred to as EA.hy 926 cells. These cells express at least one highly differentiated function of vascular endothelium, i.e. factor VIII-related antigen, which has been maintained in these cells for more than 100 cumulative population doublings, including more than 50 passages and three cloning steps (Edgell *et al.* 1983). These cells were used in our earlier studies performed on PTFE irradiated with UV light continuously or in the form of microdomains (Heitz *et al*. 2003, Mikulíková *et al.* 2005).

After screening materials using cell lines, it is necessary to verify the results on primary or low-passaged cells. These cells keep their characteristic phenotype features better than commercially available lines, e.g., they contain higher concentrations of markers

specific for or typical for a given cell type, such as alpha-actin for VSMC, vWf for endothelial cells or osteocalcin for osteoblasts (Bačáková *et al.* 2000a,b, Ding *et al.* 2006). In addition, they are more sensitive to the physical and chemical properties of the material, and thus the differences between individual tested materials are more visible. In our studies, we have often used smooth muscle cells isolated by the explantation method from the complex of the *tunica intima* and *media* of the thoracic aorta of young adult Wistar rats (Bačáková *et al*. 1997, 1999, 2000a, 2001a, 2002, 2003, 2007, Pařízek *et al*. 2009).

The highest level of material testing *in vitro* is achieved with the use of primocultures and low-passaged cells isolated from human patient tissues, isolated during surgery or in biopsies, but this requires ethical approval. An alternative and less complicated way is to use commercially available primocultured and low-passaged human cells purchased from specialized companies. However, these cells are expensive, available in limited quantities, of relatively short durability, and require specific cultivation conditions. Primocultured and low-passaged human cells are therefore used mainly for verification of selected promising results and for their further development.

Progenitor and stem cells are another important and advanced cell source for testing the cell-material interaction and for constructing bioartificial blood vessels. The most commonly used are mesenchymal stem cells (MSC) derived from the bone marrow (Suzuki *et al*. 2010), e.g. bioptically from the *crista ossis ilii*. However, MSCs have proved to be less suitable for vascular tissue engineering due to their high tendency to calcification. Alternative sources of progenitor cells are human umbilical cord cells, endothelial- and VSMC-progenitor cells from peripheral blood, adipose-derived stem cells, skeletal muscle satellite cells or amniotic fluid-derived cells (for a review, see Filová *et al.* 2009b,c).

Methods for evaluating the cell-material interaction in vitro

It is advantageous to start investigating cell-material interactions with simple, standardized and reproducible tests, which are applicable for various types of material and cells. For the first tests, two-dimensional material samples of a defined size are inserted into culture dishes, usually in multiwell plates, which enable simultaneous testing of several experimental groups of samples in multiplicates. The samples are then seeded with an appropriate concentration of cells, and the changes in cell numbers in several time intervals are observed (Bačáková *et al*. 2000a,b, 2001a, Pařízek *et al.* 2009). In our earlier studies, counting cells on days 1, 3, 5 and 7 after seeding proved to be advantageous and satisfactory for constructing growth curves with three typical phases of cell growth. These phases are (1) the lag phase, when the cells attach and spread on the tested surface, and their number does not change or even decreases slightly, (2) the exponential phase, when the cells divide and more or less increase their number, and (3) the stationary phase, when the cells reach confluence, their growth is inhibited by the cell-cell and cell-material contacts, and their number does not change or decreases due to death or spontaneous detachment of living cells from the material. For cell cultivation, a period not longer than 7 days is recommended, because longer periods usually require the culture medium to be changed, and this influences the course and shape of the growth curves. In addition to cell numbers, another important criterion for evaluating the "suitability" of a material for cell growth is the cell adhesion area, i.e. the cell area projected on the material. This area is usually measured one day after seeding, i.e. when the population density is relatively low, and thus the cell spreading is minimally influenced by contacts between cells and depends more on the material properties (Engler *et al*. 2004, Pařízek *et al*. 2009, Bačáková and Švorčík 2008). The cells on the materials can be counted either directly under a microscope or after they have been detached with the use of proteolytic enzymes or calcium chelators, e.g. trypsin combined with EDTA. Native living cells can be evaluated on transparent materials, while cells on less transparent or non-transparent materials are usually studied by fluorescence methods, e. g. after staining with fluorescent dyes, such as Texas Red C_2-Maleimide, which conjugates with proteins of the cell membrane and cytoplasm, and Hoechst #33342, which visualizes the cell nucleus (Kasálková *et al*. 2008, 2010, Pařízek *et al*. 2009, Švorčík *et al.* 2009). It is advantageous to count the trypsinized cells at later time intervals (i.e., day 5 or 7), when the cells usually reach high population densities, overlap each other and grow in several layers (this behavior is typical for VSMCs, which form so-called "hills and valleys"). Trypsinized cells in suspension can be counted manually in a haemocytometer, e.g. a Bürker chamber, or automatically in a cell counter, e.g. a Vi-CELL XR Analyzer (Beckman Coulter). This apparatus enables not only simple cell counting but also an

evaluation of the diameter and the viability of the cells, using the trypan blue-exclusion test. The cell numbers are then used not only for constructing growth curves, but also for calculating the cell population doubling time (Bačáková *et al*. 1997, 1999, 2000a,b, 2001a, 2002, Suzuki *et al*. 2010).

More advanced tests of cell-material interaction include investigations of markers of the adhesion, growth and phenotypic maturation of cells on a molecular level, i.e. on a protein or mRNA level. For protein studies, a wide range of immunocytochemical and biochemical methods can be applied, such as immunofluorescence and immunoperoxidase staining, protein electrophoresis, immunoblotting and enzyme-linked immunosorbent assay (ELISA). For mRNA studies, an advantageous technique is real-time polymerase chain reaction (real time-PCR; Kato *et al.* 1998, Ding *et al*. 2006, Nayab *et al.* 2007, Suzuki *et al*. 2010).

Molecular markers of cell adhesion include the presence, distribution, concentration and activation of various types of adhesion receptors, especially integrins, their clustering into focal adhesion plaques, their association with structural and signaling molecules, such as paxillin, talin, vinculin, focal adhesion kinase, and the assembly of an actin cytoskeleton (Bačáková *et al.* 2002, 2004, 2007, Bačáková and Švorčík 2008, Pařízek *et al*. 2009).

Molecular criteria for evaluating the proliferation activity of cells, often used in our studies, are the incorporation of bromodeoxyuridine into newly synthesized DNA, showing the S-phase fraction, i.e., the percentage of cells actually synthesizing DNA (Bačáková *et al.* 2001a), and the presence of the Ki-67 antigen (revealing the Growth Fraction, i.e., the percentage of cells capable of entering the mitotic cycle). The cell hypertrophy can be evaluated by measuring the cell volume and the total protein content, i.e., parameters which often increase with increasing cell spreading (Bačáková *et al.* 2000a, 2001b). VSMCs are prone to a specific type of hypertrophy, characterized by polyploidia, which can be revealed by counting chromosomes after arresting the cells in the metaphase, or by studies on DNA content performed by flow cytometry (Bačáková *et al.* 2000a, 2001b).

Other important indicators of the proper behavior of cells on artificial scaffolds are the presence and high concentration of molecules associated with cell differentiation and phenotypic maturation. In VSMCs, these markers are represented by contractile proteins alpha-actin and SM1 and SM2 isoforms of myosin, a protein of intermediate filaments desmin, muscle type of tropomyosin, T-troponin, h-caldesmon, h1-calponin and meta-vinculin (Brinck *et al.* 1997, Girjes *et al.* 2002, Hai and Gu 2006, Suzuki *et al*. 2010). Similarly as for molecules involved in cell adhesion, also for these proteins we evaluate their organization into specific structures, for example the formation of alpha-actin-containing filaments and filament bundles, and the concentration of alpha-actin per mg of protein or per cell in cell homogenates, usually by the ELISA method (Bačáková *et al*. 2000a,b, 2002, Filová 2009a,c, Pařízek *et al*. 2009).

Other important markers of cell behaviour on artificial materials are markers of cell viability and death, DNA damage, stress adaptation and immune activation. Markers of cell viability include the activity of mitochondrial enzymes, assessed by MTT, XTT and other related tests (Bačáková *et al*. 2002, Grausová *et al*. 2009), and also the activity of esterases, detected by commercially available kits (e.g. the LIVE/DEAD viability/cytotoxicity kit, Molecular Probes, Invitrogen; Grausová *et al*. 2009). For detecting dead cells, assays based on membrane permeability for nuclear dyes, such as ethifium homodimer-1, propidium iodide, Hoechst #33258 and #33342, and trypan blue can be used (Grausová *et al*. 2009). As a marker of DNA damage response, gamma-H2AX, i.e., a member of the histone H2A family H2AX phosphorylated at Ser139, can be detected by phosphospecific antibodies. The phosphorylation of H2AX is triggered by the formation of nuclear double-strand breaks, and this is the first step in recruiting and localizing DNA repair proteins, such as p53 binding protein 1 (53BP1) (Schultz *et al.* 2000). Heat shock proteins (HSP), such as HSP 60, 70 and 90, can be used as markers of cellular adaptation to stress, (Amberger *et al*. 1997, Kato *et al.* 1998). Long-term tolerance of the material by cells can be assessed by cultivating cells on these materials for a period of several months (Bačáková *et al.* 2000a).

Potential immune activation of cells in cultures on the tested materials can be estimated by the increased concentration of immunoglobulin and selectin adhesion molecules (ICAM-1, VCAM-1, ELAM-1), which bind cells of the immune system (Bačáková *et al*. 2000a,b, 2002). Other markers are activation of the production of interleukins (IL) and tumor necrosis factors (TNF), e.g., IL-1, IL-8 and TNF-alpha (Pešáková *et al*. 2007).

Conclusions

Vascular smooth muscle cells play important roles in the physiological function of blood vessels, and also in their remodeling under pathological conditions. Nevertheless, our earlier studies showed that these cells are also a convenient model for testing materials for potential construction of bioartificial vascular replacements by tissue engineering methods. The adhesion, migration, proliferation and differentiation abilities of these cells are important factors in the search for optimal materials and modifications to them that will applicable in clinical practice. Materials for vascular replacements of a new generation should be biomimetic, i.e. actively controlling the adhesion, growth and phenotypic maturation of vascular cells, and should serve as structures promoting the regeneration of vascular tissue. For this purpose, it is necessary to investigate the physical, chemical and biological properties and modifications of materials that are promising for the construction of bioartificial vascular replacements, and to understand the molecular mechanism of the cell-material interaction. One of the most important conclusions of this review is that besides endothelial cells, used earlier for lining the luminal surface of synthetic vascular grafts, VSMCs should become an essential part of bioartificial vascular replacements. The maturation of VSMCs into contractile phenotype can be further helped by exposure of the cell-material construct to dynamic cultivation, and by appropriate composition of the cell culture medium.

Conflict of Interest

There is no conflict of interest.

Acknowledgements

This study was supported by the Grant Agency of the Czech Republic (grants No. 305/08/0108 and P108/10/1106) and the Academy of Sciences of the Czech Republic (grant No. KAN400480701). Mr. Robin Healey (Czech Technical University, Prague) is gratefully acknowledged for his language revision of the manuscript.

References

ABRAHAM LC, ZUENA E, PEREZ-RAMIREZ B, KAPLAN DL: Guide to collagen characterization for biomaterial studies. *J Biomed Mater Res B Appl Biomater* **87**: 264-285, 2008.

AMBERGER A, MACZEK C, JURGENS G, MICHAELIS D, SCHETT G, TRIEB K, EBERL T, JINDAL S, XU QB, WICK G: Co-expression of ICAM-1, VCAM-1, ELAM-1 and Hsp60 in human arterial and venous endothelial cells in response to cytokines and oxidized low-density lipoproteins. *Cell Stress Chaperon* **2**: 94-103, 1997.

BAČÁKOVÁ-ŘEŘÁBKOVÁ L: Importance of cultivation of smooth muscle cells for understanding of the physiology and pathophysiology of the vascular wall. (in Czech) *Cs fyziol* **39**: 412-427, 1990.

BAČÁKOVÁ L, ŠVORČÍK V, RYBKA V, MÍČEK I, HNATOWICZ V, LISÁ V, KOCOUREK F: Adhesion and proliferation of cultured human vascular smooth muscle cells on polystyrene implanted with N^+, F^+ and Ar^+ ions. *Biomaterials* **17**: 1121-1126, 1996.

BAČÁKOVÁ L, WILHELM J, HERGET J, NOVOTNÁ J, ECKHARDT A: Oxidized collagen stimulates proliferation of vascular smooth muscle cells. *Exp Mol Pathol* **64**: 185-194, 1997.

BAČÁKOVÁ L, WILHELM J, HERGET J, NOVOTNÁ J: Influence of macrophages and macrophage-modified collagen I on the adhesion and proliferation of vascular smooth muscle cells in culture. *Physiol Res* **48**: 341-351, 1999.

BAČÁKOVÁ L, MAREŠ V, BOTTONE MG, PELLICCIARI C, LISÁ V, ŠVORČÍK V: Fluorine ion-implanted polystyrene improves growth and viability of vascular smooth muscle cells in culture. *J Biomed Mater Res* **49**: 369-379, 2000a.

BAČÁKOVÁ L, MAREŠ V, LISÁ V, ŠVORČÍK V: Molecular mechanisms of improved adhesion and growth of an endothelial cell line cultured on polystyrene implanted with fluorine ions. *Biomaterials* **21**: 1173-1179, 2000b.

BAČÁKOVÁ L, WALACHOVÁ K, ŠVORČÍK V, HNATOWICZ V: Adhesion and proliferation of rat vascular smooth muscle cells on polyethylene implanted with O^+ and C^+ ions. *J Biomater Sci – Polym Ed* **12**: 817-834, 2001a.

BAČÁKOVÁ L, PELLICCIARI C, BOTTONE MG, LISÁ V, MAREŠ V: A sex-related difference in the hypertrophic *versus* hyperplastic response of vascular smooth muscle cells to repeated passaging in culture. *Histol Histopathol* **16**: 675-684, 2001b.

BAČÁKOVÁ L, LISÁ V, KUBÍNOVÁ L, WILHELM J, NOVOTNÁ J, ECKHARDT A, HERGET J: Ultraviolet light-irradiated collagen III modulates expression of cytoskeletal and surface adhesion molecules in rat aortic smooth muscle cells *in vitro*. *Virchows Arch* **440**: 50-62, 2002.

BAČÁKOVÁ L, LAPČÍKOVÁ M, KUBIES D, RYPÁČEK F: Adhesion and growth of rat aortic smooth muscle cells on lactide-based polymers. *Adv Exp Med Biol* **534**: 179-189, 2003.

BAČÁKOVÁ L, FILOVÁ E, RYPÁČEK F, ŠVORČÍK V, STARÝ V: Cell adhesion on artificial materials for tissue engineering. *Physiol Res* **53** (Suppl 1): S35-S45, 2004.

BAČÁKOVÁ L, FILOVÁ E, KUBIES D, MACHOVÁ L, PROKŠ V, MALINOVÁ V, LISÁ V, RYPÁČEK F: Adhesion and growth of vascular smooth muscle cells in cultures on bioactive RGD peptide-carrying polylactides. *J Mater Sci Mater Med* **18**: 1317-1323, 2007.

BAČÁKOVÁ L, ŠVORČÍK V: Cell colonization control by physical and chemical modification of materials. In: *Cell Growth Processes: New Research.* D KIMURA (ed), Nova Science Publishers, Inc., Hauppauge, NY, USA, 2008, pp 5-56.

BAČÁKOVÁ L, FILOVÁ E, GRAUSOVÁ L, VANDROVCOVÁ M, PAŘÍZEK M, NOVOTNÁ K, ŠVORČÍK V, VACÍK J, RYPÁČEK F, KROMKA A, HEITZ J, SHARD A: Micro- and nanopatterned surfaces for guided adhesion, growth and phenotypic maturation of cells. *Engineering of Biomaterials* **89-91**: 18-21, 2009.

BANDIERA A, TAGLIENTI A, MICALI F, PANI B, TAMARO M, CRESCENZI V, MANZINI G: Expression and characterization of human-elastin-repeat-based temperature-responsive protein polymers for biotechnological purposes. *Biotechnol Appl Biochem* **42**: 247-256, 2005.

BARNES JL, TORRES ES, MITCHELL RJ, PETERS JH: Expression of alternatively spliced fibronectin variants during remodeling in proliferative glomerulonephritis. *Am J Pathol* **147**: 1361-1371, 1995.

BETTINGER CJ, BRUGGEMAN JP, MISRA A, BORENSTEIN JT, LANGER R: Biocompatibility of biodegradable semiconducting melanin films for nerve tissue engineering. *Biomaterials* **30**: 3050-3057, 2009.

BRINCK U, MIRZAIE M, KORABIOWSKA M, MEYER T: Expression rate of vinculin isoforms in human aortocoronary saphenous vein grafts. Since the cytoskeletal protein meta-vinculin is present exclusively in contractile smooth muscle cells 1. *Int J Cardiol* **59**: 125-132, 1997.

BRYNDA E, PACHERNÍK J, HOUSKA M, PIENTKA Z, DVOŘÁK P: Surface immobilized protein multilayers for cell seeding. *Langmuir* **21**: 7877-7883, 2005.

CAMPBELL GR, CAMPBELL JH: Development of the vessel wall: overview. In: *The Vascular Smooth Muscle Cell. Molecular and Biological Response to the Extracelular Matrix*. SCHWARTZ SM, MECHAM RP (eds), Academic Press, San Diego, London, 1995, pp 1-15.

CHIANG HY, KORSHUNOV VA, SEROUR A, SHI F, SOTTILE J: Fibronectin is an important regulator of flow-induced vascular remodeling. *Arterioscler Thromb Vasc Biol* **29**: 1074-1079, 2009.

CHLUPÁČ J, FILOVÁ E, RIEDEL T, BRYNDA E, REMY-ZOLGHADRI M, BAREILLE R, FERNANDEZ P, DACULSI R, BORDENAVE L, BAČÁKOVÁ L: Human endothelium on vascular prostheses modified by extracellular matrix proteins in a flow experiment. *Engineering of Biomaterials* **58-60**: 10-13, 2006.

CHLUPÁČ J, FILOVÁ E, RIEDEL T, BRYNDA E, PAMULA E, LISÁ V, BAČÁKOVÁ L: Endothelial cells on PET vascular prostheses impregnated with polyester-based copolymers and coated with cell-adhesive protein assemblies. *Engineering of Biomaterials* **81-84**: 108-111, 2008.

CHLUPÁČ J, FILOVÁ E, BAČÁKOVÁ L: Blood vessel replacement: 50 years of development and tissue engineering paradigms in vascular surgery. *Physiol Res* **58** (Suppl 2): S119-S139, 2009.

COSTA-SILVA B, DA COSTA MC, MELO FR, NEVES CM, ALVAREZ-SILVA M, CALLONI GW, TRENTIN AG: Fibronectin promotes differentiation of neural crest progenitors endowed with smooth muscle cell potential. *Exp Cell Res* **315**: 955-967, 2009.

CULLIS CF, HIRSCHLER MM: The significance of thermoanalytical measurements in the assessment of polymer flammability. *Polymer* **24**: 834-840, 1983.

DING HT, WANG CG, ZHANG TL, WANG K: Fibronectin enhances in vitro vascular calcification by promoting osteoblastic differentiation of vascular smooth muscle cells via ERK pathway. *J Cell Biochem* **99**: 1343-1352, 2006.

DUFOURCQ P, COUFFINHAL T, ALZIEU P, DARET D, MOREAU C, DUPLÀA C, BONNET J: Vitronectin is up-regulated after vascular injury and vitronectin blockade prevents neointima formation. *Cardiovasc Res* **53**: 952-962, 2002.

DUCHÁČEK V: *Polymers – Production, Properties, Processing, Application*. (in Czech) ICH, Prague, 2006.

EDGELL CJ, MCDONALD CC, GRAHAM JB: Permanent cell line expressing human factor VIII-related antigen established by hybridization. *Proc Natl Acad Sci USA* **80**: 3734-3737, 1983.

ENGLER A, BAČÁKOVÁ L, NEWMAN C, HATEGAN A, GRIFFIN M, DISCHER D: Substrate compliance versus ligand density in cell on gel responses. *Biophys J* **86**: 617-628, 2004.

FAGER G, HANSSON GK, GOWN AM, LARSON DM, SKALLI O, BONDJERS G: Human arterial smooth muscle cells in culture: inverse relationship between proliferation and expression of contractile proteins. *In Vitro Cell Dev Biol* **25**: 511-520, 1989.

FILOVÁ E, BRYNDA E, RIEDEL T, BAČÁKOVÁ L, CHLUPÁČ J, LISÁ V, HOUSKA M, DYR JE: Vascular endothelial cells on two- and three-dimensional fibrin assemblies for biomaterial coatings. *J Biomed Mater Res A* **90**: 55-69, 2009a.

FILOVÁ E, STRAKA F, MIŘEJOVSKÝ T, MAŠÍN J, BAČÁKOVÁ L: Tissue-engineered heart valves. *Physiol Res* **58** (Suppl 2): S141-S158, 2009b.

FILOVÁ E, BULLETT NA, BAČÁKOVÁ L, GRAUSOVÁ L, HAYCOCK JW, HLUČILOVÁ J, KLÍMA J, SHARD A: Regionally-selective cell colonization of micropatterned surfaces prepared by plasma polymerisation of acrylic acid and 1,7- octadiene. *Physiol Res* **58**: 669-684, 2009c.

FINK D (ed): *Fundamentals of Ion-Irradiated Polymers.* Springer Series in Materials Science **vol. 63**: 2004.

GIFFORD SM, GRUMMER MA, PIERRE SA, AUSTIN JL, ZHENG J, BIRD IM: Functional characterization of HUVEC-CS: Ca^{2+} signaling, ERK 1/2 activation, mitogenesis and vasodilator production. *J Endocrinol* **182**: 485-499, 2004.

GIRJES AA, KERIAKOUS D, COCKERILL GW, HAYWARD IP, CAMPBELL GR, CAMPBELL JH: Cloning of a differentially expressed tropomyosin isoform from cultured rabbit aortic smooth muscle cells. *Int J Biochem Cell Biol* **34**: 505-515, 2002.

GLUKHOVA MA, KOTELIANSKY VE: Integrins, cytoskeletal and extracellular matrix proteins in developing smooth muscle cells of human aorta. In: *The Vascular Smooth Muscle Cell. Molecular and Biological Response to the Extracelular Matrix*. SCHWARTZ SM, MECHAM RP (eds), Academic Press, San Diego, London, 1995, pp 37-79.

GOBIN AS, WEST JL: Val-ala-pro-gly, an elastin-derived non-integrin ligand: smooth muscle cell adhesion and specificity. *J Biomed Mater Res A* **67**: 255-259, 2003.

GRAUSOVÁ L, BAČÁKOVÁ L, KROMKA A, POTOCKÝ Š, VANĚČEK M, NESLÁDEK M, LISÁ V: Nanodiamond as a promising material for bone tissue engineering. *J Nanosci Nanotechnol* **9**: 3524-3534, 2009.

GRAVES DC, YABLONKA-REUVENI Z: Vascular smooth muscle cells spontaneously adopt a skeletal muscle phenotype: a unique Myf5(-)/MyoD(+) myogenic program. *J Histochem Cytochem* **48**: 1173-1193, 2000.

GREISLER HP, TATTERSALL CW, KLOSAK JJ, CABUSAO EA, GARFIELD JD, KIM DU: Partially bioresorbable vascular grafts in dogs. *Surgery* **110**: 645-654, 1991.

GUIDOIN R, MAUREL S, CHAKFÉ N, HOW T, ZHANG Z, THERRIEN M, FORMICHI M, GOSSELIN C: Expanded polytetrafluoroethylene arterial prostheses in humans: chemical analysis of 79 explanted specimens. *Biomaterials* **14**: 694-704, 1993.

HAI CM, GU Z: Caldesmon phosphorylation in actin cytoskeletal remodeling. *Eur J Cell Biol* **85**: 305-309, 2006.

HAMEED T, HUSSEIN IA: Effect of short chain branching of LDPE on its miscibility with linear HDPE. *Macromol Mater Eng* **289**: 198-203, 2004.

HEDIN U, THYBERG J: Plasma fibronectin promotes modulation of arterial smooth-muscle cells from contractile to synthetic phenotype. *Differentiation* **33**: 239-246, 1987.

HEITZ J, ŠVORČÍK V, BAČÁKOVÁ L, ROCKOVÁ K, RATAJOVÁ E, GUMPENBERGER T, BAUERLE D, DVOŘÁNKOVÁ B, KAHR H, GRAZ I, ROMANIN C: Cell adhesion on polytetrafluoroethylene modified by UV-irradiation in an ammonia atmosphere. *J Biomed Mater Res A* **67**: 130-137, 2003.

JEONG SI, JUN ID, CHOI MJ, NHO YC, LEE YM, SHIN H: Development of electroactive and elastic nanofibers that contain polyaniline and poly(L-lactide-co-epsilon-caprolactone) for the control of cell adhesion. *Macromol Biosci* **7/8**: 627-637, 2008.

KAKISIS JD, LIAPIS CD, BREUER C, SUMPIO BE: Links artificial blood vessel: the Holy Grail of peripheral vascular surgery. *Vasc Surg* **41**: 349-354, 2005.

KARNIK SK, BROOKE BS, BAYES-GENIS A, SORENSEN L, WYTHE JD, SCHWARTZ RS, KEATING MT, LI DY: A critical role for elastin signaling in vascular morphogenesis and disease. *Development* **130**: 411-423, 2003.

KASÁLKOVÁ N, KOLÁŘOVÁ K, BAČÁKOVÁ L, PAŘÍZEK M, ŠVORČÍK V: Cell adhesion and proliferation on modified PE. *Mater Sci Forum* **567-568**: 269-272, 2008.

KASÁLKOVÁ N, MAKAJOVÁ Z, PAŘÍZEK M, SLEPIČKA P, KOLÁŘOVÁ K, BAČÁKOVÁ L, HNATOWICZ V, ŠVORČÍK V: Cell adhesion and proliferation on plasma-treated and poly(ethylene glycol)-grafted polyethylene. *J Adhes Sci Technol* **24**: 743-754, 2010.

KATO S, AKAGI T, SUGIMURA K, KISHIDA A, AKASHI M: Evaluation of biological responses to polymeric biomaterials by RT-PCR analysis III: study of HSP 70, 90 and 47 mRNA expression. *Biomaterials* **19**: 821-827, 1998.

KUBOVÁ O, ŠVORČÍK V, HEITZ J, MORITZ S, ROMANIN C, MATĚJKA P, MACKOVÁ A: Characterization and cytocompatibility of carbon layers prepared by photo-induced chemical vapor deposition. *Thin Solid Films* **515**: 6765-6772, 2007.

LIU X, LIM JY, DONAHUE HJ, DHURJATI R, MASTRO AM, VOGLER EA: Influence of substratum surface chemistry/energy and topography on the human fetal osteoblastic cell line hFOB 1.19: Phenotypic and genotypic responses observed *in vitro*. *Biomaterials* **28**: 4535-4550, 2007.

MACKOVÁ A, ŠVORČÍK V, STRÝHAL Z, PAVLÍK J: RBS and AFM study of Ag and Au diffusion into PET influenced by plasma treatment. *Surf Interf Anal* **38**: 335, 2006.

MAROIS Y, CHAKFÉ N, GUIDOIN R, DUHAMEL RC, ROY R, MAROIS M, KING MW, DOUVILLE Y: An albumin-coated polyester arterial graft: in vivo assessment of biocompatibility and healing characteristics. *Biomaterials* **17**: 3-14, 1996.

MAXOVÁ H, BAČÁKOVÁ L, LISÁ V, NOVOTNÁ J, TOMÁŠOVÁ H, VÍZEK M, HERGET J: Production of proteolytic enzymes in mast cells, fibroblasts, vascular smooth muscle and endothelial cells cultivated under normoxic or hypoxic conditions. *Physiol Res* **59**:711-719. 2010.

MIHARDJA SS, SIEVERS RE, LEE RJ: The effect of polypyrrole on arteriogenesis in an acute rat infarct model. *Biomaterials* **29**: 4205-4210, 2008.

MIKULÍKOVÁ R, MORITZ S, GUMPENBERGER T, OLBŘICH M, ROMANIN C, BAČÁKOVÁ L, ŠVORČÍK V, HEITZ J: Cell microarrays on photochemically modified polytetrafluoroethylene. *Biomaterials* **26/27**: 5572-5580, 2005.

MILLER DC, HABERSTROH KM, WEBSTER TJ: PLGA nanometer surface features manipulate fibronectin interactions for improved vascular cell adhesion. *J Biomed Mater Res A* **81**: 678-684, 2007.

NAYAB SN, JONES FH, OLSEN I: Effects of calcium ion-implantation of titanium on bone cell function *in vitro*. *J Biomed Mater Res A* **83**: 296-302, 2007.

NEČAS O, SVOBODA A, HEJTMÁNEK M, JANISCH R, ČERVINKA M, LENHART K, KOLÁŘ Z: *General Biology.* (in Czech) H & H, Prague, 2000, pp 257-261 and 276-278.

OCHSENHIRT SE, KOKKOLI E, MCCARTHY JB, TIRRELL M: Effect of RGD secondary structure and the synergy site PHSRN on cell adhesion, spreading and specific integrin engagement. *Biomaterials* **27**: 3863-3874, 2006.

ORR AW, HASTINGS NE, BLACKMAN BR, WAMHOFF BR: Complex regulation and function of the inflammatory smooth muscle cell phenotype in atherosclerosis. *J Vasc Res* **47**: 168-180, 2009.

PAŘÍZEK M, KASÁLKOVÁ N, BAČÁKOVÁ L, SLEPIČKA P, LISÁ V, BLAŽKOVÁ M, ŠVORČÍK V: Improved adhesion, growth and maturation of vascular smooth muscle cells on polyethylene grafted with bioactive molecules and carbon particles. *Int J Mol Sci* **10**: 4352-4374, 2009.

PEŠÁKOVÁ V, KUBIES D, HULEJOVÁ H, HIMMLOVÁ L: The influence of implant surface properties on cell adhesion and proliferation. *J Mater Sci Mater Med* **18**: 465-473, 2007.

ROHATGI A, OWENS AW, KHERA A, AYERS CR, BANKS K, DAS SR, BERRY JD, MCGUIRE DK, DE LEMOS JA: Differential associations between soluble cellular adhesion molecules and atherosclerosis in the Dallas Heart Study: a distinct role for soluble endothelial cell-selective adhesion molecule. *Arterioscler Thromb Vasc Biol* **29**: 1684-1690, 2009.

ROY J, TRAN PK, RELIGA P, KAZI M, HENDERSON B, LUNDMARK K, HEDIN U: Fibronectin promotes cell cycle entry in smooth muscle cells in primary culture. *Exp Cell Res* **15**: 169-177, 2002.

SCHULTZ LB, CHEHAB NH, MALIKZAY A, HALAZONETIS TD: p53 binding protein 1 (53BP1) is an early participant in the cellular response to DNA double-strand breaks. *J Cell Biol* **151**: 1381-1390, 2000.

SHIMIZU N, YAMAMOTO K, OBI S, KUMAGAYA S, MASUMURA T, SHIMANO Y, NARUSE K, YAMASHITA JK, IGARASHI T, ANDO J: Cyclic strain induces mouse embryonic stem cell differentiation into vascular smooth muscle cells by activating PDGF receptor beta. *J Appl Physiol* **104**: 766-772, 2008.

SUZUKI S, NARITA Y, YAMAWAKI A, MURASE Y, SATAKE M, MUTSUGA M, OKAMOTO H, KAGAMI H, UEDA M, UEDA Y: Effects of extracellular matrix on differentiation of human bone marrow-derived mesenchymal stem cells into smooth muscle cell lineage: utility for cardiovascular tissue engineering. *Cells Tissues Organs* **191**: 269-280, 2010.

ŠVORČÍK V, RYBKA V, ENDRŠT R, HNATOWICZ V, KVÍTEK J: Ion implantation into polyethylene. *J Electrochem Soc* **140**: 549, 1993.

ŠVORČÍK V, RYBKA V, HNATOWICZ V, BAČÁKOVÁ L, LISÁ V, KOCOUREK F: Surface properties and biocompatibility of ion implanted polymers. *J Mater Chem* **5**: 27-30, 1995.

ŠVORČÍK V, KOLÁŘOVÁ K, SLEPIČKA P, MACKOVÁ A, NOVOTNÁ M, HNATOWICZ V: Modification of surface properties of high and low density PE by Ar plasma discharge. *Polym Degr Stab* **91**, 1219-1225, 2006.

ŠVORČÍK V, HNATOWICZ V: Properties of polymers modified by plasma discharge and ion beam, In: *Polymer Degradation and Stability Research Developments.* LB ALBERTOV (ed), Nova Science Publishers, New York, 2007, pp 171-216.

ŠVORČÍK V, KASÁLKOVÁ N, SLEPIČKA P, ZÁRUBA K, BAČÁKOVÁ L, PAŘÍZEK M, LISÁ V, RUML T, GBELCOVÁ H, RIMPELOVÁ S, MACKOVÁ A: Cytocompatibility of Ar^+ plasma-treated and Au nanoparticle-grafted PE. *Nucl Instr Meth B* **267**: 1904-1910, 2009.

VAN BILSEN PH, KRENNING G, BILLY D, DUVAL JL, HUURDEMAN-VINCENT J, VAN LUYN MJ: Heparin coating of poly(ethylene terephthalate) decreases hydrophobicity, monocyte/leukocyte interaction and tissue interaction. *Colloids Surf B Biointerfaces* **67**: 46-53, 2008.

WALACHOVÁ K, ŠVORČÍK V, BAČÁKOVÁ L, HNATOWICZ V: Smooth muscle cell interaction with modified polyethylene. *Biomaterials* **23**: 2989-2996, 2002.

WANG H, RIHA GM, YAN S, LI M, CHAI H, YANG H, YAO Q, CHEN C: Shear stress induces endothelial differentiation from a murine embryonic mesenchymal progenitor cell line. *Arterioscler Thromb Vasc Biol* **25**: 1817-1823, 2005.

XUE L, GREISLER HP: Biomaterials in the development and future of vascular grafts. *J Vasc Surg* **37**: 472-478, 2003.

YOU Q, WANG F, DUAN L, DU X, XIAO M, SHEN Z: Construction of small-caliber, polydioxanone cyclohexanone vascular stents. *Cell Biochem Biophys* **57**: 35-43, 2010.

ZAIDEL-BAR R, MILO R, KAM Z, GEIGER B: A paxillin tyrosine phosphorylation switch regulates the assembly and form of cell-matrix adhesions. *J Cell Sci* **120**: 137-148, 2007.

International Journal of Nanomedicine

Dovepress

open access to scientific and medical research

Open Access Full Text Article

ORIGINAL RESEARCH

Nanofibrous poly(lactide-co-glycolide) membranes loaded with diamond nanoparticles as promising substrates for bone tissue engineering

Martin Parizek[1]
Timothy EL Douglas[2]
Katarina Novotna[1]
Alexander Kromka[3]
Mariea A Brady[4]
Andrea Renzing[4]
Eske Voss[4]
Marketa Jarosova[3]
Lukas Palatinus[3]
Pavel Tesarek[5]
Pavla Ryparova[5]
Věra Lisa[1]
Ana M dos Santos[2]
Lucie Bacakova[1]

[1]Department of Biomaterials and Tissue Engineering, Institute of Physiology, Academy of Sciences of the Czech Republic, Prague, Czech Republic; [2]Polymer Chemistry and Biomaterials Group, Ghent University, Ghent, Belgium; [3]Institute of Physics, Academy of Sciences of the Czech Republic, Prague, Czech Republic; [4]Department of Oral and Maxillofacial Surgery, University of Kiel, Kiel, Germany; [5]Czech Technical University in Prague, Faculty of Civil Engineering, Prague, Czech Republic

Video abstract

Point your smartphone at the QR code to the left. If you have a QR code reader the video abstract will appear. Or use: http: //dvpr.es/vbovIf

Correspondence: Lucie Bacakova
Department of Biomaterials and Tissue Engineering, Institute of Physiology, Academy of Sciences of the Czech Republic, Videnska 1083, 14220 Prague 4-Krc, Czech Republic
Tel +42 02 9644 3743
Fax +42 02 9644 2488
Email lucy@biomed.cas.cz

Background: Nanofibrous scaffolds loaded with bioactive nanoparticles are promising materials for bone tissue engineering.

Methods: In this study, composite nanofibrous membranes containing a copolymer of L-lactide and glycolide (PLGA) and diamond nanoparticles were fabricated by an electrospinning technique. PLGA was dissolved in a mixture of methylene chloride and dimethyl formamide (2:3) at a concentration of 2.3 wt%, and nanodiamond (ND) powder was added at a concentration of 0.7 wt% (about 23 wt% in dry PLGA).

Results: In the composite scaffolds, the ND particles were either arranged like beads in the central part of the fibers or formed clusters protruding from the fibers. In the PLGA-ND membranes, the fibers were thicker (diameter 270 ± 9 nm) than in pure PLGA meshes (diameter 218 ± 4 nm), but the areas of pores among these fibers were smaller than in pure PLGA samples (0.46 ± 0.02 μm^2 versus 1.28 ± 0.09 μm^2 in pure PLGA samples). The PLGA-ND membranes showed higher mechanical resistance, as demonstrated by rupture tests of load and deflection of rupture probe at failure. Both types of membranes enabled the attachment, spreading, and subsequent proliferation of human osteoblast-like MG-63 cells to a similar extent, although these values were usually lower than on polystyrene dishes. Nevertheless, the cells on both types of membranes were polygonal or spindle-like in shape, and were distributed homogeneously on the samples. From days 1–7 after seeding, their number rose continuously, and at the end of the experiment, these cells were able to create a confluent layer. At the same time, the cell viability, evaluated by a LIVE/DEAD viability/cytotoxicity kit, ranged from 92% to 97% on both types of membranes. In addition, on PLGA-ND membranes, the cells formed well developed talin-containing focal adhesion plaques. As estimated by the determination of tumor necrosis factor-alpha levels in the culture medium and concentration of intercellular adhesion molecule-1, MG-63 cells, and RAW 264.7 macrophages on these membranes did not show considerable inflammatory activity.

Conclusion: This study shows that nanofibrous PLGA membranes loaded with diamond nanoparticles have interesting potential for use in bone tissue engineering.

Keywords: nanofibers, nanoparticles, electrospinning, nanotechnology, regenerative medicine, human bone cells

Introduction

Nanofibrous scaffolds have recently been recognized as promising cell carriers for advanced tissue engineering. This is mainly due to the fact that these scaffolds closely mimic the structure of the fibrous component of the native extracellular matrix formed by nano fibers of collagen, elastin and other proteins. In general, nano structured substrates are considered to be advantageous for cell adhesion and growth.

In comparison with conventionally used flat or micro structured cell growth supports, nano structured carriers improve the cell-matrix interaction, eg, by adsorption of cell adhesion-mediating molecules from biological fluids in an appropriate geometrical conformation, which enables good accessibility of specific active sites on these molecules to cell adhesion receptors.[1,2] In addition, the application of nano structured substrates can be particularly advantageous in bone tissue engineering. The reason is that from all cell adhesion-mediating molecules, these substrates preferentially adsorb vitronectin, which is recognized mainly by osteoblasts, rather than other cell types (eg, vascular endothelial and smooth muscle cells or fibroblasts).[2]

Nanofibrous scaffolds have been prepared mainly from natural or synthetic polymers, such as collagen and elastin,[3] silk fibroin,[4] chitosan,[5] peptides with ligands for cell adhesion receptors,[6] polyurethane,[7] polycaprolactone,[8] polylactide[9] and particularly its copolymers with polyglycolide.[10–15]

In our earlier studies, and also in studies by other authors, poly (lactide-co-glycolide) (PLGA) has proved to be an appropriate material for the construction of porous and fibrous scaffolds for bone tissue engineering.[16] In comparison with pure polylactic acid (PLA), the PLGA copolymer is less brittle, and in comparison with pure polyglycolide is less degradable (ie, less prone to hydrolytic degradation). Thus, PLGA provides more stable support for bone tissue regeneration, which lasts several weeks in human beings. In addition, this material has been approved by the Food and Drug Administration for medical use, including implantation into human tissues.

The main methods of nanofiber preparation are self-assembly, liquid phase separation, template synthesis, drawing, and predominantly electrospinning.[17,18] Electrospinning is a novel and effective fabrication process that uses an electric field to control the deposition of polymer fibers onto a target substrate. This electrostatic processing strategy can be used to fabricate non woven fibrous polymer meshes composed of diameters ranging from several microns down to 100 nm or less, which mimic the hierarchically organized microstructure and nanostructure of the natural tissues.[9,19]

However, the mechanical properties and bioactivity of polymer-based nanofibrous scaffolds are often unsatisfactory for tissue engineering. Some modifications of these scaffolds are therefore necessary. For example, PLA scaffolds were reinforced by copolymerization of PLA with functionalized polyaniline, which also endowed these scaffolds with electrical conductivity and antimicrobial activity.[20,21] In the case of scaffolds intended for the construction of bioartificial bone, hydroxyapatite and tricalcium phosphate have been used, because they occur in the inorganic component of the natural bone matrix. On bioactive nanofibers, these minerals can be deposited spontaneously in simulated biological fluids[22] or they can be incorporated into the nanofibers during the preparation process.[9–15] In some studies, mineral nanoparticles have been substituted by other nanosized materials, eg, by carbon nanotubes incorporated inside polylactide nanofibers.[17,23] Despite many advantageous properties of carbon nanotubes, such as excellent mechanical properties and electrical conductivity, which can enhance bone tissue regeneration, carbon nanotubes have repeatedly been shown to be associated with a risk of cytotoxicity, genotoxicity, and tumorigenicity.[24,25] Diamond nanoparticles are an alternative promising component of nanofibrous membranes. In numerous studies, they have displayed very high biocompatibility and no considerable cytotoxicity. In the form of films deposited on the biomaterial surface, nanocrystalline diamond provides excellent growth support for various cell types, particularly bone-derived cells.[26–28] In the form of dispersed nanoparticles, they have been shown not to interfere with gene expression, protein synthesis, cell cycle progression, and differentiation of cells in vitro, although they were taken up into cells via clathrin-mediated endocytosis.[29] In future uses of composite polymer-nanodiamond (ND) scaffolds in vivo, the ND particles could be cleared from the organism by glomerular filtration after degradation of the scaffolds, as is possible in the case of carbon nanotubes.[30,31]

In a recent study by Behler et al,[32] nanocrystalline diamond particles were incorporated into polyacrylonitrile or polyamide nanofibers and microfibers. However, these nanofibers were characterized only for their physical and chemical properties and were designed for use in technical applications, such as protection against ultraviolet light and improved scratch resistance of the material surfaces. In another study, diamond nanoparticles were incorporated into polymeric films, and the effects of this composite material on the growth of osteoblasts was evaluated.[33] Nevertheless, to our best knowledge, the interaction of ND-loaded nanofibers with cells and their potential use in bone tissue engineering has not yet been investigated.

In the present study, we therefore constructed nanofibrous membranes by electrospinning PLGA mixed with ND particles as potential growth supports for bone cells. We investigated the adhesion, proliferation, and viability of human osteoblast-like MG-63 cells in cultures on these materials. We expected an additional nanostructure to be created on the fiber surface by the incorporated ND, and thus further

enhancement of the scaffold bioactivity. We also anticipated enhanced mechanical properties of PLGA membranes reinforced with ND. The mechanical properties of the membranes were assessed using rupture tests[34] and tensile strength measurements.[35–37] Finally, we expected no significant inflammatory activation of cells on these scaffolds. Potential immune activation of cells was estimated by their secretion of tumor necrosis factor alpha (TNF-α) into the cell culture medium, and by the concentration of intercellular adhesion molecule-1 (ICAM-1) in cell homogenates. For these immunological tests, mouse macrophage-like RAW 264.7 cells were also used.

Materials and methods

Preparation of nanofibrous membranes

The experiments were carried out on nanofibrous membranes made of a copolymer of L-lactide and glycolide (ratio 85:15) Purasorb PLG 8531 (Purac Biomaterials, Frankfurt, Germany). The polymer was dissolved in a mixture of methylene chloride (Sigma-Aldrich, St Louis, MO) and dimethyl formamide (Sigma) at a concentration of 2.3 wt%. The ratio of the two solvents was 2:3. The nanofibrous membranes were then prepared by electrospinning in a Nanospider™ machine (Elmarco, Liberec, Czech Republic) using a vertically positioned spike-like electrode on which the polymer solution was applied with a micropipette. The electrospinning conditions were optimized prior to membrane fabrication, resulting in an applied voltage of 24.6 kV and a working distance between the electrodes of 145 mm, ie, an electric field strength of 1.79 kV/cm. The polymer solution was positioned between the two electrodes in the electrospinning setup, and when a high voltage was applied, the electric field overcame viscoelastic forces of the polymer solution and nanofibers were formed.

A polypropylene fabric, placed above the electrode, was used as a carrier substrate for collecting the nanofibers, which were stacked to several layers by repeated deposition of the PLGA solution on the same region of the substrate (a circular region approximately 10 cm in diameter). Four milliliters of the solution was used for preparing a membrane to cover this region, and this solution was applied to the top of the electrode 80 times in a quantity of 50 μL for each application.

Some nanofibrous PLGA membranes were created in combination with diamond nanoparticles.[38–41] In 1 mL of PLGA solution, 0.007 g of the ND powder was added and was homogeneously dispersed by mixing and sonication (Labsonic U-2000, B Braun Biotech, Goettingen, Germany, sonication time 5 seconds). The sonication was performed immediately before electrospinning in order to minimize clustering of diamond nanoparticles. The concentration of ND in PLGA diluted in methylene chloride and dimethyl formamide was therefore 0.7 wt%, and in the pure PLGA after evaporation of the solvents, the concentration was calculated to be almost 23 wt%.

Characterization of physicochemical properties of nanofibrous membranes

The morphology of the membranes was evaluated by scanning electron microscopy using an XL30CP device, Phillips Electron Optics GmbH, Kassel, Germany, after gold sputtering on an SCD 500 device (CAL-Tec, Ashford, UK). The following parameters were measured on scanning electron microscopy images, using Atlas Software (Tescan Ltd, Brno, Czech Republic):

- Diameter of nanofibers
- Size of pores between nanofibers; areas of void spaces among the fibers were measured on scanning electron microscopy images[23]
- Size of material clusters were measured by the area of these clusters projected on the material surface
- Density of material clusters was calculated per mm^2 of the membrane.

The distribution of diamond nanoparticles within the PLGA nanofibers was evaluated by transmission electron microscopy. The transmission electron microscopic images were recorded on a Philips CM120 microscope with an LaB_6 cathode operated at 120 kV, equipped with an SIS Veleta CCD camera. A small piece of nanofibrous membrane was placed between two carbon-coated copper grids to fix the membrane in the sample holder. Single nanofibers were observed at the edges of the membrane.

The wettability of the membranes was measured by a static method in a material-water droplet system using a reflection goniometer (Surface Energy Evaluation System, Masaryk University, Brno, Czech Republic).[28]

The mechanical properties of PLGA membranes with and without ND were evaluated by rupture tests in a texture analyzer (TA500, Lloyd Instruments, Fareham, UK) using an Instron probe method according to a protocol adapted from that of dos Santos et al.[34] Briefly, the membranes were clamped in a CellCrown (Scaffdex Oy, Tampere, Finland) of 10 mm diameter and 1 cm height. The thickness of the membranes was 20 microns, as measured by a caliper[7] (manual micrometer with limits 0–25 mm and with a precision of 0.01 mm; NSK, Tochigi, Japan). The resistance to deformation induced by a 3 mm diameter cylindrical probe

was studied. The probe penetrates and deforms the membrane causing the creation of an additional vertical force, which is measured. The maximal load and deflection is a measure of the maximum force and deformation that the membranes can undergo before permanent deformation occurs. Rupture of the fibers is considered to occur when the force drops to 50% or less of the maximum load. This parameter together with the deflection at rupture gives an indication of the resistance of the fibers to this kind of deformation.

For measurements of tensile strength, the PLGA and PLGA-ND membranes were cut into rectangular strips 40 mm in length and 21–25 mm in width. The reason for these variations in the width was raveling of the edges (margins) of the samples. The specific weight of these samples was 3.1 (±5%) g/m^2, as calculated from their total weight (determined with accuracy of 0.0005 g), and their dimensions. For each material type, six samples were prepared. The shorter sides (ends) of the tested samples were strengthened by a paper tape in order to prevent damage of the nanofibrous membranes during their preparation for the tensile test, particularly during their mounting in the gripping units of the testing machine. The LabTes4.100 SP1 machine was used, and set up to the maximal range of 50 N, with precision lower than 0.1% for a force of 2 N. The samples were loaded with a constant force until failure. The force needed for tearing the membranes (ie, maximum tensile force; also referred to as ultimate tensile strength)[35,37] was determined from the software of the testing machine.

The molecular structure of PLGA and PLGA-ND membranes was examined using attenuated total reflectance Fourier-transform infrared (FT-IR) spectroscopy. Transmittance spectra were acquired using a Biorad FT-IR spectrometer FTS 575C equipped with a "Golden Gate" attenuated total reflectance accessory. The latter was fitted with a diamond crystal. The spectra were recorded over the range 4000–500 cm^{-1}.

Cell culture on the nanofibrous membranes

The nanofibrous membranes were detached from the underlying polypropylene substrate, cut into square samples (1 × 1 cm), fixed in CellCrown inserts (Scaffdex; Figure 1A and B), and sterilized by gamma irradiation (dose 25 kGy, in accordance with the ISO 11137 standard).

The CellCrown inserts with membrane samples were inserted into polystyrene 24-well cell culture plates (TPP Techno Plastic Products, Trasadingen, Switzerland; well diameter 1.5 cm; Figure 1B), and the membranes were rinsed overnight with Dulbecco's Modified Eagle Minimum Essential Medium (Sigma). The samples were then seeded with human osteoblast-like MG-63 cells (European Collection of Cell Cultures, Salisbury, UK). Each well contained 30,000 cells (approximately 17,000 cells/cm^2) and 1.5 mL of the Dulbecco's Modified Eagle Minimum Essential Medium supplemented with 10% fetal bovine serum (Gibco, Paisley, UK) and gentamicin (40 µg/mL, LEK, Ljubljana, Slovenia). Cells were cultured for one, 3, or 7 days at 37°C in a humidified atmosphere of 5% of CO_2 in the air. The polystyrene culture well was used as a reference material. Four samples were used for each experimental group and time interval, and the experiment described below was repeated three times.

Evaluation of adhesion and growth of bone cells on nanofibrous membranes

On days 1, 3 and 7 after seeding, the samples were rinsed in phosphate-buffered saline. The cells on one sample per experimental group and time interval were fixed by 70% cold ethanol (–20°C) and stained with a combination of Texas Red C_2-maleimide fluorescent membrane dye (Molecular Probes, Invitrogen, Paisley, UK; concentration 20 ng/mL in phosphate-buffered saline) and Hoechst 33342 nuclear dye (Sigma, 5 µg/mL in phosphate-buffered saline). The morphology and distribution of cells on the membrane surface were then evaluated in pictures taken under the Nikon Eclipse Ti-E microscope equipped with a Nikon DS-Qi1 MC digital camera and NIS-Elements AR software, version 3.10.

On day 1 after seeding, the size of cell spreading area, ie, the area projected on the material, was also measured, using Atlas Software (Tescan). The cells that developed intercellular contacts were excluded from the evaluation. On each sample, 60–93 cells were evaluated.

The three remaining samples were used for evaluating the cell number. The cells were rinsed with phosphate-buffered saline, released with trypsin-EDTA solution (Sigma; incubation 5 minutes at 37°C) and counted in a Bürker hemocytometer under an Olympus IX 51 microscope. For each sample, eight cell number measurements were performed. The cell numbers obtained on days 1, 3 and 7 after seeding were used for constructing growth curves and for calculating the cell population doubling time, using the following equation:

$$DT = \log 2 \frac{t - t_0}{\log N_t - \log N_{t_0}}$$

where t_0 and t represent earlier and later time intervals after seeding, respectively, and N_{t_0} and N_t represent the number of cells at these intervals.[28,42]

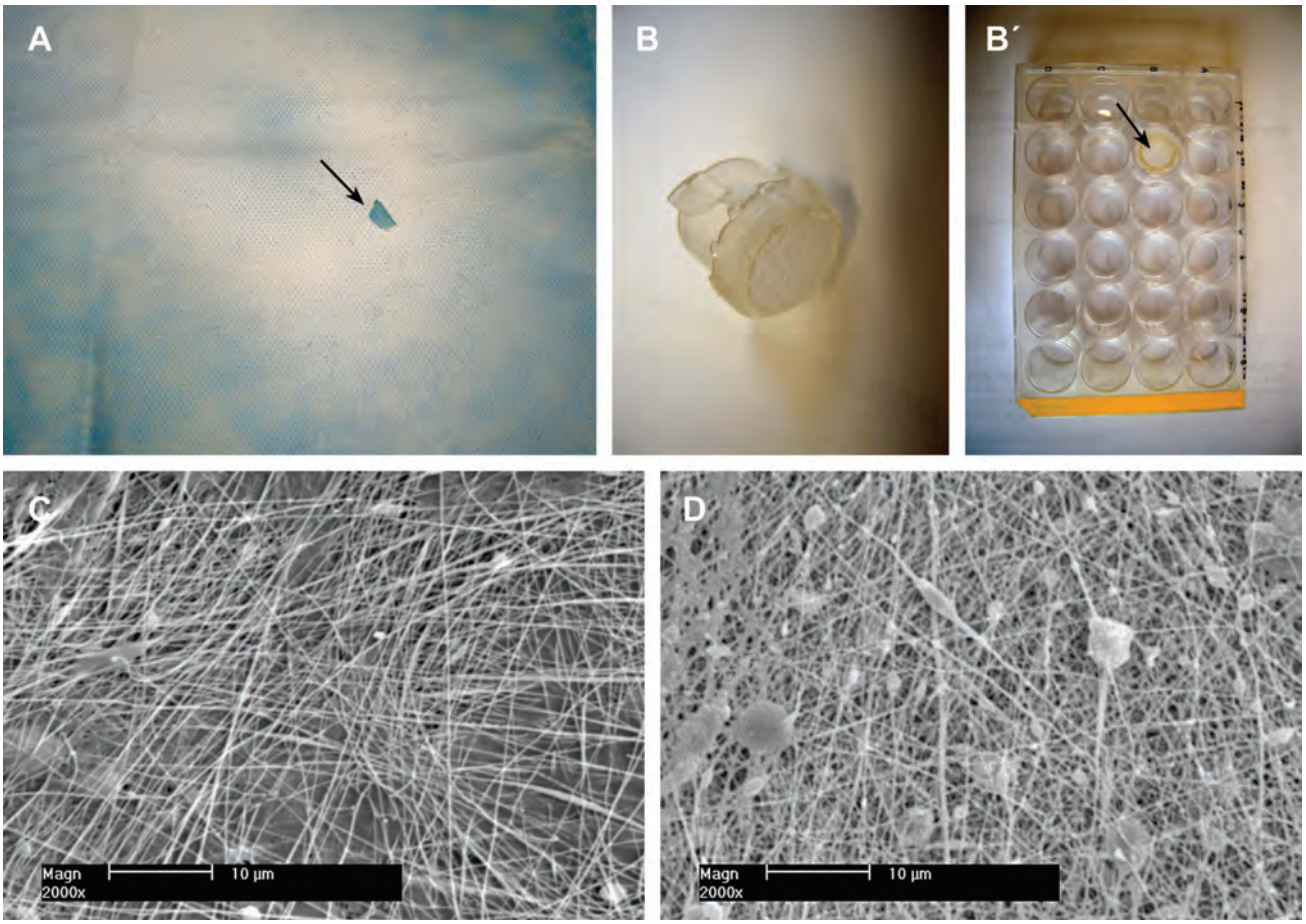

Figure 1 Morphology of nanofibrous PLGA scaffolds enriched with nanodiamond. (**A**) Gross morphology of a composite PLGA-nanodiamond membrane deposited on polypropylene fabric. An arrow indicates a site where a part of the membrane was detached. (**B**) A composite PLGA-nanodiamond membrane fixed with a Scaffdex CellCrown insert. (**B´**, Scaffdex CellCrown insert with a PLGA-nanodiamond membrane in a 24-well plate, arrow). (**C**) Pure PLGA nanofibrous membrane. (**D**) Composite PLGA-nanodiamond membrane. (**A** and **B**) Nikon Coolpix S620 digital camera and (**C** and **D**) XL30CP scanning electron microscope (Phillips Elektron Optics GmbH, Kassel, Germany), objective magnification 2000×, bar 10 µm.
Abbreviation: PLGA, copolymer of L-lactide and glycolide.

Evaluation of cell viability

On days 1, 3 and 7 after seeding, the cells were rinsed with phosphate-buffered saline, and their viability was determined by the LIVE/DEAD viability/cytotoxicity kit for mammalian cells (Molecular Probes) according to the manufacturer's protocol. Briefly, the cells were incubated for 5–10 minutes at room temperature in a mixture of two of the following probes: calcein AM, a marker of esterase activity in living cells, emitting green fluorescence, and ethidium homodimer-1, which penetrates into dead cells through their damaged membrane and produces red fluorescence. Live and dead cells were then counted in microphotographs taken under an epifluorescence microscope (Olympus IX-51, DP-70 digital camera, Japan). For each experimental group and time interval, two samples were used, and on each sample the cells were evaluated in 10 microphotographs.

Immunofluorescence staining of molecules participating in cell-matrix adhesion and cell spreading

On day 3 after seeding, the presence and spatial arrangement of the following molecules in MG-63 cells were evaluated: talin, an integrin-associated protein present in focal adhesion plaques, also reported as a protein of the "cell membrane cytoskeleton" and known to participate in cell-substrate adhesion; vinculin, another protein of focal adhesion plaques, participating in cell-substrate adhesion and stabilizing the focal adhesions;[43] beta-actin, an important component of the cell cytoplasmic cytoskeleton, associated with focal adhesion plaques.

For immunofluorescence staining of these molecules, the cells on day 3 after seeding were rinsed twice in phosphate-buffered saline and fixed with 70% ethanol (–20°C, 20 minutes) pretreated with 1% bovine serum albumin in

phosphate-buffered saline containing 0.05% Triton X-100 (Sigma) for 20 minutes at room temperature in order to block nonspecific binding sites and to permeabilize the cell membrane. The cells were then incubated with the following primary mouse monoclonal antibodies: anti-chicken talin (Sigma, clone 8D4) anti-human vinculin (Sigma) and anti-synthetic N-terminal peptide of β-actin (Sigma). All antibodies were diluted in phosphate-buffered saline to concentrations of 1:200 and applied overnight at 4°C. After rinsing with phosphate-buffered saline, the secondary antibody, represented by goat anti-mouse F(ab′)2 fragment of IgG conjugated with Alexa Fluor® 488 (dilution 1:1000; Molecular Probes) was added for 1 hour at room temperature and incubated in the dark. The cells were then rinsed in phosphate-buffered saline, mounted under microscopic glass coverslips in a Gel/Mount permanent fluorescence-preserving aqueous mounting medium (Biomeda Corporation, Foster City, CA) and evaluated under a Leica confocal laser scanning microscope (TCS SP2, Germany).

Potential immune activation of cells on nanofibrous membranes

The secretion of TNF-α into the cell culture medium and the concentration of ICAM-1 in cell homogenates were measured in human osteoblast-like MG-63 cells and murine macrophage-like RAW 264.7 cells (American Type Culture Collection, Manassas, VA). The cells were seeded on PLGA or PLGA-ND membranes fixed in CellCrown inserts in polystyrene 24-well cell culture plates (TPP; well diameter 1.5 cm). Each well contained 30,000 cells and 1.5 mL of the culture medium. MG-63 cells were cultured in the Dulbecco's Modified Eagle Minimum Essential Medium mentioned above, and for RAW 264.7, RPMI-1640 medium (Sigma; 10% fetal bovine serum, 40 μg/mL gentamicin) was used.

As reference samples, pure polystyrene wells and wells with CellCrown inserts were used. For comparison, PLGA meshes with hydroxyapatite (HAp) nanoparticles (Sigma; <200 nm particle size) were used. The concentration of HAp in PLGA was similar as in the case of ND (ie, approximately 23 wt%).

After 24 hours, the membranes were transferred into fresh wells filled with cell culture medium in order to exclude the cells adhering on the underlying well bottom from the evaluation. In the reference wells with and without CellCrown inserts, the culture medium was also changed. The cells were then cultivated for an additional 6 days. For each material and cell type, four samples were used.

After 6 days of cultivation, the cell culture medium was collected and used for measuring the concentration of TNF-α by a sandwich enzyme-linked immunosorbent assay (ELISA) using commercially available kits. A human TNF-α Quantikine ELISA kit and mouse TNF-α Quantikine ELISA kit were used for the MG-63 and RAW 264.7 cells, respectively. Both kits were purchased from R and D Systems (Minneapolis, MN) and used according to the manufacturer's protocol.

As a positive control for TNF-α production, MG-63 or RAW 264.7 cells grown in polystyrene culture wells and stimulated with lipopolysaccharide (LPS) from *Escherichia coli* (0111:B4, γ-irradiated, BioXtra, Sigma) were used. Lipopolysaccharide was applied in concentrations ranging from 0 to 10 μg/mL on day 6 after seeding for 24 hours. For each concentration, four wells were used. As a negative control, fresh Dulbecco's Modified Eagle Minimum Essential Medium or RPMI-1640 media supplemented with fetal bovine serum and gentamicin, which were not exposed to cells, were used.

The concentrations of TNF-α in cell culture media were determined from calibration curves and given in pg per 100,000 cells, ie, not per mL of the culture media, as usual.[44,45] The reason was that the cell numbers on the tested materials were different. For MG-63 cells, it ranged on average from 305,600 to 753,900 cells/sample, and for RAW 264.7 cells, from 748,900 to 1,220,600 cells/sample (Figure 9A and B).

For measuring the concentration of ICAM-1 by ELISA in cell homogenates (per mg of protein), the MG-63 cells were then harvested by trypsin-EDTA solution in phosphate-buffered saline (Sigma) and RAW 264.7 cells by 0.05% EDTA in phosphate-buffered saline and counted in a Bürker hemocytometer. The cells (10^6 cells/mL), resuspended in distilled and deionized water, were kept in a freezer at −70°C overnight. The cells were then homogenized by ultrasonication for 40 seconds in a sonicator (UP 100 H, Dr Hielscher GmbH; cycle 1, amplitude 70%), and the protein content was measured using a Coomassie Plus (Bradford) Kit (Cat. No. 23236, Thermo Fisher Scientific Inc., Rockford, IL USA).

Aliquots of the cell homogenates corresponding to 1–50 μg of protein in 50 μL of water were adsorbed on 96-well microtiter plates (Nunc-Immuno™ Plates, F96 MaxiSorp, Cat. No. 442404, Nunc a/s, Roskilde, Denmark) at 4°C overnight. After washing twice with phosphate-buffered saline (100 μL/well), the nonspecific binding sites were blocked by 0.02% gelatin in phosphate-buffered saline (100 μL/well, 60 minutes). As primary antibodies,

monoclonal mouse antihuman ICAM-1 antibody was used in MG-63 cells (Exbio, Prague, Czech Republic) and monoclonal rat anti-mouse ICAM-1 antibody (Exbio Prague, clone YN1/1.7.4). The antibodies were diluted in phosphate-buffered saline and applied for 60 minutes at room temperature (50 μL/well). Goat anti-mouse $F(ab')_2$ IgG fragment (Sigma, dilution 1:1000) was used after the mouse primary antibody, and goat anti-rat IgG (BioLegend, dilution 1:1000) was used after the rat primary antibody as secondary antibodies. Both secondary antibodies were conjugated with peroxidase and applied for 45 minutes (100 μL/well). This step was followed by double washing in phosphate-buffered saline and orthophenylendiamine reaction (Sigma, concentration 2.76 mM) using 0.05% H_2O_2 in 0.1 M phosphate buffer (pg 6.0, dark place, 100 μL/well). The reaction was stopped after 10–30 minutes by 2 M H_2SO_4 (50 μL/well), and the absorbance was measured at 490 nm and 690 nm using a Versa Max microplate reader (Molecular Devices Corporation, Sunnyvale, CA). The absorbances obtained from cells growing on PLGA and PLGA-ND membranes were expressed as a percentage of the values obtained in the control cultures on standard polystyrene wells.

Statistics

The quantitative results were presented as the mean ± standard error of mean. Statistical significance was evaluated using analysis of variance, Student-Newman-Keuls method, or the two-tailed *t*-test. Values of $P \leq 0.05$ were considered as significant.

Table 1 Morphological parameters of pure poly(lactide-co-glycolide) (PLGA) membranes and PLGA membranes with nanodiamond (PLGA-ND)

Parameters	PLGA	PLGA-ND
Fibers		
Diameter, range	124–351 nm	124–877 nm
Diameter, mean ± SEM	218 ± 4 nm	270 ± 9 nm*
Clusters		
Area, range	0.20–10.68 μm^2	0.31 to 24.10 μm^2
Area, mean ± SEM	2.13 ± 0.75 μm^2	3.54 ± 0.90 μm^2
Density, mean ± SEM	8,340 ± 1,495/mm^2	33,361 ± 6,182/mm^2
Pores		
Area, range	0.10–6.95 μm^2	0.10–1.50 μm^2
Area, mean ± SEM	1.28 ± 0.09 μm^2	0.46 ± 0.02 μm^2*

Notes: Mean ± SEM. from 129–193 measurements (fibers), 13–43 measurements (cluster area), four measurements (cluster density), and 181–192 measurements (pores). ANOVA, Student-Newman-Keuls method; statistical significance: *$P \leq 0.05$ in comparison with PLGA.

Abbreviations: ANOVA, analysis of variance; SEM, standard error of the mean.

Results

Properties of nanofibrous membranes

Both pure PLGA and composite PLGA-ND membranes formed a fine cobweb-like layer on blue polypropylene fabrics, which served as a carrier for the nanofibrous membranes. The pure PLGA membrane was white, whereas the membrane with ND was grayish. As revealed by scanning electron microscopy, both membranes were composed of mostly straight and randomly oriented fibers. These fibers were thicker and the pores between them were smaller in the composite PLGA-ND membranes. The PLGA-ND membranes also contained more material clusters. Their density, calculated per mm^2 projected on the membrane, was approximately four times higher than in pure PLGA membranes, and these clusters were on an average larger than those in PLGA membranes, although this difference was not statistically significant due to the great variation in cluster size (Figure 1, Table 1).

Transmission electron microscopy images of PLGA-ND fibers are shown in Figure 2. The images clearly show that the diamond nanoparticles form predominantly small clusters embedded in the PLGA matrix. The size of the clusters is variable, ranging from a few particles to large clusters spanning the whole width of the fibers, ie, in some cases up to 200 nm. The nanofibers exhibit great variability in thickness, from very thin threads less than 5 nm in diameter to thick fibers approaching 200 nm in diameter. The diamond nanoparticles also occurred in the form of isolated clusters attached to the surface of the PLGA nanofibers.

As revealed by reflection goniometry, the static water drop contact angle for both types of nanofibrous membranes was about 70°.

The rupture tests showed that membranes consisting of PLGA-ND resisted a load of 1.29 ± 0.22 N until rupture, significantly more than pure PLGA fiber membranes, which withstood 0.75 ± 0.19 N (Figure 3A). As indicated by Figure 3B, the deflection of the rupture probe at failure was 1.21 ± 0.08 mm and 0.97 ± 0.06 mm in the case of PLGA-ND membranes and PLGA membranes, respectively. This difference was also significant according to a two-tailed t-test ($P < 0.001$, n = 10 in both groups). However, as indicated by the tensile strength measurements, the force needed for tearing both PLGA and PLGA-ND membranes was similar, ie, approximately 0.074 (±10%) N/mm (Table 2).

With regard to the FTIR analysis, Zhao et al[46] demonstrated ND-PLA interactions by shifts in characteristic polymer bands in the FTIR spectra corresponding to the C=O stretch and bending of –OH bonds in –CH(CH_3)–OH end groups. As can be seen by comparing the FTIR spectra of

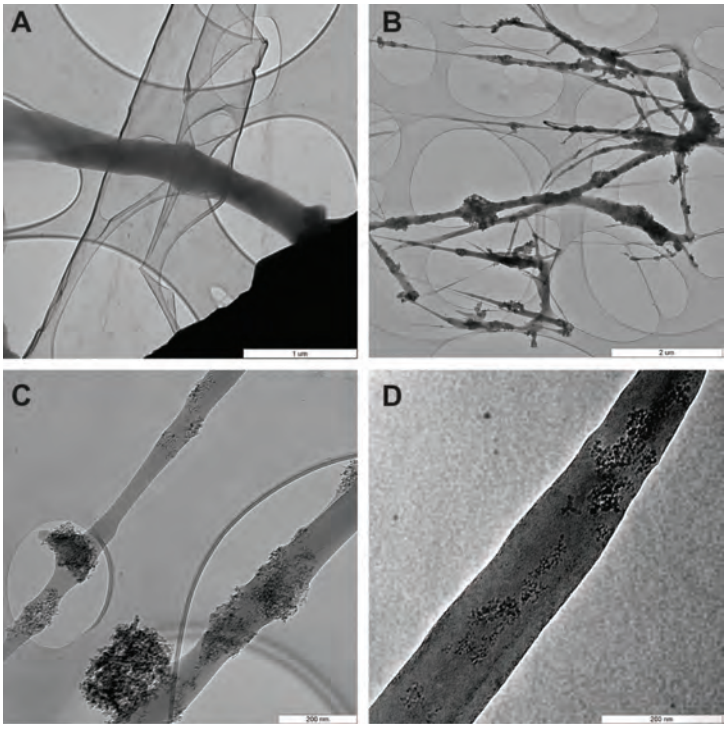

Figure 2 Transmission electron microscopy images of pure PLGA fibers (**A**) and PLGA fibers with diamond nanoparticles (**B**–**D**). (**B**) Network of PLGA with diamond nanoparticles, showing variations in fiber thickness and size of the material clusters. (**C**) Individual fibers with clusters of diamond nanoparticles. (**D**) Diamond nanoparticles relatively homogeneously distributed in a PLGA fiber.
Notes: The layers with elliptical openings (**A**–**C**) are amorphous carbon membranes of the grid used to fix the sample. A Philips CM120 transmission electron microscope, LaB6 cathode operated at 120 kV, and SIS Veleta CCD camera, were used. Scale bar 1 μm (**A**), 2 μm (**B**), and 200 nm (**C** and **D**).
Abbreviation: PLGA, copolymer of L-lactide and glycolide.

PLGA and PLGA-ND in Figure 4, only very small differences were seen in characteristic PLGA peaks, ie, C=O stretch at 1748 cm^{-1}, –OH bending in $–CH(CH_3)–OH$ end groups at 1043 cm^{-1}, and asymmetrical C–O–C stretch at 1083 cm^{-1}.[46,47]

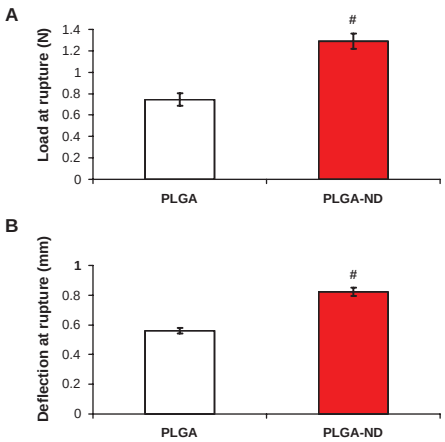

Figure 3 Load at rupture (**A**) and deflection of probe at rupture (**B**) of nanofiber membranes consisting of pure PLGA and PLGA-ND.
Notes: The mean ± standard error of the mean are presented for 10 samples from each experimental group. Two-tailed *t*-test, $P \leq 0.001$ in comparison with PLGA.
Abbreviations: PLGA, copolymer of L-lactide and glycolide; ND, nanodiamond.

Adhesion and growth of MG-63 cells on nanofibrous scaffolds

The initial adhesion and subsequent growth of MG-63 cells was similar on both pure and ND-loaded PLGA membranes. On the first day after seeding, the number of initially adhering cells on the pure PLGA membranes was 11,300 ± 1200 cells/cm^2, and on the PLGA-ND membranes, the number was 10,951 ± 1027 cells/cm^2. The highest average number of initially adhered cells was observed on the control polystyrene dishes (14,000 ± 1038 cells/cm^2). However, as revealed by analysis of variance, this value was not statistically different from the values obtained on the two nanofibrous membranes (Figure 5A). On the other hand, the cells on polystyrene dishes adhered by a significantly larger cell spreading area (1057 ± 33 μm^2) than the cells on both pure and ND-loaded PLGA membranes (442 ± 15 μm^2 and 477 ± 16 μm^2, respectively, Figure 5B).

From day 1 to 3 after seeding (ie, in an early phase of exponential cell growth) the cells on both PLGA and PLGA-ND membranes proliferated more slowly, ie, with longer cell population doubling times than the cells on

Table 2 Tensile strength of poly(lactide-co-glycolide) (PLGA) and PLGA membranes with nanodiamond (PLGA-ND) membranes

Sample	PLGA			PLGA-ND		
N	Force (N)	Width (mm)	Resultant force (N/mm)	Force (N)	Width (mm)	Resultant force (N/mm)
1	1.651	24.03	0.0687	1.655	23.24	0.0712
2	1.809	23.65	0.0765	1.954	24.46	0.0799
3	1.997	26.80	0.0745	1.867	25.75	0.0725
4	1.725	23.47	0.0735	1.877	23.43	0.0801
5	1.579	21.84	0.0723	1.773	24.73	0.0717
6	1.751	21.62	0.0810	1.648	23.88	0.0690
Mean ± SEM	1.7520 ± 0.0589	23.5683 ± 0.7628	0.0744 ± 0.0017	1.7957 ± 0.0513	24.2483 ± 0.3810	0.0741 ± 0.0019

Note: Mean ± SEM from six samples for each experimental group.
Abbreviations: ANOVA, analysis of variance; SEM, standard error of the mean.

polystyrene dishes (Table 3, Figure 5C). As a result, on day 3 after seeding, the cells on both PLGA and PLGA-ND scaffolds reached significantly lower cell population densities (36,100 ± 2200 cells/cm² and 37,000 ± 2500 cells/cm², respectively) than on polystyrene dishes (61,900 ± 2100 cells/cm²). At the same time, the cell population densities on both nanofibrous scaffolds were similar (Figure 5A and C).

From day 3 to 7 after seeding (ie, in a late phase of exponential cell growth), the cell proliferation became quicker on both types of nanofibrous membranes than on polystyrene, ie, these cells proliferated with shorter cell population doubling times (Table 3). In spite of this, on day 7 after seeding, the cell population densities still remained lower on pure and ND-loaded PLGA membranes (167,700 ± 4500 cells/cm² and 169,900 ± 6100 cells/cm², respectively) than on polystyrene dishes (220,500 ± 6300 cells/cm²).

Nevertheless, the cells on PLGA with ND were similar in shape to the cells on PLGA and polystyrene dishes, ie, polygonal or spindle-like. They were distributed homogeneously on the samples, their number rose continuously during the testing period, and at the end of the testing period, these cells were able to form a confluent layer (Figures 6 and 7). From this point of view, the MG-63 cells on PLGA-ND membranes behaved physiologically without noticeable signs of cell damage.

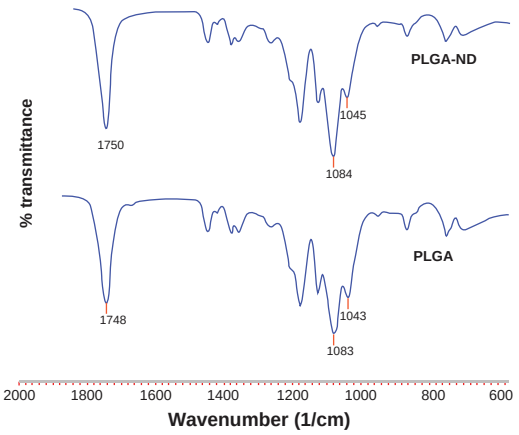

Figure 4 Fourier transform infrared spectra of nanofiber membranes consisting of pure PLGA and PLGA-ND.
Abbreviations: PLGA, copolymer of L-lactide and glycolide; ND, nanodiamond.

Viability of MG-63 cells on nanofibrous scaffolds

Staining the cells with the LIVE/DEAD viability/cytotoxicity kit showed that the percentage of living cells on all tested materials was relatively high, ranging from 92% to 99% (Figures 5D and 7). The lowest values (92%–94%) were obtained in cells on composite PLGA-ND membranes. These values were significantly lower than those obtained in cells on the control polystyrene dishes, and on days 3 and 7 were also significantly lower than the values on the pure PLGA membranes. Also, on pure PLGA membranes, cell viability was lower than that on the polystyrene dishes, except on day 7, when the two values were similar.

On the corresponding substrates, the cell viability was similar on day 1 and day 3 after seeding. However, from day 3, the viability showed a tendency to decrease, which was most pronounced on polystyrene dishes. On these substrates, the cell viability on day 7 was significantly lower than on day 1 and day 3. On PLGA-ND scaffolds, the cell viability on day 7 was lower than on day 3 (Figure 5D).

Focal adhesion plaques and actin cytoskeleton in MG-63 cells on nanofibrous scaffolds

Immunofluorescence staining showed that in cells on both types of nanofibrous membranes and the control microscopic

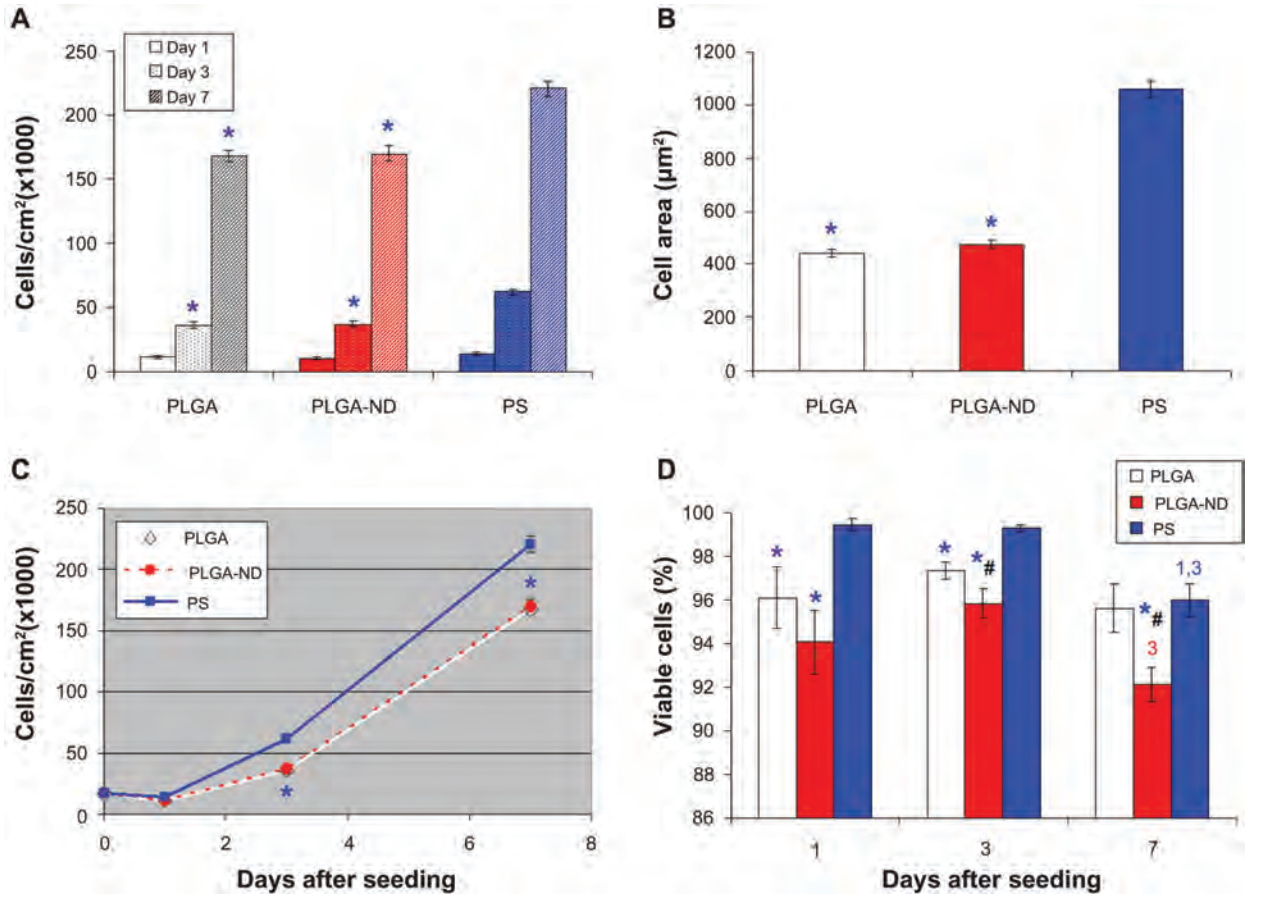

Figure 5 (**A**) Number of human osteoblast-like MG-63 cells on days 1, 3, and 7 after seeding on a pure nanofibrous PLGA membrane, a PLGA-ND membrane, and bottom of polystyrene culture wells. (**B**) Size of cell spreading area on day 1 after seeding. (**C**) Growth dynamics of cells on substrates from days 1–7. (**D**) Viability of MG-63 cells on days 1, 3 and 7 after seeding on the substrates. Mean ± standard error of the mean of three experiments. In total, 72 measurements of cell numbers (**A**, **C**) and 20 measurements of cell viability (**D**) were performed, and 200–278 cell spreading areas (**B**) were evaluated for each experimental group and time interval.
Notes: Analysis of variance, Student-Newman-Keuls method. $^{*\#}P \leq 0.05$ in comparison with polystyrene and PLGA, respectively.^{1,3} $P \leq 0.05$ in comparison with cells on days 1 and 3 after seeding on corresponding substrate.
Abbreviations: PLGA, copolymer of L-lactide and glycolide; ND, nanodiamond; PS, polystyrene.

glass coverslips, talin either was distributed diffusely throughout all the cells or was organized into focal adhesion plaques. These plaques were more apparent in cells on glass and PLGA membranes with ND than in cells on the pure PLGA scaffolds. On both nanofibrous scaffolds, the focal adhesion plaques were usually relatively small, dot-like, and distributed on the ventral part of the cell membrane in its central region. On glass, these plaques were bigger, streak-like, and distributed in both peripheral and central parts of the cells (Figure 8A–C).

A similar morphology and distribution was also observed for vinculin-containing focal adhesion plaques, though they were usually smaller and less numerous than those containing talin (Figure 8D–F).

Beta-actin in cells on all three tested substrates was organized into fine fibers running in parallel between the opposite cell edges. These fibers were most apparent in cells on glass, while on both nanofibrous substrates, a considerable amount of β-actin was also distributed diffusely without forming specific structures (Figure 8G–I).

Table 3 Cell population doubling time (DT) of MG 63 cells on poly(lactide-co-glycolide) (PLGA) membranes with and without nanodiamond (ND), and tissue culture polystyrene dishes (PS) as a reference material

Material/DT	PLGA	PLGA-ND	PS
DT_{1-3} (hours)	32.5 ± 3.2*	27.5 ± 1.3	22.5 ± 0.6
DT_{3-7} (hours)	43.6 ± 1.7*	45.6 ± 2.0*	52.8 ± 1.2
DT_{1-7} (hours)	37 ± 0.5	36.8 ± 1.1	36.2 ± 0.6

Notes: Mean ± SEM from four measurements, ANOVA, Student-Newman-Keuls method. Statistical significance: $^{*}P \leq 0.05$ in comparison with PS.
Abbreviation: ANOVA, analysis of variance.

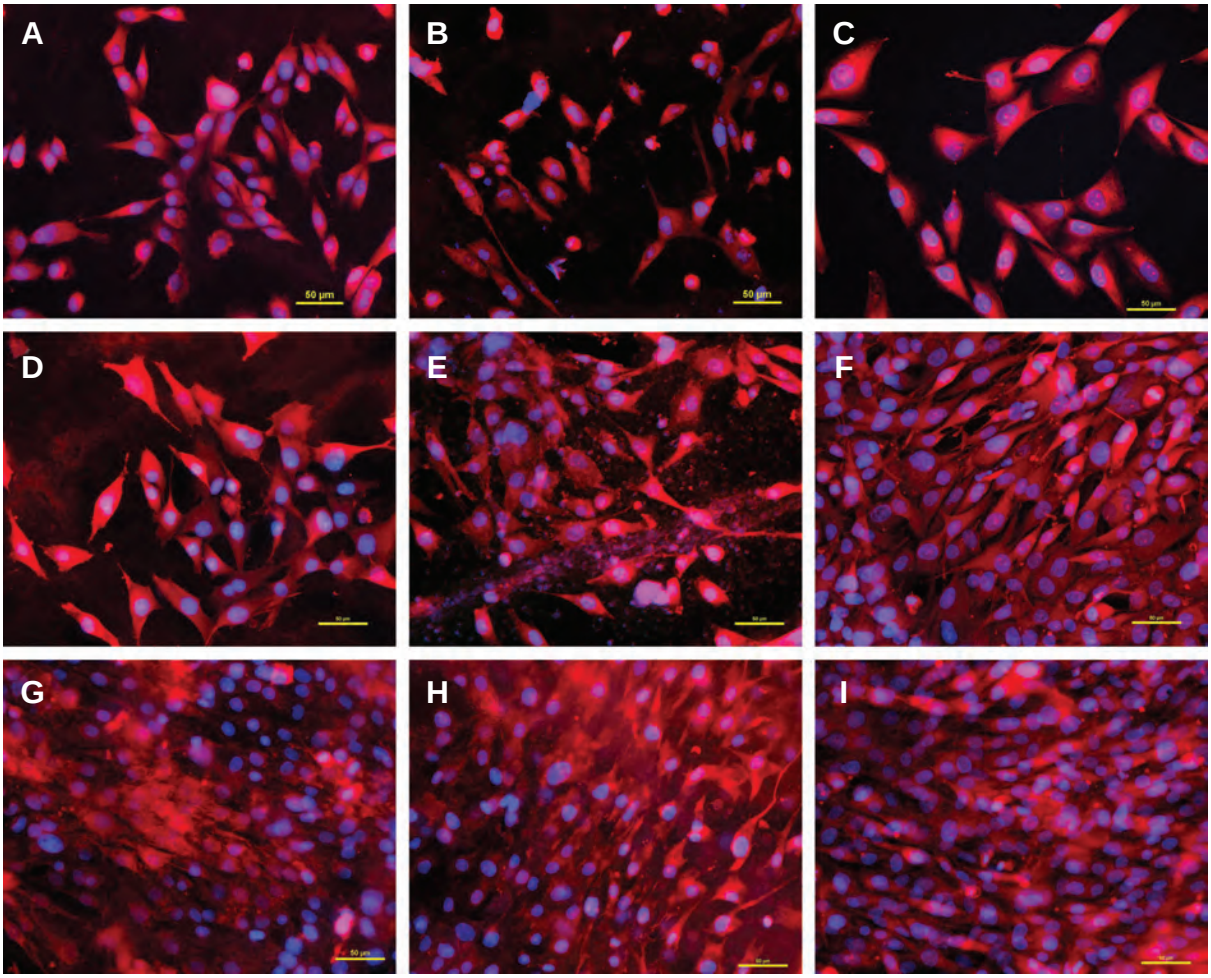

Figure 6 Morphology of human osteoblast-like MG-63 cells on days 1 (**A**–**C**), 3 (**D**–**F**), and 7 (**G**–**I**) after seeding on pure PLGA scaffolds (**A**, **D**, and **G**), composite PLGA-ND scaffolds (**B**, **E**, and **H**), and a polystyrene culture well (**C**, **F**, and **I**). The cell membrane and cytoplasm were stained with Texas Red C_2-maleimide (red fluorescence), and the cell nuclei with Hoechst 33342 (blue fluorescence).

Notes: A Nikon Eclipse Ti-E microscope, objective 20 × 1.5; Nikon DS-Qi1 MC digital camera, NIS-Elements AR software, version 3.10, were used. Summarization of Z-sections with deconvolution, bar 50 μm.

Abbreviations: PLGA, copolymer of L-lactide and glycolide; ND, nanodiamond.

Immune activation of cells on nanofibrous membranes

From days 2–7 after seeding of human osteoblast-like MG-63 cells on the tested materials, the concentration of human TNF-α in the culture medium ranged on average from 0.74 to 2.31 pg per 100,000 cells. The concentration of TNF-α in the medium from PLGA, PLGA-ND, and PLGA-HAp meshes was significantly higher than in the medium from control polystyrene dishes with and without CellCrowns (Figure 9C). The highest value (2.31 ± 0.21 pg/100,000 cells) was found in the medium taken from MG-63 cells on PLGA-ND meshes. Nevertheless, this concentration of TNF-α was very low. As follows from the calibration curve (Figure 9E), it was almost at the limit of detection by the human TNF-α Quantikine ELISA kit. Even after relatively long stimulation of MG-63 cells with a relatively high dose of bacterial lipopolysaccharide (10 μg/mL for 24 hours), the concentration of TNF-α in the culture medium reached only 5.07 ± 0.24 pg/100,000 cells, which still remained at the detection limit (Figure 9G).

On the other hand, the values obtained for RAW 264.7 macrophages were higher by 1–2 orders of magnitude. On the tested samples, the concentration of TNF-α in the culture medium reached on average 12.9 to 51.1 pg/100,000 cells. Similarly, as for MG-63 cells, the concentrations of TNF-α released into the culture medium by cells on all PLGA-based membranes were significantly higher than the values for control polystyrene wells. Nevertheless, the concentration of TNF-α released by the cells on PLGA-ND was similar as in cultures on pure PLGA (Figure 9D). The highest

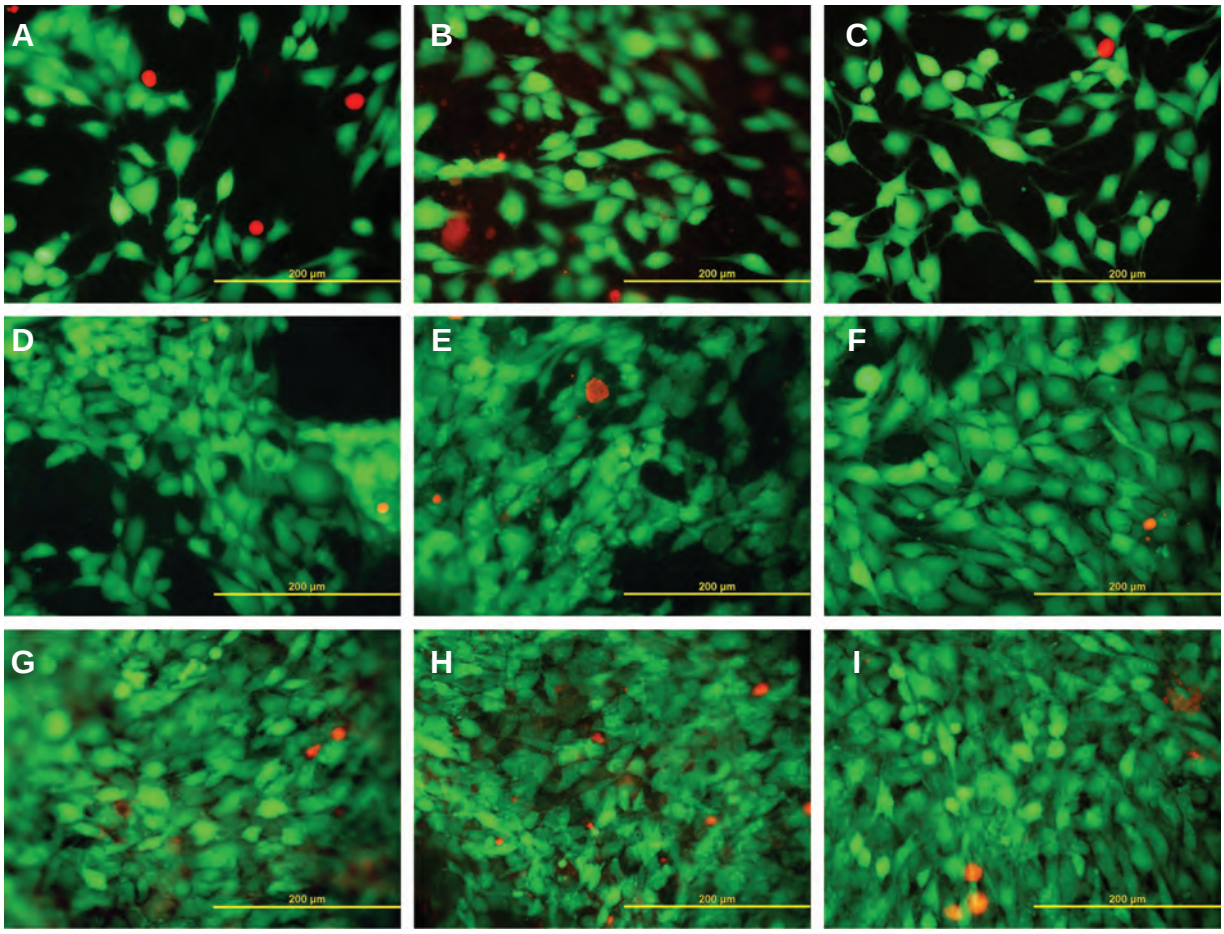

Figure 7 Live (green) and dead (red) human osteoblast-like MG-63 cells on days 1 (**A**–**C**), 3 (**D**–**F**), and 7 (**G**–**I**) after seeding on pure PLGA scaffolds (**A**, **D**, and **G**), composite PLGA-ND scaffolds (**B**, **E**, and **H**) and a polystyrene culture well (**C**, **F**, and **I**).
Notes: Stained with the LIVE/DEAD viability/cytotoxicity kit for mammalian cells. Olympus IX-51, objective 20×, DP-70 digital camera, bar 200 µm.
Abbreviations: PLGA, copolymer of L-lactide and glycolide; ND, nanodiamond.

concentration (51.1 pg/100,000 cells) was obtained in the medium from PLGA-HAp membranes, and it was significantly higher than the values obtained in all other tested materials. In spite of this, it was much lower (about eight times) in comparison with the concentration of TNF-α released from RAW 264.7 cells after stimulation with the lowest concentration of lipopolysaccharide (0.05 µg of lipopolysaccharide, Figure 9H). For comparison, 10 µg/mL of lipopolysaccharide in our study induced a massive release of TNF-α from RAW 264.7 cells, manifested by a high concentration of TNF-α in the culture medium (731 ± 7 pg/100,000 cells; Figure 9H). No TNF-α was detected in the pure culture media not exposed to cells, which served as a negative control.

As for ICAM-1, no significant differences in the concentration of this immunoglobulin in MG-63 cells or RAW 264.7 cells were detected on any tested materials (Figure 9I and J). In other words, all three types of PLGA-based membranes, ie, pure PLGA, PLGA-ND, and PLGA-HAp, did not evoke significantly higher concentrations of ICAM-1 in MG-63 or RAW 264.7 cells than the conventional cell culture system on polystyrene dishes.

Discussion

In this study, we constructed nanofibrous membranes by electrospinning pure PLGA or PLGA with approximately 23 wt% of ND. Recently, the first synthetic polymeric fibers of nanoscale or microscale diameter loaded with ND were created by Behler et al[32] by electrospinning polyacrylonitrile or polyamide and ND powder produced via detonation synthesis. Similar to our study, the ND particles were not dispersed homogeneously in the polymeric matrix, but they formed agglomerates. However, these agglomerates were much smaller than those in our present study, ie, usually not exceeding the fiber diameter. At the same time, the concentration of ND particles reached 80 wt% in polyacrylonitrile,

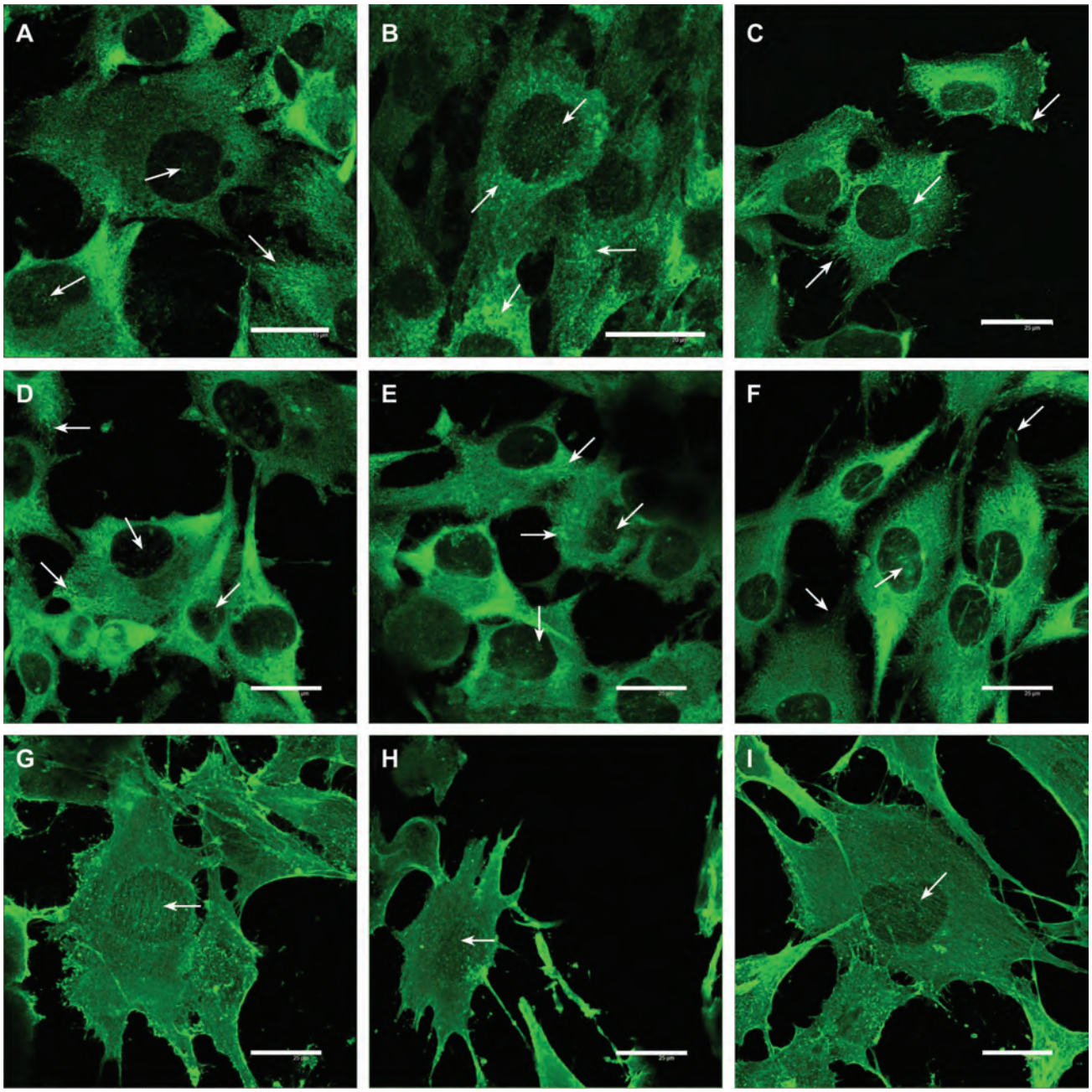

Figure 8 Immunofluorescence of talin (**A**–**C**), vinculin (**D**–**F**), and beta-actin (**G**–**I**) in human osteoblast-like MG-63 cells on day 3 after seeding on pure PLGA scaffolds (**A**, **D**, and **G**), composite PLGA-ND scaffolds (**B**, **E**, and **H**), and polystyrene culture well (**C**, **F**, and **I**).
Notes: Leica confocal laser scanning microscope (TCS SP2, Germany), objective 20×, zoom 8× (**A**) 8.5× (**B**), or 6× (remainder of pictures); bar 25 μm.
Abbreviations: PLGA, copolymer of L-lactide and glycolide; ND, nanodiamond.

while on PLGA in our study, the concentration was only 23 wt%. The optimum ND concentration for creating polyamide-based fibers was 40 wt%.[32] The optimum ND concentration for forming composite fibers therefore seems to depend on the type of the polymer used. Other factors influencing ND agglomeration include sonication, stirring, and shaking the ND suspension, the diameter of the newly formed fibers, polymer surface tension, strength of the electrostatic forces pulling the fibers in electrospinning, type of solvent, and time of its evaporation. The concentrations of polymer and ND are also important. In the study by Behler et al,[32] a relatively low polymer concentration (6 wt%) in the solvent decreased the viscosity and increased the highest obtainable loading of ND. If the ND concentration increased above 20 wt%, the fibers showed a more uniform distribution of these nanoparticles. On the other hand, excessively high

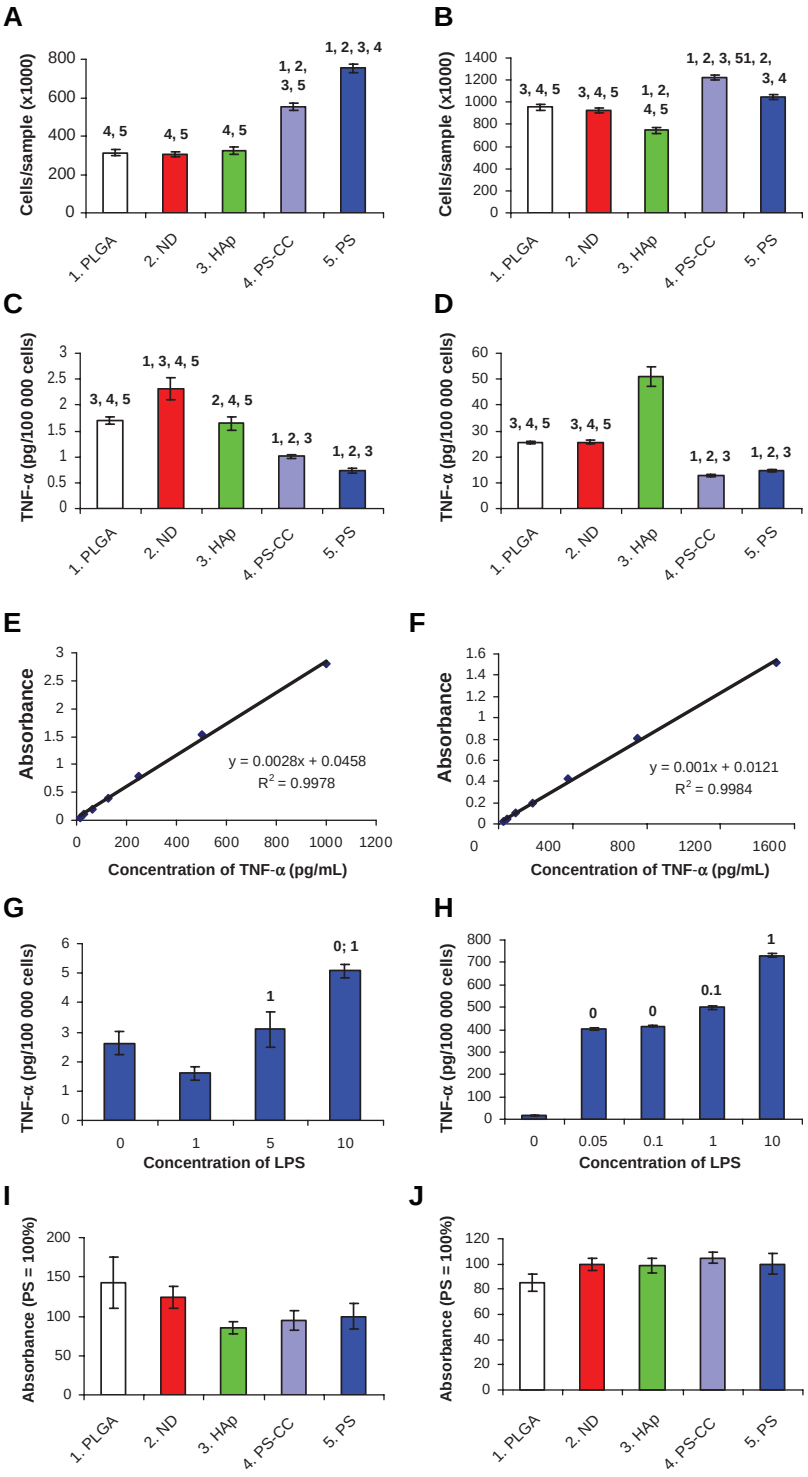

Figure 9 Markers of cell immune activation in human osteoblast-like MG-63 cells (**A**–**I**) and murine macrophage-like RAW 264.7 cells (**B**–**J**) on day 7 after seeding on pure nanofibrous PLGA membranes, PLGA membranes with ND, PLGA membranes with HAp, and bottom of polystyrene culture wells with and without CellCrown inserts (PS-CC and PS, respectively). (**A** and **B**) Cell number, with which the markers were correlated. (**C** and **D**) Concentration of TNF-α in the cell culture media taken from MG-63 or RAW 264.7 cells cultured on the tested materials. (**E** and **F**) Calibration curves for TNF-α measured by human and mouse TNF-α Quantikine enzyme-linked immunosorbent assay kits, respectively. (**G** and **H**) Concentration of TNF-α in culture media taken from MG-63 or RAW 264.7 cells after 24-hours of stimulation with bacterial lipopolysaccharide (0–10 μg/mL). (**I** and **J**) Concentration of ICAM-1 (per mg of protein) in homogenates of MG-63 or RAW 264.7 cells grown on the tested materials. Mean ± standard error of the mean for four samples from each experimental group. In total, for each experimental group, 72 (**A** and **B**), eight (**C**, **D**, **G**, and **H**) or 24–26 (**I** and **J**) measurements were performed. Analysis of variance, Student-Newman-Keuls method. The numbers above the columns indicate the type of tested sample (**A**–**D**) or lipopolysaccharide concentration (**G** and **H**) with significantly different values.

Note: $P \leq 0.05$.

Abbreviations: PLGA, copolymer of L-lactide and glycolide; ND, nanodiamond; HAp, hydroxyapatite; PS, polystyrene; ICAM-1, intracellular adhesion molecule-1; LPS, lipopolysaccharide; TNF-α, tumor necrosis factor alpha.

concentrations of ND disabled the formation of fibers. An attempt to electrospin a 90 wt% ND-polyacrylonitrile composite resulted in electrospraying of droplets, in which most of the ND particles were agglomerated, and the clumps were connected with small fibers.[32] In our study, a relatively low concentration of the polymer in the solvent was also used (ie, 2.3 wt%), and the concentration of ND exceeded 20 wt% in the polymer, being 23 wt%. Despite this, ND-containing clusters were present in our meshes. Thus, additional factors should be taken into account, particularly the different setup of the electrospinning process. While in our study the membranes were formed purely by electrostatic forces, in the study by Behler et al[32] these forces were potentiated by continuously pumping the ND dispersions through the syringe with a needle at 0.015 cm/minute. A similar technique, ie, a combination of an electrical field with active pumping and ejection of PLGA or PLA with HAp nanoparticles through a syringe with a needle, was also successfully used for electrospinning composite nanofibrous scaffolds for potential bone tissue engineering applications.[9,12,14,15] In these studies, PLGA was dissolved in dichloromethane or 1,1,1,3,3,3-hexafluor-2-propanol at concentrations in the range of 2%–30% w/v. The HAp particles were 100–200 nm in size, and they reached concentrations of 1–20 wt% in PLGA. At lower concentrations (up to 5 wt%), the HAp nanoparticles were homogeneously dispersed inside or on the surface of PLGA fibers without forming clusters. At higher concentrations (10 wt% and especially 20 wt%), HAp nanoparticles showed a tendency to agglomerate, which resulted in an increase in surface roughness, in porosity, and also in the fiber diameter. Good results were obtained with composite PLGA-tricalcium phosphate nanofibers, prepared by electrospinning 8% (w/w) PLGA in chloroform, containing 5% (w/w) of the surfactant Tween 20, and enriched with amorphous tricalcium phosphate (particle size 20–50 nm) in concentrations of 10–40 wt% in PLGA. The tricalcium phosphate nanoparticles were homogeneously distributed in the PLGA matrix, although fractures on the fiber surface occurred at higher concentrations.[13]

As for the PLA-HAp composite fibers, PLA was dissolved in trifluoroethanol at a concentration of 10 wt%, and the concentration of HAp nanoparticles (size $<$100 nm) ranged between 5 wt% and 20 wt% of PLA. At all concentrations, HAp nanoparticles were homogeneously distributed inside the nanofibers without forming aggregates and prominences on the fiber surface.[9]

A combination of PLA (dissolved in chloroform and dimethyl formamide at a ratio of 3:1 at a concentration of 20 wt%) with multiwall carbon nanotubes (diameter 15 ± 5 nm and length 5–20 μm, concentration 1 wt% in PLA) also led to electrospinning of fibers with multiwall carbon nanotubes aligned with the long axis. Only occasional fibers with incompletely encapsulated MWNT were observed.[23] Interestingly, nanocomposite PLA-multiwall carbon nanotubes fibers had a markedly smaller average diameter (700 nm) than PLA without multiwall carbon nanotubes (approximately 5–8 μm). In contrast, when HAp nanoparticles were added to PLGA or PLA, the fiber diameter increased proportionally to the nanoparticle concentration, eg, from 300 nm (neat PLGA) to 700 nm (20% nano-HAp).[14] Also in our study, the PLGA-ND fibers were thicker than pure PLGA fibers (270 ± 9 nm versus 218 ± 4 nm in diameter, Table 1).

Evaporation of the solvent during the electrospinning process is limited in the system using a needle and a syringe, whereas in our system a drop placed with a micropipette on the spike-like electrode was freely exposed to air. This allowed quick evaporation of the solvent and an increase in the polymer concentration and in the ND concentration in the dispersion. These changes may increase the viscosity of the dispersion, an important parameter which influences the spinnability of the materials. High viscosities are known to hamper electrospinning due to the flow instability caused by the high cohesiveness of the solution, while very low viscosities lead to the formation of droplets.[17] Viscosity was not measured in our present study. However, the solution viscosity is proportional to polymer concentration.[48,49] Polymer concentration plays a decisive role in the outcome of the electrospinning process: a low concentration led to the formation of beaded fibers; an intermediate concentration yielded good quality fibers; a high concentration resulted in a bimodal size distribution, and a distributed deposition at even higher concentration.[49] In accordance with this, our preliminary experiments showed that a PLGA concentration of 2.3 wt% in the solvent enabled electrospinning of long and smooth nanofibers, whereas a relatively small decrease in this concentration to 2.0 wt% resulted in the formation of several μm large polymer clusters connected with a small number of short fibers (Figure 10), which may be due to low viscosity of the mixture. In a review article by Huang et al,[17] a concentration of 5 wt% is recommended for PLGA. However, when the concentration of PLGA in our experiments was increased to 2.5 wt% or 3.0 wt%, the results were also not ideal, ie, they were similar to the results obtained at the lower PLGA concentration of 2.0 wt%.

As mentioned above, PLGA has often been dissolved in dichloromethane[12] or 1,1,1,3,3,3-hexafluor-2-propanol.[10,14,15]

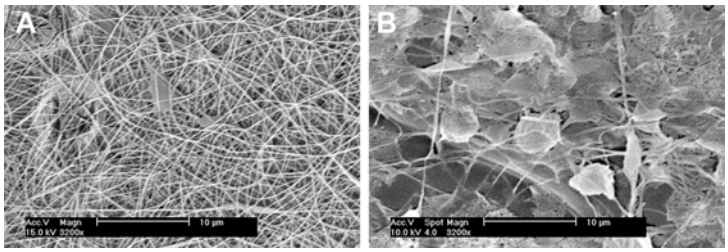

Figure 10 Morphology of nanofibrous PLGA scaffolds created by electrospinning of PLGA diluted in methylene chloride and dimethyl formamide (2:3) at a concentration of 2.3 wt% (**A**) or 2.0 wt% (**B**).
Note: XL30CP scanning electron microscope (Phillips Elektron Optics GmbH, Kassel, Germany), objective magnification 3200×, bar 10 μm.
Abbreviation: PLGA, copolymer of L-lactide and glycolide.

Some investigators have also used N,N-dimethylformamide,[50] chloroform,[13] or a combination of tetrahydrofuran and N,N-dimethylformamide at a ratio of 1:1[17] or 3:1.[11] In our preliminary experiments, a mixture of methylene chloride and N,N-dimethylformamide (ratio 2:3) proved to be the most appropriate solvent combination for our open-air electrospinning system. In this combination, methylene chloride is a relatively quickly evaporating solvent, while the evaporation of N,N-dimethylformamide is slower. Pure methylene chloride or other quickly evaporating solvents (ie, chloroform) did not give good results in our system, where the material, placed in a relatively small quantity on the top of the spike-like electrode, was freely exposed to air. From this point of view, the use of a pure slowly evaporating solvent (eg, N,N-dimethylformamide) seemed to be ideal. However, in our study, PLGA was less soluble in this type of solvent. Therefore, the abovementioned combination of quickly and slowly evaporating solvents was established in our study. In future experiments, we intend to use this combination in a Nanospider machine equipped with a bath-like vessel for the spun material instead of the experimental spike-like electrode used in this study. This "free liquid surface electrospinning" is expected to result in more effective production of nanofibrous meshes of excellent uniformity, controlled diameter of the nanofibers, and narrow fiber diameter distribution.

In addition to the properties of the polymer-solvent mixture, namely type and concentration of both polymer and solvent, evaporation of the solvent, type, size and concentration of the added nanoparticles, viscosity of the solution, and the forces pulling the nanofibers discussed above, other parameters are also important for successful electrospinning of nanofibers. In particular, these parameters include the voltage and the distance between the needle and target. During preparation of polycaprolactone nanofibers, the fiber length and diameter decreased with increasing voltage (10–20 kV), while the uniformity of the fibers increased.[51] On the other hand, in the case of superelastic polymer ink formulations, the viscoelastic nature of these polymer inks enables continuous electrospinning at a very low voltage of 200 V.[52] As for the distance between the needle and target, when this distance is short, the electrospun fibers tend to stick to the collector as well as to each other, which is due to incomplete solvent evaporation.[35] An increase in needle-collector distance represents a weaker electric field, a greater distance to be covered by the fibers and a longer flight time, presumably favoring the formation of thinner fibers. On the other hand, during electrospinning of poly(ethylene oxide), higher solvent evaporation led to a local increase of concentration and viscosity, and the viscoelastic forces opposing stretching caused an increase of fiber diameter with needle-collector distance.[49]

The number of initially adhering cells, their spreading area, their subsequent growth dynamics, and the numbers achieved on pure PLGA and composite PLGA-ND membranes in our study were similar. Although this is the first study on composite polymer-ND scaffolds used as growth supports for cells, and thus no comparison with studies by other authors is available, it is known that the addition of nanoparticles to polymeric nanofibrous scaffolds usually supports cell colonization of these materials. For example, on PLA-multiwalled carbon nanotube scaffolds, the number of human adipose-derived human mesenchymal stem cells on day 14 after seeding significantly exceeded the value on pure PLA fibers. This was attributed to the smaller diameter of PLA-multiwalled carbon nanotube fibers and smaller pores among them. In other words, there was a finer network which enabled the attachment of human mesenchymal stem cells at multiple focal points.[23] In our study, the pores among the PLGA-ND fibers were also significantly smaller than in pure PLGA membranes. Thus, the cells bridged over smaller gaps and were able to come into more intense contact with the fibers. In accordance with these findings, the cells on PLGA-ND formed more numerous and more homogeneously distributed talin-containing focal adhesion plaques than the

cells on pure PLGA membranes (Figure 8A and B). At the same time, these plaques were smaller (ie, finer) than those in cells on polystyrene dishes, particularly at the cell periphery. Streak-like and thick focal adhesion plaques have been considered as an artifact of the classical cell culture system, where the cells are cultivated on "two-dimensional" substrates such as polystyrene or glass under static conditions.[53] Focal adhesion plaques of this type do not occur in tissues in vivo or in an advanced cell culture system with cells on "three-dimensional" substrates, including nanofibrous scaffolds, and cultured under dynamic conditions. From this point of view, the fine focal adhesion plaques in cells on nanofibrous meshes in our study can be considered as more physiological and better reflecting the morphology of focal adhesions on cells under in vivo conditions.

Another reason for the better developed talin-containing focal adhesion plaques on PLGA-ND membranes may be better mechanical properties of these membranes compared with pure PLGA scaffolds. Mechanically resistant materials are less deformed by tractional forces produced by the actin cytoskeleton, and thus they can better stimulate the cell spreading and assembly of focal adhesion plaques.[54] In accordance with this, the rupture tests showed that PLGA-ND membranes were able to deform further and withstand a higher force than pure PLGA membranes. Two possible contributing factors to both these observations are the reinforcement of individual nanofibers by ND incorporation, which was demonstrated by transmission electron microscopy (Figure 2), and an increase in the number and strength of contacts between individual fibers by ND. Scanning electron microscopy images (Figure 1C and D) demonstrated that more material clusters were present in PLGA-ND membranes. It is conceivable that such clusters are reinforced by the presence of ND. Similarly, addition of nanodiamond has increased the hardness and stiffness of the polymer, polyvinyl alcohol, particularly in synergy with single-wall carbon nanotubes or graphene,[55] and PLA[33,46] Electrospun fibers of polyacrylonitrile also became harder and stiffer after incorporation of ND.[32] However, to the best of our knowledge, this study is the first to demonstrate reinforcement of electrospun PLGA nanofibers by ND. The addition of ND to polymers has been proposed to cause reinforcement by interaction between functional groups on nanodiamond surfaces with polymer chains[46] and an enhancement of polymer crystallinity.[46,55] FTIR analysis revealed band shifts which were small compared with those observed by Zhao et al.[46] One explanation is that the chemical interactions between PLGA and ND are weak. In this case, due to the weakness of these interactions, it would be expected that ND does not significantly increase the material crystallinity. This, in turn, would suggest that improved mechanical properties are due to an increased number of interfiber contacts in PLGA-ND membranes. Another explanation is that the concentration of ND is low at the surface and is thus not detected by FTIR, which is supported by the transmission electron microscopy images showing the presence of ND predominantly in the center of fibers. One cause for the "internalization" of ND is its poorer solubility compared with PLGA, leading to phase separation. Another factor is the lower size and therefore greater motility of the PLGA molecule compared with ND, allowing faster migration of PLGA to the fiber surface.

On the other hand, the more numerous and larger material clusters (often microsized) in the composite PLGA-ND membranes may hamper the adhesion, spreading, and growth of MG-63 cells on this material. In our earlier study, performed on bone MG-63 cells and vascular smooth muscle cells in cultures in carbon fiber-reinforced carbon composites, microsized irregularities distributed in microscale distances on the material surface exerted a negative influence on cell adhesion, spreading, and subsequent growth.[56]

Other nanoparticles have also been described to improve the mechanical properties (eg, their tensile modulus and tensile strength) and bioactivity of nanofibrous scaffolds made of synthetic polymers. These nanoparticles include multiwall carbon nanotubes,[23] bioglass nanofibers,[36] nanosized dispersed silica xerogel,[37] tricalcium phosphate,[13] and HAp.[9,14] However, in PLGA-HAp composites, the material reinforcement by HAp occurred only at lower HAp concentrations (1–10 wt%), whereas higher concentrations (20 wt%) led to a decrease in storage modulus and fiber-breaking.[14] On the other hand, a higher HAp concentration enhanced osteogenic differentiation of bone-forming cells. For example, the HAp component of PLGA/HAp composite nanofibers increased the activity of alkaline phosphatase, expression of osteogenic genes (eg, collagen, alkaline phosphatase, osteocalcin, bone sialoprotein), and calcium mineralization in human mesenchymal stem cells in cultures on these scaffolds.[15] In addition, the release of BMP-2 from fibrous PLGA/HAp composite scaffolds was accelerated with increasing HAp content (5–10 wt%).[12] These positive findings have been explained by the hydrophilicity of HAp, by increased adsorption of cell adhesion-mediating proteins from the serum of the culture medium on HAp-containing scaffolds, and by the more rigid and spacious scaffold structure.[12,15]

Mechanical properties and bioactivity of nanofibrous scaffolds made of conventional polymers (ie, PLA) have been markedly improved by copolymerization with polyaniline.

Recent publications by Gizdavic-Nikolaidis et al[20,21] showed that functionalized polyaniline/PLA nanofibrous blends not only allow mammalian cells to attach and proliferate, but also kill pathogenic bacteria cells, and are novel conductive materials that are potentially well suited for use as biocompatible scaffolds for tissue engineering and as antimicrobial wound dressings that have the advantage of being able to kill microorganisms without use of an antiseptic.

The size of the cell spreading area, and the cell proliferation and cell population densities achieved on both PLGA and PLGA-ND scaffolds in our study were significantly lower than the values on the bottom of polystyrene wells. This may be due to the relatively small diameter of both PLGA and PLGA-ND fibers (on average 218 nm and 270 nm, respectively), which limited the cell-material contact that is necessary for good colonization of a material with cells. In a study performed on NIH 3T3 fibroblasts in cultures on PLGA meshes, the cell spreading areas on meshes with fiber diameters of 140 nm and 760 nm were significantly lower than on continuous PLGA films, and were equal to the value on these films only at a fiber diameter of 3600 nm.[10] In a study by Kumbar et al,[11] who created PLGA fibers from 150 to 6000 nm in diameter (by electrospinning PLGA in increasing concentrations), the range of the fiber diameter optimal for spreading, proliferation, and collagen III gene expression in human skin fibroblasts was 350–1100 nm. These findings were attributed to the optimum range of the material surface wettability (which increased with increasing fiber diameter), and a favorable cell-fiber interaction.[11] The cell spreading on the nanofibrous membranes in our study may also be limited by the random orientation of the fibers in these scaffolds. It has been reported that increasing fiber orientation (from random to parallel) enlarged the cell spreading area.[10]

The increase in cell number on nanofibrous scaffolds in our study may also be reduced by lower viability of cells on these scaffolds in comparison with the values on the control polystyrene dishes. This lower cell viability may be due to limited cell-material contact and relatively small cell spreading areas. In anchorage-dependent cells, adequate contact with a material and spreading on it is decisive not only for proper functioning of the cells but primarily for survival of the cells. For example, human capillary endothelial cells cultured on fibronectin-coated islands larger than 1500 μm^2 spread and progressed through the cell cycle, whereas cells restricted to areas smaller than 500 μm^2 failed to extend and underwent apoptosis.[57]

In addition, on PLGA scaffolds loaded with ND, the cell viability on days 3 and 7 after seeding was lower than the cell viability on pure PLGA scaffolds. This may be attributed to a less favorable morphology of PLGA-ND meshes, ie, the presence of microsized clusters of ND, which could further hamper the cell-material contact. However, some adverse effects of the ND powder on cells also cannot be excluded. ND particles are generally considered to be noncytotoxic, nonimmunogenic, and nonallergenic. This is because there is no significant production of oxygen radicals by ND[26,27] or even because ND has antioxidative effects.[38] However, some authors have reported damaging effects of diamond nanoparticles on white and red blood cells in vitro and in vivo.[58,59] This has been explained by the relatively high concentrations (1 mg/mL or more) of diamond nanoparticles used in these studies. In addition, ND powders often contain impurities, mainly other forms of carbon, such as graphite[60] or iridium.[39] The ND powder used in our study was grayish in color, which suggests the presence of these impurities. In our earlier study, performed on nanocrystalline diamond films, the presence of other carbon forms, namely graphite and amorphous carbon, was also indicated by Raman spectroscopy.[28]

The size of the diamond particles was also important for their potentially damaging effects on cells. In cultures of HeLa cells, microsized diamond crystals (diameter approximately 1 μm) caused considerable stress to the cells and attenuated their growth and viability.[61] Microsized ND clusters in our PLGA-ND scaffolds might have similar effects, especially if they were released from the scaffolds and penetrated into the cells.

Nevertheless, cell viability above 90% can be considered as very high, comparable with the values in physiological cell populations, which also exhibit a certain cell turnover. In our earlier studies, focused on gender-related differences in the growth activity of rat aortic smooth muscle cells derived from male and female donors, cell loss (ie, spontaneous cell detachment often followed by cell death) in cultures of these cells on standard tissue culture polystyrene ranged from 3.0% ± 1.4% to 22.4% ± 1.7%.[62]

An important finding of this study was that the presence of diamond nanoparticles did not evoke any considerable inflammatory activation of osteoblast-like MG-63 cells and RAW 264.7 macrophages, as revealed by the concentrations of TNF-α in cell culture media and ICAM-1 in cell homogenates.

TNF-α is a cytokine involved in systemic inflammation and is a member of a group of cytokines that stimulate the acute phase reaction. It is produced mainly by activated macrophages, although it can be produced by other cell types as well, such as lymphoid cells, mast cells, endothelial cells,

cardiac myocytes, adipose tissue, fibroblasts, cells of the nervous system, and also MG-63 cells.[44,63] The release of TNF-α is highly stimulated by lipopolysaccharide, a component of the outer membrane of Gram-negative bacteria. [63,64]

ICAM-1, also referred to as CD54, is an immunoglobulin adhesion molecule in the cell membrane, which binds to β_2-integrin adhesion receptors on inflammatory cells (eg, leukocytes, monocytes, macrophages). It is expressed by leucocytes, macrophages, endothelial cells, and also by osteoblasts and osteoblast-like cell lines.[65] Its expression can be induced by cytokines (TNF-α) and is associated with osteoarthritis and osteoporosis.[66,67]

The concentration of TNF-α in the culture medium taken from MG-63 grown on PLGA-ND was significantly higher than in the media from pure PLGA, PLGA HAp, and control polystyrene cell culture wells. This increased cytokine production might be due to impurities in the ND powder, such as graphite and amorphous carbon.[68,69] On the other hand, the production of TNF-α by MG-63 cells in our study can be quantified as very low and almost at the limit of detection by the human TNF-α Quantikine ELISA kit. Even after intensive stimulation of MG-63 cells with bacterial lipopolysaccharide, the concentration of TNF-α in the culture medium still remained at the detection limit, which suggests low sensitivity of MG-63 cells to inflammatory activation. In accordance with this finding, MG-63 and other human osteoblast-like cells, ie, SaOS-2, did not produce significant levels of TNF-α even after infection with *Brucella abortus*. A significant increase in TNF-α production (almost 600 pg/mL of the culture medium) was achieved only in cocultures of these cells with human THP-1 monocytes.[45] When RAW 264.7 macrophage-like cells, which are much more sensitive to the inflammatory activation than MG 63 cells, were used, the concentration of TNF-α in the cell culture medium from PLGA-ND samples (about 26 pg/100,000 cells, which corresponded to about 237 pg/mL of the medium) was similar to that in the medium from PLGA samples, and even lower than in the medium from PLGA-HAp. For comparison, after stimulation of RAW 264.7 macrophages with hydrogel particles (0.03 to 3 vol%) the concentration of TNF-α reached about 1000 pg/mL of the culture medium, and after stimulation with 0.1 μg/mL of lipopolysaccharide for 24, it has reached more than 15,000 pg/mL.[44]

Although the concentration of TNF-α released by RAW 264.7 cells grown on PLGA membranes with HAp was significantly higher than in cells on pure PLGA, PLGA-ND, and polystyrene wells in our study, HAp is generally considered to be a material with a relatively low inflammatory potential. For example, RAW 264.7 macrophages in 24-hour cultures on a microfibrous composite of polyethylene terephthalate with 10 wt% of nanograde HAp released only 25 pg of TNF-α per mL of culture medium, while after 24 hours of stimulation of these cells with 10 μg/mL of lipopolysaccharide, TNF-α concentrations reached 566 pg/mL.[70]

In addition, the concentration of ICAM-1 in homogenates prepared from MG-63 or RAW 264.7 cells on PLGA-ND and PLGA-HAp membranes was also similar to that for cells on pure PLGA meshes and control polystyrene wells. Similar results were also obtained in our earlier studies on pure and boron-doped nanocrystalline diamond films.[28] Thus, it can be concluded that the immune activation of cells on nanofibrous PLGA-ND membranes is very low, which correlates well with studies reporting no or a very low (and not significant) inflammatory reaction of cells and tissues in contact with ND particles.[26,27,38] From this point of view, PLGA-ND composites seem to be a suitable material for bone tissue engineering.

Conclusion and further perspectives

Using an electrospinning technique, we constructed fibrous membranes made of pure PLGA and PLGA with 23 wt% of ND. The fiber diameter was 218 ± 4 nm and 270 ± 9 nm, and the area of the pores among the fibers was 1.28 ± 0.09 μm^2 in PLGA membranes and 0.46 ± 0.02 μm^2 in PLGA-ND membranes. Both pure PLGA and composite PLGA-ND membranes supported attachment, spreading, subsequent proliferation, and viability of human osteoblast-like MG-63 cells in cultures on these materials, although the cell numbers were lower than on the control polystyrene dishes. This could be attributed to relatively thin fibers and numerous microsized clusters in these membranes, which could limit the cell-material contact and hamper cell spreading. Nevertheless, our composite PLGA-ND scaffolds showed improved mechanical properties and did not evoke a considerable inflammatory response. Thus, after several improvements, the PLGA-ND scaffolds could be applied as carriers for cells in bone tissue engineering. Investigations on the osteogenic differentiation of the cells on these scaffolds are in progress.

Acknowledgments

This study was supported by grants from the Academy of Sciences of the Czech Republic (KAN 400480701 and IAAX00100902), the Czech Science Foundation (106/09/1000 and P108/11/0794), the European Union (MyJoint Project, FP-6 NEST 028861), and the Research Foundation Flanders. TELD is supported by a Research Foundation Flanders

postdoctoral fellowship. Robin Healey (Czech Technical University, Prague, Czech Republic) is gratefully acknowledged for his language revision of the manuscript.

Disclosure

The authors report no conflicts of interest in this work.

References

1. Webster TJ, Ergun C, Doremus RH, Siegel RW, Bizios R. Specific proteins mediate enhanced osteoblast adhesion on nanophase ceramics. *J Biomed Mater Res*. 2000;51:475–483.
2. Price RL, Waid MC, Haberstroh KM, Webster TJ. Selective bone cell adhesion on formulations containing carbon nanofibers. *Biomaterials*. 2003;24:1877–1887.
3. Boland ED, Matthews JA, Pawlowski KJ, Simpson DG, Wnek GE, Bowlin GL. Electrospinning collagen and elastin: preliminary vascular tissue engineering. *Front Biosci*. 2004;9:1422–1432.
4. Meinel AJ, Kubow KE, Klotzsch E, et al. Optimization strategies for electrospun silk fibroin tissue engineering scaffolds. *Biomaterials*. 2009;30:3058–3067.
5. Park YJ, Kim KH, Lee JY, et al. Immobilization of bone morphogenetic protein-2 on a nanofibrous chitosan membrane for enhanced guided bone regeneration. *Biotechnol Appl Biochem*. 2006;43:17–24.
6. Sargeant TD, Rao MS, Koh CY, Stupp SI. Covalent functionalization of NiTi surfaces with bioactive peptide amphiphile nanofibers. *Biomaterials*. 2008;29:1085–1098.
7. Stylianopoulos T, Bashur CA, Goldstein AS, Guelcher SA, Barocas VH. Computational predictions of the tensile properties of electrospun fiber meshes: effect of fiber diameter and fiber orientation. *J Mech Behav Biomed Mater*. 2008;1:326–335.
8. Pektok E, Nottelet B, Tille JC, et al. Degradation and healing characteristics of small-diameter poly(epsilon-caprolactone) vascular grafts in the rat systemic arterial circulation. *Circulation*. 2008;118:2563–2570.
9. Jeong SI, Ko EK, Yum J, Jung CH, Lee YM, Shin H. Nanofibrous poly(lactic acid)/hydroxyapatite composite scaffolds for guided tissue regeneration. *Macromol Biosci*. 2008;8:328–338.
10. Bashur CA, Dahlgren LA, Goldstein AS. Effect of fiber diameter and orientation on fibroblast morphology and proliferation on electrospun poly(D,L-lactic-co-glycolic acid) meshes. *Biomaterials*. 2006;27:5681–5688.
11. Kumbar SG, Nukavarapu SP, James R, Nair LS, Laurencin CT. Electrospun poly(lactic acid-co-glycolic acid) scaffolds for skin tissue engineering. *Biomaterials*. 2008;29:4100–4107.
12. Nie H, Soh BW, Fu YC, Wang CH. Three-dimensional fibrous PLGA/HAp composite scaffold for BMP-2 delivery. *Biotechnol Bioeng*. 2008;99:223–34.
13. Schneider OD, Loher S, Brunner TJ, et al. Cotton wool-like nanocomposite biomaterials prepared by electrospinning: in vitro bioactivity and osteogenic differentiation of human mesenchymal stem cells. *J Biomed Mater Res B Appl Biomater*. 2008;84:350–362.
14. Jose MV, Thomas V, Johnson KT, Dean DR, Nyairo E. Aligned PLGA/HA nanofibrous nanocomposite scaffolds for bone tissue engineering. *Acta Biomater*. 2009;5:305–315.
15. Lee JH, Rim NG, Jung HS, Shin H. Control of osteogenic differentiation and mineralization of human mesenchymal stem cells on composite nanofibers containing poly[lactic-co-(glycolic acid)] and hydroxyapatite. *Macromol Biosci*. 2010;10:173–182.
16. Pamula E, Filova E, Bacakova L, Lisa V, Adamczyk D. Resorbable polymeric scaffolds for bone tissue engineering: the influence of their microstructure on the growth of human osteoblast-like MG 63 cells. *J Biomed Mater Res A*. 2009;89:432–443.
17. Huang Z-M, Zhang Y-Z, Kotaki M, Ramakrishna S. A review on polymer nanofibers by electrospinning and their applications in nanocomposites. *Compos Sci Technol*. 2003;63:2223–2253.
18. Vasita R, Katti DS. Nanofibers and their applications in tissue engineering. *Int J Nanomedicine*. 2006;1:15–30.
19. Tan J, Saltzman WM. Biomaterials with hierarchically defined micro- and nanoscale structure. *Biomaterials*. 2004;25:3593–3601.
20. Gizdavic-Nikolaidis M, Ray S, Bennett JR, Easteal AJ, Cooney RP. Electrospun functionalized polyaniline copolymer-based nanofibers with potential application in tissue engineering. *Macromol Biosci*. 2010;10:1424–1431.
21. Gizdavic-Nikolaidis MR, Bennett JR, Swift S, Ray S, Bowmaker G. Electrospun poly(aniline-co-ethyl 3-aminobenzoate)/poly(lactic acid) nanofibers and their potential in biomedical application. *J Polym Sci A Polym Chem*. 2011;49:4902–4910.
22. Kim HW, Lee HH, Chun GS. Bioactivity and osteoblast responses of novel biomedical nanocomposites of bioactive glass nanofiber filled poly(lactic acid). *J Biomed Mater Res A*. 2008;85:651–663.
23. McCullen SD, Stevens DR, Roberts WA, et al. Characterization of electrospun nanocomposite scaffolds and biocompatibility with adipose-derived human mesenchymal stem cells. *Int J Nanomedicine*. 2007;2:253–263.
24. Sargent LM, Reynolds SH, Castranova V. Potential pulmonary effects of engineered carbon nanotubes: in vitro genotoxic effects. *Nanotoxicology*. 2010;4:396–408.
25. Wang L, Luanpitpong S, Castranova V, et al. Carbon nanotubes induce malignant transformation and tumorigenesis of human lung epithelial cells. *Nano Lett*. 2011;11:2796–2803.
26. Schrand AM, Huang H, Carlson C, et al. Are diamond nanoparticles cytotoxic? *J Phys Chem B*. 2007;111:2–7.
27. Amaral M, Dias AG, Gomes PS, et al. Nanocrystalline diamond: in vitro biocompatibility assessment by MG 63 and human bone marrow cells cultures. *J Biomater Res A*. 2008;87:91–99.
28. Grausova L, Kromka A, Burdikova Z, et al. Enhanced growth and osteogenic differentiation of human osteoblast-like cells on boron-doped nanocrystalline diamond thin films. *PLoS One*. 2011;6:e20943.
29. Liu KK, Wang CC, Cheng CL, Chao JI. Endocytic carboxylated nanodiamond for the labeling and tracking of cell division and differentiation in cancer and stem cells. *Biomaterials*. 2009;30:4249–4259.
30. McDevitt MR, Chattopadhyay D, Jaggi JS, et al. PET imaging of soluble yttrium-86-labeled carbon nanotubes in mice. *PLoS One*. 2007;2:e907.
31. Ruggiero A, Villa CH, Bander E, et al. Paradoxical glomerular filtration of carbon nanotubes. *Proc Natl Acad Sci U S A*. 2010;107:12369–12374.
32. Behler KD, Stravato A, Mochalin V, Korneva G, Yushin G, Gogotsi Y. Nanodiamond-polymer composite fibers and coatings. *ACS Nano*. 2009;3:363–369.
33. Zhang Q, Mochalin VN, Neitzel I, et al. Fluorescent PLLA-nanodiamond composites for bone tissue engineering. *Biomaterials*. 2011;32:87–94.
34. Dos Santos AM, Dierck J, Troch M, Podevijn M, Schacht E. Production of continuous electrospun mats with improved mechanical properties. *Macromol Mater Eng*. 2011;296:637–644.
35. Huang L, Nagapudi K, Apkarian RP, Chaikof EL. Engineered collagen-PEO nanofibers and fabrics. *J Biomater Sci Polym Ed*. 2001;12:979–993.
36. Jo JH, Lee EJ, Shin DS, et al. In vitro/in vivo biocompatibility and mechanical properties of bioactive glass nanofiber and poly(epsilon-caprolactone) composite materials. *J Biomed Mater Res B Appl Biomater*. 2009;91:213–220.
37. Jang TS, Lee EJ, Jo JH, et al. Fibrous membrane of nano-hybrid poly-L-lactic acid/silica xerogel for guided bone regeneration. *J Biomed Mater Res B Appl Biomater*. 2011 Nov 21. [Epub ahead of print.]
38. Mitura S, Mitura K, Niedzielski P, Louda P, Danilenko V. Nanocrystalline diamond, its synthesis, properties and applications. *J AMME*. 2006;16:9–16.

39. Kromka A, Rezek B, Remes Z, et al. Formation of continuous nanocrystalline diamond layer on glass and silicon at low temperatures. *Chem Vapor Depos*. 2008;14:181–186.
40. Kromka A, Rezek B, Kalbacova M, et al. Diamond seeding and growth of hierarchically structured films for tissue engineering. *Adv Eng Mater*. 2009;11:B71–B76.
41. Kromka A, Babchenko O, Kozak H, Rezek B, Vanecek M. Role of polymers in CVD growth of nanocrystalline diamond films on foreign substrates. *Phys Stat Sol B*. 2009;246:2654–2657.
42. Janicki P, Boeuf S, Steck E, Egermann M, Kasten P, Richter W. Prediction of in vivo bone forming potency of bone marrow-derived human mesenchymal stem cells. *Eur Cell Mater*. 2011;21:488–507.
43. Maheshwari G, Brown G, Lauffenburger DA, Wells A, Griffith LG. Cell adhesion and motility depend on nanoscale RGD clustering. *J Cell Sci*. 2000;113:1677–1686.
44. Yim ES, Zhao B, Myung D, et al. Biocompatibility of poly(ethylene glycol)/poly(acrylic acid) interpenetrating polymer network hydrogel particles in RAW 264.7 macrophage and MG-63 osteoblast cell lines. *J Biomed Mater Res A*. 2009;91:894–902.
45. Delpino MV, Fossati CA, Baldi PC. Proinflammatory response of human osteoblastic cell lines and osteoblast-monocyte interaction upon infection with Brucella spp. *Infect Immun*. 2009;77:984–895.
46. Zhao Y-Q, Lau K-T, Kim J-K, Xu C-L, Zhao D-D, Li H-L. Nanodiamond/poly (lactic acid) nanocomposites: Effect of nanodiamond on structure and properties of poly (lactic acid). *Composites: Part B*. 2010;41:646–653.
47. Jose MV, Thomas V, Dean DR, Nyairo E. Fabrication and characterization of aligned nanofibrous PLGA/collagen blends as bone tissue scaffolds. *Polymer*. 2009;50:3778–3785.
48. Deitzel JM, Kleinmeyer J, Harris D, Beck Tan NC. A review on polymer nanofibers by electrospinning and their applications in nanocomposites. *J Nanosci Nanotechnol*. 2009;9:3535–3545.
49. Henriques C, Vidinha R, Botequim D, Borges JP, Silva JA. A systematic study of solution and processing parameters on nanofiber morphology using a new electrospinning apparatus. *J Nanosci Nanotechnol*. 2009;9:3535–3545.
50. Liang D, Luu YK, Kim K, Hsiao BS, Hadjiargyrou M, Chu B. In vitro non-viral gene delivery with nanofibrous scaffolds. *Nucleic Acids Res*. 2005;33:e170.
51. Beachley V, Wen X. Effect of electrospinning parameters on the nanofiber diameter and length. *Mater Sci Eng C Mater Biol Appl*. 2009;29:663–668.
52. Bisht GS, Canton G, Mirsepassi A, et al. Controlled continuous patterning of polymeric nanofibers on three-dimensional substrates using low-voltage near-field electrospinning. *Nano Lett*. 2011;11:1831–1837.
53. Hu J, Liu X, Ma PX. Induction of osteoblast differentiation phenotype on poly(L-lactic acid) nanofibrous matrix. *Biomaterials*. 2008;29:3815–3821.
54. Engler A, Bacakova L, Newman C, Hategan A, Griffin M, Discher D. Substrate compliance versus ligand density in cell on gel responses. *Biophys J*. 2004;86:617–628.
55. Prasad KE, Das B, Maitra U, Ramamurty U, Rao CN. Extraordinary synergy in the mechanical properties of polymer matrix composites reinforced with 2 nanocarbons. *Proc Natl Acad Sci U S A*. 2009;106:13186–13189.
56. Bacakova L, Stary V, Kofronova O, Lisa V. Polishing and coating carbon fiber-reinforced carbon composites with a carbon-titanium layer enhances adhesion and growth of osteoblast-like MG63 cells and vascular smooth muscle cells in vitro. *J Biomed Mater Res*. 2001;54:567–578.
57. Huang S, Chen CS, Ingber DE. Control of cyclin D1, p27(Kip1), and cell cycle progression in human capillary endothelial cells by cell shape and cytoskeletal tension. *Mol Biol Cell*. 1998;9:3179–3193.
58. Puzyr AP, Neshumaev DA, Tarskikh SV, Makarskaia GV, Dolmatov VI, Bondar VS. Destruction of human blood cells upon interaction with detonation nanodiamonds in experiments in vitro. *Biofizika*. 2005;50.101–106. Russian.
59. Karpukhin AV, Avkhacheva NV, Yakovlev RY, et al. Effect of detonation nanodiamonds on phagocyte activity. *Cell Biol Int*. 2011;35:727–733.
60. Krueger A. New carbon materials: biological applications of functionalized nanodiamond materials. *Chemistry*. 2008;14:1382–1390.
61. Fucikova A, Valenta J, Pelant I, Brezina V. Novel use of silicon nanocrystals and nanodiamonds in biology. *Chem Pap*. 2009;63:704–708.
62. Bacakova L, Mares V, Lisa V, Bottone MG, Pellicciari C, Kocourek F. Sex-related differences in the migration and proliferation of rat aortic smooth muscle cells in short and long term culture. *In Vitro Cell Dev Biol*. 1997;33:410–413.
63. Huang TH, Lu YC, Kao CT. Low-level diode laser therapy reduces lipopolysaccharide (LPS)-induced bone cell inflammation. *Lasers Med Sci*. October 16, 2011. [Epub ahead of print.]
64. Takaoka Y, Matsuura S, Boda K, Nagai H. The effect of mesoporphyrin on the production of cytokines by inflammatory cells in vitro. *Jpn J Pharmacol*. 1999;80:33–40.
65. Kurokouchi K, Kambe F, Kikumori T, et al. Effects of glucocorticoids on tumor necrosis factor alpha-dependent activation of nuclear factor kappaB and expression of the intercellular adhesion molecule 1 gene in osteoblast-like ROS17/2.8 cells. *J Bone Miner Res*. 2000;15:1707–1715.
66. Shi Q, Benderdour M, Lavigne P, Ranger P, Fernandes JC. Evidence for two distinct pathways in TNFalpha-induced membrane and soluble forms of ICAM-1 in human osteoblast-like cells isolated from osteoarthritic patients. *Osteoarthritis Cartilage*. 2007;15:300–308.
67. Tanaka Y, Maruo A, Fujii K, et al. Intercellular adhesion molecule 1 discriminates functionally different populations of human osteoblasts: characteristic involvement of cell cycle regulators. *J Bone Miner Res*. 2000;15:1912–1923.
68. Whitehead GS, Grasman KA, Kimmel EC. Lung function and airway inflammation in rats following exposure to combustion products of carbon-graphite/epoxy composite material: comparison to a rodent model of acute lung injury. *Toxicology*. 2003;183:175–197.
69. Li Q, Xia YY, Tang JC, Wang RY, Bei CY, Zeng Y. In vitro and in vivo biocompatibility investigation of diamond-like carbon coated nickel-titanium shape memory alloy. *Artif Cells Blood Substit Immobil Biotechnol*. 2011;39:137–142.
70. Dimitrievska S, Petit A, Ajji A, Bureau MN, Yahia L. Biocompatibility of novel polymer-apatite nanocomposite fibers. *J Biomed Mater Res A*. 2008;84:44–53.

International Journal of Pharmaceutics 427 (2012) 311–319

Contents lists available at SciVerse ScienceDirect

International Journal of Pharmaceutics

journal homepage: www.elsevier.com/locate/ijpharm

A perivascular system releasing sirolimus prevented intimal hyperplasia in a rabbit model in a medium-term study

Ivo Skalský[a], Ondrej Szárszoi[a], Elena Filová[b,c,*], Martin Pařízek[b,c], Andriy Lytvynets[b], Jana Malušková[a], Alena Lodererová[a], Eduard Brynda[d], Věra Lisá[b], Zuzana Burdíková[b], Martin Čapek[b], Jan Pirk[a], Lucie Bačáková[b,c]

[a] Institute for Clinical and Experimental Medicine, Videnska 1958/9, 140 21 Prague 4, Czech Republic
[b] Institute of Physiology, Academy of Sciences of the Czech Republic, v.v.i., Videnska 1083, 142 20 Prague 4, Czech Republic
[c] Centre for Cardiovascular Research, Videnska 1083, 142 20 Prague 4, Czech Republic
[d] Institute of Macromolecular Chemistry, Academy of Sciences of the Czech Republic, v.v.i., Heyrovsky Sq. 2, 162 06 Prague 6, Czech Republic

ARTICLE INFO

Article history:
Received 11 December 2011
Received in revised form 12 February 2012
Accepted 13 February 2012
Available online 21 February 2012

Keywords:
Sirolimus
Perivascular wrap
Controlled drug release
Autologous vein
Intimal hyperplasia

ABSTRACT

The main complication of aortocoronary reconstruction with vein grafts is restenosis in the course of time. The aim was to assess the effect of a periadventitial polyester mesh releasing sirolimus on intimal hyperplasia of autologous grafts. We implanted *v. jugularis ext.* into *a. carotis communis* in rabbits. The vein graft was either intact, or was wrapped with a pure polyester mesh, or with a sirolimus-releasing mesh. Three and six weeks after surgery, the veins were subjected to standard histological staining and the thicknesses of the *tunica intima*, the media and the intima–media complex were measured. Wrapping the vein with a mesh releasing sirolimus or with a pure mesh decreased the thickness of the intima in comparison with a vein graft by 73 ± 11% or 73 ± 8% after 3 weeks, and by 73 ± 9% or 59 ± 12% after 6 weeks, respectively. Sirolimus-releasing meshes reduced the thickness of the media by 65 ± 9% and 20 ± 12% after 3 and 6 weeks. The thickness of the intima–media complex in grafts with sirolimus-releasing meshes decreased by 60 ± 6% and 30 ± 13% in comparison with pure PES meshes, after 3 and 6 weeks, respectively. A periadventitial polyester mesh releasing sirolimus has the potential to become an effective device in preventing vein graft restenosis.

1. Introduction

Occlusion of the graft lumen is considered as the main complication in the follow-up of patients after aortocoronary vein bypass grafting. This occurs almost in 15% within the first year, and increases up to 50% of occluded veins after 10 years (Motwani and Topol, 1998). In patent vein grafts, 7% show signs of degeneration after 1 year and 77% after 10 years (Fitzgibbon et al., 1996).

Due to a mechanical mismatch after implantation, an autologous vein graft in arterial circulation is prone to remodelling. This is accompanied by excessive proliferation of vascular smooth muscle cells (VSMC), which can migrate into the intima and produce extracellular matrix. Graft remodelling thus results in intimal hyperplasia and graft stenosis. In clinical practice, autologous graft stenosis is usually dealt with (after percutaneous transluminal angioplasty) by inserting stents, often loaded with antiproliferative drugs, e.g. sirolimus-eluting stents (Cypher™, Cordis J&J, NJ), or paclitaxel-eluting stents, into the graft lumen (Colombo and Iakovou, 2004). However, the use of stents is limited by the relatively complicated process for inserting them, by increased mechanical strain on the vessel wall, and by local damage to the endothelium and VSMC leading to reactivation of VSMC growth and restenosis of the vessel. In addition, the stents can be released and can move inside the vessel (Jeremy et al., 2004). Similar problems are associated with drug-releasing polymeric films covering the luminal surface of a vessel, e.g. hydrogel films loaded with paclitaxel (Livnat et al., 2005).

From this point of view, an external drug delivering system, i.e. placed on the adventitial surface of the vascular graft, seems to be more advantageous. Periadventitial delivery of heparin from matrices placed adjacent to rat carotid arteries was successfully

* Corresponding author at: Department of Biomaterials and Tissue Engineering, Institute of Physiology of the Academy of Sciences of the Czech Republic, Videnska 1083, 142 20, Prague 4-Krc, Czech Republic. Tel.: +420 296443742; fax: +420 241062488.
E-mail addresses: ivo.skalsky@ikem.cz (I. Skalský), ondrej.szarszoi@ikem.cz (O. Szárszoi), filova@biomed.cas.cz (E. Filová), parizek@biomed.cas.cz (M. Pařízek), litvinec@biomed.cas.cz (A. Lytvynets), jana.maluskova@ikem.cz (J. Malušková), alena.lodererova@ikem.cz (A. Lodererová), brynda@imc.cas.cz (E. Brynda), lisa.v@biomed.cas.cz (V. Lisá), burdikova@biomed.cas.cz (Z. Burdíková), capek@biomed.cas.cz (M. Čapek), japx@ikem.cz (J. Pirk), lucy@biomed.cas.cz (L. Bačáková).

0378-5173/$ – see front matter © 2012 Elsevier B.V. All rights reserved.
doi:10.1016/j.ijpharm.2012.02.023

used in the case of heparin, which is well known to attenuate proliferation of VSMC (Edelman et al., 1990). Other antiproliferative drugs have also been found to inhibit neointimal hyperplasia of vein grafts in animal experimental models after local extraluminal application, for example suramin, C-type natriuretic peptide, cilostazol, and sirolimus (Schachner et al., 2004a,b; Hu et al., 1999; Fujinaga et al., 2004). Especially sirolimus (Rapamycin) is a drug well known for its potent antiproliferative action. In addition to its application in drug-eluting stents (Colombo and Iakovou, 2004), this macrocyclic lactone has also been used clinically for immunosuppressive therapy after organ transplantation (Roque et al., 2001). The mechanism of its antiproliferative effect is very complex (Yakupoglu and Kahan, 2003; Regar et al., 2001), involving mainly blocking the transition from the G1 phase to the S phase of the cell cycle by interacting with a specific target protein (mTOR, mammalian target of sirolimus) and inhibiting its activation. Our earlier study focused on the kinetics of the release of sirolimus from polyester meshes *in vitro* (Filova et al., 2011). In these experiments, the release of sirolimus from polyester meshes coated with a degradable copolymer loaded with sirolimus was detected for several weeks. The proliferation of VSMC in culture plates was inhibited if sirolimus-releasing meshes were used. For the present study, we assumed that the graft wall of the vessel would be thin enough to enable diffusion of sirolimus released from a periadventitially placed mesh into the tunica media, so that VSMC proliferation could be inhibited.

It has been suggested that thickening of the intima of the vein grafts increased in the distended regions, where the grafts were subjected to low flow velocity (Dobrin, 1995). Thus, we expected that in addition to the antiproliferative effects of sirolimus, our meshes would also reduce the risk of graft restenosis by minimizing distension of the graft. From this point of view, encouraging results were obtained in an *in vivo* study performed on sheep. Sheathing the implanted vein grafts with a pressure-resistant polyester (torlen/dacron) mesh significantly reduced intima thickening in these grafts compared to control untreated vein grafts within 12 weeks after implantation (Krejca et al., 2002). Taken together, the mesh placed around the graft should serve as a mechanical support for the graft wall, which increases the resistance of the graft against high pressure, decreases tangential stress and retards graft degeneration (Jeremy et al., 2004; Krejca et al., 2002).

We therefore developed a novel combined device composed of two synergistically effective components: a mechanically supportive polyester mesh, and an antiproliferative drug (sirolimus). Our work extended previous preliminary study about early intimal changes in the autologous vein grafts (Skalsky et al., 2011). We evaluated the dynamics of the vascular wall changes during a medium-term examination in vein grafts in rabbits, wrapped with a sirolimus-releasing polyester mesh. Sustained release of sirolimus within a period of several weeks suppressed VSMC proliferation for the time necessary for re-endothelialization of the graft. These effects reduced autologous graft remodelling and the need for subsequent treatment.

2. Materials and methods

2.1. Materials

Polyester mesh (CHS 50, PES mesh) was obtained from VUP Joint-Stock Co., Brno, CR. Purasorb PLC 7015, and a grade copolymer of L-lactide and ε-caprolactone (70/30 molar ratio, inherent viscosity midpoint of 1.5 dl/g) was purchased from PURAC biomaterials. Sirolimus (Rapamycin from Streptomyces hygroscopicus, Cat. No. R0395) was obtained from Sigma–Aldrich (Germany).

2.2. Mesh impregnation

Polyester mesh impregnation was described in a previous paper (Filova et al., 2011). Briefly, the mesh was coated with a solution containing 5.2 mg of sirolimus and 36.4 mg of purasorb in 1 ml of chlorobenzene–ethanol (1.75:1, v/v). It was dried, and then coated for a second time with the same solution and dried again. Finally, the impregnated mesh contained 0.14 mg of sirolimus per cm^2. The mesh was dried out in a vacuum oven for 3 weeks, and was then sterilized with ethylene oxide (sirolimus-releasing PES mesh).

2.3. Implantation procedures

The experiments on laboratory animals were approved by the Authorization No. 48/2009 issued by the Chief Hygienist of the Czech Republic, the Ministry of Health of the Czech Republic according to the law No. 246/1992 of the Collection and in compliance with further regulations, for the protection of animals against suffering, and in accordance with the Project of Experiments and the statement of the Ethical Committee. Male Giant Chinchilla rabbits (3.0–3.5 kg; $n = 65$; Table 1) were anaesthetized using an intramuscular injection of ketamine hydrochloride (30.0 mg/kg). Anaesthesia was maintained with isoflurane (2.5–3.0%), inhaled through a mask. Heparin (300 IU/kg) was given intravenously to the animals. The operative procedure was performed with an aseptic technique with operating glasses (magnification 2.5×). The right external jugular vein and the right common carotid artery were exposed through a vertical midline cervical incision. The vein bypass grafts were constructed using an anastomotic cuff technique (Jiang et al., 2004) (Fig. 1).

A segment of the external jugular vein approximately 2 cm in length was harvested for an autologous reversed-vein graft; the segments were also used as the graft_0 control group. The polymer cuffs were prepared from a 4F endovascular catheter (Terumo Medical Corp, Elkton, MD). The jugular vein ends were passed through a cuff, everted, and fixed using 8-0 monofilament polypropylene silk. The common carotid artery was clamped distally and proximally, and the lumen was then exposed using a small arteriotomy, and the cuffed, reversed vein ends were inserted. A second 8-0 polypropylene silk was used to ligature (i.e. secure) the artery around the cuff on both sides. The back wall of the carotid artery between the cuffs was excised to allow a vein graft extension (an untreated autologous graft). Finally, a pure PES mesh or a sirolimus-releasing PES mesh was put on around the vein graft and fixed by polypropylene 8/0 on the side (autologous graft wrapped with a PES mesh, an autologous graft wrapped with sirolimus-releasing PES mesh) (Jiang et al., 2004).

Groups of animals were euthanized 3 and 6 weeks after implantation. The specimens were equally divided in the middle of the vein graft (without the cuff segment) to obtain equal parts for histology and for immunohistochemistry.

2.4. Histology and immunohistochemistry

The venous grafts were divided into two parts. One part was fixed in 10% formalin and then it was embedded in paraffin. The second part was embedded in Sakura Finetek Tissue Tek© Cryomold holders and Sakura Finetek Tissue Tek© OCT Compound (both from Sakura Finetek, Tokyo, Japan). The samples were subsequently frozen in 2-methylbutane (Fluka Chemika, Buchs, Switzerland) cooled by liquid nitrogen, and then stored at −80 °C.

2.5. Histological analysis

The samples embedded in paraffin were cut into 3–4 μm sections and stained with haematoxylin-eosin, Van Gieson with

Table 1
Number of CD4+ cells, CD8+ cells, plasmocytes, macrophages and Fe particles in transverse histological sections through untreated autologous grafts (Graft), grafts wrapped with a pure PES mesh (PES mesh) or with a sirolimus-releasing PES mesh (Sirolimus) 3 and 6 weeks (3w, 6w) after implantation. Mean ± SEM from 7 to 10 rabbits (10 microscopic fields per animal). Olympus BX41 microscope, magnification 600×, numbers of rabbits with any kind of thrombus, with oblitering or recanalized thrombi are also given. Non-parametric Kruskal–Wallis one-way analysis of variance (ANOVA) was used.

	1. Graft 0w	2. Graft 3w	3. PES mesh 3w	4. Sirolimus 3w	5. Graft 6w	6. PES mesh 6w	7. Sirolimus 6w
No of animals	12	7	9	9	10	8	10
CD4+	[#] vs. 2 [**] vs. 3 1.1 ± 0.4	[#] vs. 1 [#] vs. 4 50.7 ± 19.9	[**] vs. 1 [*] vs. 4 30.0 ± 2.6	[#] vs.2 [*] vs. 3 0.6 ± 0.4	10.7 ± 1.1	12.8 ± 4.5	12.8 ± 3.8
CD8+	[**] vs. 3 [#] vs. 2, 6 0.6 ± 0.2	[#] vs. 1 27.5 ± 17.3	[#] vs. 5, 7 [**] vs. 1, 4 17.0 ± 2.4	[**] vs.3 0.8 ± 0.4	[#] vs. 3 2.9 ± 0.3	[#] vs. 1 10.0 ± 3.4	[#] vs. 3 1.8 ± 0.5
Plasmocytes	[**] vs. 5 0 ± 0	4.6 ± 1.8	3.2 ± 1.6	[*] vs. 5 0 ± 0	[*] vs. 4, [#] vs.7 [**] vs. 1 6.9 ± 2.0	2.5 ± 0.7	[#] vs. 5 0.4 ± 0.4
Macrophages	[**] vs. 7 0 ± 0	1.6 ± 1.1	5.7 ± 4.0	[*] vs. 7 0 ± 0	2.8 ± 1.3	1.2 ± 0.6	[**] vs. 1 [*] vs. 4 13.2 ± 9.6
Fe particles	[*] vs. 5 0 ± 0	[#] vs. 5 0 ± 0	[*] vs. 5 0 ± 0	[*] vs. 5 0 ± 0	[*] vs. 1, 3, 4, 7[#] vs. 2 120.8 ± 79.1	5.1 ± 5.1	[*]vs. 5 0 ± 0
Rabbits with any kind/oblitering/ recanalized thrombus	0/0/0	3/0/1	5/1/3	5/0/1	5/3/0	5/1/2	3/0/0

[#] $p < 0.05$ in comparison with the sample labelled with the same number (statistical significance).
[*] $p < 0.01$ in comparison with the sample labelled with the same number (statistical significance).
[**] $p < 0.001$ in comparison with the sample labelled with the same number (statistical significance).

elastica, von Kossa and Pearl's stains. The sections were taken from the midportion of the graft to avoid tissue that may have reacted to the suture material. Each section stained with Van Gieson with elastica was photographed using an Olympus IX 51 microscope and a DP 70 digital camera.

2.6. Immunohistochemical staining

Information concerning the primary antibodies used for the immunohistochemical analyses is shown in Table 2.

2.6.1. Formol fixed, paraffin embedded tissues

Immunohistochemistry was performed on 4 μm-thick paraffin sections using a three-step indirect method. The slides were deparaffinized in xylene and rehydrated in graded ethanol. After deparaffinization and rehydration, the slides were cooked in a microwave oven using 0.01 M citrate buffer pH 6.0 (detection of smooth muscle actin), or EDTA buffer pH 8.0 (detection of PCNA) for target retrieval, or proteinase K was applied (detection of macrophages and CD31). Endogenous peroxidase was blocked by 0.3% H_2O_2 in 70% methanol for 30 min. Endogenous biotin was blocked with the biotin-blocking system (Dako, Glostrup, Denmark). The tissues were then preincubated with a 10% horse serum (Vector laboratories, Burlingame, CA) for 20 min to prevent nonspecific binding and FcR binding. The primary antibody was applied for 30 min RT or incubated overnight at 4 °C (CD31). Detection of the monoclonal antibody was performed using biotinylated horse anti-mouse IgG (Vector laboratories, Burlingame, CA, USA) diluted 200× for 30 min. The specimens were then incubated with RTU Vectastain Elite ABC Reagent for 30 min. Finally, the specimens

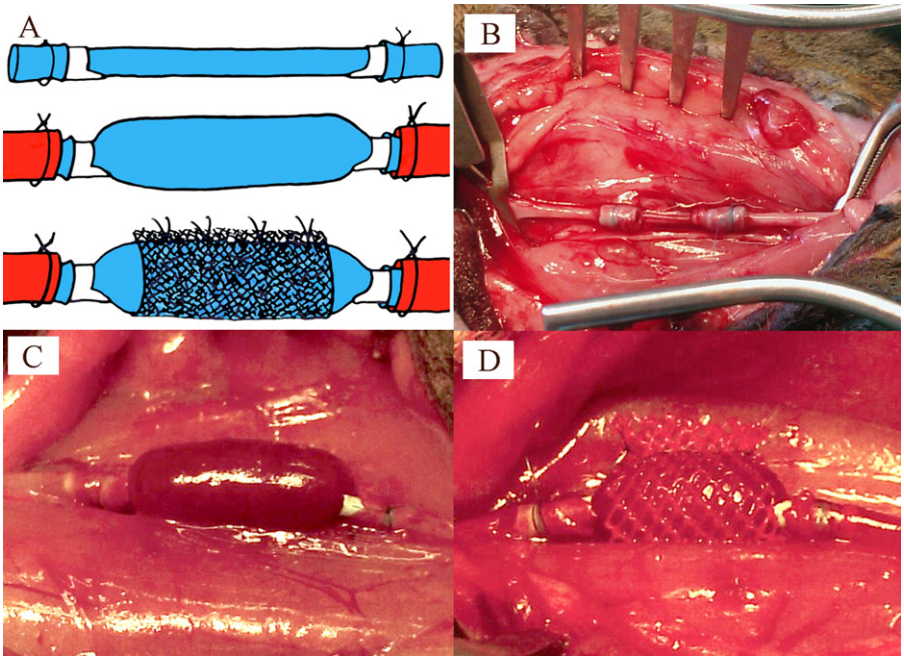

Fig. 1. Scheme of the surgical technique for graft implantation (A), the autologous vein before a clip release (B), the dilated vein graft (C) and the dilated vein graft wrapped with a PES mesh (D).

Table 2
The list of monoclonal antibodies used for immunohistochemical staining.

Specificity	Origin	Company	Dilution	Clone
CD4+ cells	Mouse	Novus Biological, CO, USA	50×	KEN-4
CD8+ cells	Mouse	LifeSpan Biosciences, WA, USA	100×	NA
α-Smooth muscle actin	Mouse	Sigma, MO, USA	900×	1A4
Macrophage	Mouse	Abcam, UK	200×	MAC387
CD31	Mouse	Abcam, UK	20×	JC/70A
PCNA	Mouse	Dako, Denmark	6000×	PC 10

were stained with Dako Liquid DAB+ Substrate-Chromogen System (Dako, Glostrup, Denmark) for 5 min, and were counterstained with Harris's haematoxylin before they were embedded in Entellan (both from Merck, Germany).

2.6.2. Snap-frozen tissue samples

Immunohistochemistry was performed on sections 8 μm in thickness, using a three-step indirect method. The sections were fixed for 10 min in cold acetone. Following this, the sections were rinsed in 0.2% Triton X-100 and phosphate-buffered saline, and endogenous biotin was blocked with a biotin-blocking system (Dako, Glostrup, Denmark). The tissues were then incubated in 10% horse serum, after which a primary antibody (anti-CD4/CD8) was applied for 60 min. In addition, endogenous peroxidase was blocked in 0.3% H_2O_2 and 70% methanol for 30 min. The specimen was incubated with a secondary biotinylated horse anti-mouse antibody (Vector Lab, Burlingame, CA, USA), followed by incubation with RTU Vectastain Elite ABC Reagent (Vector Lab, Burlingame, CA, USA). Finally, the specimens were incubated for 5 min with the Dako Liquid DAB+ Substrate-Chromogen System (Dako, Glostrup, Denmark), counterstained with Harris's haematoxylin and embedded in Entellan (both from Merck, Germany).

The total numbers of CD4+ cells, CD8+ cells, neutrophils, plasmocytes, eosinophils, macrophages, foreign body giant cells, Fe and Ca particles were counted in the entire cross-section of the vein grafts in 10 microscopic fields per rabbit at magnification 600×.

2.7. Thickness of intima, media, media–intima complex, media–intima ratio

The following parameters were measured: the thickness of the intima from the endothelial surface to the inner border of the tunica media, the thickness of the media from the inner border of tunica media to the border between tunica media and adventitia, and the thickness of the media–intima complex from the endothelial surface to the media–adventitia border. Data was collected from 32 to 84 measurements per rabbit in 12–28 microscopic fields, using the MeasureStackLines plug-in module of Ellipse Software (ViDiTo Systems, Slovakia). The media/intima ratio was calculated from the measured values. The mean value and the Standard Error of Mean (mean ± SEM) were calculated for each vein and for each animal group. Grafts with thrombosis were not measured.

2.8. Statistical methods

Non-parametrical one-way Kruskal–Wallis ANOVA was used for a statistical evaluation of the histology and histomorphometry. Two-way ANOVA and the Tukey studentized range method were used for the data analyses of the thickness of the intima, media, intima/media complex and the media/intima ratio. The variables were tested for normality by Shapiro and Wilk's statistics. Since normality was rejected, the logarithmic transformation was applied. The effects of time, drug, and the interaction between time and drug were tested, and $p < 0.05$ was considered to be significant.

3. Results

3.1. Histology and immunohistochemical staining

3.1.1. Tunica intima

In all experimental groups of animals, the luminal surface of the venous graft was covered by a layer of endothelial cells (Figs. 2 and 3). In some grafts, thrombi were observed on the luminal surface of tunica intima (Table 1). Some thrombi entirely obliterated the graft lumen, while others were only parietal or recanalized, but no significant differences were found among the rabbit groups. However, there was a significant difference in the thickness of the intima among the samples (see also below in Section 3.3). Focally, smooth muscle cells were observed in the neointima, especially in samples from animals without the application of sirolimus.

3.1.2. Tunica media

In all groups, the adaptation process of vein grafts to arterial pressure led to the formation of multiple smooth muscle cells layers, which resulted in thickening of the media (Fig. 3; see also below in Section 3.3). This was accompanied by an increased number of PCNA+ cells (Fig. 2; see also below in Section 3.2). In the venous autograft with the sirolimus-releasing mesh, the infiltration of CD4+ and CD8+ cells was remarkably decreased in the vessel wall (i.e. complex of intima, media and adventitia) compared to the untreated autologous graft and the graft wrapped with a PES mesh after 3 weeks (Table 1, Fig. 4).

The number of plasmocytes and macrophages was very small in all groups. There were only sporadic neutrophils and eosinophils in the venous grafts (data not shown). After 6 weeks, a lower number of plasmocytes was found in veins with a sirolimus-releasing mesh compared to the untreated autologous graft. However, in veins with a sirolimus-releasing mesh, the number of macrophages increased significantly between the 3rd week and the 6th week, although they were similar in number to those in both control groups after 6 weeks (Table 1). No calcium particles were found in any of the groups. No infectious wound complications were observed in any of the groups of animals. One rabbit died during the operation, and two rabbits due to systemic infection.

3.1.3. Tunica adventicia

Histological staining revealed the presence of PES meshes and sirolimus-releasing PES meshes in the adventitia of the vein grafts. In all groups, the distribution of immunocompetent cells, i.e. plasmocytes, CD4+ and CD8+ cells, was similar to the distribution of these cells in the tunica media (Fig. 4A), see Section 3.1.2 (Table 1). Small deposits of iron were sometimes observed, probably as a histological correlate of haematoma resorption (Fig. 4B). In addition, in groups with a PES mesh and a sirolimus-releasing PES mesh, foreign-body giant cells were observed around the meshes (Fig. 4C and D).

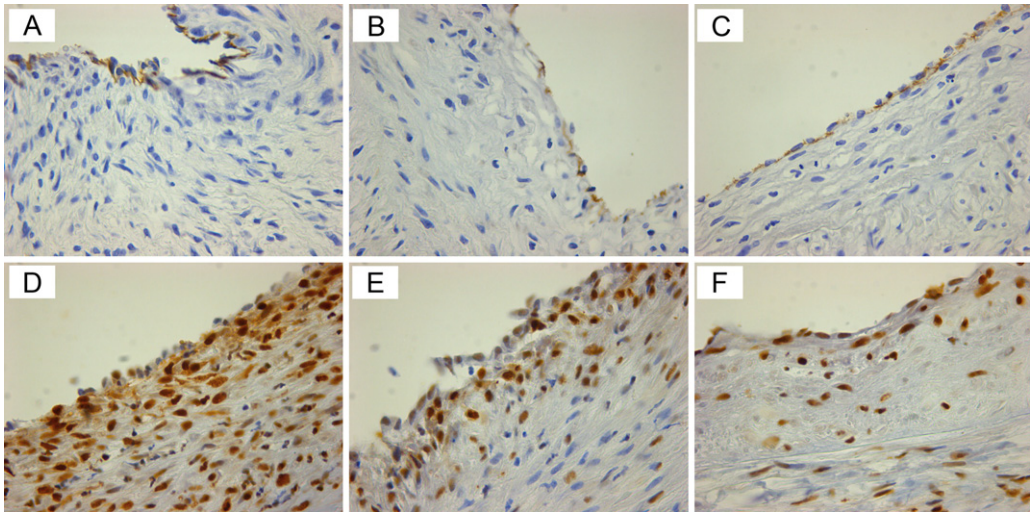

Fig. 2. Immunohistochemical staining of CD31 (A–C) and proliferating cell nuclear antigen (PCNA, D–F) in an untreated autologous graft (A, D), an autologous graft wrapped with a PES mesh (B, E), an autologous graft wrapped with a sirolimus-releasing PES mesh (C, F) 3 weeks after implantation into rabbits, Olympus BX41 microscope original magnification 400×, positively stained cells are brown. (For interpretation of the references to colour in this figure legend, the reader is referred to the web version of this article.)

3.2. Proliferating cell nuclear antigen (PCNA)

Most of the PCNA+ cells were found in the media and intima (Figs. 2 and 5), and fewer in the adventitia. The highest number of PCNA+ cells was observed in the control untreated grafts 3 weeks after implantation (graft_3w). After 3 weeks, wrapping the vein graft with a pure PES mesh reduced the number of PCNA+ cells by 59 ± 15%, while wrapping with sirolimus-releasing PES meshes reduced the number by 84 ± 13%. After 6 weeks, the number of PCNA+ cells decreased significantly in the control untreated graft (graft_6w); however, the number did not change in grafts wrapped with a pure PES mesh or with a sirolimus-releasing mesh.

3.3. Thickness of the intima, media, media–intima complex, and the media/intima ratio

The intima measurements (Fig. 6A) after 3 weeks showed the highest intima thickness value in the control graft. In grafts wrapped with a PES mesh or with a sirolimus-releasing mesh, the thickness of the intima was reduced by 73 ± 8% and 73 ± 11%, respectively, compared to the untreated graft.

Between the 3rd and 6th weeks, the intimal thickness of the untreated autologous grafts, the grafts with a pure PES mesh and the grafts with a sirolimus-releasing PES mesh remained constant. After 6 weeks, the relative reduction of the thickness of the intima in the grafts wrapped with a PES mesh or with a sirolimus-releasing PES mesh was 59 ± 12% and 73 ± 9%, respectively, in comparison to the untreated graft. The sirolimus-releasing meshes had a significantly stronger effect reducing intimal hyperplasia than the pure PES meshes after 6 weeks.

The increase in media thickness (Fig. 6B) was significantly reduced by 65 ± 9% by the use of sirolimus-releasing meshes after 3 weeks of implantation. Concurrently, a pure PES mesh did not influence the hyperplasia of the tunica media compared to the control untreated autologous graft, at both time intervals. After 6 weeks, the media was significantly thinner by 20 ± 12% in grafts wrapped with a sirolimus releasing PES mesh than in the untreated autologous grafts. The thickness of the intima–media complex

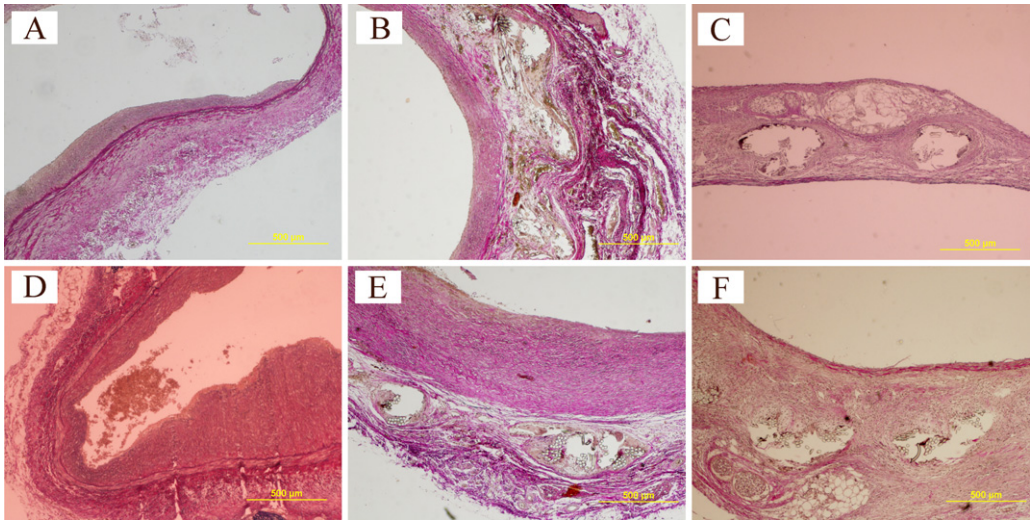

Fig. 3. An autologous vein graft A, D), an autologous vein graft wrapped with a polyester mesh (B, E) and an autologous vein graft wrapped with a polyester mesh releasing sirolimus (C, F) after 3 (A–C) and 6 weeks (D–F) in rabbits, van Gieson and elastica staining, objective 4×, scale bar = 500 μm, Olympus IX51 microscope, DP70 digital camera.

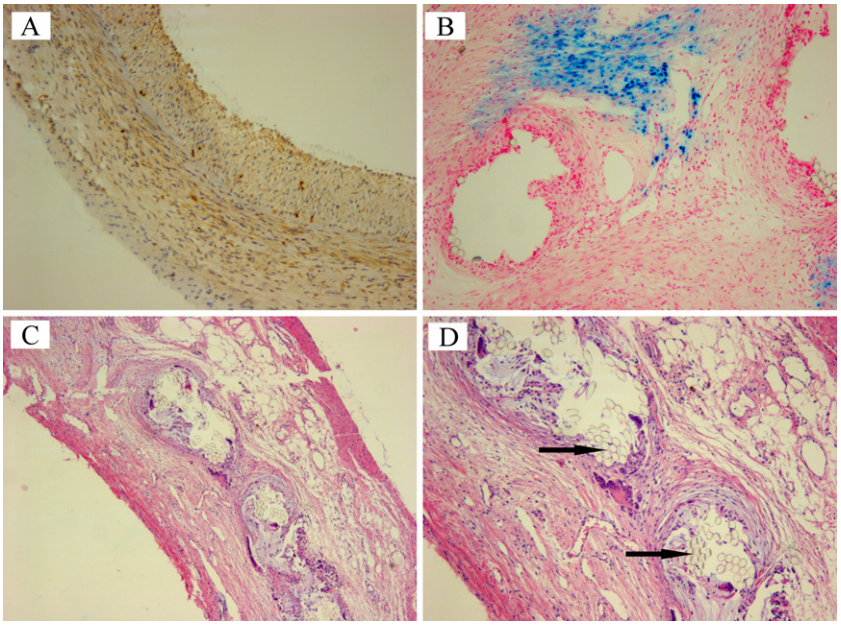

Fig. 4. Immunohistochemical staining of CD4 in an untreated autologous graft after 3-week implantation in a rabbit (A), Pearl's staining of iron (B) in an autologous graft wrapped with a sirolimus-releasing PES mesh after 3-week implantation in a rabbit, and haematoxylin-eosin staining of an autologous graft wrapped with a sirolimus-releasing PES mesh after 3-week implantation in a rabbit (C and D), magnification 50× (A, C), 200× (B) and 100× (D), Olympus BX41 microscope; CD4+ cells are stained brown (A), Fe is stained blue (B), arrows (D) indicate PES mesh fibres grown in the vein graft; the foreign-body giant cells are localized around the PES mesh fibres. (For interpretation of the references to colour in this figure legend, the reader is referred to the web version of this article.)

(Fig. 6C) was remarkably reduced by the sirolimus-releasing mesh by 76 ± 5% and 37 ± 9% in comparison with the control grafts after 3 and 6 weeks, respectively. At 3 weeks, a pure PES mesh reduced thickening of the intima–media complex by 41 ± 6% compared to the untreated autologous graft.

The control autologous grafts and the sirolimus treated graft after 3 weeks had an intima to media ratio that was similar to the ratio in a healthy vein, i.e. graft_0. After 3 weeks, the sirolimus releasing mesh was able to keep a media/intima ratio similar to that of graft_0. After 6 weeks, selective thickening of the media caused an increase in the media/intimal ratio in a graft wrapped with sirolimus-releasing meshes, probably due to the minimal concentration of sirolimus in the meshes at this time interval [14]. The highest media/intima ratio was observed in grafts wrapped with a pure PES mesh after 3 and 6 weeks. In these groups the ratio was higher than the ratio of the untreated autologous graft.

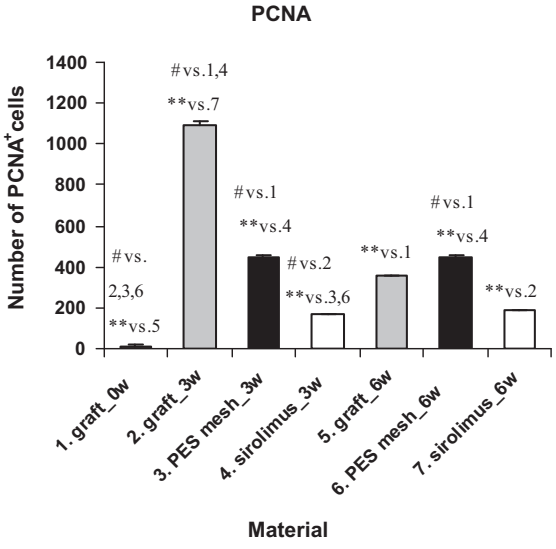

Fig. 5. The number of proliferating cell nuclear antigen-positive (PCNA+) cells in an untreated autologous vein graft (*graft*), an autologous vein graft wrapped with a polyester mesh (*PES mesh*), and an autologous vein graft wrapped with a polyester mesh releasing sirolimus (*sirolimus*), after 3 and 6 weeks (3w, 6w) in rabbits. The values are presented as mean ± SEM (standard error of mean). Two-way ANOVA and a Tukey pairwise comparison were used for statistical analyses. Statistical significance: $^{*}p \leq 0.01$ and $^{\#}p < 0.05$ in comparison with the sample labelled with the same number.

4. Discussion

In the present study, we created a unique periadventitial system with controlled release of the antiproliferative drug sirolimus to prevent neointimal hyperplasia in the vein graft interposed to the arterial system in rabbits. In addition, our study confirmed the hypothesis of the synergistic effects of a PES mesh and sirolimus on vein wall remodelling.

Several experimental and clinical studies have investigated the effects of external wall support on reducing the vessel wall stress and inhibiting neointimal proliferation (Mehta et al., 1998). The external torlen/dacron mesh tubing around an autologous vein graft in sheep retarded overgrowth of both the intima and the media within 12 weeks; the effect was especially pronounced in the intima (Krejca et al., 2002). The external wrap acts as a barrier against distension of the vein graft. The polyester periadventitial mesh works in the same way as the external elastic membrane of native arterial vessels, and allows them to withstand higher pressures in arterial circulation. It has been suggested that haemodynamic forces, especially excessively high wall shear stress, promote intimal hyperplasia. The wall thickness in grafts tends to adapt to the same value as the wall thickness in the grafted artery, which indicates that wall thickening occurs to normalize the tangential wall stress (Dobrin et al., 1989). While shear stress is a dominant regulator of lumen caliber, wall tension is a more critical determinant of wall thickness. Animal models indicate that there is a structurally optimal lumen radius/wall thickness ratio to support arterial pressure with minimal wall stress (Owens, 2010).

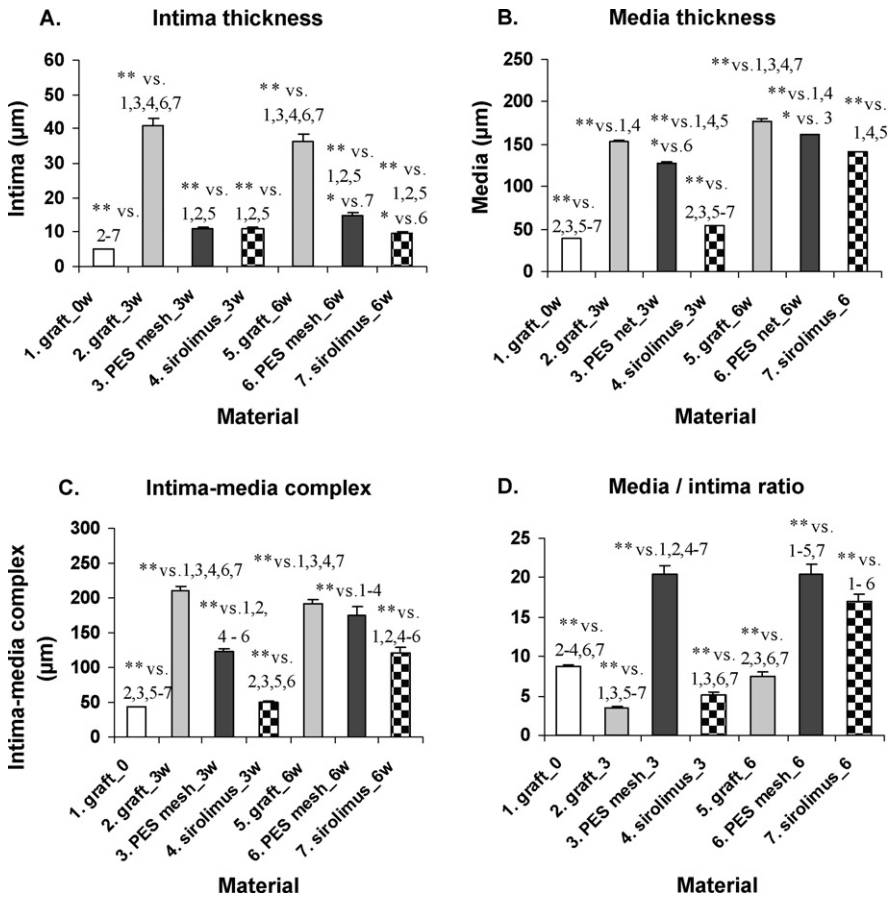

Fig. 6. The thickness of the intima (A), the media (B), and the intima–media complex (C) of an untreated autologous vein graft (*graft*), an autologous vein graft wrapped with a polyester mesh (*PES mesh*), and an autologous vein graft wrapped with a polyester mesh releasing sirolimus (*sirolimus*), after 3 (A–D) and 6 weeks (3w, 6w) in rabbits (B–D); media/intima ratio (D). The values are presented as mean ± SEM (standard error of mean). The Tukey studentized range method was used for the statistical analyses; $^{**}p \leq 0.01$ and $^{*}p \leq 0.05$ in comparison with the sample labelled with the same number.

The adventitia plays an important role in the neointimal formation mechanism (Shi et al., 1996; Scott et al., 1996). Mechanical injury of the vessel induces an adventitial angiogenic response. It has been suggested that adventitial myofibroblasts play a role in proliferation, in synthesizing growth factors and finally in migration into the neointima. Applying the antiproliferative drug from the outer space of the vessel lumen has the advantage of hitting the target area for administering the drug in a controlled manner.

In our study, both a PES mesh and a sirolimus-releasing PES mesh significantly reduced intimal thickness in comparison with the control untreated grafts 3 and 6 weeks after implantation. Between the 3rd and 6th weeks, there was no difference in intima thickness in all groups.

There is no convincing evidence of the durability and the maximal effective period of external sheaths or wraps, due to the unfavourable inflammatory response to the synthetic material used as a permanent mechanical support (Bunt, 1983). In addition, biodegradable materials may cease to fit, and may allow the vein graft to expand under arterial pressure. Then the increased level of circumferential wall stress would not be controlled, due to the loss of mechanical support. The mechanical support in our study was provided by a mesh made from polyester yarns. A yarn 90 µm in width was formed by fibres 17.5 µm in diameter; the area of an individual hole in the mesh was approximately 0.44 mm^2. This material was used on the basis on the results of previously published studies of the porosity, flexibility, biocompatibility and non-inflammatory response (Mehta et al., 1998; Hinrichs et al., 1994). Macroporosity is crucial for the efficacy of external stents in reducing neointima formation in porcine vein grafts. In addition, macroporous stents allow adventitial microvessels to connect with the vasculature outside the stent, thereby potentially improving oxygenation. Although external stenting is highly effective in reducing neointima formation after vein grafting, the properties of the stent material necessary for this effect have not been defined (Georgie et al., 2001). Non-degradable wraps could elicit long-term mechanical damage, especially in coronary artery bypass grafting, where the moving heart will be directly juxtaposed to an external wrap. New types of biodegradable wraps could provide a future option for solving this problem.

Another important role of the external periadventitial wrap developed in our study is in delivering sirolimus to the vein wall. Sirolimus is used as immunosuppressant for patients with organ transplants. This drug has been observed to inhibit IL-2 induced T cell proliferation (Ballou and Lin, 2008). This can explain the reduced numbers of CD4+ and CD8+ cells that we observed in the graft wall wrapped with a sirolimus-releasing mesh after 3 weeks in rabbits. After 6 weeks, the difference among the groups of rabbits disappeared, probably due to the kinetics of sirolimus release from the purasorb coating. In our earlier *in vitro* study, 67% of the sirolimus was released after 11 days of incubation in a phosphate-saline buffer (Filova et al., 2011).

The counts of other cells in our grafts, such as macrophages, plasmocytes, neutrophils and eosinophils, were very low, and their distribution was similar to that in normal tissues. A slightly increased number of macrophages is associated with the presence of foreign material, i.e. a PES mesh. The foreign-body giant

cells correlate with tissue reaction to the presence of a PES mesh.

The presence of thrombi in all tested groups of grafts probably resulted from the activation of blood coagulation due to damage to the endothelium during surgery and expansion of the graft lumen by relatively high blood pressure in the venous graft interposed into the arterial bed. This expansion then exposed tissues underlying the endothelium to the blood stream. A second reason might be blood coagulation due to reduced blood flow in the vein graft. Sirolimus did not increase the incidence of thrombi in either of the time intervals.

Sirolimus inhibits vascular smooth muscle cell migration and proliferation, and decreases the reocclusion of coronary arteries following angioplasty (Moses et al., 2003). There is a significant inhibitory effect of sirolimus on the proliferation of endothelial cells (Liuzzo et al., 2005). Regeneration of the injured endothelium after surgery depends on growth factor, such as FGF, VEGF, PDGF, and other molecules derived from endothelial cells or circulating cells. Sirolimus inhibits FGF-2 stimulated proliferation of human endothelial cells. Endothelium re-establishment is completed in the range of weeks after extensive injury. We observed a confluent layer of endothelial cells in the lumen of all vein grafts after 3 and 6 weeks. Due to the final position of the periadventitial wrap in the tunica adventitia, smooth muscle cells in the vicinity of the sirolimus-releasing mesh were exposed to high sirolimus concentrations, while distant endothelial cells were affected by a lower sirolimus concentration. Earlier findings that there was an increased rate of apoptosis in the graft adventitia and a lower rate of apoptosis in the neointima after perivascular application of pluronic gel with rapamycin may also be explained by the sirolimus concentration gradient (Schachner et al., 2005).

In our experiments, the vein grafts were wrapped after dilatation in the arterial system. In another study (Hinrichs et al., 1994), they were wrapped before dilatation of the vein graft, which prevents intimal tears; however, similar results were observed in the thickness of the intima–media complex after 3 and 6 weeks.

In rabbits, the reduction of intimal hyperplasia depended on the sirolimus dosage in stents containing 60–200 μg of sirolimus (Suzuki et al., 2001). The sirolimus concentration used in our study was 140 μg/cm^2, and a maximum of 3 cm^2 of PES mesh was used per graft. Reduced thickness of the tunica intima and also the tunica media was observed in veins wrapped with a sirolimus-releasing mesh after 3 and 6 weeks. The effective concentration of sirolimus necessary for inhibiting smooth muscle cell growth is relatively low (IC 50 = 5 ng/ml) (Owen et al., 2010), and allows a sufficient amount of the drug to be dispersed for long-term release (in the range of 4–6 weeks). The content of sirolimus in Cypher^{TM} stents is in the range from 70 to 300 μg (Venkatraman and Boey, 2007). 100 or 200 μg of sirolimus was applied in a pluronic gel into the perivascular space on a model of interposition of the inferior vena cava into the common carotid artery in mice. After 1 and 2 weeks, but not after 4 and 6 weeks, a significant decrease in intima thickness was observed only in the group with a higher sirolimus concentration (Schachner et al., 2004a). Our sirolimus-releasing mesh decreased intimal hyperplasia to the non-wrapped graft by 73 ± 11% and 73 ± 9% after 3 and 6 weeks, respectively. A perivascular wrap prepared from poly(ε-caprolactone) with rapamycin (sirolimus) reduced the thickness of the intima by 76% after 3 weeks (Pires et al., 2005). Rapamycin-eluting homogeneous films made of copolymer of L-lactide and ε-caprolactone with 8 μg, 80 μg, and 800 μg (i.e. 1.4, 14 and 140 μg/cm^2; Kawatsu et al., 2007) of the drug were applied externally to a femoral vein graft anastomosed to the proximal femoral artery in end-to-end fashion in dogs. After 4 weeks, only the highest rapamycin concentration significantly attenuated intimal hyperplasia compared to the control. This was accompanied by a decreased number of PCNA positive cells in the neointima and adventitia.

The intima thickness values were almost the same in the grafts wrapped with a sirolimus-releasing mesh after 3 and 6 weeks. This is in agreement with the observation that maximum initial proliferation accrual of both smooth muscle and endothelial cells appears during the first weeks after implantation of a vein graft into the arterial bed. The cell proliferation returns to standard values after 12 weeks (Kalra and Miller, 2000; Zwolak et al., 1987). According to the described time course of intimal hyperplasia, it is probable that the intitial burst release of sirolimus during the first week can have a stronger protective effect against the development of intimal hyperplasia than a stable but lower sirolimus concentration released during the following weeks.

5. Conclusions

We have developed a novel device with a sustained release of sirolimus, made of a polyester mesh coated with a degradable copolymer of L-lactide and ε-caprolactone loaded with sirolimus, and we have evaluated its effect on inhibiting intimal hyperplasia *in vivo* in a rabbit model. After wrapping the mesh around the autologous vein graft, sirolimus was released into the vascular wall through the tunica adventitia. This perivascular sirolimus-releasing wrap significantly decreased the thickness of the intima and prevented neointimal hyperplasia of the autologous vein graft in a rabbit model within 6 weeks.

The mechanical support of the wrapped periadventitial polyester mesh and the antiproliferative effect of the released sirolimus have a joint synergetic effect on preventing thickening of the intima. Thus this system is a promising method for prolonging the "lifetime" of the vein grafts in arterial circulation.

Both the sirolimus content in the polymer coated mesh and the kinetics of its release seem to be favourable, since there is no intimal hyperplasia in the rabbit model in the course of the study. In clinical practice, this device could be effective in preventing restenosis of autologous vein grafts.

Acknowledgements

The research presented here has been supported by the Grant Agency of the Ministry of Health of the CR (project no. NR9358), by the Centre for Cardiovascular Research (project no. 1M6798582302), by Research program no. AV0Z50110509, and by the Czech Science Foundation (projects no. 102/08/0691 and P108/11/0794). We also thank Dr. Zdeněk Plichta (Institute of Macromolecular Chemistry, Acad. Sci. CR) for mesh coating. Mr. Robin Healey (Czech Technical University, Prague, CR) is gratefully acknowledged for his language revision of the manuscript.

References

Ballou, L.M., Lin, R.Z., 2008. Rapamycin and mTOR kinase inhibitors. J. Chem. Biol. 1, 27–36.

Bunt, T.J., 1983. Synthetic vascular graft infections. I. Graft infections. Surgery 93, 733–746.

Colombo, A., Iakovou, I., 2004. Drug-eluting stents: the new gold standard for percutaneous coronary revascularisation. Eur. Heart J. 25, 895–897.

Dobrin, P.B., Littoy, F.N., Endean, E.D., 1989. Mechanical factors predisposing to intimal hyperplasia and medial thickening in autogenous vein grafts. Surgery 105, 393–400.

Dobrin, P.B., 1995. Mechanical factors associated with the development of intimal and medial thickening in vein grafts subjected to arterial pressure. A model of arteries exposed to hypertension. Hypertension 26, 38–43.

Edelman, E.R., Adams, D.H., Karnovsky, M.J., 1990. Effect of controlled adventitial heparin delivery on smooth muscle cell proliferation following endothelial injury. Proc. Natl. Acad. Sci. U. S. A. 87, 3773–3777.

Filova, E., Parizek, M., Olsovská, J., Kamenik, Z., Brynda, E., Riedel, T., Skalsky, I., Szarszoi, O., Vandrovcova, M., Lisa, V., Suchy, T., Bacaková, L., 2011. Perivascular sirolimus-delivery system. Int. J. Pharm. 404, 94–101.

Fitzgibbon, G.M., Kafka, H.P., Leach, A.J., Keon, W.J., Hooper, G.D., Burton, J.R., 1996. Coronary bypass graft fate and patient outcome: angiographic follow-up of 5,065 grafts related to survival and reoperation in 1,388 patients during 25 years. J. Am. Coll. Cardiol. 28, 616–626.

Fujinaga, K., Onoda, K., Yamamoto, K., Imanaka-Yoshida, K., Takao, M., Shimono, T., Shimpo, H., Yoshida, T., Yada, I., 2004. Locally applied cilostazol suppresses neointimal hyperplasia by inhibiting tenascin-c synthesis and smooth muscle cell proliferation in free artery grafts. J. Thorac. Cardiovasc. Surg. 128, 357–363.

Georgie, S.J., Izzat, M.B., Gadsdon, P., Johnson, J.L., Yim, A.P., Wan, S., Newby, A.C., Angelini, G.D., Jeremy, J.Y., 2001. Macro-porosity is necessary for the reduction of neointimal and medial thickening by external stenting of porcine saphenous vein bypass grafts. Atherosclerosis 155, 329–336.

Hinrichs, W.L.J., Zweep, H.P., Satoh, S., Feijen, J., Wildevuur, C.R.H., 1994. Supporting, microporous, elastomeric, degradable prostheses to improve the arterialization of autologous vein grafts. Biomaterials 15, 83–91.

Hu, Y., Zou, Y., Dietrich, H., Wick, G., Xu, Q., 1999. Inhibition of neointima hyperplasia of mouse vein grafts by locally applied suramin. Circulation 100, 861–868.

Jeremy, J.Y., Bulbulia, R., Johnson, J.L., Gadsdon, P., Vijayan, V., Shukla, N., Smith, F.C.T., Angelini, G.D., 2004. A bioabsorbable (polyglactin), nonrestrictive, external sheath inhibits porcine saphenous vein graft thickening. J. Thorac. Cardiovasc. Surg. 127, 1766–1772.

Jiang, Z., Wu, L., Miller, B.L., Goldman, D.R., Fernandez, C.M., Abouhamze, Z.S., Ozaki, C.K., Berceli, S.A., 2004. A novel vein graft model: adaptation to differential flow environments. Am. J. Physiol. Heart Circ. Physiol. 286, H240–H245.

Kalra, M., Miller, V.M., 2000. Early remodeling of saphenous vein grafts: proliferation, migration, and apoptosis of adventitial and medial cells occur simultaneously with changes in graft diameter and blood flow. J. Vasc. Res. 37, 576–584.

Kawatsu, S., Oda, K., Saiki, Y., Tabata, Y., Tabayashi, K., 2007. External application of rapamycin-eluting film at anastomotic sites inhibits neointimal hyperplasia. Ann. Thorac. Surg. 84, 560–567.

Krejca, M., Skarysz, J., Szmagala, P., Plewka, D., Nowaczyk, G., Plewka, A., Bochenek, A., 2002. A new outside stent—does it prevent vein graft intimal proliferation? Eur. J. Cardiothorac. Surg. 22, 898–903.

Liuzzo, J.P., Ambrose, J.A., Coppola, J.T., 2005. Sirolimus- and taxol-eluting stents differ towards intimal hyperplasia and re-endothelialization. J. Invasive Cardiol. 17, 497–502.

Livnat, M., Beyar, R., Seliktar, D., 2005. Endoluminal hydrogel films made of alginate and polyethylene glycol: physical characteristics and drug-eluting properties, J. Biomed. Mater. Res. A 75, 710–722.

Mehta, D., George, S.J., Jeremy, J.Y., Izzat, M.B., Southgate, K.M., Bryan, A.J., Newby, A.C., Angelini, G.D., 1998. External stenting reduces long-term medial and neointimal thickening and platelet derived growth factor expression in a pig model of arteriovenous bypass grafting. Nat. Med. 4, 235–239.

Moses, J.W., Leon, M.B., Popma, J.J., Fitzgerald, P.J., Holmes, D.R., O'Shaughnessy, C., Caputo, R.P., Kereiakes, D.J., Williams, D.O., Teirstein, P.S., Jaeger, J.L., Kuntz, R.E., 2003. Sirolimus-eluting stents versus standard stents in patients with stenosis in a native coronary artery. N. Engl. J. Med. 349, 1315–1323.

Motwani, J.G., Topol, E.J., 1998. Aortocoronary saphenous vein graft disease: pathogenesis, predisposition, and prevention. Circulation 97, 916–931.

Owen, S.C., Li, H., Sanders, W.G., Cheung, A.K., Terry, C.M., 2010. Correlation of tissue drug concentrations with in vivo magnetic resonance images of polymer drug depot around arteriovenous graft. J. Control. Release 146, 23–30.

Owens, C.D., 2010. Adaptive changes in autogenous vein grafts for arterial reconstruction: clinical implications. J. Vasc. Surg. 51, 736–746.

Pires, N.M.M., van der Hoeven, B.L., de Vries, M.R., Havekes, L.M., van Vlijmen, B.J., Hennink, W.E., Quax, P.H., Jukema, J.W., 2005. Local perivascular delivery of anti-restenotic agents from a drug-eluting poly(ε-caprolactone) stent cuff. Biomaterials 26, 5386–5394.

Regar, E., Sianos, G., Serruys, P.W., 2001. Stent development and local drug delivery. Br. Med. Bull. 59, 227–248.

Roque, M., Reis, E.D., Cordon-Cardo, C., Taubman, M.B., Fallon, J.T., Fuster, V., Badimon, J.J., 2001. Effect of p27 deficiency and rapamycin on intimal hyperplasia: in vivo and in vitro studies using a p27 knockout mouse model. Lab. Invest. 81, 895–903.

Schachner, T., Oberhuber, A., Zou, Y., Tzankov, A., Ott, H., Laufer, G., Bonatti, J., 2005. Rapamycin treatment is associated with an increased apoptosis rate in experimental vein grafts. Eur. J. Cardiothorac. Surg. 27, 302–306.

Schachner, T., Zou, Y., Oberhuber, A., Tzankov, A., Mairinger, T., Laufer, G., Bonatti, J., 2004a. Local application of rapamycin inhibits neointimal hyperplasia in experimental vein grafts. Ann. Thorac. Surg. 77, 1580–1585.

Schachner, T., Zou, Y., Oberhuber, A., Mairinger, T., Tzankov, A., Laufer, G., Ott, H., Bonatti, J., 2004b. Perivascular application of C-type natriuretic peptide attenuates neointimal hyperplasia in experimental vein grafts. Eur. J. Cardiothorac. Surg. 25, 585–590.

Scott, N.A., Cipolla, G.D., Ross, C.E., Dunn, B., Martin, F.H., Simonet, L., Wilcox, J.N., 1996. Identification of a potential role for the adventitia in vascular lesion formation after balloon overstretch injury of porcine coronary arteries. Circulation 93, 2178–2187.

Shi, Y., Pieniek, M., Fard, A., O'Brien, J., Mannion, J.D., Zalewski, A., 1996. Adventitial remodeling after coronary arterial injury. Circulation 93, 340–348.

Skalský, I., Filová, E., Szárszoi, O., Pařízek, M., Lytvynets, A., Malušková, J., Lodererová, A., Brynda, E., Lisá, V., Burdíková, Z., Čapek, M., Pirk, J., Bačáková, L., 2011. A periadventitial sirolimus-releasing mesh decreased intimal hyperplasia in a rabbit model. Physiol. Res. 60, 585–588.

Suzuki, T., Kopia, G., Hayashi, S., Bailey, L.R., Llanos, G., Wilensky, R., Klugherz, B.D., Papandreou, G., Narayan, P., Leon, M.B., Yeung, A.C., Tio, F., Tsao, P.S., Falotico, R., Carter, A.J., 2001. Stent-based delivery of sirolimus reduced neointimal formation in a porcine coronary model. Circulation 104, 1188–1193.

Venkatraman, S., Boey, F., 2007. Release profiles in drug eluting stents: issues and uncertainties. J. Control. Release 120, 149–160.

Yakupoglu, Y.K., Kahan, B.D., 2003. Sirolimus: a current perspective. Exp. Clin. Transplant. 1, 8–18.

Zwolak, R.M., Adams, M.C., Clowes, A.W., 1987. Kinetics of vein graft hyperplasia: association with tangential stress. J. Vasc. Surg. 5, 126–136.

Hindawi Publishing Corporation
BioMed Research International
Volume 2013, Article ID 371430, 18 pages
http://dx.doi.org/10.1155/2013/371430

Research Article

Adhesion, Growth, and Maturation of Vascular Smooth Muscle Cells on Low-Density Polyethylene Grafted with Bioactive Substances

Martin Parizek,[1] Nikola Slepickova Kasalkova,[2] Lucie Bacakova,[1] Zdenek Svindrych,[1] Petr Slepicka,[2] Marketa Bacakova,[1] Vera Lisa,[1] and Vaclav Svorcik[2]

[1] *Institute of Physiology, Academy of Sciences of the Czech Republic, Videnska 1083, 142 20 Prague 4-Krc, Czech Republic*
[2] *Institute of Chemical Technology, Technicka 5, 166 28 Prague 6-Dejvice, Czech Republic*

Correspondence should be addressed to Lucie Bacakova; lucy@biomed.cas.cz

Received 28 August 2012; Accepted 14 February 2013

Academic Editor: Benaissa El Moualij

The attractiveness of synthetic polymers for cell colonization can be affected by physical, chemical, and biological modification of the polymer surface. In this study, low-density polyethylene (LDPE) was treated by an Ar^+ plasma discharge and then grafted with biologically active substances, namely, glycine (Gly), polyethylene glycol (PEG), bovine serum albumin (BSA), colloidal carbon particles (C), or BSA+C. All modifications increased the oxygen content, the wettability, and the surface free energy of the materials compared to the pristine LDPE, but these changes were most pronounced in LDPE with Gly or PEG, where all the three values were higher than in the only plasma-treated samples. When seeded with vascular smooth muscle cells (VSMCs), the Gly- or PEG-grafted samples increased mainly the spreading and concentration of focal adhesion proteins talin and vinculin in these cells. LDPE grafted with BSA or BSA+C showed a similar oxygen content and similar wettability, as the samples only treated with plasma, but the nano- and submicron-scale irregularities on their surface were more pronounced and of a different shape. These samples promoted predominantly the growth, the formation of a confluent layer, and phenotypic maturation of VSMC, demonstrated by higher concentrations of contractile proteins alpha-actin and SM1 and SM2 myosins. Thus, the behavior of VSMC on LDPE can be regulated by the type of bioactive substances that are grafted.

1. Introduction

Construction of tissue replacements and tissue engineering are very important areas of contemporary medicine and biotechnology. They have great potential for the future, due to increased life expectancy, civilization disorders, and thus increased requirements for medical care. Advanced tissue replacements consist of two basic components: cells and cell carriers. Artificial materials are usually applied as cell carriers, and for this purpose they should be adapted to act as analogues of the extracellular matrix, that is, to control the adhesion, growth, phenotypic maturation, and proper functioning of the cells. Synthetic polymers are an important type of materials that can be used for constructing substitutes for various tissues of the human body. These materials have a wide range of advantages, such as relatively easy availability and low cost, defined and versatile chemical composition, tunable mechanical properties, and tailored biodegradability at physiological conditions. These properties have made these polymers an obvious choice of material for many biotechnological and medical applications, for example, as growth supports for cell cultures *in vitro* or for constructing nonresorbable, fully resorbable, or semiresorbable vascular prostheses [1–4], artificial heart valves [5], bone and joint replacements [6, 7], implants for plastic surgery [8], bioartificial skin [9], and carriers for cell, drug or gene delivery [10]; for a review, see [11–14].

For biomedical applications, it is generally accepted that synthetic polymeric materials have to be biocompatible; that is, they must match the mechanical properties of the replaced tissue and not act as cytotoxic, mutagenic, or immunogenic. In addition, the physicochemical characteristics of the surface

of these biomaterials are of great importance, because they can directly influence and control the cell adhesion, spreading, and signaling events that further regulate a wide range of biological functions, for example, cell growth, differentiation, and extracellular matrix synthesis [15].

However, in their pristine state, many polymeric materials have unfavorable physical and chemical surface properties, which are limiting for their colonization with cells and for their integration with the surrounding tissues in the patient's organism. A typical example is the high hydrophobicity of synthetic polymers; that is, the water drop contact angle on the material surface is often higher than 90°. Fortunately, a wide range of physical and chemical modifications is available that can be used to create more hydrophilic bioactive surfaces attractive for cell colonization. For example, the polymers can be irradiated with ions [2, 3], with ultraviolet light [14, 16, 17], or exposed to plasma [18]. These treatments induce degradation of the polymer chains, release of noncarbon atoms, and creation of radicals. These radicals react with oxygen in the ambient atmosphere, leading to the formation of oxygen-containing functional chemical groups on the polymer surface (i.e., carbonyl, carboxyl, hydroxyl, ether, or ester groups). These groups enhance the polymer polarity and wettability and promote the adsorption of cell adhesion-mediating molecules in appropriate geometrical conformations, which enable specific amino acid sequences (e.g., RGD) in these molecules to be reached by cell adhesion receptors. In addition, conjugated double bonds between carbon atoms are created, and this renders the polymer surface electrically conductive. It is known that the electrical conductivity of a material surface enhances its attractiveness for cell colonization, even without active electrical stimulation (for a review, see [11–13, 19]).

In addition, the radicals, oxygen-containing groups, and double bonds that provide chemically reactive sites on the material surface can subsequently be grafted with various bioactive molecules, such as amino acids, proteins, other synthetic polymers, or nanoparticles. The grafted substances can further enhance the attractiveness of the modified polymer surface for cell adhesion and growth [18, 20–22].

In this study, we have therefore evaluated the adhesion, growth, and phenotypic maturation of vascular smooth muscle cells (VSMC) derived from rat aorta and cultured on low-density polyethylene (LDPE) modified by an Ar^+ plasma discharge and subsequent grafting with glycine (Gly), bovine serum albumin (BSA), polyethylene glycol (PEG), colloidal carbon nanoparticles (C), or BSA+C. The aim of these modifications was to create surfaces attractive for cell colonization, and furthermore to be able to control the extent of cell adhesion, cell growth activity, and cell differentiation. Growth supports of this kind are particularly important for VSMC, in order to prevent their so-called phenotypic modulation, that is, transition from their quiescent differentiated state to a synthetic and proliferative phenotype (for a review, see [23]). This modulation is associated with the risk of restenosis of an artificial vascular graft. For this reason, VSMCs have been avoided in the construction of vascular replacements. However, VSMCs are the most numerous cell component of the natural blood vessel wall. Thus, these cells have to be included in advanced bioartificial vascular replacements, provided their phenotype, and proliferation activity is controlled by appropriate cell culture conditions, including the physical and chemical properties of their material carrier.

LDPE was chosen as a carrier for VSMC in this study. Unlike other polymers, namely, polytetrafluoroethylene (PTFE) and polyethylene terephthalate (PET), LDPE is not used for constructing clinically applied vascular prostheses. However, due to its relatively simple and well-defined chemical composition, polyethylene provides a good model for studying the correlations between physicochemical changes of the material surface and the cell behavior. This model has been used with success in numerous earlier studies that we have carried out (e.g., [18, 20–22]).

Another aim of this study was to compare the sensitivity of LDPE and high-density polyethylene (HDPE), used in most of our earlier studies, to plasma treatment and subsequent grafting, and the influence of these modifications on cell behavior.

2. Experimental

2.1. Preparation of the Polymer Samples. The experiments were carried out on low-density polyethylene foils (LDPE) of Granoten S^*H type (thickness 0.04 mm, density 0.922 $g{\cdot}cm^{-3}$, and melt flow index 0.8 g/10 minutes), made by the Granitol Joint-Stock Company, Moravsky Beroun, Czech Republic. The polyethylene samples were cut into circles (diameter 2 cm) using a metallic perforator. The foils were modified by an Ar^+ plasma discharge (gas purity: 99.997%) using a Balzers SCD 050 device. The time of modification was 50 seconds, and the discharge power was 1.7 W. The chamber parameters were: Ar flow 0.3 $l\,s^{-1}$, Ar pressure 10 Pa, electrode area 48 cm^2, interelectrode electrode distance 50 mm, chamber volume 1000 cm^3, and plasma volume 240 cm^3. After this process, the samples were immersed in water solutions of glycine (Gly; Merck, Darmstadt, Germany, product number 104201), bovine serum albumin (BSA; Sigma-Aldrich, Germany, product number A9418) or polyethylene glycol (PEG; Merck, Darmstadt, Germany, product number 817018, m.w. 20000). Some plasma-treated samples and samples grafted with BSA were exposed to a suspension of colloidal carbon particles (C; Spezial Schwartz 4, Degussa AG, Germany) [18, 24]. All substances mentioned here were used in a concentration of 2 wt.%, and the time of the grafting process was 12 hours at room temperature [18]. Unmodified LDPE and standard cell culture polystyrene dishes were used as reference samples.

2.2. Characterization of the Polymer Samples. It is known that after plasma treatment changes occur in a wide range of parameters in the modified layer during the aging process [25]. For this reason, all analyses (and also cell culture experiments) were performed 20 days after modification (i.e., on aged samples).

The surface wettability was determined by measuring the contact angle using the static water drop method. The measurement was performed by distilled water in 10 different positions at room temperature with error 5% on the Surface

Energy Evaluation System (SEE System, Advex Instruments, Czech Republic).

The surface free energy (SFE) was evaluated on the basis of the contact angle of two liquids (water and glycerol). From these values, the SEE System calculates the surface energy according to the Owens-Wendt model [26].

The concentration profile of oxygen in the modified surface was determined by Rutherford Backscattering Spectroscopy (RBS). The RBS analysis was performed in a vacuum target chamber with 2.72 MeV He^+ ions. The elemental depth profiles were inspected at an accessible depth of a few hundred nm. The RBS spectra were evaluated by the GISA 3.99 code. The typical RBS detection limit is 0.1 at.% for oxygen.

The changes in surface morphology and roughness were determined by Atomic Force Microscopy (AFM), using a VEECO CP II in tapping mode. We used an RTESPA-CP Si probe, with spring constant 20–80 N/m. By repeated measurements of the same region ($1 \times 1\,\mu m^2$), it was proven that the surface morphology did not change after three consecutive scans. The mean roughness value (R_a) is the arithmetic average of the deviations from the centre plane of the sample.

2.3. Cells and Culture Conditions. Each LDPE sample 2 cm in diameter was cut into four smaller parts of equal size, and these parts were used for evaluating the cell number and the cell morphology and for immunofluorescence staining. Whole samples were used for an evaluation of the molecular markers of cell adhesion and differentiation by enzyme-linked immunofluorescence assay (ELISA). All LDPE samples were sterilized with 70% ethanol for one hour. The smaller samples were inserted into 24-well plates (TPP, Switzerland; well diameter 1.5 cm), while for the bigger (i.e., whole) samples, 12-well plates from the same company (diameter 2.1 cm) were used. After sterilization, the samples were air-dried for 12 hours in a sterile environment in order to prevent possible negative effects of ethanol on the cells. After the drying process, the samples were fixed to the bottom of the culture wells by plastic rings (inner area 0.38 cm^2 for the smaller samples and 1.77 cm^2 for the bigger samples) in order to prevent the samples floating in the cell culture media. The samples were seeded with VSMC isolated by an explantation method from rat aorta. The cells were used in the third passage, and their seeding density was 17000 cells per cm^2 [18]. The cells were cultivated in Dulbecco's Modified Eagle Minimum Essential Medium (DMEM, Sigma, USA), supplemented with 10% foetal bovine serum (Sebak GmbH, Aidenbach, Germany) and gentamicin (40 μg/mL, LEK, Slovenia), for 1, 2, 4, 5, or 7 days (temperature 37°C, humidified atmosphere of 5% of CO_2 in the air). For the smaller samples, 1.5 mL of the medium was used, and for the bigger samples, 3 mL of the medium. For the evaluation of the cell numbers and the cell spreading area, 4 smaller samples for each experimental group and time interval were used. For ELISA, 8 large samples for each experimental group were used, and the cultivation time was 7 days. For immunofluorescence staining, the time of cultivation was 4 days, and the cells were grown on the smaller samples.

2.4. Evaluation of the Cell Number and Cell Morphology. The cells on the smaller polymer samples were rinsed in phosphate-buffered saline (PBS). On one sample per each experimental group, the cells were fixed by 70% cold ethanol (−20°C) and stained with a combination of Texas Red C_2-maleimide fluorescent membrane dye (Molecular Probes, Invitrogen, Cat. number T6008; concentration 20 ng/mL in PBS) and Hoechst nuclear dye number 33342 (Sigma, USA; 5 μg/mL in PBS). The cell number and cell morphology were then evaluated using an Olympus IX 51 microscope equipped with an Olympus DP 70 digital camera.

The size of the cell spreading area was measured using Atlas software (Tescan Ltd, Czech Republic) on pictures taken on days 1 and 2 after seeding.

On the three remaining smaller samples, the cells were counted in a Cell Viability Analyzer (Vi-cell XR, Beckman Coulter). After rinsing with PBS, the cells were harvested by 5 min treatment in a trypsin-EDTA solution (Sigma, Cat. number T4174). The device performed an automatic analysis of the number of viable and dead cells, based on the trypan blue exclusion test.

2.5. Construction of Growth Curves and Calculation of Cell Population Doubling Time. The cell numbers obtained on days 1, 2, 5, and 7 after seeding were expressed as cells per cm^2 (i.e., the cell population densities) and were used for constructing growth curves. The cell population doubling time (DT) was determined by the equation

$$\mathrm{DT} = \log(2)\,\frac{t - t_0}{\log N_t - \log N_{t_0}}, \tag{1}$$

where N_{t_0} and N_t are the cell population densities at the beginning and at the end of the studied culture interval [2, 3].

2.6. Immunofluorescence Staining. On day 4 after seeding, the cells were rinsed twice in PSB, fixed with precooled 70% ethanol (−20°C, 15 min), and pretreated with 1% bovine serum albumin in PBS containing 0.05% Triton X-100 (Sigma) for 20 minutes at room temperature, in order to block nonspecific binding sites and permeabilize the cell membrane. The cells were then incubated with primary antibodies against several molecular markers of adhesion and phenotypic maturation of VSMC, namely, integrin-associated focal adhesion proteins talin vinculin and paxillin, α-actinin, a protein present in focal adhesions and also binding the actin cytoskeleton, cytoskeletal protein β-actin, and contractile proteins α-actin and SM1 and SM2 myosins, markers of VSMC phenotypic maturation (Table 1).

The primary antibodies were diluted in PBS to concentrations of 1 : 200 and applied overnight at 4°C. After rinsing with PBS, the secondary antibodies (dilution 1 : 400) were added for 1 hour at room temperature. These antibodies were goat anti-mouse or goat anti-rabbit F(ab′)2 fragments of IgG (H + L), both conjugated with Alexa Fluor 488 and purchased from Molecular Probes, Invitrogen (Cat. number A11017 and A11070, resp.). The cells were then rinsed twice in PBS, mounted under microscopic glass coverslips in a Gel/Mount permanent fluorescence-preserving aqueous

Table 1: Primary antibodies used for immunofluorescence staining (Immf.) and enzyme-linked immunosorbent assay (ELISA) of markers of adhesion and phenotypic maturation of VSMCs.

Antibody against	Developed in, type	Company, Cat. number	Dilution	Incubation
Chicken talin	Mouse, monoclonal	Sigma[a] T 3287	Immf.: 1 : 200 ELISA: 1 : 500	Immf.: overnight, 4°C ELISA: 60 min, RT[c]
Human vinculin	Mouse, monoclonal	Sigma[a] V9131	Immf.: 1 : 200 ELISA: 1 : 400	Immf.: overnight, 4°C ELISA: 60 min, RT[c]
Recombinant human paxillin	Rabbit, polyclonal	Chemicon[b] P1093	Immf.: 1 : 200 ELISA: 1 : 400	Immf.: overnight, 4°C ELISA: 60 min, RT[c]
Chicken α-actinin	Rabbit, polyclonal	Sigma[a] A2543	Immf.: 1 : 200 ELISA: 1 : 500	Immf.: overnight, 4°C ELISA: 60 min, RT[c]
Synthetic peptide of α-smooth muscle actin	Mouse, monoclonal	Sigma[a] A2547	Immf.: 1 : 200 ELISA: 1 : 400	Immf.: overnight, 4°C ELISA: 60 min, RT[c]
Synthetic peptide of β-actin	Mouse, monoclonal	Sigma[a] A 5441	Immf.: 1 : 200 ELISA: 1 : 400	Immf.: overnight, 4°C ELISA: 60 min, RT[c]
Human smooth muscle SM1 and SM2 myosin	Mouse, monoclonal	Sigma[a] M7786	Immf.: 1 : 200 ELISA: 1 : 500	Immf.: overnight, 4°C ELISA: 60 min, RT[c]

[a]Sigma, St. Louis, MO, USA; Czech Dealer: Sigma-Aldrich S.R.O., Prague, Czech Republic.
[b]Chemicon International Inc., Temecula, CA, USA; Czech dealer: Scintilla S.R.O., Jihlava, Czech Republic.
[c]Room temperature (RT).

mounting medium (Biomeda Corporation, Foster City, CA, U.S.A.), and evaluated under an Olympus IX 51 microscope (obj. 100x), using an Olympus DP 70 digital camera [18].

2.7. Enzyme-Linked Immunosorbent Assay (ELISA). The differences in the concentration of the adhesion and differentiation molecules on the tested materials were evaluated semiquantitatively, using enzyme-linked immunosorbent assay (ELISA) in homogenized cells per mg of protein.

For this purpose, the cells were cultured for 7 days and then rinsed with PBS, released with trypsin-EDTA solution (Sigma, Cat. number T4174, incubation 5 min at 37°C), and counted in the Cell Viability Analyzer (Vi-CELL XR, Beckman Coulter). Trypsinized cells were resuspended in PBS, centrifuged, resuspended in distilled and deionized water (10^6 cells/in 200 μL), and kept in a freezer at −70°C overnight. The cells were then homogenized by ultrasonication for 40 seconds (cycle 1, amplitude 70%) in a sonicator (UP 100 H, Dr. Hielscher GmbH), and the total protein content was measured using a modified method originally developed by Lowry [18, 27]. Aliquots of the cell homogenates corresponding to 1–50 μg of protein in 50 μL of water were adsorbed on 96-well microtiter plates (Maxisorp, Nunc) at 4°C overnight. After washing twice with PBS (100 μL/well), the nonspecific binding sites were blocked by 0.02% gelatin in PBS (100 μL/well, 60 min) and then treated by 1% Tween (Sigma, Cat. number P1379, 100 μL/well, 20 min). The primary antibodies (Table 1) were diluted in PBS (1 : 200 to 1 : 500) and applied for 60 minutes at room temperature (50 μL/well). The secondary antibodies, that is, goat anti-mouse IgG Fab specific (dilution 1 : 1000) or goat anti-rabbit IgG whole molecule (dilution 1 : 1000), both conjugated with peroxidase and purchased from Sigma (Cat. number A3682 and A0545, resp.), were applied for 45 min at room temperature (50 μL/well). This step was followed by double washing in PBS and an orthophenylenediamine reaction (Sigma, Cat. number P1526, concentration 2.76 mM) using 0.05% H_2O_2 in 0.1 M phosphate buffer (pH 6.0, dark place, 100 μL/well). The reaction was stopped after 10–30 minutes by 2 M H_2SO_4 (50 μL/well), and the absorbance was measured at 490 and 690 nm by a Versa Max Microplate Reader (Molecular Devices Corporation, Sunnyvale, CA, USA). The absorbance of the cell samples taken from modified LDPE foils was given as a percentage of the value obtained in the cells on pure LDPE [18].

2.8. Statistics. The biological results were presented as mean ± SEM (Standard Error of Mean). The statistical significance was evaluated by the One-Way Analysis of Variance (ANOVA), Student-Newman-Keuls method. For the cell number and the size of the cell spreading area, multiple comparisons of values obtained on all tested samples were performed. For the data obtained from ELISA, values on tested samples were compared only with values on the control unmodified LDPE. For ELISA, Dunnett's posttest was also used. Values $P \leq 0.05$ were considered significant.

3. Results and Discussion

3.1. Physicochemical Properties of Polymer Samples. It is known that Ar plasma discharge can cause changes in the chemical structure and surface morphology of a modified layer. These changes significantly affect the surface wettability [28]. The degree of wettability, characterized by the contact angle, is shown in Figure 1 for pristine LDPE, plasma-treated LDPE, and plasma treated and subsequently grafted with biomolecules. The contact angle decreases dramatically after plasma treatment. This is due to the creation of free radicals and subsequent oxidation of the layer exposed to the air [29]. This leads to the formation of new oxygen

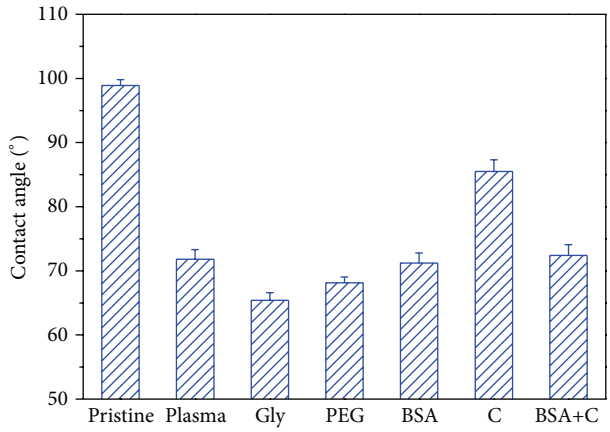

Figure 1: The water drop contact angle of pristine LDPE (pristine), plasma-treated LDPE (plasma), LDPE treated with plasma and then grafted with glycine (Gly), polyethylene glycol (PEG), bovine serum albumin (BSA), colloidal carbon particles (C), or a combination of BSA and C (BSA+C).

Table 2: Surface free energy (SFE, in $mJ \cdot m^{-2}$) of pristine LDPE, plasma-treated LDPE (plasma), LDPE treated with plasma and then grafted with glycine (Gly), polyethylene glycol (PEG), bovine serum albumin (BSA), colloidal carbon particles (C), or with a combination of BSA and C (BSA+C). γ_{total} is the total SFE of the polymer and consists of nonpolar (γ_{LW}) and polar components (γ_{AB}).

	γ_{total}	γ_{LW}	γ_{AB}
Pristine	24.54	23.16	1.37
Plasma	28.56	25.01	3.55
Gly	36.20	31.89	4.31
PEG	34.91	5.01	29.90
BSA	26.56	20.28	6.28
C	26.59	19.22	7.37
BSA+C	25.58	12.86	12.72

The values are the mean of 10 to 15 measurements for each experimental group and were calculated automatically by the Surface Energy Evaluating System (SEE System, Masaryk University, Brno, Czech Rep.).

structures, for example, carbonyl, carboxyl, and ester groups [30]. Subsequent grafting of glycine and PEG to the plasma-activated surface resulted in a further decrease in the contact angles on these samples. The molecules of Gly and PEG contain polar groups, which increase the hydrophilicity of the material surface. However, the presence of BSA and BSA+C had no significant effect on the wettability of LDPE, because the contact angles on these samples were comparable with the values on samples treated only with plasma. Different behavior was observed in samples after modification with colloidal C particles. These samples had much lower wettability than the plasma-treated samples. This result is in accordance with the previous finding by ourselves and by other authors that carbon-based coatings, for example, with amorphous diamond-like carbon, graphite or nonfunctionalized fullerenes, are often hydrophobic (for a review, see [19]). Nevertheless, the wettability of C-modified LDPE in this study still remained higher than on pristine LDPE.

The total surface free energy (SFE) of the LDPE samples was inversely correlated with the water contact angle; that is, samples with a relatively low contact angle had a higher total SFE (LDPE grafted with Gly or PEG), while samples with a high contact angle had lower total SFE (pristine LDPE, Table 2). In other words, the total SPE was positively correlated with the hydrophilicity of the material surface. On all modified samples, the total SFE and its polar component increased in comparison with pristine LDPE. Similar differences between pristine and UV light-treated LDPE were described by O'Connell et al. [31]. The highest polar component of SFE was found on samples modified with plasma and subsequently grafted with PEG. This result is consistent with relatively high hydrophilicity of this sample (Figure 1), and also with the results obtained by RBS, which revealed a high concentration of oxygen in PEG-grafted LDPE (Figure 2). Surprisingly, the increase in the polar component was relatively small in LDPE grafted with Gly (Table 2), which exhibited the lowest water drop contact angle and the highest oxygen concentration at the material surface (Figures 1 and 2). In addition, the changes in the nonpolar component were variable. This component increased on samples modified in plasma or on samples subsequently grafted with glycin, while on samples grafted with BSA, C, or BSA+C, this value decreased. Similar variability has been described on LDPE, UHMWPE, and Sarlink polymers after treatment with UV light and has been explained by configuration changes of chemical functional groups at the material surface during its modification [31].

The concentration depth profile of oxygen modified LDPE was determined from RBS measurements. The concentration of oxygen in a modified layer and the oxygen depth profile is shown in Figure 2. The highest concentration of oxygen was found in the surface layers of all modified substrates. With increasing depth from the surface, the oxygen concentration decreased, and at a depth of 80 nm the amount of oxygen was minimal. Most oxygen in the modified layer was determined on a sample treated by plasma and grafted with glycine. More oxygen was also detected on a sample modified with plasma discharge and PEG. A comparable amount of oxygen was measured on substrates exposed to plasma or exposed to plasma and subsequently grafted with BSA or BSA+C. These results, obtained by the RBS method, are consistent with the results determined by goniometry, except that the samples grafted with C showed a similar oxygen content as the samples grafted with BSA and BSA+C, although their water drop contact angle was higher.

Changes in surface morphology and surface roughness that occurred due to plasma exposure and the subsequent grafting process were studied by the AFM method. AFM scans of pristine and modified samples are shown in Figure 3. Plasma modification leads to ablation of the surface layer. Its amorphous phase is ablated preferably [32]. This leads to enhanced branching of LDPE structures. Subsequent grafting with glycine and PEG on the plasma modified surface does not significantly change the surface morphology, but it slightly increases the surface roughness. Figure 3 shows that the bonding of carbon particles highlights the fine details of the structure and also leads to the formation of small

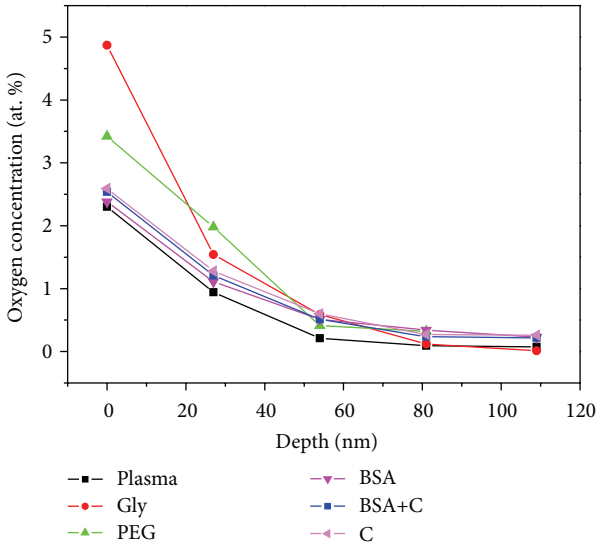

Figure 2: Oxygen concentration in the modified layer and depth concentration profile of oxygen, determined from RBS measurements, on plasma-treated LDPE (plasma), LDPE treated with plasma and then grafted with glycine (Gly), polyethylene glycol (PEG), bovine serum albumin (BSA), colloidal carbon particles (C), or a combination of BSA and C (BSA+C).

spherical units corresponding to carbon nanoparticles. In the case of BSA and BSA+C grafting, large cluster formations that strongly affect the surface roughness were detected, in agreement with previous observations for BSA published by Wang et al. [33].

3.2. Initial Adhesion and Subsequent Growth of Cells on Polymer Samples. On the first day of the experiment, the highest number of initially adhered cells was found on the control PS dishes (17,100 ± 3,300 cells/cm^2). The cell numbers on all LDPE samples showed no statistically significant differences, when compared with each other (Figure 4(a)). Nevertheless, the highest average cell number was observed on LDPE grafted with BSA (10,950 ± 1,030 cells/cm^2), while the lowest number was found on LDPE grafted with PEG (4,770 ± 1,400 cells/cm^2). This number was even slightly lower than the value found on pristine LDPE (5,720 ± 1,780 cells/cm^2). This result contrasts with our earlier findings on HDPE foils [18], where the lowest initial cell number was found on the control PS, and the highest values were found on HDPE grafted with PEG. This disproportion in the cell behavior on LDPE and on HDPE could be explained by the different arrangements of the PEG chains on the surfaces of LDPE and HDPE samples. It is known that if PEG chains are attached to a surface only by one end, and dangle on the surface in a water environment (including cell culture media), this has a repulsive effect on cell adhesion. Cell adhesion on artificial materials *in vitro* is mediated by specific proteins adsorbed on the material surface from the serum supplement of the culture medium, mainly fibronectin and vitronectin. This adsorption is hampered or even disabled on mobile surfaces, especially if the surface mobility is combined with relatively high hydrophilicity, which occurs in PEG due to the presence of -OH groups in its molecules and which was also proven in this study (Figure 1). PEG—also known as polyethylene oxide (PEO), if its molecular mass is above 20,000—has been widely used for constructing surfaces that are nonadhesive for cells, especially those which were designed for the attachment of oligopeptidic ligands for cell adhesion receptors in defined types, concentrations, and distributions and which should prevent uncontrolled protein adsorption and aberrant cell adhesion [4, 34]; for a review, see [11–13]. PEG can also be attached to the material surface through several sites on one chain. In this case, PEG chains are not mobile and can support the adsorption of cell adhesion-mediating proteins and subsequent cell adhesion and growth [21]; for a review, see [18]. In our experiments, the cell-repulsive effects of PEG probably prevailed on LDPE, while PEG promoted cell adhesion on HDPE. This topic needs further investigation, but it can be supposed that the different behavior of PEG was due to the different structure of LDPE and HDPE. For example, LDPE molecules have more branching than HDPE molecules, so their intermolecular forces are weaker. The tensile strength of LDPE is lower, but its resilience is higher. Because of the side branches, LDPE molecules are less tightly packed and less crystalline than HDPE molecules. All these factors may lead to different attachment, distribution, and mobility of PEG chains on LDPE and HDPE surfaces, particularly if the branched LDPE structure is further enhanced by plasma treatment, as mentioned previously.

In spite of the relatively low number of initially adhered cells on PEG-grafted LDPE, the spreading area of cells on day 1 after seeding on this material (1,527 ± 98 μm^2) was on an average larger than the areas on the other modified LDPE samples (which ranged from 1,282 ± 49 μm^2 to 1,361 ± 60 μm^2), significantly larger than the areas on unmodified LDPE (687 ± 57 μm^2) and similar to those found on PS (1,664 ± 104 μm^2; Figure 4(b)). One explanation is that the cells had more space for spreading due to the lower number of adhering cells. In any case, the cell spreading implies that PEG-grafted LDPE surfaces allowed adsorption of cell adhesion molecules. However, this adsorption may be nonhomogeneous. On some regions, the cells were well spread and polygonal, while on other sites, the cells remained round (Figure 5).

From day 1 to 2 after seeding, the cells on all LDPE-based samples started to enter the exponential phase of growth and proliferated with doubling times ranging on an average from 14.1 to 46.1 hours (Table 3), while the cells on polystyrene dishes remained rather in the lag phase and proliferated more slowly (doubling time 59.0 hours). As a result, the statistically significant differences between the LDPE samples and PS, observed on day 1, disappeared on day 2 after seeding (Figure 4(c)). Only on LDPE grafted with PEG did the cell number still remain significantly lower than on PS (10,000 ± 1,800 cells/cm^2 versus 22,700 ± 2,300 cells/cm^2 on PS).

The cell spreading area on day 2 after seeding was (similarly as on day 1) significantly larger on all modified LDPE samples (1,037 ± 36 μm^2–1,714 ± 71 μm^2) than on unmodified LDPE (441 ± 18 μm^2), but at the same time

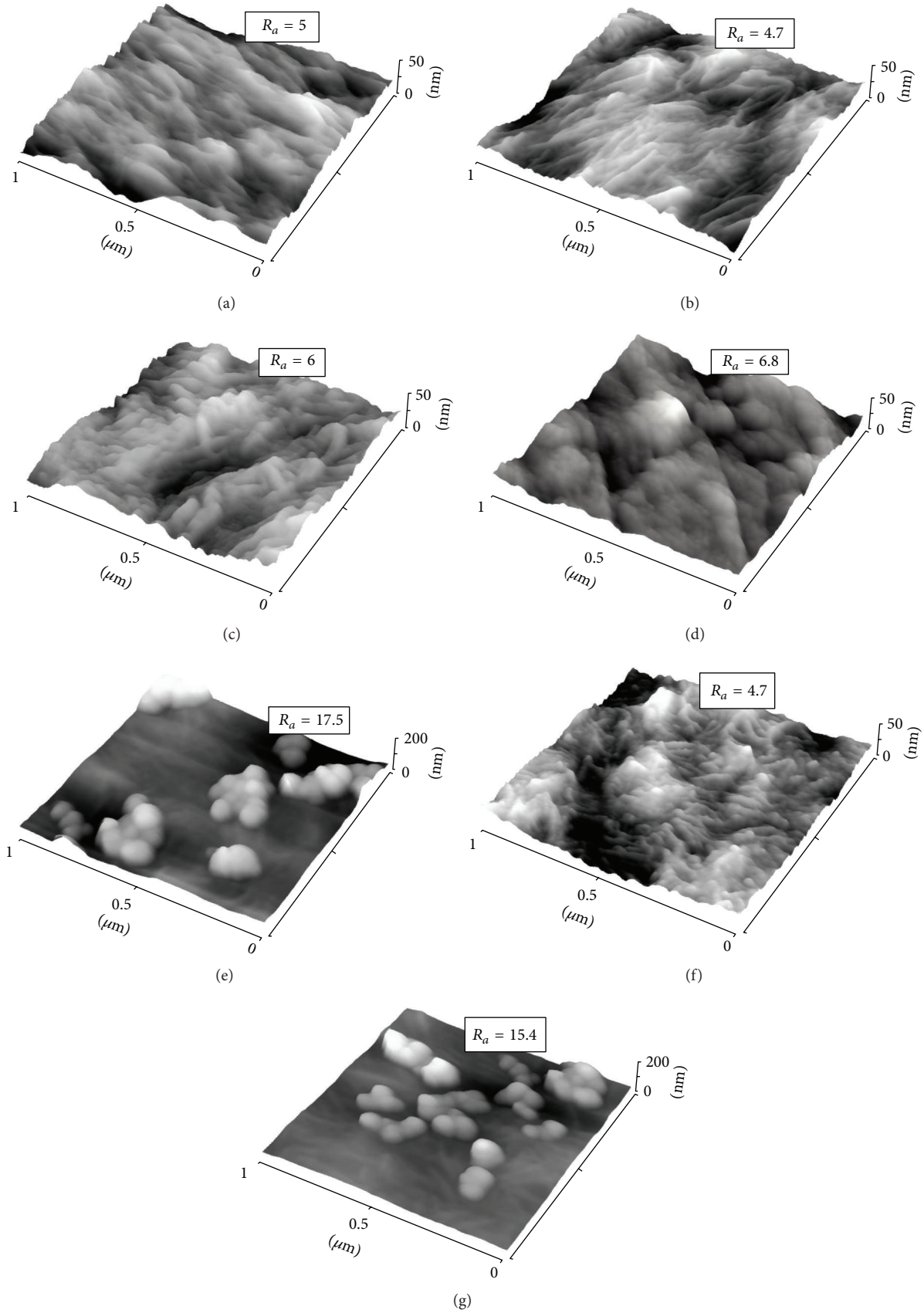

Figure 3: AFM scans of pristine LDPE (a), plasma-treated LDPE (b), LDPE treated with plasma and grafted with glycine (c), PEG (d), BSA (e), C (f), or BSA+C (g). R_a is the surface roughness in nm.

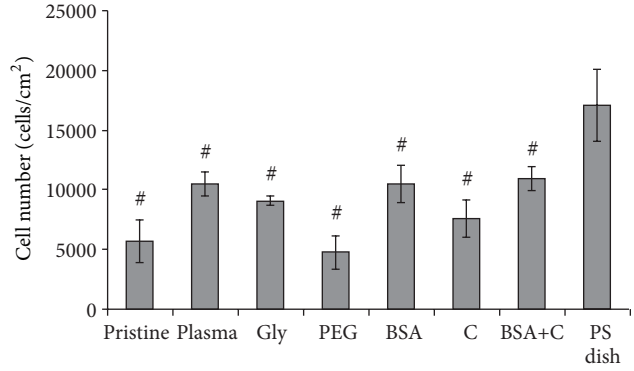

(a) Cell number, day 1

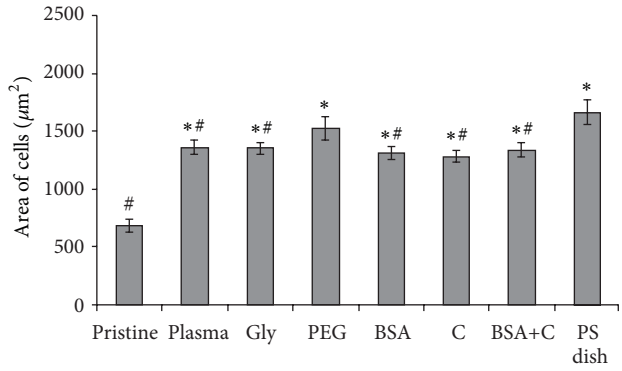

(b) Spreading area, day 1

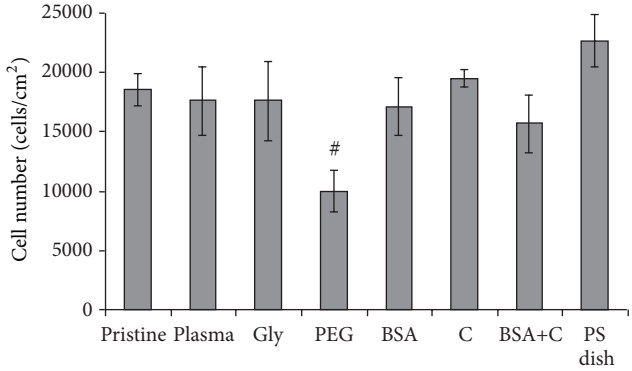

(c) Cell number, day 2

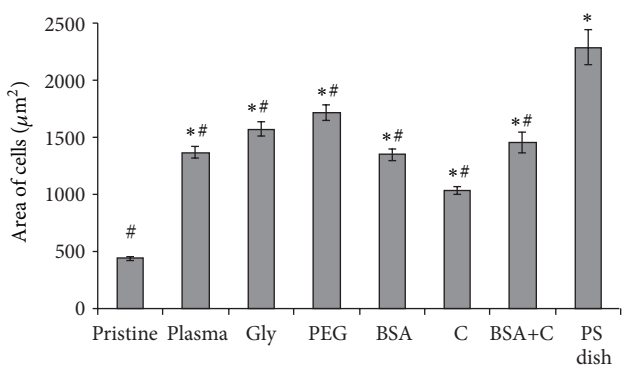

(d) Spreading area, day 2

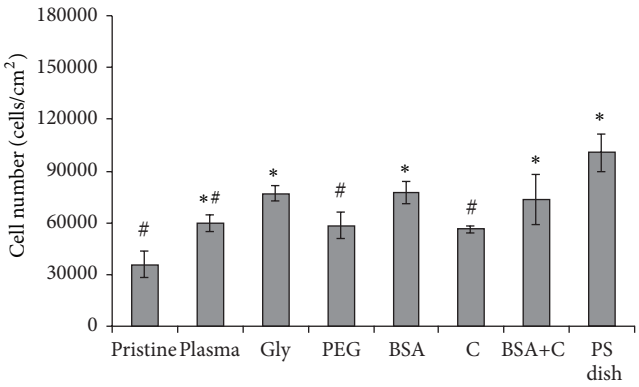

(e) Cell number, day 5

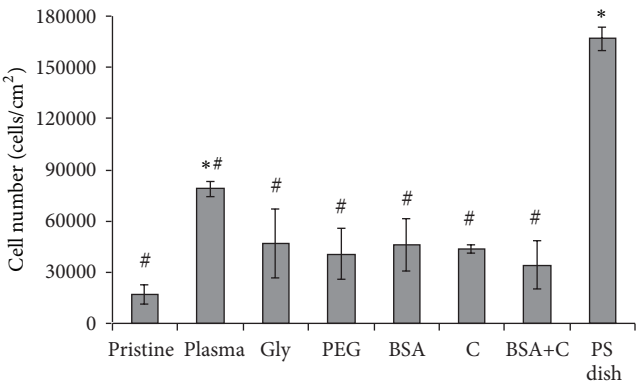

(f) Cell number, day 7

Figure 4: The number (a, c, e, and f) and the size of the spreading area (b, d) of rat aortic smooth muscle cells in cultures on nonmodified LDPE (pristine), on LDPE irradiated with plasma (plasma), on LDPE irradiated with plasma and grafted with glycine (Gly), on polyethylene glycol (PEG), on bovine serum albumin (BSA), on colloidal carbon particles (C), or on bovine serum albumin and C (BSA+C). A tissue culture polystyrene dish (PS dish) was used as a reference material. Days 1, 2, 5, and 7 after seeding. Mean ± SEM from 3 samples, each measured 50 times (cell number, Vi-CELL Analyser) or from 119 to 229 cells for each experimental group (spreading area). ANOVA, Student-Newman-Keuls method. Statistical significance: $^{*,\#}P \leq 0.05$ compared to the value on pristine PE and a polystyrene dish, respectively.

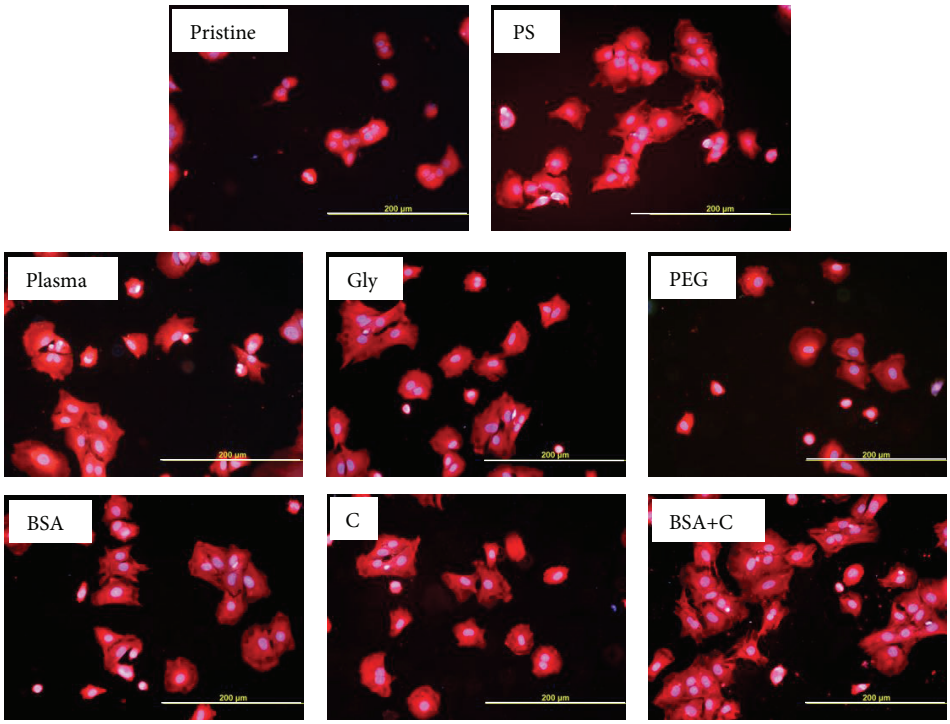

Figure 5: Morphology of rat aortic smooth muscle cells on day 1 after seeding on pristine LDPE (pristine), on a tissue culture polystyrene dish (PS), on LDPE irradiated with Ar^+ plasma (plasma), on LDPE irradiated with plasma and grafted with glycine (Gly), on polyethyleneglycol (PEG), on bovine serum albumin (BSA), on colloidal carbon particles (C), or on bovine serum albumin and carbon particles (BSA+C). Cell membrane and cytoplasm stained with Texas Red C_2-maleimide (red fluorescence), cell nuclei with Hoechst 33342 (blue fluorescence). Olympus IX 51 microscope, DP 70 digital camera, obj. 20x, bar = 200 μm.

it was significantly smaller than on PS (2,289 ± 149 μm^2; Figure 4(d)). Similar results were obtained in our earlier study performed on cultures on HDPE. The cell spreading areas of VSMC on HDPE treated with the same modifications as LDPE in the present study were larger than the spreading areas of the unmodified polymer. This can be explained by the increase in oxygen concentration on the surface of the modified polymer samples, their optimized wettability, and also changes in their surface roughness and morphology (Figures 1–3; [18]).

It is known that the size of the spreading area correlates positively with cell proliferation activity, at least to a certain extent [35, 36]; for a review, see [11–13]. In accordance with this, from day 2 to 5 after seeding, the cells on all modified samples proliferated more quickly (doubling time from 9.4 to 13.6 hours) than the cells on pristine LDPE (doubling time 25.5 hours); see Table 3, Figure 6. On day 5 after seeding, the cells on the modified LDPE samples (except the samples grafted with PEG and C) reached a significantly higher cell population density (59,940 ± 4,850–77,530 ± 6,460 cells/cm^2) than the cells on pristine LDPE (35,680 ± 7,760 cells/cm^2). On LDPE grafted with Gly, BSA, or BSA+C, the cell population densities reached values not significantly different from those obtained on the PS dishes (100,740 ± 10,930 cells/cm^2), which are considered as the "gold standard" for cell cultivation (Figure 4(e)). The samples grafted with BSA or BSA+C were covered by almost confluent cell layers (Figure 7). Similar results were also obtained in our earlier study performed on HDPE, but the cell population densities on BSA and BSA+C significantly exceeded the values on the PS dishes [18].

The improved spreading and growth of VSMC on LDPE irradiated with plasma can be explained by physicochemical changes in the polymer surface which lead to an increased oxygen content and increased wettability of the surface. These surfaces are then more susceptible to adsorption of adhesion-mediating extracellular matrix proteins, for example, vitronectin, fibronectin, collagen, or laminin, in a near physiological and bioactive conformations, suitable for binding by the cell adhesion receptors (for a review, see [11–13]).

The reactive sites formed in a polymer when it is exposed to plasma can be used for grafting various molecules which further modulate the effects of polymer treatment on cell adhesion, growth, phenotypic maturation, and functioning. Glycine, used for grafting the plasma-activated LDPE in this study, is a component of a well-known ligand for integrin cell adhesion receptors, that is, Arg-Gly-Asp (RGD), though Gly alone cannot be bound by these receptors. Nevertheless, Gly grafting enriches the irradiated polymer surface with additional oxygen-containing and also amine groups, which are known to improve the adsorption of cell adhesion-mediating proteins and cell colonization [16]; for a review, see [12]. In addition, Gly and PEG slightly increased the size of the nanoscale irregularities on the polymer surface; that is, they enhanced the material nanostructure, which has been

Table 3: Cell population doubling time (hours) of rat aortic smooth muscle cells from day 1 to 2, day 2 to 5, and day 5 to 7 after seeding on nonmodified LDPE (pristine), LDPE irradiated with plasma (plasma), LDPE irradiated with plasma and grafted with glycine (Gly), polyethyleneglycol (PEG), bovine serum albumin (BSA), colloidal carbon particles (C), bovine serum albumin and C (BSA+C), and polystyrene dishes (PS dish).

Material/time interval	Pristine	Plasma	Gly	PEG	BSA	C	BSA+C	PS dish
Days 1-2	14.1	32.0	25.0	22.5	33.8	17.7	46.1	59.0
Days 2–5	25.5	13.6	11.3	9.4	11.0	15.7	10.8	11.2
Days 5–7	−21.8*	60.3	−33.6*	−45.5*	−32.1*	−66.9*	−21.9*	33.0

*Nonproliferating cells.

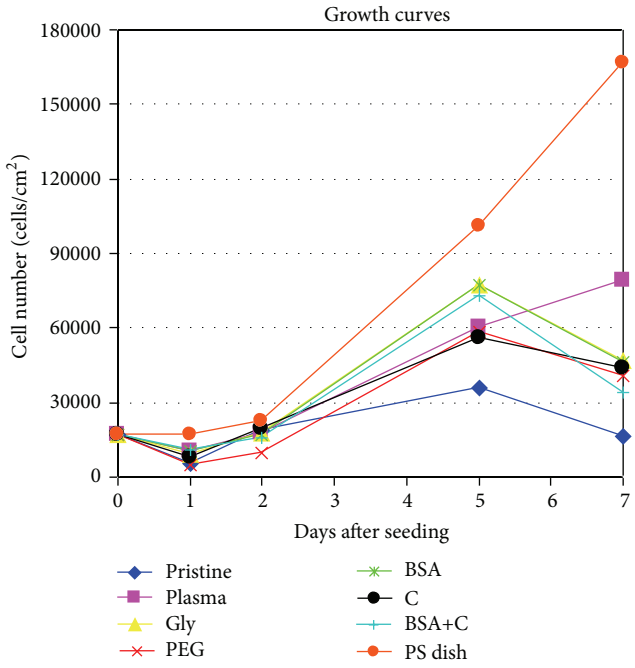

Figure 6: Growth dynamics of rat aortic smooth muscle cells in cultures on nonmodified PE (pristine), on PE irradiated with plasma (plasma), on PE irradiated with plasma and grafted with glycine (Gly), on polyethyleneglycol (PEG), on bovine serum albumin (BSA), on colloidal carbon particles (C), or on bovine serum albumin and C (BSA+C). A tissue culture polystyrene dish (PS dish) was used as the reference material. Means from three samples for each experimental group and time interval (each sample measured 50 times).

shown, like surface wettability, to optimize the spectrum and the geometrical conformations of adsorbed cell adhesion-mediating molecules (for a review, see [12]).

Albumin, a protein that is nonadhesive for cells, has been used for constructing cell-repulsive surfaces. From this point of view, our result that albumin grafting improved the colonization of LDPE with cells might be surprising. However, albumin preadsorbed on the material surfaces improved the geometrical conformation of the cell adhesion-mediating molecules, for example, fibronectin and vitronectin, and their accessibility for cell adhesion receptors [37, 38]; for a review, see [12, 18]. In addition, BSA grafted on the LDPE formed nanosized (i.e., smaller than 100 nm) and submicron-sized (i.e., smaller than 1 μm) cluster structures (Figure 3). Irregularities of this size are believed to promote the adsorption of cell adhesion-mediating molecules in a more physiological conformation than the conventional flat surfaces, and this markedly improves the adhesion and further functioning of the cells [39, 40].

From day 5 to 7 after seeding, the cells on most modified LDPE samples stopped proliferating (i.e., entered the stationary phase of growth), and they even decreased in number. Cell proliferation continued only on the polystyrene dishes and on the plasma-irradiated LDPE (Figure 6, Table 3). On all LDPE samples, the final cell population density was significantly lower than on the PS dishes (Figure 4(f)). However, the cell proliferation on all modified HDPE samples in our earlier study continued from day 5 to 7, and the final cell population density on these samples was similar to or even higher than on the PS dishes [18].

Thus, the positive effects of plasma treatment and subsequent grafting on the adhesion and growth of VSMC were more apparent in HDPE than in LDPE. Analogous results were obtained when a terpolymer of polytetrafluoroethylene, polyvinyldifluoride and polypropylene (PTFE/PVDF/PP), and polysulfone (PSU) was mixed with carbon nanotubes. The addition of nanotubes significantly improved the adhesion and growth of human osteoblast-like MG 63 cells on the terpolymer, while this effect was much less apparent on PSU. This difference was explained by the high hydrophobicity of pristine PTFE/PVDF/PP (water drop contact angle ~100°), while the pristine PSU was more hydrophilic (contact angle ~85°). In addition, PSU contains bioactive sulphone groups, which can also mediate the positive effects of this polymer on cell adhesion. Sulphonated polystyrene promoted the adsorption of fibronectin in an advantageous geometrical conformation for cell adhesion [41]. Thus, pristine PSU is more suitable for cell colonization, and thus the cells were less sensitive to the modifications, further improving the cell adhesion and growth (for a review, see [42]). However, in our studies, both LDPE and HDPE were relatively hydrophobic, having a similar water drop contact angle of 98.6 ± 1.90° and 102.5 ± 2.31°, respectively. Thus, the different sensitivity of cells to modifications of LDPE and HDPE may be due to other differences in the physical and chemical properties of these polymers (see above), for example, differences in chain branching, tensile strength, resilience, crystallinity, packing density, and so forth. A further investigation of this topic is needed.

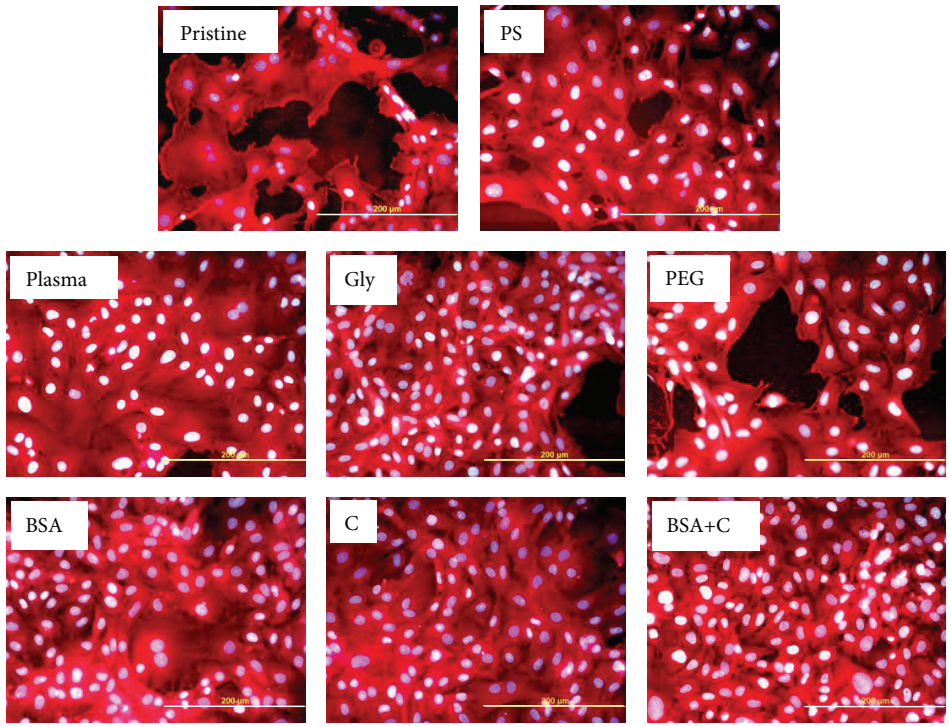

Figure 7: Morphology of rat aortic smooth muscle cells on day 5 after seeding on pristine LDPE (pristine), on a tissue culture polystyrene dish (PS), on LDPE irradiated with Ar^+ plasma (plasma), on LDPE irradiated with plasma and grafted with glycine (Gly), on polyethyleneglycol (PEG), on bovine serum albumin (BSA), on colloidal carbon particles (C), or on bovine serum albumin and carbon particles (BSA+C). Cell membrane and cytoplasm stained with Texas Red C_2-maleimide (red fluorescence), cell nuclei with Hoechst mumber 33342 (blue to white fluorescence). Olympus IX 51 microscope, DP 70 digital camera, obj. 20x, bar = 200 μm.

3.3. Distribution and Concentration of Molecular Markers of Cell Adhesion and Phenotypic Maturation. Immunofluorescence staining showed that the cells on all modified LDPE samples had better developed focal adhesion plaques containing talin and vinculin than the cells on pristine LDPE samples (Figure 8). This result correlates well with the size of the cell spreading area, which was generally larger on all modified samples than on pristine LDPE.

ELISA revealed that the concentration of talin in cells on LDPE modified with plasma, or plasma with subsequent grafting of Gly or PEG, was significantly higher than in cells on pristine LDPE. The concentration of vinculin, which stabilizes focal adhesion plaques (for a review, see [12]), was also higher in cells on LDPE grafted with Gly or PEG (Figure 9). In accordance with these findings, the cells on LDPE modified with plasma, Gly, and particularly PEG achieved on an average the largest cell spreading areas (Figures 4(b) and 4(d)).

However, the concentration of paxillin (i.e., another protein of focal adhesion plaques) was lower in cells on LDPE modified with plasma, Gly, PEG, and BSA+C than in cells on pristine LDPE (Figure 9). Only in cells on LDPE modified with BSA or C the concentration of paxillin was similar as in the cells on pristine polymer. This result corresponded, at least partly, with immunofluorescence staining of paxillin (Figure 10). In cells on LDPE modified with plasma, Gly, or PEG, the paxillin-containing focal adhesions were equally developed or even worse developed than in cells on pristine LDPE, while the paxillin focal adhesions on polymer modified with BSA or C were similarly developed or better developed than in cells on pristine LDPE. Only in cells on BSA+C the paxillin-containing focal adhesions were well-developed, though the concentration of paxillin in these cells was relatively low (Figures 9 and 10). In this context, it should be pointed out that the ELISA method used in our study measured the total number of focal adhesion molecules in the cells, and not only the molecules located in focal adhesion plaques. A more exact method might be to extract the cytosolic fraction of the focal adhesion proteins (i.e., not bound in the focal adhesion plaques) by detergents [43] or to use antibodies against phosphorylated antigens. It can be supposed that phosphorylated paxillin (i.e., activated paxillin exerting its function in cell adhesion) is located in the focal adhesion plaques, while in the cytosolic fraction, nonactive paxillin is not phosphorylated [44–46].

Alpha-actinin is associated with both focal adhesion plaques and the actin cytoskeleton, in which it acts as a crosslinker and stabilizer of the contractile apparatus [47, 48]. In cells on the modified LDPE samples and on PS, its concentration was usually similar to that in cells on pristine LDPE (Figure 9). Only in cells on plasma-irradiated LDPE the concentration of α-actinin was significantly lower. From the cells on all modified samples, only the cells on plasma-modified LDPE continued their proliferation from day 5 to 7 (Figure 6,

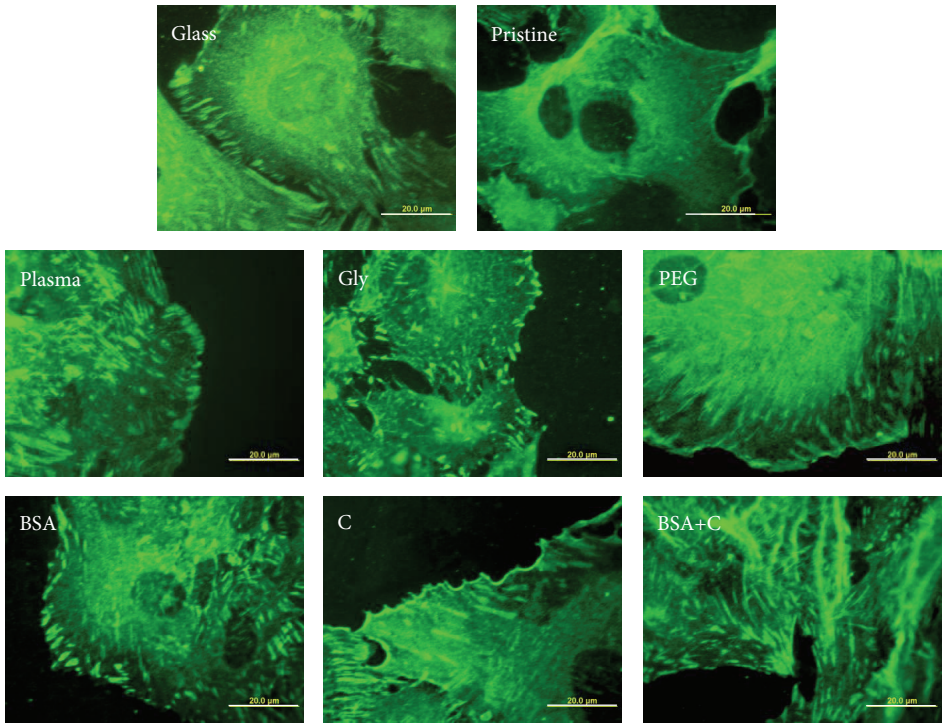

Figure 8: Immunofluorescence of talin, an integrin-associated protein of focal adhesion plaques, in rat aortic smooth muscle cells on day 4 after seeding on a microscopic glass coverslip (glass), on pristine LDPE (pristine), on LDPE irradiated with plasma (plasma), on LDPE irradiated with Ar^+ plasma and grafted with glycine (Gly), on polyethylene glycol (PEG), on bovine serum albumin (BSA), on colloidal carbon particles (C), and on bovine serum albumin with C (BSA+C). Olympus IX 51 microscope, DP 70 digital camera, obj. 100x, bar = 20 μm.

Table 3). Thus, the decreased concentration of α-actinin may be a sign of certain instability of the actin cytoskeleton, which is reorganized during cell division. This presumption is further supported by the immunofluorescence staining pattern of α-actinin. In cells on plasma-modified LDPE, the structures containing α-actinin are relatively short and are located predominantly at the cell periphery, while in the cells on the other samples, the α-actinin-containing structures are long, filament like, often running in parallel through the entire cell (Figure 11).

VSMCs exist in two basic phenotypes, referred to as contractile and synthetic. The contractile phenotype occurs in mature healthy blood vessels and is characterized by the presence of desmin, that is, a protein of intermediate filaments, muscle type of tropomyosin, T-troponin, h-caldesmon, h1-calponin, and metavinculin, and particularly by contractile proteins α-actin and SM1 and SM2 isoforms of myosin. On the other hand, the synthetic phenotype is characterized by the accumulation of cell organelles involved in proteosynthesis, such as endoplasmic reticulum, ribosomes or Golgi complex, and predominance of β- and γ-isoforms of actin and nonmuscle myosin. This phenotype occurs physiologically in immature blood vessels under development, pathologically in diseased blood vessels, for example, during atherosclerosis and hypertension, and artificially after disintegration of the vascular wall and seeding VSMC *in vitro* (for a review, see [48]). However, the synthetic phenotype of VSMC *in vitro* can be reversed, at least partly, to the contractile phenotype by appropriate cell culture conditions, such as the use of serum-free media, dynamic stimulation of VSMC, and particularly the physical and chemical properties of the adhesion substrate. In cells on our materials, the distribution and concentration of α-actin or SM1 and SM2 myosins were therefore evaluated as markers of phenotypic maturation of VSMC, that is, their transition toward a more differentiated contractile phenotype.

We found that α-actin formed thick and brightly stained filament bundles in cells on all samples, including pristine LDPE (Figure 12), while bundles containing SM1 and SM2 myosins were more apparent in cells on modified LDPE than on pristine LDPE (Figure 13). However, as revealed by ELISA, the concentration of α-actin and SM1 and SM2 myosins was significantly higher only in cells on LDPE grafted with BSA and BSA+C, respectively, compared to cells on pristine LDPE (Figure 9). The cells on the samples grafted with BSA or BSA+C had a relatively high cell population density on day 5 after seeding, approaching the value found on cell culture PS, and reached confluence. In addition, these cells had relatively large spreading areas and well-developed talin- and vinculin-containing focal adhesion plaques (Figures 4(b), 4(d), and 8). These factors, that is, good cell-cell adhesion in confluent cultures together with good cell-matrix adhesion, are associated with cell differentiation (for a review, see [11–13]). At the same time, the concentration of β-actin, that is,

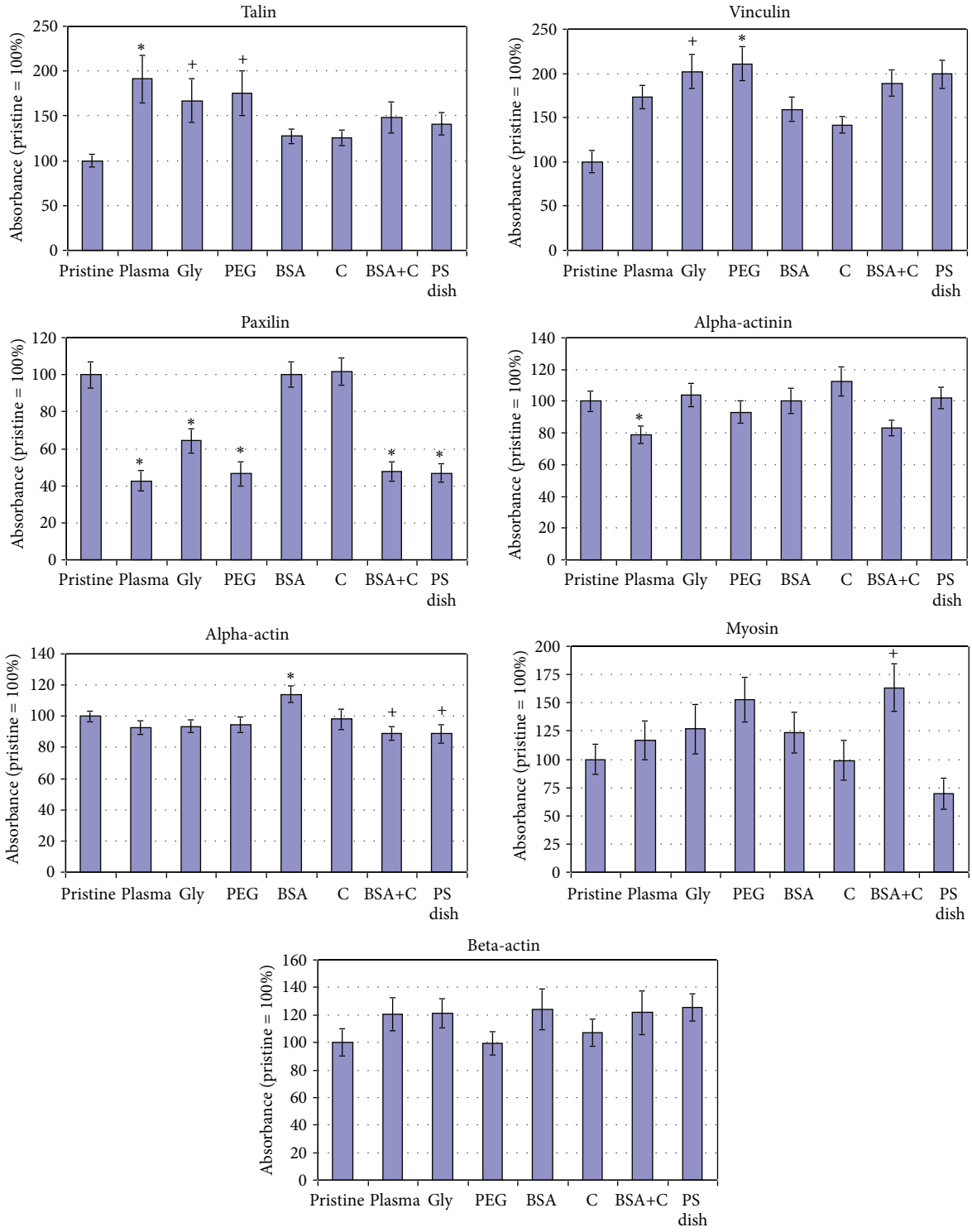

Figure 9: Concentration of focal adhesion, cytoskeletal, and contractile proteins in rat aortic smooth muscle cells in 7-day-old cultures on pristine PE (pristine), on PE activated with plasma (plasma), on PE grafted with glycine (Gly), on polyethylene glycol (PEG), on bovine serum albumin (BSA), on colloidal carbon particles (C), or on BSA with C (BSA+C), and on a tissue culture polystyrene dish (PS dish). Measured by ELISA per mg of protein. Means ± SEM from three to seven experiments, each performed in duplicate or in triplicate. Absorbance values were normalized to the values obtained in cell samples from pristine PE, that is, given as a percentage of the values on pristine PE. ANOVA, statistical significance: $^{*,+}P \leq 0.05$ compared to the value on pristine PE (Student-Newman Keuls method and Dunnett's posttest, resp.).

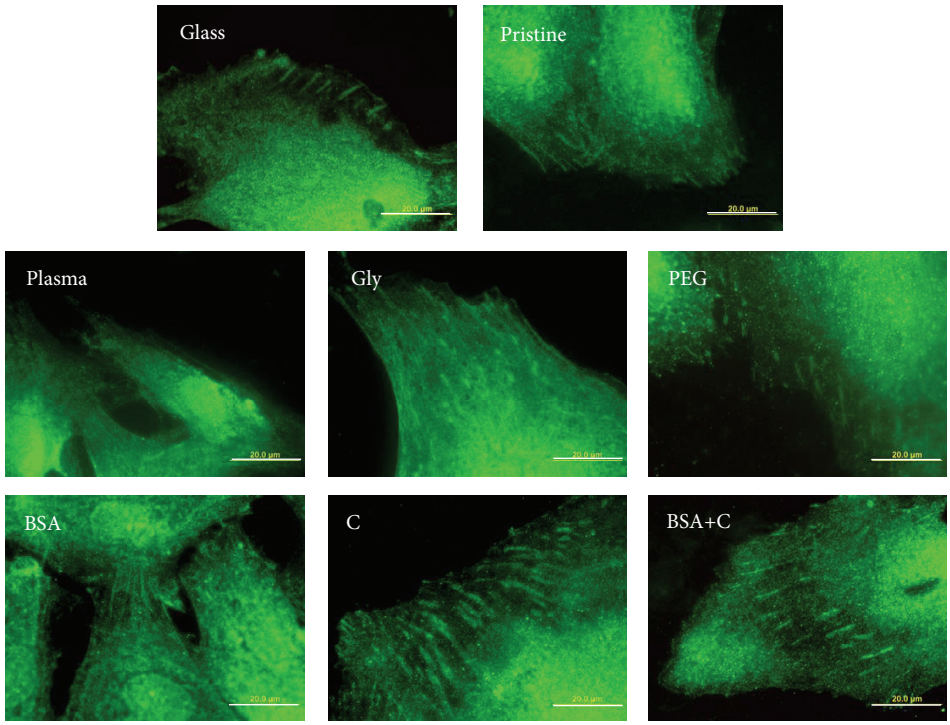

Figure 10: Immunofluorescence of paxillin, an integrin-associated protein of focal adhesion plaques, in rat aortic smooth muscle cells on day 4 after seeding on a microscopic glass coverslip (glass), on pristine LDPE (pristine), on LDPE irradiated with plasma (plasma), on LDPE irradiated with Ar^+ plasma and grafted with glycine (Gly), on polyethylene glycol (PEG), on bovine serum albumin (BSA), on colloidal carbon particles (C), and on bovine serum albumin with C (BSA+C). Olympus IX 51 microscope, DP 70 digital camera, obj. 100x, bar = 20 μm.

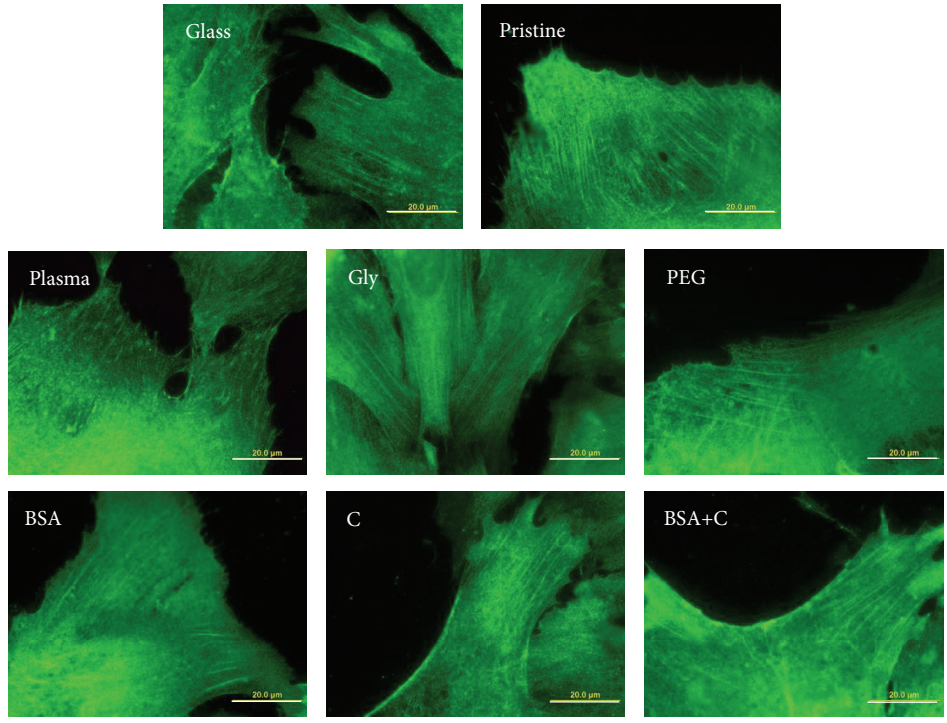

Figure 11: Immunofluorescence of α-actinin, a protein associated with both focal adhesion plaques and the actin cytoskeleton, in rat aortic smooth muscle cells on day 4 after seeding on a microscopic glass coverslip (glass), on pristine LDPE (pristine), on LDPE irradiated with plasma (plasma), on LDPE irradiated with Ar^+ plasma and grafted with glycine (Gly), on polyethylene glycol (PEG), on bovine serum albumin (BSA), on colloidal carbon particles (C), and on bovine serum albumin with C (BSA+C). Olympus IX 51 microscope, DP 70 digital camera, obj. 100x, bar = 20 μm.

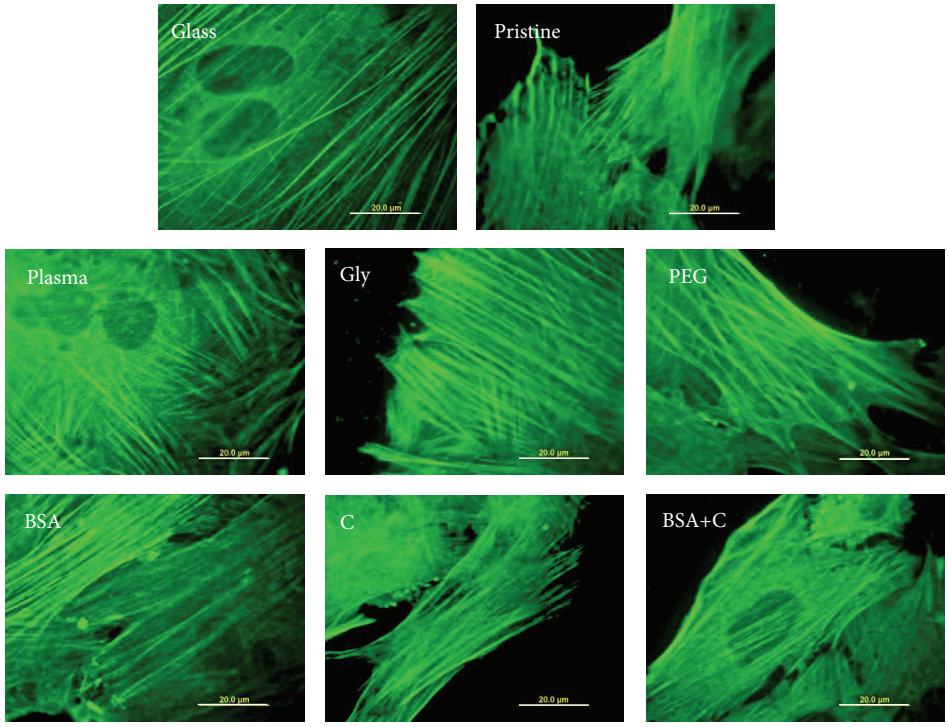

Figure 12: Immunofluorescence of contractile protein α-actin in rat aortic smooth muscle cells on day 4 after seeding on a microscopic glass coverslip (glass), on pristine LDPE (pristine), on LDPE irradiated with plasma (plasma), on LDPE irradiated with Ar^+ plasma and grafted with glycine (Gly), on polyethylene glycol (PEG), on bovine serum albumin (BSA), on colloidal carbon particles (C), and on bovine serum albumin with C (BSA+C). Olympus IX 51 microscope, DP 70 digital camera, obj. 100x, bar = 20 μm.

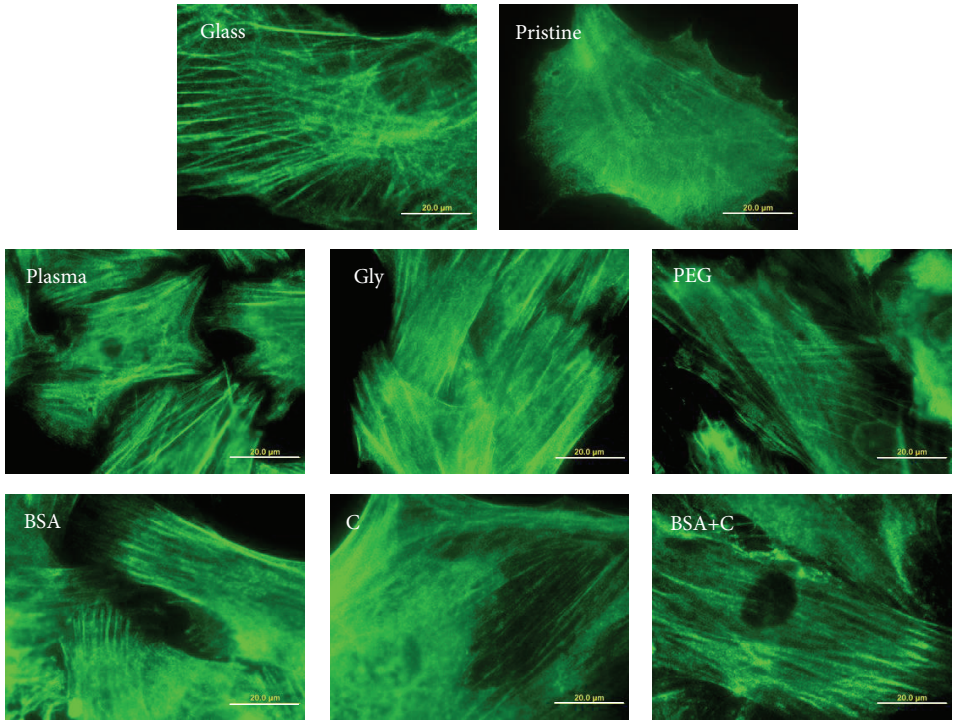

Figure 13: Immunofluorescence of contractile proteins SM1 and SM2 myosins in rat aortic smooth muscle cells on day 4 after seeding on a microscopic glass coverslip (glass), on pristine LDPE (Pristine), on LDPE irradiated with plasma (plasma), on LDPE irradiated with Ar^+ plasma and grafted with glycine (Gly), on polyethylene glycol (PEG), on bovine serum albumin (BSA), on colloidal carbon particles (C), and on bovine serum albumin with C (BSA+C). Olympus IX 51 microscope, DP 70 digital camera, obj. 100x, bar = 20 μm.

an actin isoform nonspecific for VSMC and also present in nonmuscle cell types, was similar in the cells on all tested samples (Figure 9).

Taken together, like the changes in cell number and in spreading area, the changes in the concentration of molecular markers of the adhesion and maturation of VSMC were also generally less apparent on LDPE than on HDPE, after the same modifications of the two polymers (for comparison, see [18]). LDPE grafted with Gly or PEG supported mainly the cell spreading and formation of talin- and vinculin-containing focal adhesion plaques, while the functionalization of LDPE with BSA or BSA+C tended to promote the growth of VSMC to high population densities and their phenotypic maturation, manifested by a higher concentration of α-actin and SM1 and SM2 myosins.

4. Conclusion and Further Perspectives

Modifications of LDPE samples with an Ar^+ plasma discharge and subsequent grafting with glycine, PEG, BSA, C particles, and BSA with C particles improved the colonization of LDPE with VSMC. Grafting with glycine or PEG mainly increased the cell spreading and the concentration of focal adhesion proteins talin and vinculin, which could be attributed to the relatively high oxygen content and wettability of these samples. Grafting LDPE with BSA and BSA+C supported the growth of VSMC to confluence and increased the concentration of α-actin and myosins (SM1 and SM2) in these cells. This could be explained by an enhanced nano- and submicron-scale structure and also by the wettability of the samples. Thus, the plasma treatment and grafting with bioactive substances used in this study improved the adhesion, growth, and phenotypic maturation of VSMC, though these changes were less pronounced than those observed on HDPE in our earlier study [18]. Nevertheless, the polymer modifications developed in this study have a potential for creating a bioartificial vascular wall with reconstructed *tunica media*.

Conflict of Interests

There is no conflict of interests in this study.

Acknowledgments

This study was supported by the Grant Agency of the Czech Republic Grant no. P108/12/G108 ("Center of Excellence"). Mr. Robin Healey (Czech Technical University, Prague, Czech Republic) is gratefully acknowledged for his language revision. The authors also thank Mrs. Ivana Zajanova and Mrs. Jana Vobornikova for their technical assistance.

References

[1] H. P. Greisler, C. W. Tattersall, J. J. Klosak, E. A. Cabusao, J. D. Garfield, and D. U. Kim, "Partially bioresorbable vascular grafts in dogs," *Surgery*, vol. 110, no. 4, pp. 645–654, 1991.

[2] L. Bacakova, V. Mares, M. G. Bottone, C. Pellicciari, V. Lisa, and V. Svorcik, "Fluorine-ion-implanted polystyrene improves growth and viability of vascular smooth muscle cells in culture," *Journal of Biomedical Materials Research*, vol. 49, no. 3, pp. 369–379, 2000.

[3] L. Bačáková, V. Mareš, V. Lisá, and V. Švorčík, "Molecular mechanisms of improved adhesion and growth of an endothelial cell line cultured on polystyrene implanted with fluorine ions," *Biomaterials*, vol. 21, no. 11, pp. 1173–1179, 2000.

[4] L. Bacakova, E. Filova, D. Kubies et al., "Adhesion and growth of vascular smooth muscle cells in cultures on bioactive RGD peptide-carrying polylactides," *Journal of Materials Science*, vol. 18, no. 7, pp. 1317–1323, 2007.

[5] S. H. Daebritz, B. Fausten, B. Hermanns et al., "New flexible polymeric heart valve prostheses for the mitral and aortic positions," *The Heart Surgery Forum*, vol. 7, no. 5, pp. E525–532, 2004.

[6] N. Saito and K. Takaoka, "New synthetic biodegradable polymers as BMP carriers for bone tissue engineering," *Biomaterials*, vol. 24, no. 13, pp. 2287–2293, 2003.

[7] S. A. Atwood, D. W. Van Citters, E. W. Patten, J. Furmanski, M. D. Ries, and L. A. Pruitt, "Tradeoffs amongst fatigue, wear, and oxidation resistance of cross-linked ultra-high molecular weight polyethylene," *Journal of the Mechanical Behavior of Biomedical Materials*, vol. 4, no. 7, pp. 1033–1045, 2011.

[8] C. F. Schierle and L. A. Casas, "Nonsurgical rejuvenation of the aging face with injectable poly-L-lactic acid for restoration of soft tissue volume," *Aesthetic Surgery Journal*, vol. 31, no. 1, pp. 95–109, 2011.

[9] K. W. Ng, D. W. Hutmacher, J. T. Schantz et al., "Evaluation of ultra-thin poly(ε-caprolactone) films for tissue-engineered skin," *Tissue Engineering*, vol. 7, no. 4, pp. 441–455, 2001.

[10] T. Garg, O. Singh, S. Arora, and R. Murthy, "Scaffold: a novel carrier for cell and drug delivery," *Critical Reviews in Therapeutic Drug Carrier Systems*, vol. 29, no. 1, pp. 1–63, 2012.

[11] L. Bacakova, E. Filova, F. Rypacek, V. Svorcik, and V. Stary, "Cell adhesion on artificial materials for tissue engineering," *Physiological Research*, vol. 53, supplement 1, pp. S35–S45, 2004.

[12] L. Bacakova, E. Filova, M. Parizek, T. Ruml, and V. Svorcik, "Modulation of cell adhesion, proliferation and differentiation on materials designed for body implants," *Biotechnology Advances*, vol. 29, no. 6, pp. 739–767, 2011.

[13] L. Bacakova and V. Svorcik, "Cell colonization control by physical and chemical modification of materials," in *Cell Growth Processes: New Research*, D. Kimura, Ed., pp. 5–56, Nova Science, Hauppauge, NY, USA, 2008.

[14] I. Pashkuleva, A. P. Marques, F. Vaz, and R. L. Reis, "Surface modification of starch based biomaterials by oxygen plasma or UV-irradiation," *Journal of Materials Science*, vol. 21, no. 1, pp. 21–32, 2010.

[15] S. Tajima, J. S. F. Chu, S. Li, and K. Komvopoulos, "Differential regulation of endothelial cell adhesion, spreading, and cytoskeleton on low-density polyethylene by nanotopography and surface chemistry modification induced by argon plasma treatment," *Journal of Biomedical Materials Research A*, vol. 84, no. 3, pp. 828–836, 2008.

[16] J. Heitz, V. Svorcik, L. Bacakova et al., "Cell adhesion on polytetrafluoroethylene modified by UV-irradiation in an ammonia atmosphere," *Journal of Biomedical Materials Research A*, vol. 67, no. 1, pp. 130–137, 2003.

[17] R. Mikulikova, S. Moritz, T. Gumpenberger et al., "Cell microarrays on photochemically modified polytetrafluoroethylene," *Biomaterials*, vol. 26, no. 27, pp. 5572–5580, 2005.

[18] M. Parizek, N. Kasalkova, L. Bacakova et al., "Improved adhesion, growth and maturation of vascular smooth muscle cells on polyethylene grafted with bioactive molecules and carbon particles," *International Journal of Molecular Sciences*, vol. 10, no. 10, pp. 4352–4374, 2009.

[19] L. Bacakova, L. Grausova, J. Vacik et al., "Nanocomposite and nanostructure carbon-based films as growth substrates for bone cells," in *Advances in Diverse Industrial Applications of Nanocomposites*, B. Reddy, Ed., pp. 399–435, Intech, 2011.

[20] V. Svorcik, N. Kasalkova, P. Slepicka et al., "Cytocompatibility of Ar^+ plasma-treated and Au nanoparticle-grafted PE," *Nuclear Instruments and Methods in Physics Research B*, vol. 267, no. 11, pp. 1904–1910, 2009.

[21] N. Kasalkova, Z. Makajova, M. Parizek et al., "Cell adhesion and proliferation on plasma-treated and poly(ethylene glycol)-grafted polyethylene," *Journal of Adhesion Science and Technology*, vol. 24, no. 4, pp. 743–754, 2010.

[22] N. Slepickova, N. Kasalkova, P. Slepicka et al., "Cell adhesion and proliferation on polyethylene grafted with Au nanoparticles," *Nuclear Instruments and Methods in Physics Research B*, vol. 272, pp. 391–395, 2012.

[23] M. Parizek, K. Novotná, and L. Bačáková, "The role of smooth muscle cells in vessel wall pathophysiology and reconstruction using bioactive synthetic polymers," *Physiological Research*, vol. 60, no. 3, pp. 419–437, 2011.

[24] A. Van Amerongen, J. H. Wichers, L. B. J. M. Berendsen et al., "Colloidal carbon particles as a new label for rapid immunochemical test methods—quantitative computer image analysis of results," *Journal of Biotechnology*, vol. 30, no. 2, pp. 185–195, 1993.

[25] P. Slepicka, S. Trostova, N. Slepickova-Kasalkova, Z. Kolska, P. Sajdl, and P. V. Svorcik, "Surface modification of biopolymers by argon plasma and thermal treatment," *Plasma Processes and Polymers*, vol. 9, no. 2, pp. 197–206, 2012.

[26] V. Bursikova, P. Stahel, Z. Navratil, J. Bursik, and J. Janca, *Surface Energy Evaluation of Plasma Treated Materials By Contact Angle Measurement*, Masaryk University, Brno, Czech Republic, 2004.

[27] O. H. Lowry, N. J. Rosebrough, A. L. Farr, and R. J. Randall, "Protein measurement with the Folin phenol reagent," *The Journal of Biological Chemistry*, vol. 193, no. 1, pp. 265–275, 1951.

[28] K. Rockova, V. Svorcik, L. Bacakova, B. Dvorankova, J. Heitz, and V. Hnatowicz, "Bio-compatibility of ion beam-modified and RGD-grafted polyethylene," *Nuclear Instruments and Methods in Physics Research B*, vol. 225, no. 3, pp. 275–282, 2004.

[29] V. Švorčík, V. Rybka, V. Hnatowicz, and K. Smetana, "Structure and biocompatibility of ion beam modified polyethylene," *Journal of Materials Science*, vol. 8, no. 7, pp. 435–440, 1997.

[30] V. Svorcik and V. Hnatowicz, "Properties of polymers modified by plasma discharge and ion beam," in *Polymer Degradation and Stability Research Developments*, L. B. Albertov, Ed., pp. 171–216, Nova Science, New York, NY, USA, 2008.

[31] C. O'Connell, R. Sherlock, M. D. Ball et al., "Investigation of the hydrophobic recovery of various polymeric biomaterials after 172 nm UV treatment using contact angle, surface free energy and XPS measurements," *Applied Surface Science*, vol. 255, no. 8, pp. 4405–4413, 2009.

[32] V. Švorčík, K. Kolářová, P. Slepička, A. Macková, M. Novotná, and V. Hnatowicz, "Modification of surface properties of high and low density polyethylene by Ar plasma discharge," *Polymer Degradation and Stability*, vol. 91, no. 6, pp. 1219–1225, 2006.

[33] Q. Wang, Y. X. Guan, S. J. Yao, and Z. Q. Zhu, "Controllable preparation and formation mechanism of BSA microparticles using supercritical assisted atomization with an enhanced mixer," *Journal of Supercritical Fluids*, vol. 56, no. 1, pp. 97–104, 2011.

[34] Y.-S. Lin, S.-S. Wang, T.-W. Chung et al., "Growth of endothelial cells on different concentrations of Gly-Arg-Gly-Asp photochemically grafted in polyethylene glycol modified polyurethane," *Artificial Organs*, vol. 25, no. 8, pp. 617–621, 2001.

[35] S. Huang, C. S. Chen, and D. E. Ingber, "Control of cyclin D1, p27(Kip1), and cell cycle progression in human capillary endothelial cells by cell shape and cytoskeletal tension," *Molecular Biology of the Cell*, vol. 9, no. 11, pp. 3179–3193, 1998.

[36] S. Huang and D. E. Ingber, "Shape-dependent control of cell growth, differentiation, and apoptosis: switching between attractors in cell regulatory networks," *Experimental Cell Research*, vol. 261, no. 1, pp. 91–103, 2000.

[37] A. L. Koenig, V. Gambillara, and D. W. Grainger, "Correlating fibronectin adsorption with endothelial cell adhesion and signaling on polymer substrates," *Journal of Biomedical Materials Research A*, vol. 64, no. 1, pp. 20–37, 2003.

[38] J. E. Koblinski, M. Wu, B. Demeler, K. Jacob, and H. K. Kleinman, "Matrix cell adhesion activation by non-adhesion proteins," *Journal of Cell Science*, vol. 118, no. 13, pp. 2965–2974, 2005.

[39] T. J. Webster, C. Ergun, R. H. Doremus, R. W. Siegel, and R. Bizios, "Specific proteins mediate enhanced osteoblast adhesion on nanophase ceramics," *Journal of Biomedical Materials Research*, vol. 51, no. 3, pp. 475–483, 2000.

[40] J. Lu, C. Yao, L. Yang, and T. J. Webster, "Decreased platelet adhesion and enhanced endothelial cell functions on nano and submicron-rough titanium stents," *Tissue Engineering A*, vol. 18, no. 13-14, pp. 1389–1398, 2012.

[41] H. M. Kowalczyńska, M. Nowak-Wyrzykowska, R. KoThlos, J. Dobkowski, and J. Kamiński, "Semiquantitative evaluation of fibronectin adsorption on unmodified and sulfonated polystyrene, as related to cell adhesion," *Journal of Biomedical Materials Research A*, vol. 87, no. 4, pp. 944–956, 2008.

[42] L. Bacakova, L. Grausova, M. Vandrovcova et al., "Carbon nanoparticles as substrates for cell adhesion and growth," in *Nanoparticles: New Research*, S. L. Lombardi, Ed., pp. 39–107, Nova Science, Hauppauge, NY, USA, 2008.

[43] H. Mao, Y. Wang, Z. Li et al., "Hsp72 interacts with paxillin and facilitates the reassembly of focal adhesions during recovery from ATP depletion," *The Journal of Biological Chemistry*, vol. 279, no. 15, pp. 15472–15480, 2004.

[44] C. A. Carter and T. Bellido, "Decrease in protein tyrosine phosphorylation is associated with F-actin reorganization by retinoic acid in human endometrial adenocarcinoma (RL95-2) cells," *Journal of Cellular Physiology*, vol. 178, no. 3, pp. 320–332, 1999.

[45] C. E. Turner, "Paxillin interactions," *Journal of Cell Science*, vol. 113, part 23, pp. 4139–4140, 2000.

[46] R. Zaidel-Bar, R. Milo, Z. Kam, and B. Geiger, "A paxillin tyrosine phosphorylation switch regulates the assembly and

form of cell-matrix adhesions," *Journal of Cell Science*, vol. 120, part 1, pp. 137–148, 2007.

[47] N. F. Worth, B. E. Rolfe, J. Song, and G. R. Campbell, "Vascular smooth muscle cell phenotypic modulation in culture is associated with reorganisation of contractile and cytoskeletal proteins," *Cell Motility and the Cytoskeleton*, vol. 49, no. 3, pp. 130–145, 2001.

[48] B. Sjöblom, A. Salmazo, and K. Djinović-Carugo, "Alpha-actinin structure and regulation," *Cellular and Molecular Life Sciences*, vol. 65, no. 17, pp. 2688–2701, 2008.